University of East Anglia

British Heart Foundation

Investigating a microRNA-499-5p network during cardiac development

Thesis for a PhD degree

Submitted to University of East Anglia

by Johannes Gottfried Wittig

Principal Investigator: Prof. Andrea Münsterberg

Submission Date: 10.05.2019

Declaration of own work

I, Johannes Wittig, confirm that the work for the report with the title:

“Investigating a microRNA-499-5p network during cardiac development”

was undertaken by myself and that no help was provided from other sources than those allowed. All sections of the report that use quotes or describe an argument or development investigated by other scientist have been referenced, including all secondary literature used, to show that this material has been adopted to support my report.

Place/Date Signature

Acknowledgements

I am very happy that I had the chance to be part of the Münsterberg-lab for my PhD research, therefore I would very much like to thank Andrea Münsterberg for offering me this great position in her lab. I especially want to thank her for her patience with me in all the moments where I was impatient and complained about slow progress. I also would like to say thank you for the incredible freedom I had during my PhD work and the support she gave me in the lab but also the understanding for all my non-science related activities.

I also would like to say thank you to Grant Wheeler, Tracey Chapman and Tamas Dalmay who supervised the progression of my PhD and were always open for questions.

Further I would like to thank Geoffrey Mok, for getting me started in the lab by teaching me relevant techniques, showing me around but more importantly for introducing me to the English culture and making every day funny and sarcastic in the lab.

Furthermore, a big thanks goes to Camille Viaut and Timothy Grocott for discussions and technical advice during my experiments. Thank you for teaching me important techniques in the lab and discussing my troubles when experiments went wrong.

Another big shout out goes to Leighton Folkes and Simon Moxon the bioinformatic brains at UEA, who helped me relentlessly to solve RNAseq challenges but also were great chaps for nerdy discussions.

I also would like to acknowledge Paul Thomas from the imaging facility who always helped when there was trouble with imaging tasks.

A special thanks goes to the various members of the Münsterberg, Wheeler and Grocott lab for discussion support and making my time in the UK joyful.

Very important and not to forget: I would like to thank a few friends of mine: Gerry Giese, Isabell Weber and Marcus Blohs for helping during my PhD research. All the discussions we had were a great input to improve my work and all the advice about science life was invaluable. Thank you guys for the help!

Last but not least, I would like to thank my Mum and Dad, as well as my sisters for all the support during my studies. Specifically, I am very thankful for your patience with me when I had spontaneous ideas about moving somewhere else or going abroad and when I needed advice about my future plans. Thank you very much! I am very lucky to have you.

Abstract

Cardiovascular disease is a major cause of death world-wide, which makes it important to study cardiac development. Research into the heart, the first functioning organ in the body, will provide new knowledge to understand potential causes of different heart conditions. Cardiac maturation is a complex process depending on several different signalling cascades, which are fine-tuned by microRNAs. Alterations in NOTCH1 and ETS1 signalling have been linked to congenital heart defects and diseases. NOTCH1 is vital for cardiac septation and trabeculation, whereas ETS1 is necessary for neural crest cell coordination and proper maturation of the endocardial cushions. Further, both of them are important for inducing epithelial to mesenchymal transition in different tissues. Next generation sequencing of small RNAs has identified several microRNAs (miR-126, miR-499 & miR-451) upregulated during cushion formation (HH17-20 chicken). This was confirmed by RT-qPCR. Interestingly, one of these microRNAs (microRNA-499-5p) targets a site present in the ETS1 and NOTCH1 3'UTR and microRNA-499-5p mimics repressed expression of a luciferase reporter gene. A cardiac injection procedure was developed in the context of this project to asses differential expression and phenotypes after AntagomiR mediated microRNA-499-5p knockdown *in vivo*. RNAseq revealed strong modulation of extracellular matrix genes, which are connected to ETS1 and upregulation of a NOTCH signalling cascade that affected cardiac Troponin. Along with these gene expression changes we have observed increased ECM deposition at the sites of endocardial cushions by sectioning hearts and subsequent 3D-reconstruction and volume measurements. Moreover, a reduced heart rate in knockdown animals has been observed which was linked to cardiac contraction defects due to reduced TNNT2 expression which may have caused Ca^{2+} desensitization. TNNT2 reduction came with reduced TBX3 expression which potentially links the observed defects to the conduction system. Future experiments should strengthen the observed links and specify TNNT2s and TBX3s relation to cardiac conduction.

Table of Contents

Figure Index

Table Index

Abbreviations

Abbreviation	Meaning
ACAN	Aggrecan
ACTA1	alpha 1 skeletal muscle actin
ACTC1	Actin, Alpha, Cardiac Muscle 1
ADAMTS	a disintegrin and metalloproteinase with thrombospondin motifs
AVC	Atrio-ventricular canal
BMP	Bone morphogenetic protein
CDS	Coding sequence
CJ	*Cardiac Jelly*
CX40, GJA5	Connexin 40, Gap junction alpha-5 protein
DGCR8	DiGeorge syndrome critical region 8
DLL4	Delta-like protein 4
DMSO	Dimethyl sulfoxide
DNase	Deoxyribonuclease
DRP1	Dynamin-related protein-1
EC	Endocardial cushions
ECM	Extra cellular matrix
EET	Extra embryonic tissue
EGR1	Early Growth Response 1
EGR2	Early Growth Response 2
EMSA	electrophoretic mobility shift assay
EMT	epithelial to mesenchymal transition
ETS1	v-ets avian erythroblastosis virus E26 oncogene homolog 1
FGF	Fibroblast Growth Factor
FOS	FBJ osteosarcoma oncogene
GATA4	GATA Binding Protein 4
HA	Hyaluronan
HAPLN1, CRTL1	hyaluronan and proteoglycan link protein 1, cartilage link protein
HAS2	Hyaluronan Synthase 2
HBEGF	Heparin Binding EGF Like Growth Factor
hCMPC	Human cardiac myocyte progenitor cells
HF	Heart field
HH	Hamburger and Hamilton stage
hpi	Hours post injection
IAS	Interatrial septum
IHC	Immunohistochemistry
ISH	In situ hybridisation
JAG1	Jagged1
IVT	In vitro transcription
LB	Lysogeny broth
MEF2C	Myocyte Enhancer Factor 2C
miRISC	Mature microRNA RNA-induced silencing complex
mirRNA, miR	Micro ribonucleic acid

Abbreviation	Meaning
MMP	Matrix Metalloproteinase
mRNP	nuclear messenger ribonucleoprotein
MSX1	Msh homeobox 1
MVB	Multivesicular bodies
MYH	Myosin Heavy Chain
NCC	Neural crest cells
NFATC1	Nuclear factor of activated T-cells, cytoplasmic 1
NGS	Next Generation Sequencing
NICD	NOTCH intracellular domain
NOTCH1	NOTCH homolog 1, translocation-associated
NPPB	natriuretic peptide precursor type B
NRG1	Neuregulin 1
nt	Nucleotide
OFT	Outflow tract
PAX3	Paired Box 3
PEO	Proepicardial organ
PLAU	Plasminogen Activator, Urokinase
POSTN	Periostin
PS	Penicillin Streptomycin
PVDF	polyvinylidene fluoride membrane
rER	Rough endoplasmatic reticulum
RISC	RNA-induced silencing complex
RNase	Ribonuclease
RNAseq	Ribonucleic acid sequencing
RT	Room temperature
RT-qPCR	Real time quantitative Polymerase Chain Reaction
SG	Stress granules
SIM	Septum intermedium
SMAD	Mothers against decapentaplegic homolog
SMC	Smooth muscle cells
SOX	SRY-Box
SRF	Serum response factor
TBX	T-Box
TG	Transgenic
TGN	Trans Golgi network
TIMP	Tissue inhibitor of metalloproteinase
TNC	Tenascin C
TNNT2	Troponin T2, Cardiac Type
TM	Melting Temperature
UTR	Untranslated region
VCAN	Versican
VIC	valvular interstitial cells
VS	Ventricular septum
WISH	Whole mount in situ hybridization

1 Aims of Project

The goal of this project was to investigate the role of microRNAs (Figure 1A) during heart development and to acquire new information about their involvement in regulating the many signalling pathways within the heart, such as for example NOTCH, WNT or Bone morphogenetic protein (BMP) (MacGrogan et al., 2018a, van Eif et al., 2018). The complexity of the organ, which comprises of multiple chambers and different tissues makes adequate regulation and fine tuning a necessity to ensure proper formation of a healthy heart. The primary interest of this study was to learn how microRNAs affect the development of endocardial cushions (EC), the precursors of cardiac valves and septa (Person et al., 2005). There are seven ECs which arise at different time-points of development (Figure 1B). The first two form in the atrioventricular canal (AVC), the second set of three form in the outflow tract (OFT) and the remaining two form much later in development lateral to the left and right of the heart and will aid the formation of tricuspid and mitral valves. The first two groups of ECs arise earlier in development and thus were the main focus of this study. For experimentation two model systems, the chick and cultured cells (chicken fibroblasts) were used.

A microRNA expressed in the heart was selected based on NGS for this study, microRNA-499-5p. Literature and experiments in the Münsterberg lab indicated target interaction of said microRNA with the transcription factor ETS1 (= v-ets avian erythroblastosis virus E26 oncogene homolog 1) (Wei et al., 2012, Wilson et al., 2010). Therefore, the initial aim was to confirm this observation in cell culture experiments and simultaneously determine other target interaction partners. A second aim of the project was to develop a technique for *in vivo* knockdown of microRNAs by using microRNA inhibitors (AntagomiRs) in the heart. These manipulated embryos were then used in a third stage for various downstream analyses to dissect the role of microRNA-499-5p in heart development. Experiments included phenotypical analyses (heartbeat, morphology), differential expression analysis using transcriptomics/RNAseq and determination of changes in mRNA expression by ISH or RT-qPCR.

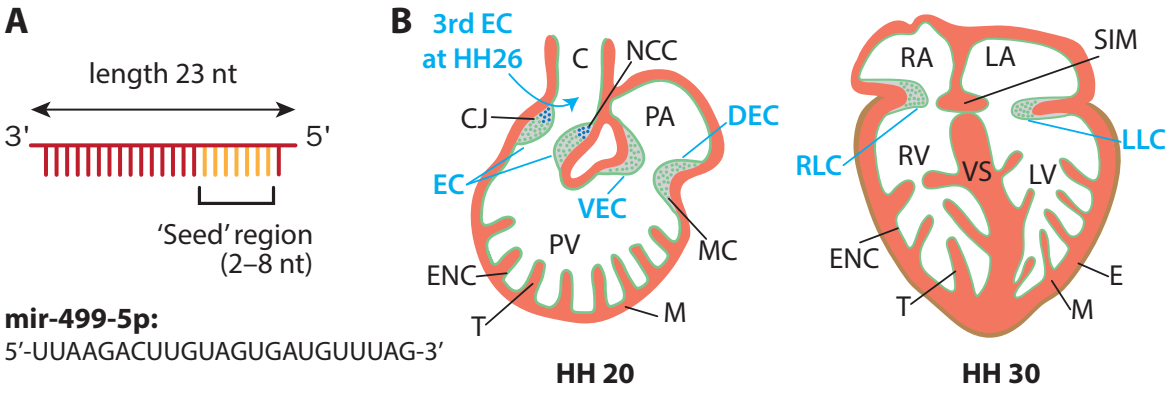

Figure 1: Aim of Project

(A) Core structure of a microRNA with seed for target binding (5' nucleotide 2-8), sequence information for microRNA-499-5p below. (B) Illustrations of chicken hearts at HH20 & HH30 showing locations of endocardial cushions (turquoise labels) formation. At HH20 two cushions stretch along the OFT. A third one forms later at the distal region which is relevant for aorticopulmonary septation. At HH30 two more lateral cushions are forming that aid the development of the tricuspid & mitral valve. (C) conus, (CJ) cardiac jelly, (DEC) dorsal endocardial cushion, (E) Epicardium, (EC) endocardial cushion, (LA) left atrium, (LLC) left lateral cushion, (LV) left ventricle, (M) myocardium, (PA) primitive atrium, (PV) primitive ventricle, (RA) right atrium, (RLC) right lateral cushion, (RV) right ventricle, (T) Trabeculae, (VEC) ventral endocardial cushion, (VS) ventricular septum

2 Introduction

2.1 MicroRNAs small but potent regulators

Gene regulation through microRNAs (miRNA or miR) is still an under investigated field in today's research community. Nevertheless, the importance of these small molecules should not be underestimated. Their combined impact has shown to be essential for proper development and the first footsteps for microRNAs to become future drugs and biomarkers have been made (Liu and Olson, 2010, Tian et al., 2017, van Rooij and Olson, 2012).

MicroRNAs are small double stranded hairpin molecules that after various processing steps become incorporated as a single strand into a protein complex which allows them to bind to specific gene transcripts and affect their translation. Most microRNAs are transcribed via RNA-Polymerase II producing the "primary" or pri-microRNAs, the earliest form of the microRNA. The pri-microRNAs can originate from three different locations in the genome. There are exonic, intronic (intragenic) and intergenic microRNAs. The first two relate to microRNAs produced from an exon or intron within a host gene, whereas intergenic microRNAs comprise their own independent transcriptional unit, in between other genes. The majority of currently known microRNAs originate from intronic regions (Figure 2). The pathways for microRNA processing can be classified into a canonical cascade and a non-canonical one. The primary pathway for microRNA processing is the canonical biogenesis pathway (Bartel, 2004, Luo et al., 2015, O'Brien et al., 2018).

After initial transcription the pri-microRNA structure forms, which contains double-stranded hairpins with mismatched base pairing and terminal stem loops. This structure is recognised by the ribonuclease III enzyme Drosha, DiGeorge syndrome critical region 8 (DGCR8) and other co-factors and subsequently cleaved to liberate a 60-70nt long RNA with a typical hairpin structure, the "precursor" or pre-microRNA. Particularly for intragenic microRNAs this cotranscriptional process has high similarity with splicing which removes introns and reconnects exons during transcription. Recently, a report has shown splicing function of Drosha outside microRNA biogenesis (Havens et al., 2014). Moreover, this process requires high specificity since one pri-microRNA can produce multiple different microRNAs of the same family or of different families. Once the pre-microRNA is released it is transported to the cytoplasm via exportin-5 and potentially by other as yet unknown mechanisms. In the cytoplasm, the pre-microRNA is further processed by the RNase III endonuclease, Dicer, and TRBP yielding a double stranded microRNA-5p/microRNA-3p duplex, which consists of imperfectly matching strands around 21-25 nts long. In principal, both strands can be functional and mediate a biological effect. However, usually the inactive microRNA (also termed passenger strand) is removed and degraded when the microRNA duplex matures and becomes integrated into the RNA-induced silencing complex (RISC), a multiprotein complex consisting of several Argonaute proteins (Bartel, 2004, van Rooij and Olson, 2012) (Figure 2). Strand selection occurs in an ATP dependent manner and depends on thermodynamic stability at the 5' ends of the microRNA duplex or the presence of a 5' Uracil. In most cases strands with 5'-U or lower thermodynamic stability are prioritised for loading into RISC. This so-called guide strand guides RISC to target mRNAs.

Non-canonical microRNA processing occurs in a similar fashion to canonical processing. However, in the various forms of non-canonical biogenesis that have been reported some of the components

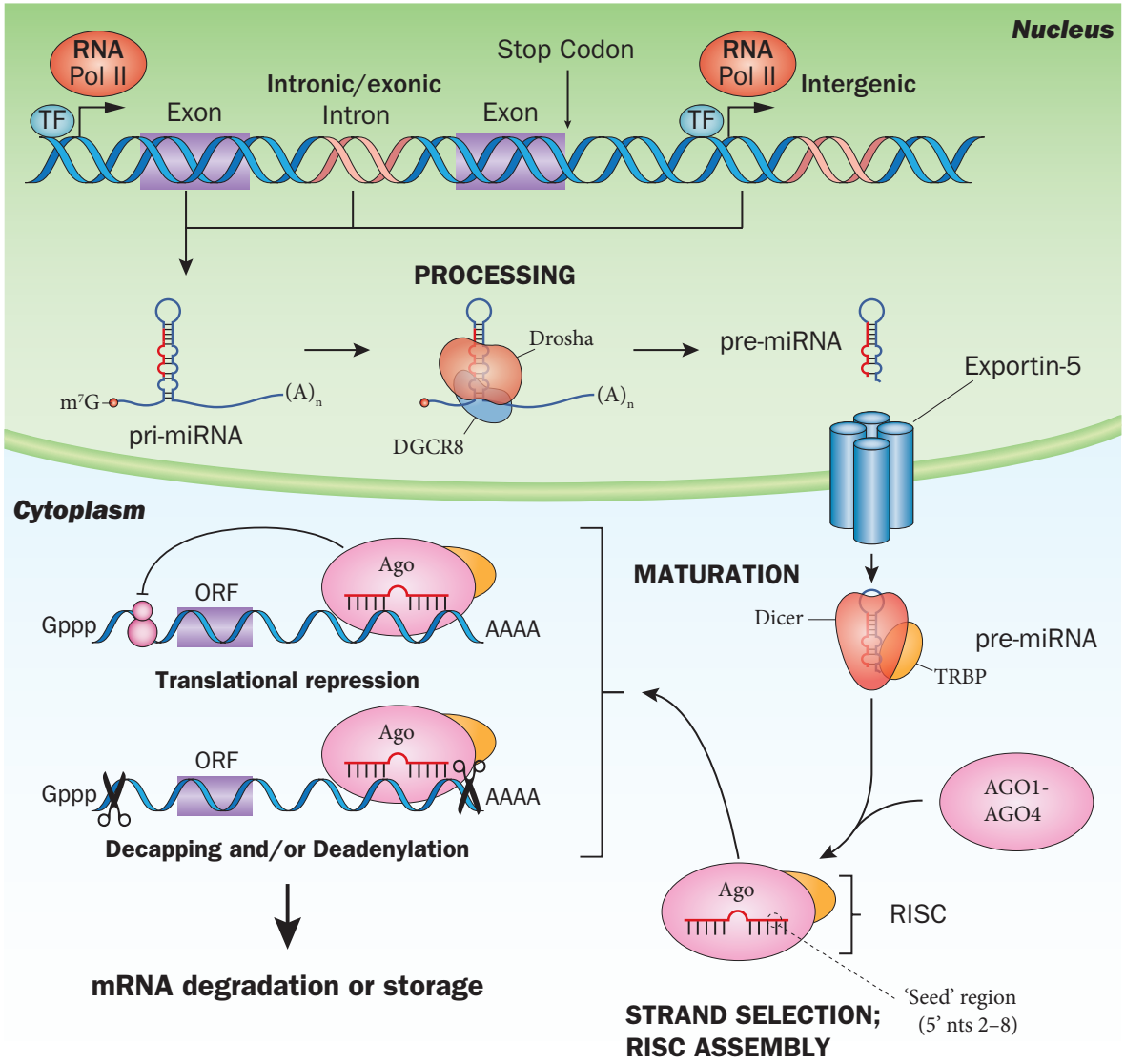

Figure 2: Biogenesis and functions of microRNAs

The schematic illustrates the three genomic locations from which microRNA can be synthesized, intronic, exonic and intergenic. Whereas the first two refer to locations within a protein-coding gene, the latter refers to a location between two genes. MicroRNAs are synthesized by RNA polymerase II and form immediately a looped and self-hybridizing pri-microRNA, which is subsequently processed by Drosha and results in the pre-microRNA. This pre-microRNA is then transported by Exportin-5 into the cytoplasm where it is further processed by the endo-ribonuclease Dicer and TRBP, which yields a microRNA duplex. One strand is selected and incorporated into RISC which can modulate mRNAs in different ways and the unused strand usually gets degraded. The possible effects of RISC on target mRNAs are shown: (1) Translational repression and (2) Decapping and/or De-adenylation together these mechanisms lead to either mRNA degradation or storage for later use. Importantly, complementarity of the seed region is a major determinant for microRNA:mRNA-target interactions in Metazoans. The seed region corresponds to nucleotides 2-8 at the 5' end of the microRNA. (Figure adapted from (Inui et al., 2010, Luo et al., 2015))

of the canonical pathway are omitted. MicroRNAs that are processed independently of Drosha/DGCR8 as for example mirtrons, which are produced from the introns of mRNA during splicing are directly exported to the cytoplasm and processed by Dicer only, before they are loaded into the RISC complex. There are also Dicer-independent processed microRNAs and these need further processing by AGO for maturation and incorporation into the RISC complex (O'Brien et al., 2018).

After formation of a mature complex (miRISC), which includes the remaining active microRNA

strand (guide strand), the miRISC is guided to target mRNAs in the cytoplasm by interacting directly with sequences in the mRNA, typically located in the 3'UTR, via Watson-Crick base pairing. Although there are also some reports showing microRNA interaction with 5'UTRs, coding sequences (CDS) and promoter regions (O'Brien et al., 2018). This interaction affects the translation of the mRNA. A major determinant for target interaction in metazoans is the degree of complementarity of the microRNA seed sequence with the UTR of the target mRNA. The seed sequence corresponds to nucleotides 2 to 8 at the 5' end of the guide strand. If the seed sequence is identical or highly similar between different microRNAs, they are considered as family members with potentially similar signalling roles (Inui et al., 2010, O'Brien et al., 2018). Nevertheless, the remaining nucleotides of the microRNA also support the binding process to achieve specific interactions. Finally, the interaction of RISC with the mRNA can trigger different effects, the following three are the most common ones: (1) mRNA cleavage (Li et al., 2018a, Li et al., 2018b) (2) translational repression and (3) Poly(A)-deadenylation and de-capping (Bartel, 2004, Luo et al., 2015, van Rooij and Olson, 2012). Together they then cause mRNA degradation or storage for later use (Figure 2). The mechanism selected is often dependent on the degree of complementarity, high complementarity leads to cleavage which is mainly occurring in plants and low complementarity leads to translational repression, which is the primary mode of action in animals (Li et al., 2018a, Li et al., 2018b). Furthermore, these different silencing mechanisms require additional protein functions. Cleavage for example can be executed by AGO2 after fully complimentary binding, whereas de-capping requires proteins like DCP2 and poly(A)-deadenylation is orchestrated by a complex of PAN2/3 and CCR4-NOT (O'Brien et al., 2018).

Localisation of miRISC is broad and not restricted to the cytoplasm. Various reports (summarised in O'Brien et al. (2018)) showed miRISC presence at early/late endosomes, lysosomes, mitochondria, multivesicular bodies (MVB), the nucleus, processing (P)-bodies, the rough endoplasmatic reticulum (rER), stress granules (SG) and the trans Golgi network (TGN). Presence of miRISC at Polysomes and P-bodies has been observed together with increased levels of mRNA degradation and block of translation. P-bodies themselves are strongly enriched for the degradation enzymes described above. Another location for miRISC, the nucleus is not only related to nuclear mRNA degradation but also to modulation of transcription, where it can interact with nascent mRNA to promote more efficient splicing or alternate splicing profiles as well as interact with DNA to promote active or inactive chromatin states. Furthermore, miRISC can promote mRNA storage in P-bodies or be stored as a miRISC- nuclear messenger ribonucleoprotein (mRNP) complex itself in SG to allow the cell a dynamic response under stress conditions. Last but not least miRISC can also be exported to the extracellular matrix where they function as chemical messengers to mediate cell-cell communication (O'Brien et al., 2018).

2.1.1 Conservation and species differences

Interestingly the microRNA processing and how microRNAs mediate gene regulation is evolutionary conserved among different kingdoms, meaning that the key players or variants of those described above occur in many different species. The strongest differences to the described mechanisms above from the animal kingdom exist in plants. Their microRNA biogenesis for example is completed in the nucleus leading to microRNAs with universally methylated 3' ends. Prior to export the microRNA-5p/microRNA-3p complex gets 3'-terminal 2'-O-methylated, to prevent degradation

in the cytoplasm. They also do not possess Drosha genes and all the processing is carried out by dicer-liker proteins. Furthermore a broader range of AGO proteins (1-10) is available in plants compared to the animal kingdom (1-4), potentially allowing more fine control in their function (Li et al., 2018a, Li et al., 2018b). In contrast to metazoans, microRNA target interaction in plants relies on almost perfect matches with little tolerance for mismatches, resulting in higher efficacy the better the complementarity is. Nonetheless, the biological impact of microRNAs is equally important in in both kingdoms. One thing they have in common is that their regulatory effect on a single target is often minor, however clever mechanisms have evolved to significantly increase their potential. One of these is the presences of several microRNA target sites within their binding regions, that allows binding of different microRNAs to their respective target sites which in turn allows for synergistic or additive effects on one gene. Another one is that a single microRNA often targets multiple genes within a certain pathway, which in turn leads to a stronger overall impact (Liu and Olson, 2010). Besides their function as gene regulator, microRNAs also have recently been identified as hormone like messengers both in animals and plants. As mentioned, means for microRNAs export exist that allows them to travel to target cells and tissues where they can be reabsorbed and modulate gene expression (Li et al., 2018a, Li et al., 2018b). Furthermore, the presence of such circulating microRNAs can be exploited for diagnostics and treatment which is explained further in the section on 'MicroRNAs in heart development and disease'. In summary microRNA synthesis and the acting mechanism of action show a strong degree of similarities between animals and plants even though various subtle differences exist.

2.1.2 Target identification and experimental validation

As described above the effects of microRNAs on gene expression are subtle and microRNAs often serve more for fine tuning to establish a constant baseline expression. This in turn makes the evaluation of microRNA target binding more challenging, since analysis of individual microRNA:target interactions might not achieve changes of gene expression that are easily detectable by commonly used assays.

The most commonly used assay for studying modulation of gene expression by microRNAs uses luciferase-reporter constructs. These constructs include a luciferase linked to a 3'UTR of interest and a secondary luciferase for normalization of transfection efficiency (Figure 3A, B). Such constructs are transfected into cell lines, which allows readout of microRNA target interaction with the 3'UTR since the expression strength of the 3'UTR-linked luciferase will be affected by microRNA binding to its target site (Figure 3C). Thanks to the high sensitivity even minor changes in luciferase expression can be detected and correlated with biological relevance (Liu and Olson, 2010). Still, such assays are only partially supportive since even though interaction can be shown in the *in vitro* assay the commonly used immortalised cell lines provide a different cellular environment (O'Brien et al., 2018) than is the case *in vivo* in the animal. For example, other mechanisms or microRNAs of the same family with structural homology can potentially compensate for microRNA loss or overexpression. Recently, such cases were described for miR-143 and miR-145 in a review about microRNAs during cardiac development (Liu and Olson, 2010) and for microRNA-499 in regard to SRY-Box 6 (SOX6) target interaction (Shieh et al., 2011).

An alternative method to luciferase assays is a more recent adaptation for electrophoretic

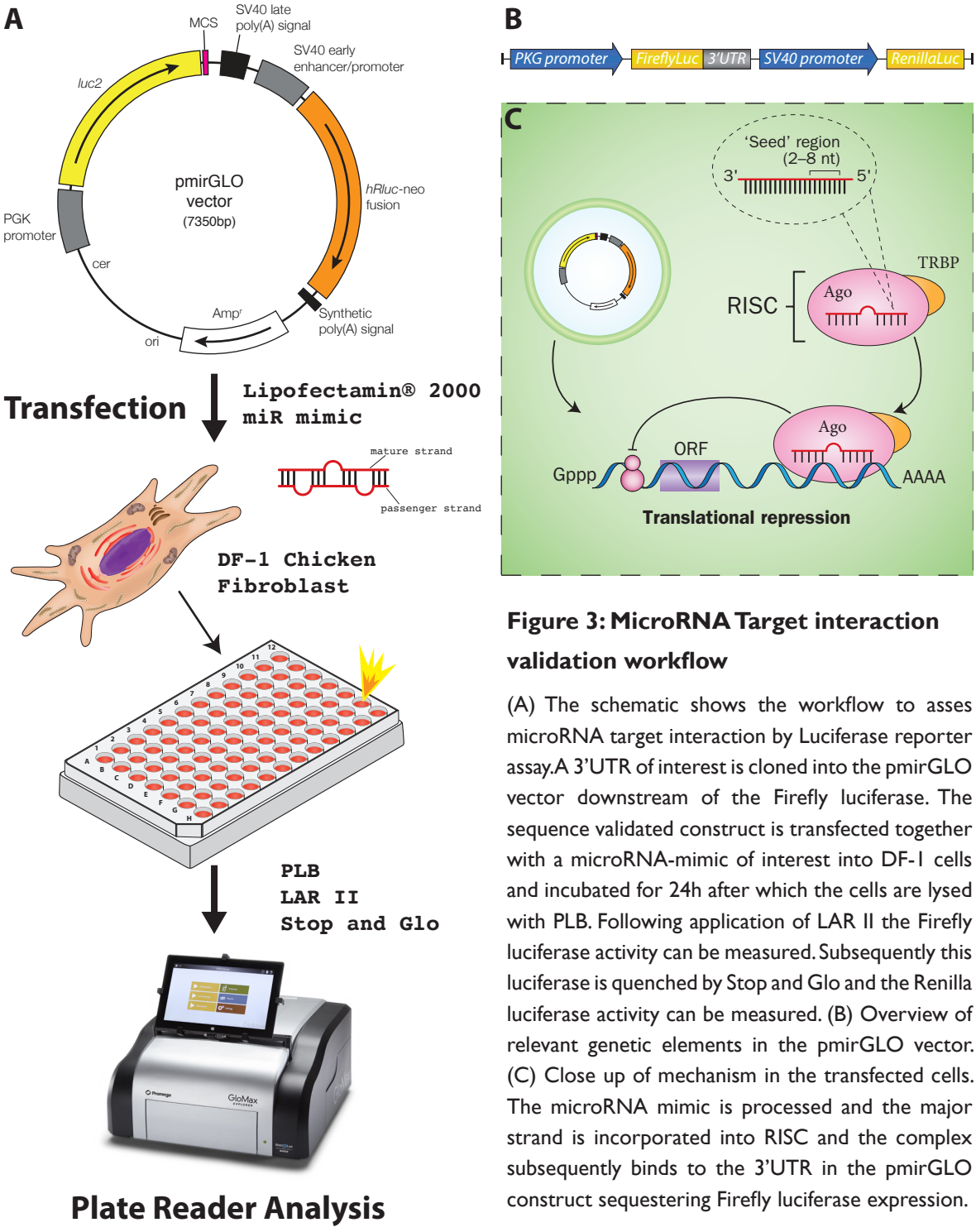

Figure 3: MicroRNA Target interaction validation workflow

(A) The schematic shows the workflow to asses microRNA target interaction by Luciferase reporter assay.A 3'UTR of interest is cloned into the pmirGLO vector downstream of the Firefly luciferase. The sequence validated construct is transfected together with a microRNA-mimic of interest into DF-1 cells and incubated for 24h after which the cells are lysed with PLB. Following application of LAR II the Firefly luciferase activity can be measured. Subsequently this luciferase is quenched by Stop and Glo and the Renilla luciferase activity can be measured. (B) Overview of relevant genetic elements in the pmirGLO vector. (C) Close up of mechanism in the transfected cells. The microRNA mimic is processed and the major strand is incorporated into RISC and the complex subsequently binds to the 3'UTR in the pmirGLO construct sequestering Firefly luciferase expression.

mobility shift assays (EMSA) for microRNA target interaction studies. In an EMSA a microRNA and a 3'UTR of interest are run on a native gel, either separately or together. For visualisation at least one of the two needs to be labelled. The authors of the method have used radioactive labels to do so, but other options should work as well. When run together a shift in mobility compared to the separate conditions should be visible if the microRNA is interacting with the 3' UTR. Ideally the 3'UTR is labelled since it will lead to a more easily detectable signal due to the larger fragment size. Labelling of the microRNA though will allow visualisation of microRNA conformations as it was shown for miR-224. To confirm that different bands correspond to microRNA secondary structures a denaturing gel can be used which resolves these (Sole et al., 2013). In summary the EMSA method can successfully proof target interactions but will not provide any information that this interaction

leads to an actual expression change.

For this project we employed a dual luciferase reporter system based on the pmirGLO Dual-Luciferase microRNA Target Expression Vector from Promega to confirm target interaction of selected microRNAs (Table 1) against genes of interest that are relevant during cardiac development. The plasmid encodes for two luciferases, Firefly and Renilla luciferase, which are driven by different promoters. Further Firefly luciferase is affected by a downstream UTR, which is cloned into the plasmid whereas Renilla luciferase is not and therefore serves as internal control for transfection efficiency (Figure 3A, B). This single plasmid allows for better normalisation compared to other systems which were based on two individual plasmids one harbouring the UTR construct and the other one only a luciferase for normalisation. The schematic in Figure 3 describes the experimental procedure and components.

2.1.3 MicroRNAs in heart development and disease

Several microRNAs have been studied in context to heart development and function. The best known ones include the muscle specific miR-1 (Zhao et al., 2005) and miR-133 (Chen et al., 2006). Both of these microRNAs are evolutionary conserved across their entire length, which is an uncommon feature but also emphasizes their importance for regulation. Both of them repress non-muscle specific lineages but act contradictory in regard to cardiomyocyte differentiation which is promoted by miR-1 and inhibited by miR-133. Furthermore, they are involved in several other roles. Both of them have regulatory effects on cardiac conduction and hypertrophy, cardiomyocyte proliferation and sarcomeric actin organization. MicroRNA-1 also regulates myoblast differentiation and miR-133 takes part in regulation of smooth muscle cell (SMC) gene expression and myoblast proliferation (Liu and Olson, 2010). Different knockout and overexpression studies focussing on these two microRNAs showed ventricular-septal defects and either an increase or decrease in cardiomyocyte proliferation (Liu et al., 2008, Zhao et al., 2007, Zhao et al., 2005). Further to those two microRNAs, cardiac specific knockout of Dicer using the Cre-LoxP system in mice driven by the α-myosin or Homeobox protein NKX-2.5 (*NKX2.5*) promoter led to greatly reduced cardiac function and even embryonic lethality, respectively. In fact, many human heart diseases show differential expression of microRNAs and/ or reduced amounts of Dicer itself, emphasizing the fundamental role of microRNAs in heart development (Tian et al., 2017). However not only miR-1 and miR-133 have been reported to affect cardiac development and function. Other micro RNAs include miR-138 which is involved cardiac patterning in zebrafish (Morton et al., 2008) and miR-143 and miR-145 which are involved in fate of SMCs and specifically vascular SMCs (Cordes et al., 2009). In addition, miR-126 is important for regulation of angiogenesis. Interestingly, miR-126 expression is promoted by the transcription factor ETS1 (Wang et al., 2008), which also directs neural crest migration in the heart and thus contributes to development of the endocardial cushions (Gao et al., 2010). ETS1 itself is also a predicted target of several microRNAs (Agarwal et al., 2015) including one of the MyomiRs, which are important regulators for cardiac remodelling of myofiber content, muscle performance and muscle myosin content. Members of this family are miR-208a, miR-208b (not conserved in gallus gallus) and miR-499 which is the one predicted to target ETS1 (van Rooij et al., 2009, van Rooij et al., 2007). The former two regulate the switch of their host genes myosin heavy chain (*MYH)6* and *MYH7*, by repressing the respective other gene. Studies have shown,

that overexpression of miR-208a alone can cause cardiac hypertrophy and defects in the cardiac conduction system. In addition to its regulatory function for *MYH7*/miR208b it also controls myosin heavy chain 7B (*MYH7B)*/miR-499 expression. MicroRNA-499 is the primary target of study in this project. Available information about miR-499 and particularly its role during development is limited. MicroRNA-499 is known to regulate sarcomeric genes and some studies indicated regulation of *SOX6*, CalcineurinA (*CNA)α* and *CNA*β. Furthermore, downregulation of miR-499 itself has been shown to contribute to cardiac hypertrophy. In human disease, it has been noted that after acute myocardial infarction increased levels of microRNAs, such as miR-1, miR-133a, miR-208 and miR-499, can be detected in the blood serum and overexpression of miR-499 in human cardiac stem cells showed improved cardiac specification. This indicates miR-499 could be a potential drug for regenerative medicine. In contrast to is regenerative potential overexpression in mouse has shown to cause enlarged hearts, contractile dysfunction and increased heart-to-body weight ratios when compared with littermate controls, showing that a fine balance of the microRNA is necessary for natural development and function (Shinji et al., 2014, Tian et al., 2017). Therefore, the aim of this project is to elucidate microRNA-499's role during cardiac development, to more precisely define its necessity and interaction partners.

2.2 Investigating the signalling network surrounding microRNA-499

As described above microRNAs are important regulators during development of the heart and further research is required to more precisely describe their role in development. One of the areas where microRNA related signalling function is under-investigated, is the formation of the endocardial cushions and the subsequent formation of the heart valves. Therefore, this study aims to shed some new light on these areas of the heart. During a previous project in the Münsterberg lab a microRNA profiling study was conducted, which determined microRNAs that are expressed during the time of endocardial cushion formation, starting at around stage HH17 in chicken embryos. Several microRNAs showed a 100-fold increased expression at this time point (Figure 4A). A summary of those microRNAs is depicted in Table 1.

Based on the profiling data three microRNAs were selected for further investigation, miR-126, miR-451 and miR-499. Among those, microRNA-499 was the most promising candidate. It has a predicted target site in the 3'UTR of *ETS1*, along with miR-1. Preliminary data confirmed the interaction of miR-499 with the *ETS1* 3'UTR, opening an exciting topic for investigation. ETS1 itself is a transcription factor, which has been shown to be important in multiple cardiac lineages where it controls GATA Binding Protein 4 (*GATA4*) in early cardiogenesis (Schachterle et al., 2012). Later, ETS1 becomes restricted to the endocardium where it remains active throughout cardiogenesis.

Table 1: microRNAs peaking during the time of endocardial cushion formation

Fourteen microRNAs show a >100-fold increase in normalised read numbers at HH17-20 compared to HH5. Of these, 6 microRNAs have known roles in heart development and function (underlined) and 3 of them are highly correlated (bold) (McCormick, 2015).

miRNAs with a fold change larger than 100 in at least one sample				
miR-1	**miR-126**	miR-187	**miR-451**	miR-9
miR-10	miR-145	miR-199	miR-490	miR-99
miR-100	miR-1451	miR-449	**miR-499**	

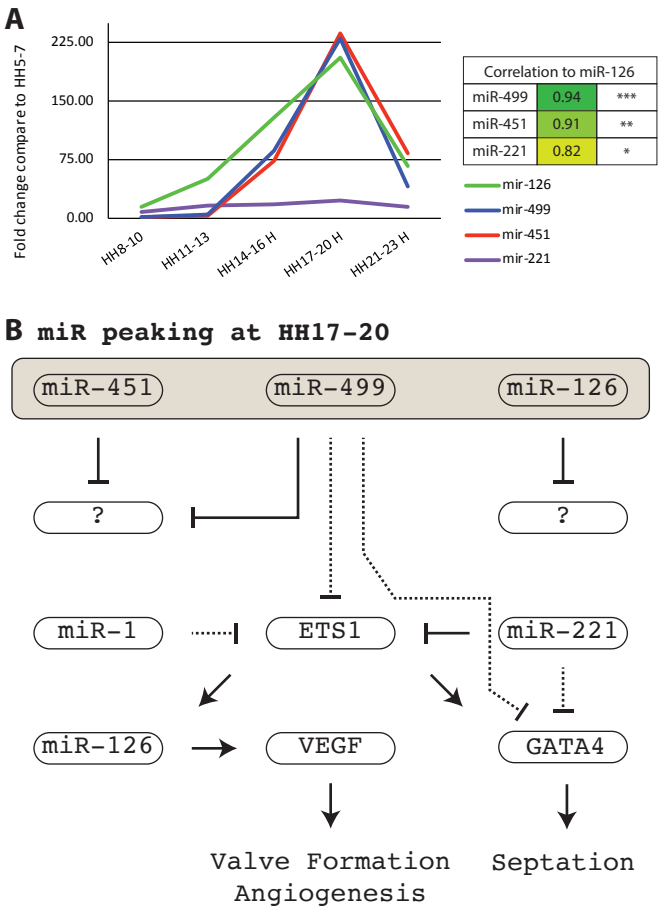

Figure 4: Project background and working hypothesis

(A) Expression profiling revealed candidate micro-RNAs which increase more than 100-fold (miR-126, miR-449 and mir-451) and correlate with the timing of endocardial cushion development. In addition, miR-221 shows a similar trend, but has a smaller increase in expression. (B) The schematic illustrates a candidate gene for this study that might be regulated by the selected microRNAs above. ETS1 is a transcription factor known to be involved in septation and valve formation via GATA4 and miR-126 respectively. The interaction of miR-221 with the ETS1 3'UTR has been confirmed previously. The aim of this study is to gain a better understanding of this signalling network as several microRNA target interactions have been predicted and to further elucidate other targets of the selected microRNAs that are vital for cardiac development. (dotted lines for target predictions, full lines for published interactions)

Interestingly it is known that ETS1 is a regulator for miR-126 which is required for cushion and valve formation. In this context miR-126s role is to repress inhibitors of VEGF. Expression of VEGF is required as it was shown that its signalling directs the morphogenesis of AVC cushions into mature, elongated valve leaflets (Stankunas et al., 2010). In addition to the regulatory function of ETS1 protein, it was recently shown that its transcript is also regulated by miR-221-3p in synovial fibroblasts (Xu et al., 2016). Furthermore, the expression profile of miR-221 correlates with the above chosen microRNAs of interest (Table 1) thus pointing towards a potential role in heart development. Taken together, these observations (Figure 4), place ETS1 in the centre of a microRNA regulation network as target and effector in the heart.

2.2.1 Origin of microRNA-499 and known functions in heart development

MicroRNA-499 belongs to the so-called MyomiRs as introduced above. It is coded intragenic between Exons 24 and 25 of *MYH7B* (Figure 5A) located on chromosome 20 in the chicken. The expression of *MYH7B* is specific to cardiac and slow skeletal muscle, and microRNA-499 is co-expressed at the same locations (van Rooij and Olson, 2012). However, other reports even state that microRNA-499 and *MYH7B* are exclusive to the heart (Sluijter et al., 2010). Genomic sequence alignment shows (Figure 5B) that microRNA-499 is broadly conserved among several species, in particular the 3p arm shows better alignment. The main guide-strand and therefore the primary signal conductor used in the heart is however the 5p arm where there is a single nucleotide change in the chicken sequence compared to the human sequence (Kiezun et al., 2012, Shieh et al., 2011).

MicroRNA-499 has been previously studied in transgenic mice which revealed that overexpression

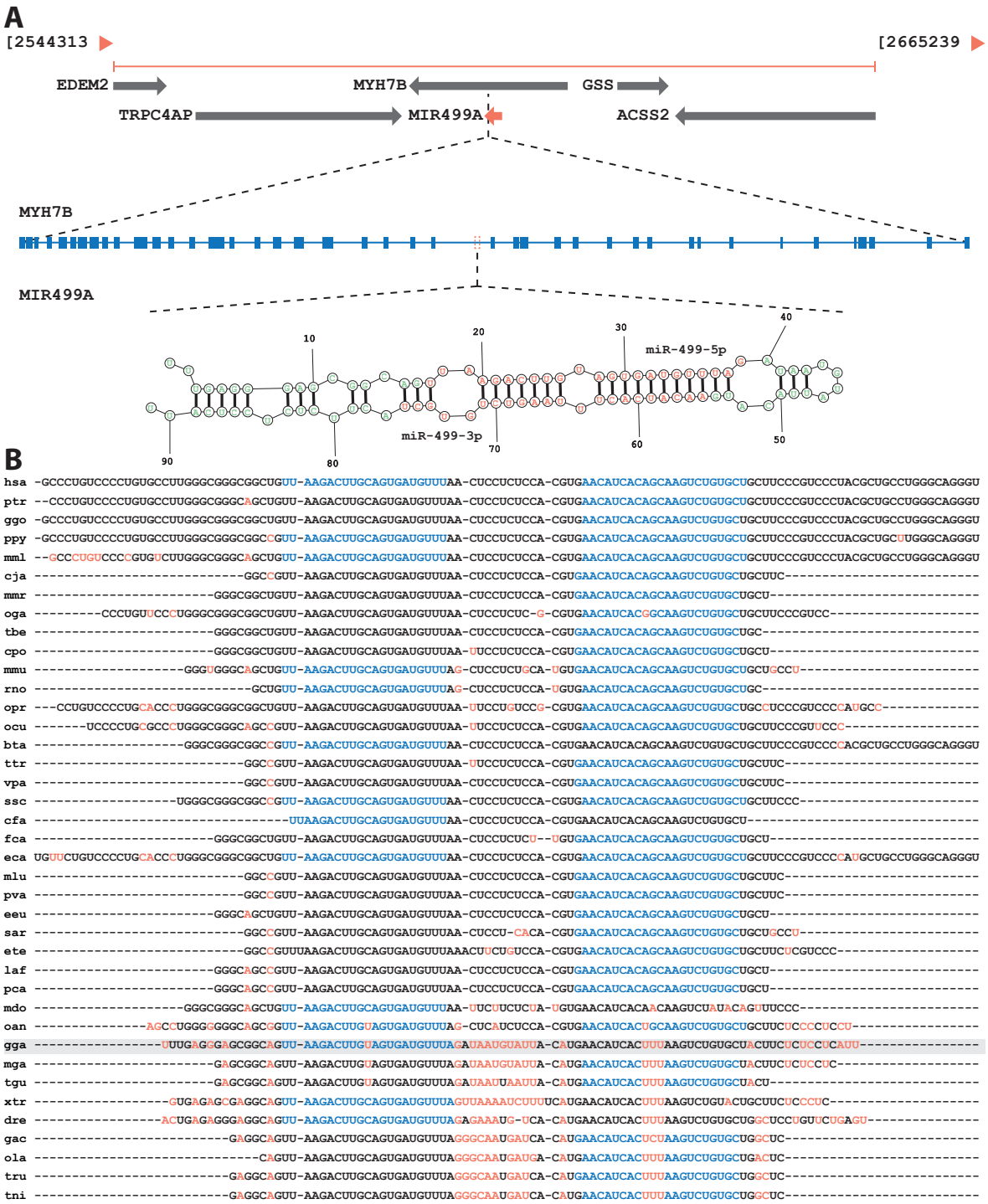

Figure 5: MicroRNA-499 locus, structure and conservation

(A) Schematic showing the genomic region around *MYH7B* (gallus gallus) the host gene of microRNA499A. Magnification shows that microRNA499A lies in between exon 24 and 25. Further zoom shows secondary structure of microRNA499A with red lettering for their active 3p (bottom) and 5p (top) form. (B) Sequence alignment of microRNA499 with several different animal species (grey box shows chicken) shows there is a strong conservation particularly for the 3p variant. Within each miRNA group, multiple alignment is coloured black for aligned sequences, red for mismatches and blue for mature miRNA region (Kiezun et al., 2012).

causes an acute hypertrophy phenotype, leading to much bigger hearts. In this study they observed in the transgenic animals an increased expression of natriuretic peptide precursor type B (*NPPB*), *MYH7* and alpha 1 skeletal muscle actin (*ACTA1*) and a reduction in early stress responders, early growth response 1 (*EGR1*), early growth response 2 (*EGR2*) and FBJ osteosarcoma oncogene (*FOS*). Interestingly for the downregulated genes, *EGR1*, *EGR2* and *FOS*, luciferase assays did not confirm

a direct target interaction. In addition, the *in vivo* results did not show reduced levels of serum response factor (*SRF*), their upstream activator, pointing towards an as of yet unknown signalling cascade or mechanism. Further target interaction analysis identified *SOX6* as a suitable target. However, target interaction could only be shown in cell based luciferase assays but not *in vivo* in the mouse (Shieh et al., 2011).

In another study, cell culture experiments with human cardiac myocyte progenitor cells (hCMPC) were performed that showed upon differentiation increased levels of microRNAs such as miR-1, miR-133a, miR-133b and interestingly also miR-499. They were able to show that addition of either miR-1 or miR-499 reduces cell proliferation which is necessary for differentiation and that beating cell clusters can be achieved in a much shorter timeframe than without microRNA supplementation. Strikingly, upon miR-499 transfection cardiomyocyte specific genes increased in expression, including cardiac Troponin T (*TNNT2*), Actin, Alpha, Cardiac Muscle 1 (*ACTC1*) and Myosin regulatory light chain 2 (*MLC-2V*) (Sluijter et al., 2010). Further experiments also identified SOX6 as a direct target of miR-499 regulation by luciferase reporter assays similar to the study above (Shieh et al., 2011). However, in contrast to their results, miR-499 transfection into hCMPCs was accompanied by reduced SOX6 protein levels and promoted myocyte differentiation, suggesting species specific differences (Sluijter et al., 2010).

Yet another study at that time (Wang et al., 2011) investigated miR-499s role in apoptosis regulation. A strong link was established that showed P53 as a repressor of miR-499 which in turn attenuates Calcineurins, *CNAα* and *CNA*β. Both Calcineurins are responsible for dynamin-related protein-1 (DRP1) dephosphorylation, which allows its translocation into mitochondria. Within mitochondria DRP1 is able to trigger mitochondrial fission (“self-destruction”) which causes cell death. Particularly this mechanism has been shown to play an important role in cardiac infarction. Further to apoptosis regulation, the authors were able to show that miR-499 mediated Calcineurin repression prevents hypertrophy.

In summary microRNA-499 has been linked to different processes in the heart but no information about a potential involvement in cushion morphogenesis has yet been published.

2.3 Formation and Development of the heart

Of the many organs which are required for a fully functional organism, the heart is the one which forms first. When having a closer look at anatomy this easily makes sense, because every organ is dependent on uninterrupted function of the heart. Any variant of failure or defect of the organ results in one of many heart related diseases like arrhythmias, myopathies, myocardial infarction, cardiac hypertrophy, vascular stenosis and fibrosis or finally heart failure and subsequent death. Unfortunately, congenital heart diseases are the most abundant birth defect among humans and heart disease is also still a leading cause of death (Liu and Olson, 2010, van Rooij and Olson, 2012). The fight against those diseases and abnormalities is still ongoing and research is extensive in this field. In fact, it is more often the case that answering one question leads to multiple new ones. Therefore, it is important to continue research to decrease the critical impact of heart related conditions in the future. This translates to the aim of this PhD project, to improve our understanding of the components of correct heart development.

2.3.1 The endocardial cushions and their path to become valves

The first appearance of heart related cell types occurs as early as stage HH3 (12-13 hours) in chicken embryos, where only a primitive streak has formed. Cardiac precursor cells of the mid-primitive streak ingress and migrate laterally and cranially to form bilateral heart fields (HF) by stage HH4 (16 hours) (Person et al., 2005). This process is coordinated by signals including WNT3A, BMP2, and Fibroblast growth factor (FGF)8 which are expressed in the primitive streak and ensure proper migration. After formation of the HFs in the lateral plate mesoderm, precursor cells will differentiate and form somatic and splanchnic layers of which the latter comprises of cardiogenic cells. By stage HH5 (19 hours) a combination of other signals, BMP2, FGF4/8, and inhibitors of canonical WNT signalling become important to specify cardiac fate and direct heart development towards a straight heart tube, which is achieved by HH9 (29 hours) (Wittig and Münsterberg, 2016). Soon after, contraction of the heart becomes apparent (HH10, 33hours) and the heart tube begins to loop (HH12, 2 days) and starts its remodelling process to achieve the four-chambered form it has at birth. Just after initiation of looping first signs of cardiac jelly (CJ) deposition at the OFT and AVC can be observed, marking the beginning of endocardial cushion formation (Martinsen, 2005, Person et al., 2005). The jelly is composed of various extracellular matrix (ECM) components such as hyaluronan (HA), versican (VCAN), collagens and others, which are synthesized by cells of the myocardium in response to BMP2 and WNT6 signals (Person et al., 2005). Further, epithelial to mesenchymal transition (EMT) is induced triggering endocardial cells to migrate into the CJ and differentiate into mesenchymal cells where they proliferate and further contribute to ECM synthesis to expand the cushions. In chick embryos EMT takes place between stages HH14 and HH19 (Mercado-Pimentel and Runyan, 2007). Overall, these ECM components are critical for cushion development as knockout of Hyaluronan Synthetase 2 (*HAS2*), one of the synthesizing enzymes led to hearts without endocardial cushions in mice (Camenisch et al., 2000).

2.3.1.1 AVC cushions

At around stage HH16 (2.1 days) AVC cushions emerge as small ridges (Figure 6) and soon get populated by mesenchymal cells originating from the endocardium which have undergone myocardium induced EMT (Harris and Black, 2010). EMT causes the endothelial cells to loosen cell-cell adhesions and become migratory to invade the ECM. These now formed early form of AVC cushions will contribute over the course of extensive remodelling to the septum intermedium (SIM), mitral valve and tricuspid valve. Until roughly HH21-23 (3.5-4.0 days), the AVC cushions expand until they touch each other but don't fuse yet. This point of development also marks the time when pre-valve leaflet formation at the AVC mesenchyme begins. Later, at around HH26 (4.5 days) the fusion of the AVC cushions begins which will form the SIM. Starting at HH 28 (5.5d days) AV valve formation starts and takes roughly until HH36 (10 days). AV valve formation involves restructuring of the cushions into valve leaflets and differentiation of cells to connective tissue fibroblasts (Martinsen, 2005). During this period at approximately HH30 (6.5 days), the cushion fusion resulting in the SIM is complete, and the atrio-ventricular junction is divided into right and left openings (Figure 6). Simultaneously during fusion, looping continues resulting in the initial form of a four-chambered heart. Further morphogenesis of the septum intermedium accompanies the formation of the aortic leaflet of the mitral valve and the posterior inferior and septal leaflets of the tricuspid

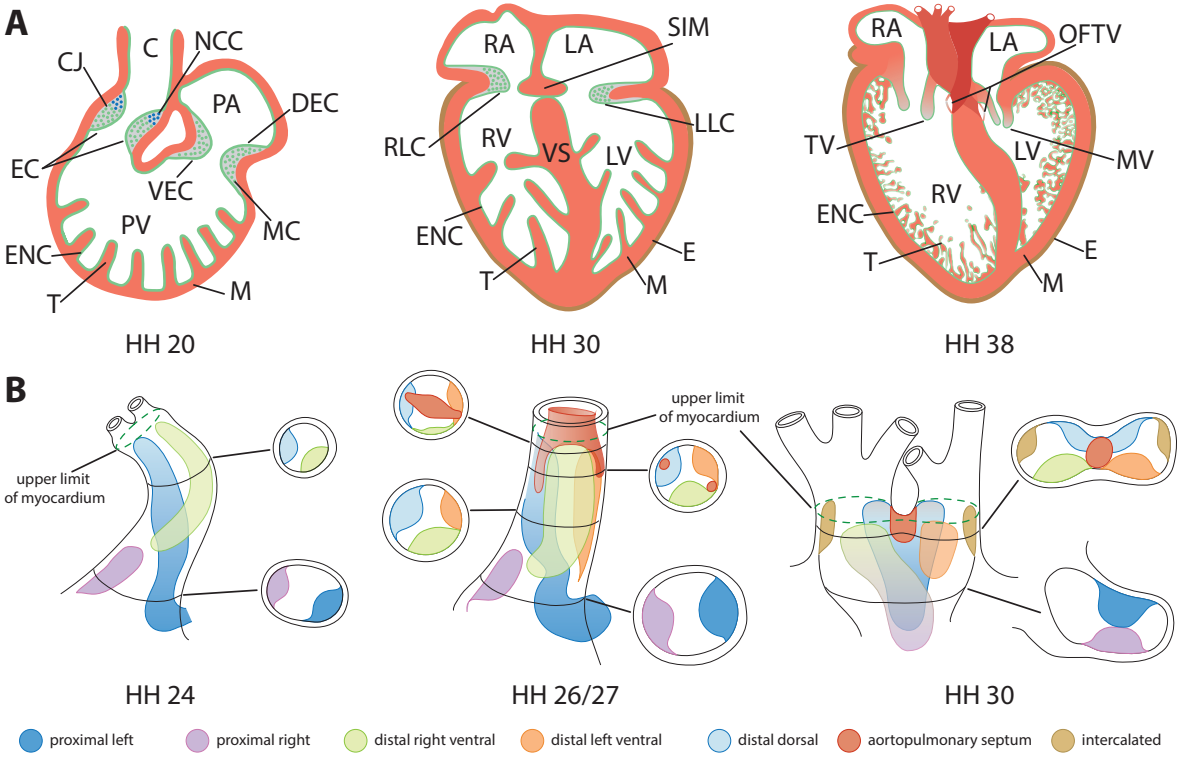

Figure 6: From Cushion to Valves - important stages

(A) The schematic shows illustrations of whole hearts of three different stages which depict important steps of cardiac cushion maturation to valves and septa in the chicken embryo. (HH20) Endocardial cushions have formed in the OFT and at the AVC junction. Mesenchymal cells have populated the cushions, originating from EMT induced by the Endocardium. (HH30) The dorsal endocardial cushion and ventral endocardial cushion have fused and formed the septum intermedium which itself joined with the interatrial septum. More cushions have developed, namely the left lateral cushion and right lateral cushion, which will contribute to the formation of tricuspid valve and mitral valve later in development. Growth of the ventricular septum towards the septum intermedium has not finished by this stage. (HH38) All valves have finished development and the ventricular septum has separated the ventricles from each other. (B) Detailed schematics of OFT cushion development in chicken (Illustration remade from Qayyum et al. (2001)). (HH24) Initially there are two pairs of cushions whereby one of them is a continuous structure along the OFT. (HH26/27) A third distal cushions arises (distal left ventral) and the aortopulmonary septum grows inwards the OFT from distal to proximal. (HH30) The proximal cushions start fusing which will lead to another septum which is only temporary. Meanwhile the aortopulmonary septum separates aortic and pulmonary channels in the dorsal OFT and intercalated cushions arise. The three cushions in each dorsal outflow channel will later form an aortic valve. Conus (C), Cardiac jelly (CJ), Dorsal endocardial cushion (DEC), Endocardial cushions (EC), Endocardium (ENC), Epicardium (E), Left atrium (LA), Left lateral cushion (LLC), Left ventricle (LV), Myocardium (M), Mitral valve (MV), Outflow tract valves (OFTV), Primitive atrium (PA), Primitive Ventricle (PV), Right atrium (RA), Right lateral cushion (RLC), Right ventricle (RV), Septum intermedium (SIM), Trabeculae (T), Tricuspid Valve (TV), Ventral endocardial cushion (VEC), Ventricular Septum (VS)

valve. All in all, it takes up to stage HH36 (10 days) to complete formation of valves and septa (Martinsen, 2005, Person et al., 2005).

2.3.1.2 OFT cushions

Formation of OFT cushions initiates slightly later compared to the AVC cushions. The first protrusions in the OFT ECM can be observed at around HH18 (2.5 days) where they become populated by mesenchymal cells (Figure 6) (Person et al., 2005). Later, at around HH21 (3.5 days), pairs of distinctive cushions located proximally (left and right) and distally (dorsal and right ventral)

within OFT can be observed. In fact, those cushions are not completely separate units, the left proximal cushion stretches from the ventricular opening to the top of the OFT, where it is connected to the arterial segment and becomes the distal dorsal cushion (Figure 6)(Qayyum et al., 2001). It takes until HH25-26 (4.0-4.5 days) when the third distal OFT cushion left to the distal right ventral cushion forms, making it five OFT cushions in total (Martinsen, 2005). Over the course of the next days the aortopulmonary septum grows dorsal to ventral into the outflow tract splitting the distal dorsal cushion into two pieces and separating the OFT between the other two distal cushions. This leads to separate aortic and pulmonary channels at the dorsal OFT by HH30 (6.5 days). At the same time intercalated aortic und pulmonary cushions arise at the lateral sides of the dorsal OFT leaving each channel with a new set of three cushions. Concomitantly the proximal OFT cushions start fusing to generate a septum between the subpulmonary and subaortic outlets. The fusion process thereby occurs from ventral to dorsal. Shortly after, at around HH31 (7 days), remodelling of the distal OFT cushions into aortic and pulmonary valves is complete. In contrast to their origin on an identical plane, these valves are now positioned at different planes on the proximal-distal axis (Qayyum et al., 2001). Throughout the next few stages the initial septa in the OFT get replaced by extracardiac tissue which forms the definitive OFT septa of the heart. During this process the proximal cushions become myocardialised and contribute to the posterior wall of the free-standing subpulmonary infundibulum. OFT septation completes by HH 34 (8.0 days). In summary, the described cushions in the OFT contribute to its early septation into aortic and pulmonary channels and to the semilunar valves, which prevent blood flow back into the heart (Martinsen, 2005). Importantly, OFT cushion maturation depends not only on EMT derived mesenchyme but also neural crest cells (NCC), which migrate into the distal OFT (Kirby and Waldo, 1995) as early as stage HH18 (2.5 days) and aid in the formation of the interatrial septum (IAS) (Person et al., 2005) (Figure 6).

2.3.1.3 Signalling networks and origin of endocardial cushions

Initiation of cushion formation is dependent on a delicate signalling cascade across different tissue layers. The AVC and OFT cushions are comprised of three different layers which are, from the outside to the inside: the myocardium, the CJ and the endocardium (Figure 7). In the endocardium NOTCH is activated by Delta-like protein 4 (DLL4) and Jagged1 (JAG1) respectively. The former leads to HEY1 activation and the latter to *WNT4* expression. HEY1 functions as an inhibitor for BMP2 signalling in the endocardium whereas WNT4 activates *BMP2* expression in the myocardium (Henderson et al., 2018, MacGrogan et al., 2018b). Myocardial BMP2 activates TBX2/3 expression, which inhibits chamber specification and thus promotes cushion fate. Additionally, TGFβ2 is activated in the Myocardium, which promotes EMT. In the case of the AVC cushions T-Box 20 (TBX20) is expressed anterior and posterior to inhibit TBX2 activity, which needs to be restricted in its spatial expression to maintain chamber specification in the atria and ventricle. Furthermore, DLL4 activated endocardial NOTCH and myocardial BMP2 induces SNAIL1/2 expression, which is necessary for EMT induction within the cushion (MacGrogan et al., 2018a). Expression of these genes promotes acquisition of a mesenchymal cell type and migration into the CJ. Cell invasion into the ECM requires subtle degradation of the ECM, which is facilitated by filopodia acquired through EMT. Overall the process requires the cells to loosen their rigid structure and become more motile. Cell junction proteins such as CDH5 are downregulated, the basement membrane dissipates, cell adhesion is inhibited, apical-

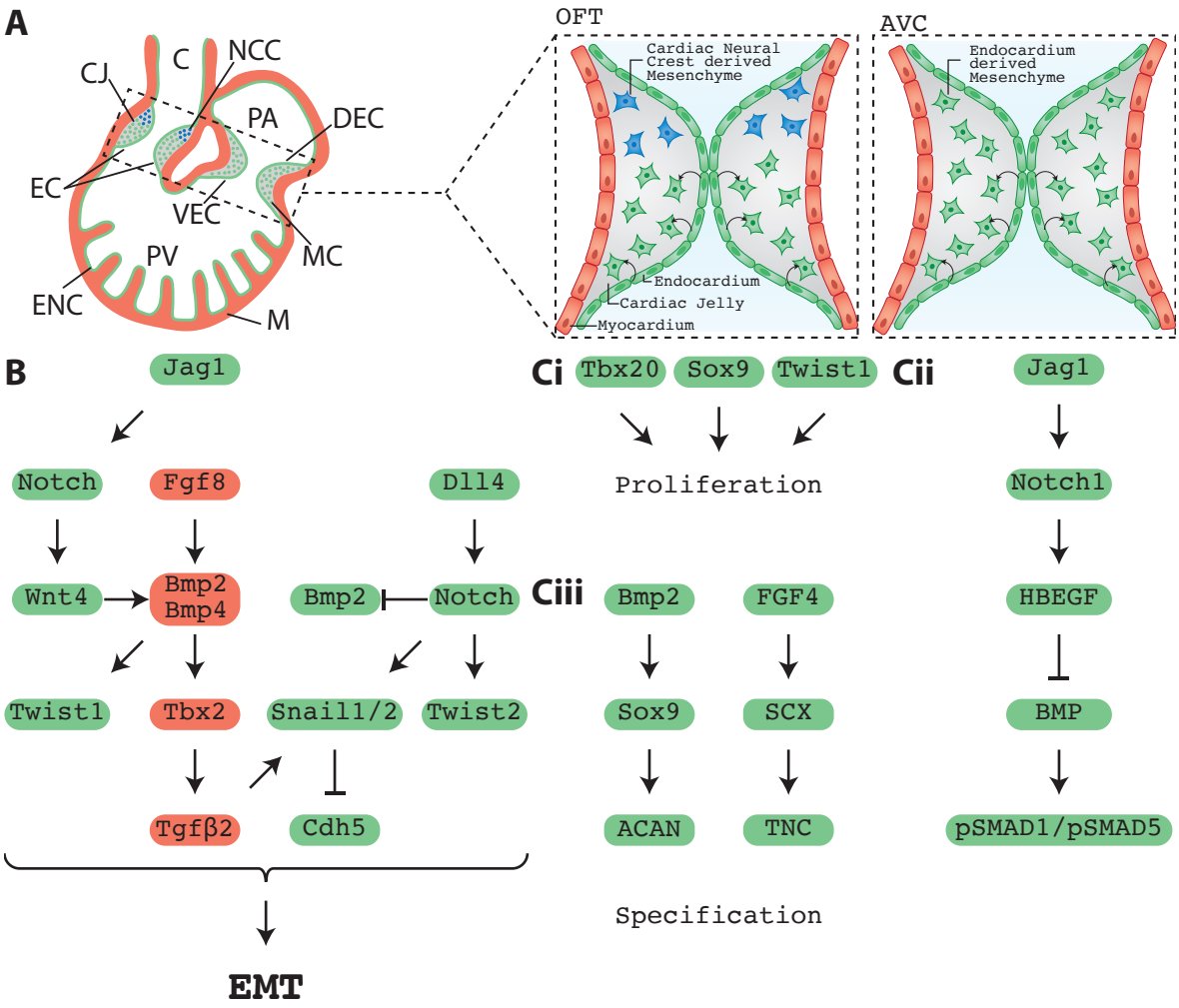

Figure 7: Cardiac Signalling to form endocardial cushions

(A) Coronal heart section representing chicken stage HH20. Dashed box shows close-up of endocardial cushions, their difference between OFT and AVC. The cushion ECM (grey) is surrounded by endocardium (green) and myocardium (red). Initiation of EMT loosens cell-cell junctions of endothelial cells and promotes their migration into the cardiac jelly where they transition to mesenchymal cells. In the OFT, a second cell population, neural crest cells contribute to the cellularisation of the endocardial cushions. (B) Signalling cascade for the induction of EMT. JAG1 activated endothelial NOTCH induces BMP2/4 in the Myocardium which activates TWIST1. Further BMP2/4 signal via TBX2 and TGFB2 to activate SNAIL1/2, which is also promoted by DLL4 activated endocardial NOTCH. SNAIL1/2 is responsible for inhibition of CDH5 a major cell-cell junction protein and others, which loosens the cells and allows migration. Moreover, DLL4 activated endothelial NOTCH inhibits BMP2 expression in the endocardium and activates TWIST2. Together TWIST1/2 and SNAIL1/2 promote the EMT process. (C) Post EMT several processes take please. Some of those signalling events are (Ci) promotion of proliferation by increased expression of TBX20, SOX9 and TWIST1, (Cii) fine tuning of proliferation to avoid hyperplastic cushions. Activated HBEGF inhibits BMP signalling which would promoter proliferation via pSMAD1/pSMAD5 and (Ciii) Specification towards valves. BMP2 activated SOX9 promotes synthesis of the ECM component ACAN and FGF4 activated scleraxis (SCX) initiates Tenascin C (TNC) which marks a transition toward a more tendon like structure.

basal cell polarity gets disrupted and a front-rear polarity is acquired. Proliferation of the early cushion mesenchyme and its expansion is supported by endocardium derived signals such as Twist-related protein (TWIST)1/2, SRY-Box 9 (SOX9) and TBX20 (Figure 7Ci). In addition, they promote expression of pro migratory factors during mesenchymal invasion (MacGrogan et al., 2018b). Importantly, proliferation needs strict regulation to avoid excessive cushion growth (Figure 7Cii). Experiments in mouse have shown that JAG1 dependent NOTCH homolog 1, translocation-associated (NOTCH1)

signalling promotes Heparin Binding EGF Like Growth Factor (HBEGF) that inhibits BMP-pSMAD1/5 signalling. Inactivation of JAG1 in *JAG1flox/flox; NKX2.5–Cre* mice led to hyperproliferation in OFT cushions and subsequent valve malformations (MacGrogan et al., 2018a). Later in development during remodelling of the cushions into valves mesenchymal cells will gradually differentiate into valvular interstitial cells (VIC) which again is promoted by the endothelium by signals as calcineurin and Nuclear factor of activated T-cells, cytoplasmic 1 (NFTATC1). The transcriptional profile of VICs is very similar to tendon and cartilage lineages as they are responsible for regulating the ECM household in the adult leaflets (Henderson et al., 2018, MacGrogan et al., 2018b).

As just described, the majority of mesenchymal cells in the endocardial cushions originate from EMT derived endothelial cells. In addition to those contributions are made by NCC and epicardial cells. NCC are long known to contribute significantly to the OFT cushions but a small proportion of NCC derived cells is also still detectable in adult AV valves (MacGrogan et al., 2018b). They are of ectodermal origin and migrate from the neural tube via the pharyngeal arches into the OFT of the heart where they populate the still acellular distal OFT cushions. However, migration of NCC doesn't stop here as they can be identified at later developmental stages in the proximal OFT cushions. (Henderson et al., 2018). Epicardial cells are contributing to both mitral and tricuspid valves. They have been localised in the parietal leaflets of both valves, which develop from the lateral cushions (MacGrogan et al., 2018b). Despite the invading mesenchyme, the majority of cushion tissue is made up of CJ, which is composed of ECM proteins. The most important ones are HA, a non-sulphated proteoglycan and versican a sulphated proteoglycan, whose expression is also BMP2 dependent (Henderson et al., 2018). Further, interaction of those two proteins is facilitated by hyaluronan and proteoglycan link protein 1 (CRTL1/HAPLN1) and mutations in any of the three leads to cardiac malformations and disease phenotypes, as for example null embryos of HAS2 (hyaluronan Synthase 2; HA synthesising enzyme) led to the complete absence of endocardial cushions in the OFT and AVC. All together sulphate-proteoglycans form a scaffold for other ECM molecules and for cell surface receptors and in general provide tissue structure. Besides those functions they can interact with growth factors promoting cell migration. HA for example together with ERBB2/B3 stimulates mesenchyme formation (Henderson et al., 2018, MacGrogan et al., 2018b). CJ composition needs fine balancing as excessive ECM deposition will introduce malformations (Gao et al., 2010). A major player for ECM synthesis is HAS2 whereas degradation is facilitated for example by a disintegrin and metalloproteinase with thrombospondin motifs (ADAMTS) proteases.

2.3.2 Additional developmental processes initiating around stage HH17 in chick

Besides the above described processes relating to cushion development a few other processes initiate around stage HH17 (2.5 days) in the chicken heart.

2.3.2.1 Atrial Septation

Early on in heart development the four chambers are not separated from each other and the necessary septa for their division arise during remodelling of the heart. The IAS arises approximately at HH16 (2.1-2.5 days) in the chicken heart, where it originates as septum primum from the cephalo-dorsal wall. In contrast to higher vertebrates, which have a septum secundum, there is only the septum primum in avian species. However, a common characteristic among avian and mammalian

development is that the IAS does not completely close until after birth to allow for interatrial blood flow. This is necessary for optimal oxygen supply, which is later ensured by the pulmonary system. In the chick embryo the fusion of the IAS with the ventral and dorsal cushion of the AVC occurs by HH24 (4 days). During this fusion a secondary foramen like structure for interatrial blood flow arises in form of multiple perforations in the middle of the IAS. This structure stays open until two days after hatching when it closes (Martinsen, 2005).

2.3.2.2 Ventricular trabeculation and septation

Trabeculae are temporary structures that form at around HH16-17 (2.1-2.5 days) in the chicken embryo where the initiated at the level of the greater curvature of the looped primitive ventricle. During the course of development they undergo a process called compaction which reduces their surfaces area and ultimately contribute their mass to the myocardial wall (Martinsen, 2005). Their function during development spans nutrient and oxygen exchange prior to coronary vascularization, routing of blood flow, increasing the myocardial mass and facilitation of intraventricular conduction (MacGrogan et al., 2018a, Martinsen, 2005). Trabeculae are a part of the myocardium which can be separated into 2 distinctive layers: a highly proliferative one the compact myocardium which is closer to the outside where the epicardium is located and a mitotically inactive layer at the inside closer to the endocardium. By stage HH17/18 (2.5 days) the trabecular meshwork expands dorso-ventrally in the un-septated ventricle and achieve by stage HH19/20 (3 days) a uniform distribution proximally until the AVC. At the same time a primitive structure of the ventricular septum (VS) can be observed. At around stage HH21/23 (3.5-4 days) distinctive trabecular bundles can be observed at the ventricular groove where the VS originates from. The VS will grow towards the atrioventricular cushions and start fusing with them by roughly stage HH28/29 (5.5-6 days) leaving a protrusion for ventricular blood flow prior birth. Prior to VS fusion at HH27 (5 days) trabeculations become transformed to fenestrated trabecular sheets, which now show differences between the left ventricle and right ventricle – the trabeculae in the left ventricle are thicker and more sheet-like. Furthermore, proliferation of the compact myocardium leads to an increase in its thickness and thus forming a multi-layered organisation. During the following days (HH29-HH34; 6-8 days), the cell density in the ventricular myocardial compact zone increases by 80%. The VS passage for blood flow remodels further during development and becomes a diagonal passageway situated right below the forming aortic semilunar valve at HH31 (7.0 days). Ventricular septation is complete by HH34 (8 days), which also triggers a change in orientation of the now unique trabecular meshwork pattern resulting in an apico-basal orientation rather than the previous radial one. Moreover, compaction ingresses the basal portions of the trabeculae into the ventricular wall. By stage HH46 (20-21 days), the rate of myocyte proliferation diminishes prior to hatching before it once more increases (Martinsen, 2005), however not much is known about postnatal proliferative capacities of chick hearts. In contrast, studies with neonatal mice have shown that their cardiomyocytes still possess proliferative capabilities post birth. Cardiac injury, like amputation of a portion of the ventricular apex within one day of birth could be completely repaired. Yet, this regeneration potential dramatically decreases within the first two weeks after birth before it is silenced (Porrello and Olson, 2014). Interestingly another study was able to show that cardiac proliferation does not disappear completely in human adults too by measuring 14C content in heart cells (Bergmann et al., 2009). This emphasises that

further research is essential to better understand heart development and particularly regeneration to tackle the needs of medicine in the future.

2.3.2.3 Formation of the epicardial cell layer

The Epicardium represents the outermost layer of the heart and is formed late in heart development compared to myocardium and endocardium. Between stage HH14-HH17 (2.1-2.5 days) the proepicardial organ (PEO) forms at the back of the heart at the location of the sinus venosus. From the PEO cells migrate outwards to form the epicardium. At around HH17-18 (2.5days), villous protrusions of the PEO reach as far as the AVC and migrate further by HH20 (3.0 days) when they surpass the inner curvature of the heart. By stage HH21-23 (3.5-4.0 days), first cells start penetrating the dorsal myocardium of the ventricles. From these stages onwards up to HH31 (7.0 days), the epicardium contributes to various cell populations of the heart, however, its formation is already completed by HH27 (5.0 days). The complete epicardium does not solely originate from the PEO, a population covering a distal portion of the OFT originates somewhere else (Martinsen, 2005).

2.4 Chicken as model for developmental research

The below section has been published in a review (Wittig and Münsterberg, 2016) but was expanded for more detail for this PhD thesis.

The chicken is a “classic” model organism and the first meaningful information obtained through its use arose in the 17th century, when it was shown that embryos are not preformed but develop body parts progressively. Further fundamental discoveries were dependent on the development of optical microscopes, which made it possible to discover the three germ layers: ectoderm, mesoderm, and endoderm. A comment on Charles Bonnet’s ideas on “fecundation” and development of the germ (egg) was published in the late 19th century (Bonnet, 1894). Since then developmental biology research has changed dramatically owing to advances in genetics and in cell and molecular biology, which enabled much progress and a “golden age” for the discipline (St Johnston, 2015). Analyses have become more sophisticated, focusing on discrete regions in the developing animal.

The chick embryo is well suited for studying the early development of the heart, the first functioning organ in the embryo. A major advantage is that the chick develops *ex utero* in an egg, which allows easy accessibility during all stages of development post-laying. This ease of access enables *in ovo* manipulations and observation of the embryo, such as dissection, grafting, micro-injection, and labelling, and this has made the chicken popular, even before the molecular age (Kain et al., 2014, Stern, 2004, Stern, 2005). For example, the process of OFT septation has been observed and described in detail in the chicken heart and consequently revealed differences to mammalian development and a better understanding of the role of the various OFT cushions (Qayyum et al., 2001). Particularly powerful have been grafting and ablation experiments. When combined with the use of quail/chick chimeras (Le Douarin, 1973), this approach allowed the tracing of grafted cells before genetic labelling became possible. With the help of this technique Kirby (1989) showed that NCC fate is determined by stage 8-10 in quail and chick. NCC were transplanted from different regions with mesencephalic, cardiac and truncal fate into the cardiac NCC region of chick embryos. The non-cardiac NCC led to severe OFT defects showing a set fate of these cells at that stage.

Establishing methods for *ex ovo* development and introduction of constructs encoding fluorescently labelled proteins by electroporation has facilitated the imaging of cell movement in live embryos using advanced microscopy (Rozbicki et al., 2015, Yang et al., 2002). More recently these tools have been used to trace migration of cardiac progenitor cells in the chick embryo to gain new insights into cell migration trajectories (Song et al., 2011). Further, advanced tools for image registration allow for the alignment and comparison of multiple specimens in the absence of morphological landmarks (Grocott et al., 2016). By directly labelling the extracellular matrix, it has also been possible to measure active versus passive motion of cells, including cardiac progenitors, during gastrulation (Zamir et al., 2006, Zamir et al., 2008). The use of CRISPR/CAS9-mediated genome editing via targeted electroporation allows the generation of genetic mosaics; combined with imaging the behaviour of mutant cells can then be studied in detail, for example in developing somites (Veron et al., 2015). Furthermore, improved methods for transgenesis and the availability of lines, both quail and chick, transgenic for fluorescent markers expressed either ubiquitously or restricted to specific cell lineages, has enhanced the utility of avian models (Balic et al., 2014, Cui et al., 2013, Macdonald et al., 2012).

Finally, the mature chick heart comprises four chambers with in- and out-flow tracts, and despite some differences, for example during septation and aortic arch remodelling (Plein et al., 2015), it resembles the human anatomy more closely than other non-mammalian model organisms. Owing to those features, and the available tool-kit described above, avian embryos will almost certainly continue to contribute significant insights into the development of the heart.

2.5 Procedures for embryo manipulation to study the heart

The below section has been published in (Wittig et al., 2018), but was expanded for more detail for this PhD thesis.

The study of heart development contributed important insights into the normal process of organ patterning and growth control but also revealed factors involved in pathological development leading to a better understanding of congenital heart disease. MicroRNAs are small non-coding RNA molecules of approximately 23 base pairs in size that regulate gene expression (Bartel, 2009). It has been demonstrated previously that they play a significant role in both cardiac development and disease (Chen and Wang, 2012, Liu and Olson, 2010), however the details of how individual microRNAs regulate gene networks remain to be elucidated. Thus, further work is needed to acquire new insights and to potentially translate this knowledge into new avenues for medical care. Cardiac microRNA networks have been studied in a number of model organisms each of them with different advantages for analysis. Two models closely resembling human heart anatomy, with a four-chambered heart comprising two atria and two ventricles, are the mouse (Mus musculus) and the chicken (Gallus gallus). The fact that mice develop *in utero* whereas chicken embryos develop *in ovo* has a strong impact on accessibility and therefore applicable methods. Commonly used approaches for altering gene expression in mice include Cre-mediated tissue specific (conditional) recombination of a selected target gene, CRISPR-mediated genome editing, or transgenic overexpression of genes of interest, allowing for permanent and/or inducible genetic alterations (Bouabe and Okkenhaug, 2013, Singh et al., 2015). Furthermore, lineage tracing experiments that reveal cell relationships have been used extensively in mice by applying genetic labelling methods (Kalhor et al., 2018, Kraus

et al., 2014). A more recent report has shown a procedure for heart manipulation of mice embryos that requires surgery of the parent animals (Fu et al., 2018), which points out that accessibility is a major challenge in mouse experiments.

In chicken, tissue grafting, electroporation and microinjections are the most commonly used techniques. The embryo is highly accessible *in ovo* and allows stage-specific manipulations with subsequent read out (Bellairs and Osmond, 2014, Stern, 2005). Recently for example a method was published that enables *in ovo* electroporation in the auditory organ (Evsen and Doetzlhofer, 2016), which might be transferable to the heart. Another tool used in chicken research are *ex ovo* cultures where embryos are transferred into specially prepared beakers which allow *ex ovo* growth and therefore better accessibility for experiments (Yalcin et al., 2010). But not only *ex ovo* techniques to gain better access exist, Spurlin and Lwigale (2013) showed a procedure that improved *in ovo* access for older embryos which allowed injection of transfected cells into said embryos at different locations, which most likely also allows targeting of the heart. Finally, even though a different subset of techniques is used in chicken embryos, lineage tracing has also been employed to study cell fate (Kretzschmar and Watt, 2012), for example the contributions of cardiac neural crest to outflow tract septation and of the second heart field to the right ventricle were first identified in the chicken (Wittig and Münsterberg, 2016).

Genetic approaches in mice have significantly increased our understanding of heart development, however, these are time-consuming, and their spatio-temporal control is limited by the ability to control the activity of the Cre-recombinase, thus making the study of specific events during heart development more challenging. The precise local administration of pharmacological agents to the mouse heart is difficult due to *in utero* development and therefore lack of access to the embryonic heart. Injections into the vasculature lead to systemic delivery and thus an impact on tissues other than the heart cannot be excluded (Goehringer et al., 2009, Krutzfeldt et al., 2005). In chicken, the effective delivery of viral based expression constructs needs high concentrations (Lambeth et al., 2014), leading to potential DNA toxicity effects. A general complication is that due to heart contractions, injected compounds are quickly washed out into circulation (Davidson et al., 2001). Virus based transduction is slightly less affected by this since the virus binds to cell surface receptors. Effective binding can be improved by slowing the heart temporarily through embryo cooling. However, nucleic acid-based constructs or synthetic compounds can quickly disperse, and their successful delivery and uptake requires steady local administration and/or temporary heart arrest, which could have non-specific effects on development.

In this study the chicken embryo has been used as model organism, its developmental stages are well-defined (Hamburger and Hamilton, 1951) and the heart is readily accessible, particularly the early and intermediate stages, which closely resemble human anatomy (Wittig and Münsterberg, 2016). Embryos are cheap to obtain and are incubated to the desired stage in controlled conditions. This facilitates *in ovo* manipulations with precise temporal and site-specific targeting and permits the study of different phases of intermediate heart development, including S-shape (heart) looping, chamber remodelling, trabeculation and septa formation. Following manipulation and further embryo development subsequent visual assessment and gene expression analysis is possible and does not require sacrificing the parent animal. Therefore, the use of chicken embryos complements

the analysis of genetically modified embryos of other model species (Bellairs and Osmond, 2014).

The injection technique into the chicken heart developed as part of this study can be applied to different subsections of the heart and thus overcomes some of the above-mentioned drawbacks. Furthermore, the targeted injections could be performed with plasmid constructs – combined with Lipofectamin (England et al., 2017), or with virus particles, synthetic compounds, antisense morpholinos or microRNA mimics and inhibitors. Delivery of microRNA inhibitors, AntagomiRs, is the primary focus of this report as it represents a new tool for studying the functions of individual or multiple microRNAs during intermediate heart development, during which the heart tube is remodelled into a mature chambered heart. Once mastered, this method can be used for heart-specific knockdown and gain-of-function studies and allows medium-throughput screening of multiple genes of interest.

3 Material and Methods

3.1 3D-Reconstruction

3.1.1 Image acquisition

Bright field photographs of heart sections of HH27 embryos were taken using a Zeiss Axioplan 2ie microscope at 5x magnification to ensure single image acquisition per slice. Histological stains as H/E of the sections improved contrast for acquisition enormously. Files were numbered in their natural order from the front of the heart to the back and saved as ZVI to maintain image calibration and ease downstream processing.

3.1.2 Image alignment

The Bio-Formats Importer was used to load images as a Hyperstack into Fiji. Thereby the option “Group Files with similar names” to ensure the whole image series is loaded was selected. Following “Stack to RGB” was performed on the image series and brightness and contrast were auto adjusted based on an image in the middle of the sequence. The stack was then saved as “colour-not-aligned”. A new TrackEM2 (blank) file was generated and the stack was imported. The next step was to unlink all images. Following unlinking, the “align layers” command was executed with standard parameters. After digital alignment manual corrections were applied by starting at the most central section. To do so the layer before or after was set as a red channel in the TrackEM2 layers panel and the transformation tool was used to move and rotate the section in place. Once one direction was finished the other one was done. Importantly when applying the transformation, it was helpful to use the option that applies the transformation for all preceding or following sections respectively. After successful alignment the

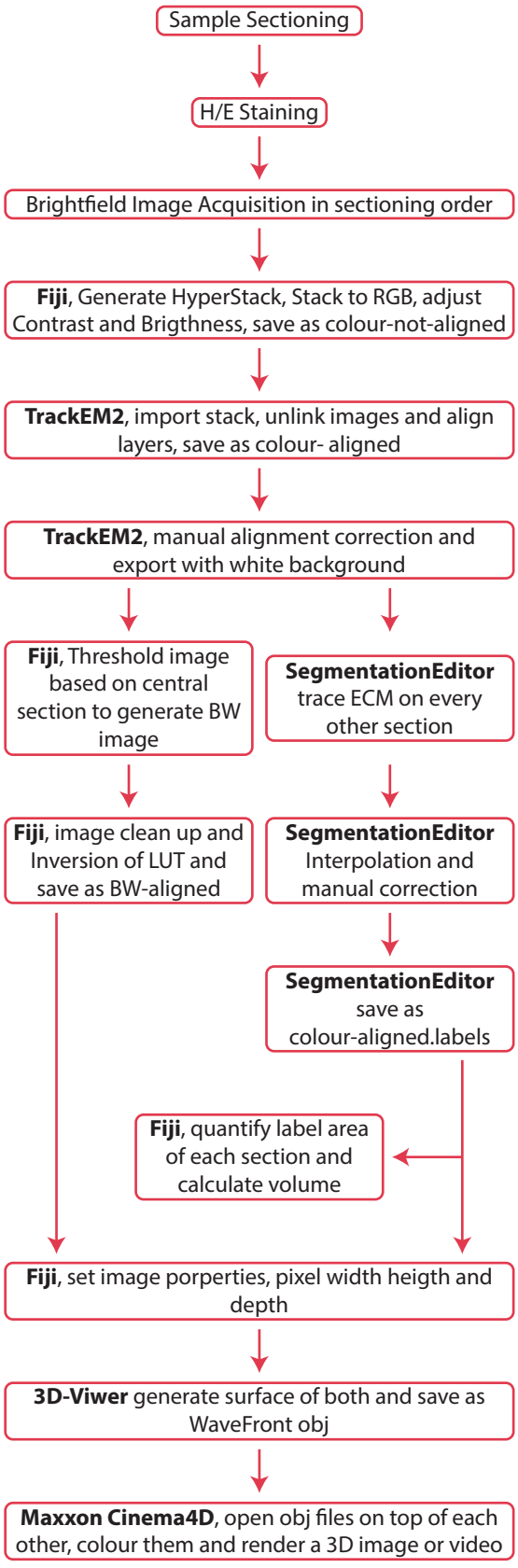

Figure 8: Flow Chart of 3D Reconstruction

Flow chart showing all steps necessary for 3D reconstruction including the calculation of ECM volume and 3D rendering of reconstructed hearts.

images were exported as a stack with white background and saved as “colour- aligned”.

3.1.3 Segmentation

The aligned colour stack was opened in Fiji and the “Segmentation Editor” was loaded. Segmentation of the cardiac ECM was performed from the back to front due to easier recognition of the ECM. The selection brush was used to label the region of interest on every other section and then interpolated (I button). Interpolated sections have than been manually corrected to ensure adequate ECM labelling. Once completed the labelled areas were exported (+ button) in an image stack with same dimensions as the “colour-aligned” one and saved as “colour-aligned.labels”.

For easier segmentation an iPad Pro 11 (2018) with an ApplePencil2 has been used in combination with AstroPad Studio to gain a mirrored screen with touch input. This allowed tracing of the ECM structure by using the pencil.

3.1.4 Volume calculation

The “colour-aligned.labels” file was opened in Fiji and the “measure stack” command was run to determine the surface area A_{total} and the mean of each image. Those two values were used to calculate the surface area of red pixels A_{red}. To do so the following relations need to be considered $mean=Pixelvalue_{black}*x+Pixelvalue_{red}*y$ where x and y represent the proportion of black and red pixels respectively. The pixel value for black was 0 and for red 1 therefore $mean=y$ applied which allowed calculation of $A_{red}=A_{total}*y$. Following $V_{total}=\sum_{n}^{1} A_{red}*d$ was determined, where n equals the number and d the thickness of sections of the analysed heart.

3.1.5 3D-Volume projection

Fiji was opened and the “colour-aligned” stack was loaded, converted to 8bit grayscale and the threshold was set to 146. The black and white image was than cleaned by overpainting dust particles from the imaging process and other irrelevant debris with white colour. Before 3D-image generation the image properties have been set according to sectioning thickness (20µm) and the LUT was inverted to gain a white heart with black background. The resulting stack was saved as “bw-aligned”. Following the “3D viewer” plugin was used to generate a surface at 0 threshold and a resampling factor of 2. The resulting 3D image was exported as WaveFront obj. The same was performed for “colour-aligned.labels” but using a resampling factor of 1. The resulting obj files were loaded together into Maxxon Cinema4D, coloured and rendered to a final image or animation.

3.2 AntagomiR design

AntagomiRs were synthesized by Dharmacon/ Horizon Discovery. They were designed to be fully complementary to the microRNA of interest and included a 5’ Fluorescein and 3’ Cholesterol addition (Table 2). Further the backbone consists of 2-O-methyl RNA and contains phosphorothioate bonds at the three most 3’ and two most 5’ bases (McGlinn et al., 2009).

3.3 Bacterial Transformation

Plasmid-DNA for transformation was added to DH5-alpha competent Escherichia coli in a tube, contents were mixed and incubated on ice for 30 min. After incubation cells were heat-shocked

Table 2: AntagomiRs used in this study

AntagomiR name	sequence
AntagomiR-SCR	5'-(FL)mC(*)mA(*)mUmCmCmAmUmCmAmCmUmCmAmCmUmCm CmAmU(*)mC(*)mA(*)mU(3'-Chl)-3'
AntagomiR-499-5p	5'-(FL)mC(*)mU(*)mAmAmAmCmAmUmCmAmCmUmAmCmAmAm GmUmCmU(*)mU(*)mA(*)mA(3'-Chl)-3'
AntagomiR-221-3p	5'(FL)-mG(*)mA(*)mAmAmCmCmCmAmGmCmAmGmAmCmAmAm UmGmUmA(*)mG(*)mC(*)mU(3'-Chl)-3'

45 seconds in a water bath at 42°C to allow plasmid uptake by the bacteria. Following heat shock 900µl of LB-media was added to the DH5-alpha bacteria and another incubation of 1h at 37°C was performed to allow plasmid expression. After incubation cells were pelleted at 8000g for 5 min. The supernatant was discarded and the pellet re-suspended in 100µl of LB media. The re-suspended cells were plated on selective LB-agar plates (Carbenicillin 100µg/ml) and incubated over night at 37°C.

Competent Escherichia coli strains were stored at -80°C.

3.4 Cryosectioning and Sample Preparation

To prepare hearts for cryosectioning a two-day procedure is necessary.

Day 1: Methanol stored Embryos were rehydrated in a series of PBT/MeOH dilutions (25%/50%/75% and 100%) for at least 15 minutes each. The hearts were then dissected and washed another 15 min in PBT. Subsequently they were transferred into 20% Sucrose/EDTA buffer (pH=7.5) for overnight incubation at 4°C.

Day 2: First the freezing medium, a sucrose/gelatine (Fisher Scientific; 10645312/Sigma-Aldrich; 48723) mixture was prepared. The media was dissolved in PBS and heated up to 65 °C. After 60 minutes of cooling to 40 °C in an oven the media was ready for use. Disposable embedding molds (18985 Polysciences, Inc.) were placed on dry ice, freezing media was added, and the heart was placed as desired, depending on the intended orientation for sectioning. After hearts were appropriately orientated the block was left until it was fully frozen. All frozen hearts were kept for at least one night at -80 °C before cryosectioning.

The embedded hearts were cut using a cryostat (LEICA CM 1959). First the frozen sample was attached to a mounting plate with OCT (Cell Path; KMA-0100-00A) and placed on a -50°C cooler plate in the cryostat. Subsequently the sample was mounted to the cryostat and aligned to the blade. At first sections were trimmed off until the heart was exposed. Then the dispensable freezing media around the heart was removed in a rectangular shape and the cryostat was switched to fine mode (20 µm sections thickness). After fine-tuning of the blade and cover-glass position, sections were cut and transferred to Superfrost- Plus slides (ThermoScientific; J1800AMNZ). The finished slides were collected and kept inside the cryostat and later frozen at -20 °C.

3.5 Embryo Development

Fertilized Dekalb White chicken eggs were ordered once a week from Henry Stewart & Co. Ltd, Fakenham, UK and kept cooled (17˚C) after arrival. To initiate development, the eggs were

transferred to a humid incubator at 37°C and incubated until the desired stage was reached according to Hamburger and Hamilton. Stage HH14-16 embryos (~66h) were used for the cardiac injection procedure (Hamburger and Hamilton, 1951).

3.6 Embryo Dissections

3.6.1 For whole mount in situ hybridization (WISH)

Embryos were dissected in DEPC-treated PBS. The extraembryonic regions were removed. Specifically, for areas around the heart this was important to improve visibility of markers for WISH. After dissection embryos were transferred into 4% PFA (SIGMA; P6148) for fixation and left at 4°C O/N. After fixation embryos were dehydrated in a series of MeOH/PBT dilutions (25%/50%/75% and 100%) for at least 15 minutes each. Once dehydrated embryos were stored at -20°C in MeOH for up to three months.

3.6.2 For RNA extraction

Embryos were dissected as before but kept in ice-cold DEPC-treated PBS until snap frozen in liquid nitrogen. Frozen samples were stored at -80°C until processed for RNA extraction (see below: RNA and microRNA extraction).

3.7 Experimental evaluation of putative microRNA targets

3.7.1 Generation of luciferase reporter constructs

Primers for a 3'UTR of interest were manually designed with overhangs complementary to the insertion (Table 3) site in pmirGLO Dual-Luciferase microRNA Target Expression Vector (Promega, E1330), which was linearized with SacI and XbaI leaving cohesive ends.

Table 3: In-Fusion Cloning primer overhangs for pmirGLO

Primer	Primer overhang sequence
Forward-SacI	CTAGTTGTTTAAACG
Reverse-XbaI	GCAGGTCGACTCTAG

Using those primers, a PCR was performed with CloneAmpTM HiFi PCR Premix (Clontech; 639298) according to Clontech's protocol, using chick cDNA from a stage where the gene of interest was expressed as template (Darnell et al., 2007). After PCR-Product purification (Qiagen; 28106), In-Fusion® HD Cloning (Clontech; 011614) was used to recombine the fragment into the linearized pmirGLO vector. The reaction setup is described in Table 4.

The reaction was thoroughly mixed and incubated at 50°C for 15 minutes and then placed on ice. Next, 2.5 µL of the reaction-mix containing the plasmid were transformed immediately using StellarTM Competent Cells (Clontech; PT5055-2). The next day a single colony was selected for plasmid preparation (usually on a mini scale). Prior to use in luciferase assays, the sequence integrity was confirmed by sequencing using pmirGLO-vector specific primers (F: GGCAAGATCGCCGTGTAATTC; R: CAATGTATCTTATCATGTCTGCTCGAAG) (Source Bioscience Sequencing, Cambridge UK).

Table 4: In-Fusion Cloning reaction setup

Reaction Component	Reaction amounts
Purified PCR fragment	5-100 ng*
Linearized vector	25-100 ng**
5X In-Fusion HD enzyme premix	1µl
dH2O	To 5µl

*<0.5 kb: 5-25 ng, 0.5-10 kb: 25-50 ng, >10 kb: 25-100 ng
**<10kb: 25-50ng, >10 kb: 25-100ng

3.7.2 PCR mediated mutation of microRNA target sites

MicroRNA-target sites were mutated using Fast-Cloning (Li et al., 2011). Therefore, self-overlapping primers in the Ampicillin-resistance gene of the pmirGLO-vector (Promega, E1330) and the site to be mutated were designed. The induced mutation was designed to introduce a new restriction site to allow easy verification. Forward mutation primer was used with reverse Ampicillin primer and reverse mutation primer was used with forward Ampicillin primer in a PCR reaction with CloneAmpTM HiFi PCR Premix (Clontech; 639298) according to Clontech's protocol with a reduced cycle number to 22 to amplify the two halves of the plasmid. To remove PCR template 5 µL of both reactions were mixed with 0.5 µL of DpnI enzyme (NEB; R0176S) and incubated for 2h at 37°C. After digest confirmation via gel-electrophoresis the PCR product mix was transformed into Escherichia coli with Carbenicillin-containing LB selection medium. Only bacteria which recombined the plasmid halves together were able to grow. Plasmid preparations of mutated constructs were sequenced to validate the sequence mutation.

3.7.3 Luciferase assay of microRNA sensing constructs

3.7.3.1 Cell culture

DF1-chicken dermal fibroblast cells were gently thawed at 37°C in a water bath and transferred to a T75 culture flask containing 10 mL of standard medium, which consists of DMEM-Glutamax (Gibco®; 21885-025) + 10% v/v FBS (Gibco®; 10500-064) and Pen/Strep (Gibco®; 15140-122). After 6 h of incubation at 37°C and 5% v/v CO_2 the culture medium was changed to remove residual DMSO from the freezing medium. Subsequently cells were left for growth until a confluency of 90-95% was reached.

To split the culture, the medium was removed, and the cells were washed in 10ml PBS (Gibco®; 10010-015). Following 1 mL Trypsin (Gibco®; 25200-072) was added and shortly incubated (~10 s). Trypsin was removed and the cells incubated for 2 min at 37°C and 5% v/v CO_2. Sufficient cell detachment was verified by microscopy and subsequently the cells were plated in fresh medium. A desired proportion was transferred into a new T75 flask and medium was filled up to 10-15 mL.

3.7.3.2 Transfection

Cells were split and counted to seed 7000 cells/well in 100 µL standard medium on a 96-well plate. After 24h incubation the medium was removed and substituted by 100 µL serum free media including the transfection mix. Following 24h incubation the mix was removed, and cells were processed for luciferase measurements.

Table 5: Luciferase assay components

Concentration/Amount	component	Vendor
50 nM	miRNA-mimic	Sigma/Qiagen
100 ng	luciferase construct DNA	Promega; E1330
0.2 µL	Lipofectamine® 2000	Thermo Fisher Scientific; 11668027

3.7.3.3 Luciferase assay

Culture medium was removed, and cells were washed twice in cold PBS (4°C). After the washes the cells were lysed with 60 µL passive Lysis Buffer (Promega; E2940) and incubated for ≥ 15 min at RT on a shaker. For luciferase measurements 10 µL cell lysate per well was transferred into a white 96-well plate. Following 50 µL LARII (Promega; E2940) were added and Firefly luciferase activity was measured with a plate Reader (Promega; GloMax Explorer). Immediately after measurement, 50 µL Stop and Glo solution (Promega; E2940) was applied and Renilla luciferase activity was measured. After measuring all wells data was exported as Excel-file and analysed in GraphPad Prism.

3.8 Fluorescence microscopy

AnatagomiR delivery was confirmed using a LEICA MZ16F microscope with a LEICA DFC 300FX camera to track the fluorescence of the Fluorescein tag. Brightfield and green channel images were taken and merged in Adobe Photoshop CC.

3.9 Gel-electrophoresis

Gels were made of 1.0% w/v agarose (Melford; MB1200) with 2.5 µL / 50 mL ethidium bromide (Sigma; E1510) diluted in 1xTAE buffer. The electrophoresis was performed in “Gel Casting Unit HU6-CU” from Fisherbrand™ using a current of between 80V and 100V. Samples contained different amounts of DNA, usually 150-400ng, diluted with nuclease free water (SIGMA; W4502) to a desired volume (5-20 µL) to which an appropriate amount 6x loading buffer (ThermoScientific; R0611) was added. The size of each product was evaluated by molecular size markers, either a 100 bp ladder or a 1000 bp ladder (New England BioLabs; N3232L and/or N0467S).

3.10 Heart Rate Assessment

To asses heart rates, a single injected egg was removed from the incubator and a circular opening was cut in the tape seal. The egg was immediately placed under the microscope and a 15-30 sec clip at 1080p/120fps was recorded using a RIBCAGE H5PRO camera. Subsequently the embryo was dissected and processed for other methods. Collected video clips were played in slow motion using Apple QuickTime and heart beats were counted manually by J.G.W. and M.R.G. Beats per minute were calculated accordingly $BPM = n_{beats} / t_{recording} * 60s$.

3.11 Hematoxylin and Eosin Staining

To stain sections, gelatine was removed by washing in PBST at 37°C for 15 min. Following they were rinsed several times in PBS before proceeding to staining. Staining was done according to standard procedures(Fischer et al., 2008). Slides were incubated for 8 min in Harris Hematoxylin solution (Thermo Scientific™, 72704) and then washed in running tap water for 5 minutes. Next,

they were dipped twice in 1% acid alcohol solution (HCL in 70% Ethanol) for differentiation (this step needs to be short and can be omitted, otherwise Hematoxylin will destain). Another wash under running tap water for 1 min followed. Then the colour was intensified using 0.1% sodium bicarbonate solution for 1 minute followed by another wash under running tap water for 5 min. Staining was briefly fixed by 10 dips in 95% ethanol.

As a second step slides were counterstained in eosin-phloxine solution (Thermo Scientific™, 71304) for 10-30 s, depending on desired staining intensity. Finally, slides were dehydrated through 95% ethanol, 2 changes of absolute alcohol for 5 min each and cleared in 2 changes of xylene for 5 minutes each before they were mounted with DPX (Thermo Fisher Scientific™, 15538321).

3.12 In situ hybridisation (ISH)

3.12.1 cDNA synthesis

To generate gene specific probes, RNA was reverse transcribed to cDNA using SuperScript®II Reverse Transcriptase (Life Technologies; 18064-014). To do so 1-2 µg RNA was mixed with 1 µL random primers (Promega; C1181) , the volume was made up to 11 µL using RNAse free water (SIGMA; W4502) and the mix was incubated 10 min at 70°C. After incubation a second mix was added consisting of:

Table 6: cDNA synthesis reaction setup

Reagent	Volume
5x Buffer (included in kit)	4 µL
100mM DTT (Promega; P1171)	2 µL
10mM dNTP (Roche; 11 969 064 001)	1 µL
RNasin® (Promega; N2611)	1 µL
Superscript Reverse Transcriptase	1 µL

The combined mix was incubated for 1 h at 42°C. After incubation the cDNA was ready as a template and frozen at -20°C until used.

3.12.2 Generation of gene specific templates for *in vitro* transcription (IVT)

A standard PCR was performed to amplify a gene of interest from cDNA (Table 8), which then was cloned into pGEM-T-Easy (Promega; A1360) after PCR-product purification (Qiagen, 28106). Gene specific primers were designed to amplify a gene fragment with little to no complementary to other genes or gene variants using NCBI Primer Blast. The gene fragment size was in between 300bp and 1500bp (Lawrence and Singer, 1985).

3.12.3 *In vitro* transcription for probe generation

To generate anti-sense RNA-probe, a standard PCR was performed using M13 forward and reverse primers. The PCR product was verified by gel-electrophoresis, purified (Qiagen, 28106) and subsequently used for an *in vitro* transcription reaction. The components listed in Table 7 were mixed.

The reaction was carried out at 37°C for 2-3 h. Subsequently 1 µl of Probe-RNA was analysed

Table 7: In-vitro transcription reaction setup

Reagent	Volume
Trans Buffer (Promega, P1181)	4 µL
100mM DTT (Promega; P1171)	2 µL
Dig Mix*	2 µL
RNasin® (Promega; N2611)	1 µL
Polymerase (T3, T7 or SP6) (Promega; P2083, P2075 or P1085)	2 µL
PCR-product	500-1000 ng
Water (SIGMA; W4502)	ad 20 µL

* 10mM dATP, dGTP, dCTP; 10mM 7:3 dUTP/Digoxigenin-11-UTP (Roche; 11 969 064 001 and 11 209 256 910)

by gel-electrophoresis and the remaining RNA was cleaned up using G50-Colums (GE-Healthcare; 27-5330-01) to remove unincorporated NTPs and small fragments, after which the probe was transferred into 10 mL Hyb-buffer.

3.12.4 Whole mount in situ hybridisation

3.12.4.1 Hybridization

Methanol treated embryos were rehydrated through a series of 75/50/25 % v/v Methanol/PBS washes. Following two short rinses in PBS, embryos were treated with 15 µg/mL Proteinase-K in PBS for 30 min. After treatment, embryos were rinsed in PBST and post-fixed in 4 % w/v PFA for 20 min at RT. Again, embryos were rinsed in PBST in preparation for hybridization. To do so, they were washed in 1/1 PBST/Hyb solution. After settling, the embryos were transferred into Hyb-solution and incubated for >2 h at 65-70°C for mRNA probes and 48°C for LNA probes. After pre-hybridization the Hyb-solution was replaced with Hyb-buffer containing the probe and incubated O/N at the same temperature as before.

Hyb-Buffer: 50% v/v Formamide, 1.3x SSC (pH 5.0), 5 mM EDTA (pH 8.0), 50 µg Yeast RNA (Sigma R6750), 0.2% v/v Tween-20, 0.5% w/v CHAPS, 100 µg/mL Heparin (Sigma, H3149) in DEPC-H2O

Hyb-Solution: 50% v/v Formamide, 1.3x SSC (pH 5.0), 0.2% v/v Tween-20 in DEPC-H2O

3.12.4.2 Immunodetection

The probe solution was removed and stored at -20°C for reuse, embryos were rinsed in Hyb-Buffer twice and then washed 4 times in Hyb-Solution for 30 min at hybridisation temperature. Following, a 10 min wash in 1/1 Hyb-Solution/MABT followed at hybridisation temperature. Subsequently 3 rinses in MABT followed and two more 30 min washes in MABT at RT. After all wash steps embryos were pre-blocked in block solution (MABT/2% w/vRoche blocking reagent, 11096176001) for 1 h at RT and then incubated in block solution + 10% v/v Goat serum for 2 h at RT. Finally, the solution was replaced with fresh block solution + 10% v/v Goat serum including the antibody in a 1:2000 dilution (anti-Dig-AP Fab fragment; Roche; 11093274910) and incubated O/N at 4°C.

MABT: 100mM Maleic acid (Sigma M0375), 150mM NaCl, 0.1% v/v Tween-20 (pH 7.5)

Table 8: Primer List for ISH Probes

Table shows all primer combinations used to clone cDNA fragments into pGEM-T-Easy for probe generation. Further their sequencing status is listed on the right.

Name	Forward Primer 5'-3'	Reverse Primer 5'-3'	sequenced
ACAN	GACCATCTGCTTTTCCTCCAGC	GAGACCTCACCACTTCCATCAACAC	yes
ACTC1	TCACAGAGCGTGGCTATTCC	TGTCGTCATCCTGAGTGGGA	yes
AMHC/MYH1C	CAGGCCCTGGATGACCTG	GGCATTGACTGCCTCCACA	yes
ETS1	CCAGAAGTTCTGCATGAACGG	CAGCGGCAGGAATGACAGG	yes
GATA 4	GTTCCAAGGCCATTAGCAATGAGAA	TTATGCCGTTATGATGTCCCCATG	yes
HAPLN1/CLP	ATGACAAGTCTACTCTTTCTGGTG	TCAGTTGTAAGCTCTGAAACAGTA	yes
HAS2	TGGAGCCCCTCTATGACCAA	ATAATTCCACGCTTCTCCCAG	yes
MEF2C	AATCAGGAACGGATGCAGGG	TCAGGGCTGTGACCTACTGA	yes
MSX1	CCGCGCCGCTTTATCAAC	GAGAAGCGGGGGCTCTG	no
NOTCH1	GACAGCTACGGGACGTACAA	TACCCGATCCGTGCACTTG	yes
NRG1	CGGATGATGTTGCTGTTTCGGAC	CAGAGGACCACAACCCGACATC	yes
PAX3	GCATCCGGCCCTGTGTCATCTC	GCTCCTGCCTGCTTCCTCCATCT	yes
PDLIM5	CAAACAAAAAACCTGCCCAGT	GCAGGGTACAGAGGTTTTTACA	yes
POSTN	CGATTTAATGCTCTCCACCAC	CCTTCCTTCTTTACTTCCTCTGAC	yes
PITX2	AGAACCGCAGAGCCAAATGGAG	TGTCCACGGGGTACTGGC	yes
SMAD6	CCTAACGACGAGCAAAAGCC	CTTTCGTCAGAGGCTGACTGTTATC	yes
SOX9	GTCACCACCTACAGCGGTAC	TATTTGCCTTCACGTGGCTTTAAG	yes
TBX3	TTCCAGCCCCGCTTCCAC	CGGCATCGCTGTCACCCT	yes
TBX18	CTTGTGCCCGCTCAGGTT	CCTAGTAAGAATGCTGTGCCGTTG	yes
TNNT2	CAAGCCCTTCATGCCCAACC	TCTTCCCACGTGCAGCCTTT	yes
VCAN	GCTGTGGTTCATGCCTACACT	GAGTATGCAGTTTCTGTCAGCTC	yes

3.12.4.3 Colour development

The antibody solution was removed, and embryos were washed in MABT 6 times for 30 min. Following the washes, the pH was adjusted for colour development by two 10 min washes in NTMT. Subsequently, the colour development solution (NBT/BCIP in NTMT, 7/9 µL per mL respectively) was applied and incubated until a satisfactory signal was developed. Embryos were then transferred to 5X TBST for background stain removal. Colour reaction were sometimes repeated starting with NTMT washes.

TBST: 20 mM Tris, 150 mM NaCl, 0.1% v/v Tween 20 (pH 7.5)

NBT: 4-Nitro blue tetrazolium chloride (Roche 11087479001), stock at 75mg/ml in 70% v/v dimethylformamide. Aliquot and store at -20°C. Protect from light.

BCIP: 5-bromo-4-chloro-3-indolyl-phosphate, 4-toluidine salt (Roche 10760994001), stock at 50mg/ml in dimethylformamide. Aliquot and store at - 20°C. Protect from light.

NTMT: 100 mM NaCl, 100 mM Tris-HCl (pH 9.5), 50 mM MgCl2, 1% v/v Tween 20 in DEPC-H2O

3.13 *In ovo* cardiac microinjections

The development of this protocol was a major part of this thesis and is included in the results section: Protocol for cardiac injections.

3.14 Immunohistochemistry

Endogenous phosphatases of dissected hearts were inactivated at 67°C in HYB buffer overnight. Following several washes according to previously described procedures (Goljanek-Whysall et al., 2011) an antibody against Fluorescein (1:2000 dilution of Anti-Fluorescein-AP, Fab fragments, Roche; 11426338910) was applied and incubated overnight (see Immunodetection above). Again, following several washes colour was developed for all samples simultaneously using BCIP/NBT (see Colour development above).

3.15 microRNA target selection

3'UTRs of genes expressed during heart development were retrieved from Ensembl (preferentially from RNA sequencing (RNAseq) data) and analysed versus micro-RNAs of interest. For analysis the customizable perl-script of Targetscan (Lewis et al., 2005) was used. If an interaction site was found it was co-confirmed by other algorithms, such as MIRANDA (Betel et al., 2008) and RNAhybrid (Rehmsmeier et al., 2004).

3.16 Northern blot

Northern blot analysis was performed as previously described (Pall and Hamilton, 2008). Briefly, 10 µg of total RNA was resolved on a 15% denaturing urea polyacrylamide gel. The RNA was transferred to a Hybond-NX nylon membrane (GE Healthcare) by semidry-blotting for 1h at 20 V and chemically crosslinked using 1-Ethyl-3-(3-dimethylaminopropyl) carbodiimide (Sigma Aldrich) at 60°C for 2h.

For Northern blot hybridization the membranes were pre-hybridized using Perfect Hyb buffer (Sigma Aldrich) and the antisense DNA oligonucleotides (Sigma-Aldrich) were end-labelled using 3000 Ci/mmol of [γ-32P]-ATP (Perkin Elmer). The hybridization of the membranes with the 5'-32P labelled DNA oligonucleotide was performed overnight at 37°C. The membranes were washed twice with 0.2x SSC and 0.1% SDS for 20 min and exposed to a phosphor imager screen for autoradiography. The membrane was imaged using the Typhoon Scanner and band intensities were quantified with the Image Quant Software (GE Healthcare).

Before re-probing of the membranes with a probe against the loading control, U6, the membranes were stripped with 0.1% SDS for 5h at 80°C.

The miR499-5p miRCURY LNA microRNA detection (Qiagen,) probe was used for the detection of microRNA 499-5p (5'-CTAAACATCACTACAAGTCTTA-3') and the membrane was re-probed with U6 snRNA as a loading control (5'-GCTAATCTTCTCTGTATCGTTCC-3').

3.17 pGEM-T-Easy cloning

A standard PCR is performed to amplify gene specific DNA (CDS or 3'UTR) for cloning into pGEM-T-Easy (Promega; A1360). After amplification, products are verified by gel-electrophoresis and purified with a PCR-Product purification kit (Qiagen; 28106). The purified PCR product is then ligated into the pGEM vector. The setup therefore is:

Table 10: pGEM cloning strategy

Component	Volume
pGEM®-T Easy Vector (50 ng/µL)	0.5 µL
T4 DNA Ligase	0.5 µL
2X Rapid Ligation Buffer	5 µL
Insert	molecular ratio based
Water (SIGMA; W4502)	ad 10 µL

The ratio for the insert was calculated as following:

$$m_{insert} = \frac{m_{vector} * kb\ size\ of\ insert}{kb\ size\ of\ vector} * ratio\left(\frac{insert}{vector}\right)$$

$$V_{insert} = \frac{m_{insert}}{c_{insert}}$$

After mixing the components, they were incubated overnight at 17°C. Next day 5µL of the mixture was transformed into competent cells.

3.18 Polymerase Chain reaction

A standard reaction consists of 12.5 µL BioMix™ (BIOLINE; BIO-25012), 1 µL Template DNA, 1 µL 10mM gene specific primers (each) and 9.5 µL water (SIGMA; W4502). PCR standard conditions are as follows:

Table 9: Standard PCR conditions

Temperature	Duration	Repetition
95°C	5 min	x1
95°C	30 s	┐
Primer specific temperature	30 s	| x35
72°C	1 min	┘
72°C	10 min	x1
4°C	infinite	x1

3.19 Purification and quantification of nucleic acids

3.19.1 Plasmid DNA purification

Plasmids preparations were performed according to manufactures procedures. For mini-preparations (reSource; SBS27106) 5 mL of Escherichia coli culture was used and for midi-preparations (Macherey Nagel™; 740412.50) 50 mL of Escherichia coli over-night culture.

3.19.2 RNA and microRNA extraction

Extraction was carried out as described below. If samples were intended for RT-qPCR optional steps involving Proteinase-K and DNase have been included as specified in the respective kit protocols.

3.19.2.1 Non-TRIzol® based extraction

Harvested embryos or dissected hearts were thawed (-80°C) and homogenized in ≥300 µL DNA/RNA ShieldTM (1X) (Zymo Research) using a 1 mL syringe with a 21Gx2" needle. The subsequent steps were as described in the manufacturer's manual of Quick-RNA™ MiniPrep Plus (Zymo Research). In short, the procedure included (1) Protein Digestion (2) Lysis with RNA Lysis Buffer (3) gDNA removal via Spin-AwayTM Filter (4) Ethanol precipitation (5) Column binding (6) DNase on column digest (7) Column preparation and two washes (8) Elution in Nuclease-Free Water.

3.19.2.2 TRIzol® based extraction

Harvested embryos or dissected hearts were thawed (-80°C) and homogenized in 1 mL TRIzol® Reagent (Invitrogen™, 15596026) using a 1 mL syringe with a 21Gx2" needle and incubated for 5 min. Following 200 µL (1/5 of TRIzol® Reagent) Chloroform was added and mixed by gentle shaking. After another incubation of 10 min at RT the samples were centrifuged at 12,000 g for 30 min at 4°C. Subsequently the transparent upper phase was transferred into a clean tube. The subsequent steps were as described in the manufacturer's manual of RNA Clean & Concentrator™-5 kit (Zymo Research). In short, the procedure included (1) Ethanol precipitation (2) Column binding (3) DNase on column digest (4) Column preparation and two washes (5) Elution in DNase/RNase-Free Water.

3.19.3 DNA and RNA quantification

DNA and RNA concentration were determined using a standard NanoDrop 1000 spectrophotometer for DNA and a NanoDrop 2000 for RNA (Thermo Scientific). A 260/280 ratio of ~1.8 and ~2.0 indicated pure DNA and RNA, respectively. The desired 260/230 value was >2.00, indicating that the sample was free of residual ethanol, which inhibits enzymes in relevant downstream reactions.

3.20 RT-qPCR

cDNA was synthesized from 200 ng RNA in a 20 µl reaction using a Maxima First Strand cDNA synthesis kit (Thermo Fisher Scientific; K1671). For microRNAs, cDNA was synthesized from 10 ng in a 10 µl reaction using miRCURY LNA RT Kit (Qiagen; 339340). RT-qPCR was performed on a 7500 Real-Time PCR System (Applied Biosystems) using SYBR Green PCR Master Mix (Thermo Fisher Scientific; 4309155) according to the manufacturer's instructions. MicroRNA specific primers have been designed by Qiagen (mir-449-5p: YP02111236, mir-451: YP02110557, mir-126-3p: YP02111065, mir-221-3p: YP00204532). Primers (Sigma-Aldrich) used for mRNA detection are shown in the table below (Table 11). RT-qPCR was normalized to β-Actin for mRNA, and miR-451 and miR-126-3p for micro RNA. Analysis was done using the DeltaCt method and according to Livak and Schmittgen (2001) and significance was determined by unpaired t-test using GraphPad Prism.

β-Actin was chosen for normalisation as GAPDH showed differential expression in the context of microRNA-499-5p knockdown experiments. Initial aim was to use two genes for normalisation (Bustin et al., 2009). Internal control for RT-qPCR was expression of technical replicates of β-Actin within one Ct.

Table 11: Primers for RT-qPCR on mRNA

A list of all primers designed for RT-qPCR during the course of this PhD project. The two right columns indicate if melt curve analysis showed a single (+) peak or multiple (-). The latter indicates lack of target specificity. Not all primers could be used for experiments within the time frame of the project, but are intended for use of follow up studies.

Name	Forward Primer 5'-3'	Reverse Primer 5'-3'	24hpi	48hpi
ACAN	TTACCTGAACCCTGCCAACC	CAGCTCCACCTCAGTCTGTG	-	
ACAN - 2	GATACGCCTTCTCCTTCATCC	TTGTCTCCTACACAGTTGCTG	-	-
ACAN - 3	CTTGAAATAGAGCCCTCCACTC	GAACTTGATCCAGCCTTCCTC		-
ACTC1	TGTTCTTGACTCTGGTGATGG	CTTCATGAGGTAGTCGGTCAG		
BMP10	CTCTCCGACATTCCTCTGC	ATTTCCGAACTCCTATGACGC	+	-
BMP10 - 2	CACCAGAGTACATGTTAGAGCTG	TGGAGACATTGAACAGAAGGG	+	+
CLIC5	GCTGGATGACTATCTGAGAACC	CATCTCTGTTGGGAACTCGAAG		
ETS1	TGTGCCTTTGTTAACCCCCA	ATTCACTGCCCACATCACCC	+	-
ETS1 - 2	GCCTGACTTTGTGGGAGATATC	GTATAGCGGGATTCTGGATACG	+	+
FGF8	TCATGCACTTGTTCGTCCTC	CTGAGCTGATCTGTCACCAG	-	
FGF8 - 2	AAGAAAATCAATGCGATGGCC	TTGTTCTCCAGCACGATCTC	-	-
FGF8 -3	CTCGCTCTTCAGCTACGTG	CATGCTGTGTAAAATTAGGTGGG	+	+
HAPLN1	GCAGTGAGAACGATGCCTCT	TTGTAACGACCCAGACGTGG	+	+
HAS2	CAGCACGTATCTCAGCTGGT	ATCGCCTCCAACTCCTCCAA	+	-
HAS2 - 2	AAGTGCGATTTGATCTTTTACCTC	TGTGGTTCCAAGTATTCTCAGG		-
HCN2	CCCTTATGAAGATCAGTCCGTG	CAATTGCTGGGCTTGTAACC	+	+
HCN4	CTTCCTGATAGTTGAGACCCG	CAGATCGTAGGTCATGTGGAAG	+	+
HES1	TCAATTCGCCTTCCTCATCC	TGATGTCAAGCCCTGCAC	+	
HES1 - 2	AAAACCCACCGCTTCCC	GTCCAGGATGAGCATCTTCAG	+	-
HEY1	TGTCTGCGTTCCCCTTTTC	GCTTCCCCACCCTTACTAAAG	-	
HEY1 - 2	TGGATCACCTGAAGATGCTG	CTGAGAGGCGTAGTTATTGAGG	+	-
HEY2	GAAACTACCTCAGACAGCGAC	CGCCTTTTCTCTATAATCCCTCTTC	-	
HEY2 - 2	CGGAAATACTGCAAATGACGG	ACCTCGCAACTTCAGTCAAG	+	+
HNRNPK	CTTCCTGATAGTTGAGACCCG	CGTTTGCCATTTGTCTCTGTG		
KCNIP2	AAGAATGAGTGCCCGAGTG	ACAAAGTCCTCAAAGCTGACG	+	+
KCNIP2 - 2	CAGCGATTCCTCAAACTGC	TCGGGCACTCATTCTTGAAG		+
MEF2C -1	AGCACGGATATGGACAAAGTG	CCTACTGAATCGTCTGCATCG		
MEF2C -2	AGTGTCTGAGGATGTTGATCTG	GTTGAGATGGCTGATGGGTAT		
MEF2C -3	TCCTACTCTACCAGGGCAAG	AGCCAGTCACAGAACCAAG		
MSX1	CAGAGAGCCCCGAGAAGC	TGCTTCTGGCGGAATTTCCT	-	
MSX1 - 2	GCGCACGTGGGATATAGTATG	GGTTGAAGGTCTGGATGAAGG	+	+
NOTCH1	TCAATGAGTGCCAGAGCCAG	GCCGTTGATCTTGTCGATGC	+	+
NRG1	CTGGTGATCGCTGCCAAAAC	GTAGGCCACCACACACATGA	+	-
NRG1 - 2	TCACCCTTCCCCATACCTAG	GACCACAACCCGACATCTAG	+	+
PAX3	AGAACTCGCACAAAGAGCCA	CAGAGAGCTGGTATGTCGGC	-	
PAX3 - 2	ATTATGCCCTGTCCCCTTTG	ACTTTGTCCATACTGTCCATACTG	-	-
POSTN	TTGAGCGTCTTCCAAGAGGA	TCACCATCACAGCCAACTTCA	+	+
Pre-miR-499	TTTGAGGGAGCGGCAGTTAA	TGAGGAGAGAAGTAGCACAGACT	+	+
SMAD3	CGCAGAACATCAACACCAAG	CGTACTCGCACATCTCCATG	-	+
SMAD3 - 2	CCAGAGAACACTAACTTCCCAG	TGCCGGAGACATAGGATTTG	+	+
SMAD6	GCTGAAGCGGCTGAAGGA	ATTCGCACAGGGCCTTCAG	-	
SMAD6 - 2	GAAGGCCCTGTGCGAATGTC	GGCTTTTGCTCGTCGTTAGG	+	+
SOX9	AAGTACCAACCACGCAGGAG	CTGCTGAGCGTCCGTTTTG	-	

Name	Forward Primer 5'-3'	Reverse Primer 5'-3'	24hpi	48hpi
SOX9 - 2	CAGCAAGAACAAACCCCAC	CGCTTCTCGCTCTCATTCAG	+	+
TBX20	GAGAGGGAAAGTGTGGAGAG	GTTGAAGAGGATACCCAGGAAC	+	+
TBX3	ATAAAAGAGGCACGGAGATGG	TCTTTGGCATTTCAGGGTCAG		
TNNT2 -1	GATGAAACAAAAGCACCAGGAG	TGTCATCGAAATCCAGGCG		
TNNT2 -2	AAGCATGTCGGACTCTGAAG	TTCCTCTGTCTCCTCTTCCTC		
TNNT2 -3	GGCAGAAGTACGAGATCAACG	CTTCAGAGCCATCTACTTCCAC		

3.21 RNAseq and Transcriptome Analysis

Total RNA was isolated using the above described Non-TRIzol® based extraction method. Illumina RNAseq was performed by Novogene Co., Ltd in Hongkong. Samples were submitted as RNA as described below.

Quality assessment of the RNAseq data was done using the FastQC (Andrews, 2010) with default setting. This was followed by TrimGalore (Krueger, 2015), using default settings to trim reads and another FastQC quality asessment. Quality filtered reads generated by the tool were then aligned to the chick reference Gallus-gallus-5.0 (transcripts) using the Kallisto (Bray et al., 2016) aligner with 100 bootstratps (parameter b=100, other settings were default). Differential gene expression analysis was done using Sleuth (v. 0.30.0) (Pimentel et al., 2017). (Performed by Bioinformation Dr. Leighton Folkes.)

Read counts obtained from Sleuth (Pimentel et al., 2017) were normalized by dividing each sample transcript count by the median of each transcript count across all samples of one timepoint. The averaged normalized expression values of the samples were used to calculate fold change. Cutoff values of fold change between -0.75 and 0.75 and p values less than 0.05 were then used to select for differentially expressed transcripts between sample group comparisons. Significant pathway enrichment analysis was performed using PANTHER Overrepresentation Test, GO biological process complete (Mi et al., 2019).

3.22 Western Blot

3.22.1 Protein Isolation and SDS-page

Dissected hearts were pooled, dissolved in NP40 buffer and mechanically lysed by using a syringe needle (1 ml syringe with 25Gx 5/8" needle). Lysed protein amounts were quantified using the Pierce™ BCA Protein Assay Kit (Thermo™ Scientific, 23227) against a BSA standard curve prepared in NP40 buffer. Protein amount is relative to emission at 562nm, which was measure with a GloMax® Explorer (Promega, GM3500).

Desired protein amounts (15-30 µg) and Ladder (Thermo Scientific™, 26616) were mixed with 5% v/v 2-Mercaptoethanol (Sigma-Aldrich, M6250-100ML) and 1x sample buffer (BIO RAD, 1610747) and loaded onto a Mini-PROTEAN® TGX™ Precast Protein Gel (BIO RAD, 4561086) and run at 100V for 1-2 hours. After successful run the gel was ready for transfer.

3.22.2 Western transfer

After SDS-PAGE proteins were transferred to a polyvinylidene fluoride membrane (PVDF

membrane, BIO RAD, 1620177) by tank (wet) electro transfer. The membrane was pre-soaked in methanol. Before starting the transfer all components (membrane, gel, fiber pads and papers) were soaked in transfer buffer (10X solution 0.25M TRIS, 2M Glycine, pH 8.3) and stacked up in correct order (fiber pad, 2x filter papers, gel, PVDF membrane, 2 filter papers, fiber pad). Everything was locked in a gel holder cassette. The transfer was then performed at 115V for 75 min in transfer buffer. The transfer was executed in a "Mini Trans-Blot® Cell" from Biorad.

3.22.3 Immunolabeling and Imaging

After transfer the membrane was rinsed three times in PBST and subsequently blocked for 2h or o/n in 5% w/v milk PBST. After blocking the membrane was rinsed a few times in PBST and then incubated in primary antibody in 5% w/v milk PBST o/n. After Incubation the membrane was washed four times for five minutes in PBST. Following the washes, the membrane was incubated in secondary antibody in 5% milk PBST for 1h and washed again four times for five minutes in PBST. After the final wash 1ml of the detection agent, ECL™ Prime Western Blotting System (GE Healthcare, RPN2232) was applied and incubated for three minutes. After incubation the membrane was image immediate while still wet. For short term storage membranes were kept in PBST.

Table 12: List of used primary antibodies

List of primary antibodies used within this study to analyse microRNA-499-5p knockdown phenotype

Antibody name	Manufacturer	Dilution	Expected size	Compatibility chick
Anti-Actin antibody [ACTN05 (C4)]	Abcam, ab3280	1:1000	42 kDa	Yes confirmed
Anti-ETS1 antibody	Abcam, ab26096	1:500	50 kDa	Could not be confirmed, but predicted
HSC 70 (B-6)	Santa Cruz Biotechnology, sc-7298	1:1000	70 kDa	Yes confirmed
Anti-NOTCH1 intracellular domain antibody	Abcam, ab83232	1:1000	88 kDa	Could not be confirmed, but predicted
Cleaved NOTCH1 (Val1744) (D3B8) Rabbit mAb	Cell Signalling, #4147	1:1000	110 kDa	Could not be confirmed, worked previously
Anti-SMAD6 (AB2) antibody produced in rabbit	Sigma, AV32690	1:1000	53 kDa	Could not be confirmed, but specified to work

4 Results

4.1 Validation of microRNAs of interest during development

The interest to study microRNAs during endocardial cushion development arose from a microRNA sequencing study preceding this project (McCormick, 2015). This study revealed that several microRNAs are upregulated at the time when cushion development initiates in the chicken embryo, which is at around HH17. Among the most promising candidates from this study were microRNA-499-5p, microRNA-451, microRNA-126-3p and microRNA-221-3p (Figure 9A). Before moving on to experiments confirming target interaction and functional in vivo experiments we wanted to obtain additional evidence for their upregulation since the RNA sequencing experiments contained no biological replicates which was the accepted standard practice at the time the experiment was conducted. To acquire confirmation RT-qPCR was performed on heart samples from HH17 embryos as well as well as HH stage 13 (approx. 16 hours before) and HH stage 21 (approx. 18 hours after). The RT-qPCR data confirmed the trend of upregulation of the four microRNAs (Figure 9B). For further experimental analysis microRNA-499-5p and microRNA-221-3p were chosen as published reports supported (Liu and Olson, 2010, Luo et al., 2015, Tijsen et al., 2012) their relation to heart development and the ETS1 signalling cascade (see Figure 4).

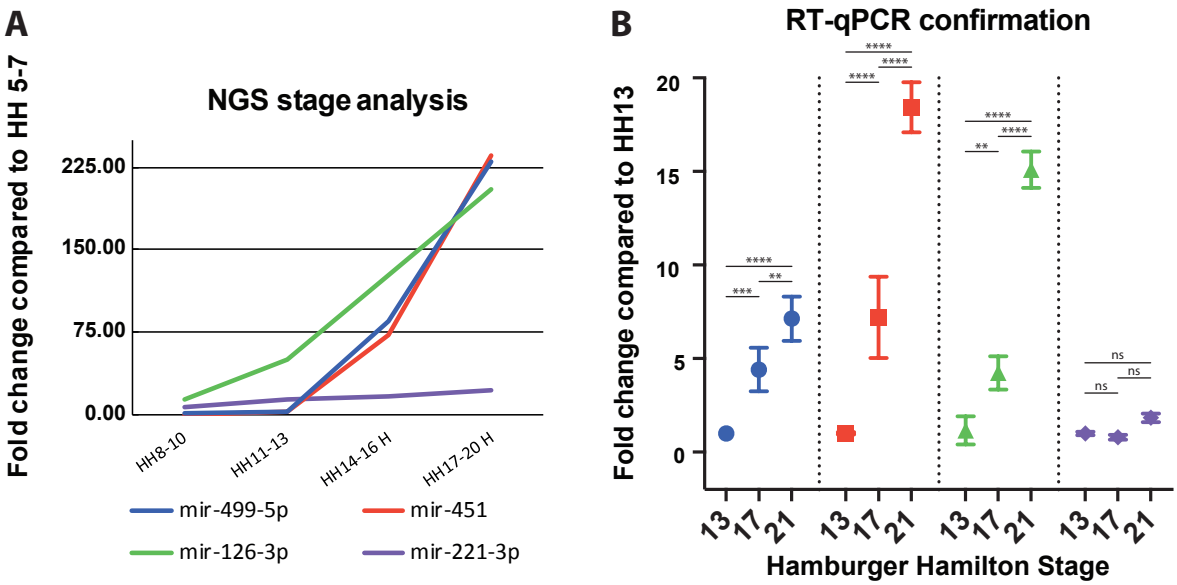

Figure 9: MicroRNA upregulation during heart development

Several microRNAs are upregulated during the initiation of cushion development. (A) Results prior to project start showed upregulation of four candidate microRNAs. Samples were pooled hearts of multiple stage from which small RNA libraries were constructed and sequenced using Solexa (Illumina forerunner) at that time a single replicate was standard practice for high throughput sequencing. (B) Independent RT-qPCR confirmation of upregulation trends observed in the small RNAseq. Samples are pooled hearts of the single HH-stage indicated (Mean with SD; n=3; 2way ANOVA for statistical analysis with Tukey correction; some error bars are shorter than symbols)

4.2 *In vitro* confirmation of target interaction

Prior to project start *ETS1* was selected as a promising target for microRNA-499-5p target interaction. Target sequence analysis at that point of time revealed only a cryptic binding site

according to microRNA nomenclature (Bartel, 2004, Bartel, 2009). Cryptic binding sites signal in a non-canonical manner and are less well understood. Nevertheless, luciferase assays using an UTR sequence with this cryptic binding site led to a reduction of luciferase expression, concluding successful target interaction (data not shown). Initial experiments within this PhD project addressed

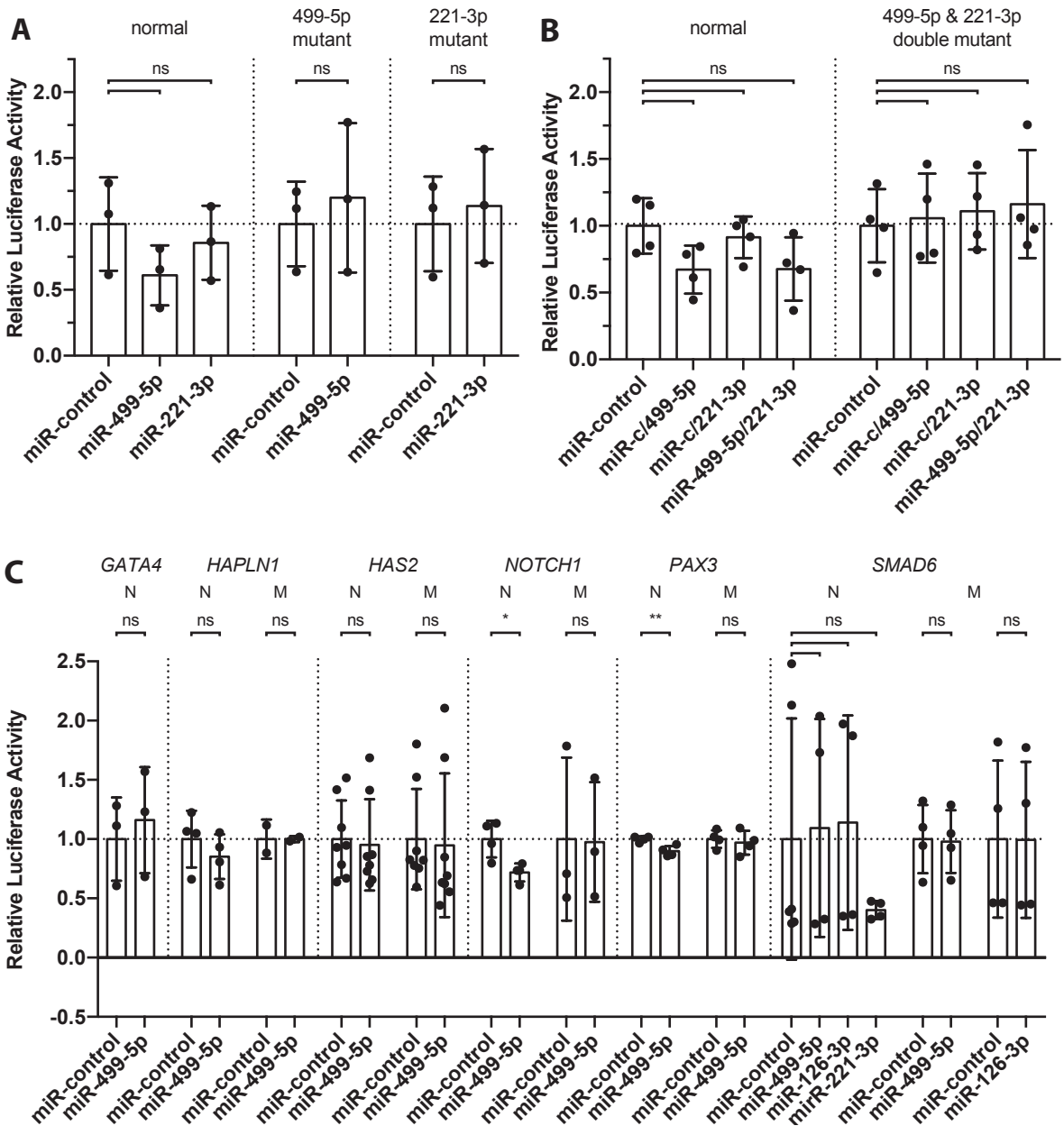

Figure 10: Validation of 3'UTR interactions via Luciferase Assays.

Luciferase Assay analysis of target genes. Columns labelled with used microRNA-mimic and column header indicates construct type, normal (N) and mutated (M) (A) Confirmation of microRNA-499-5p and microRNA-221-3p target interaction with the *ETS1* 3'UTR. Mutation of both seed sequences individually recovered expression to base levels respectively (n=3) (statistical significance was not achieved, students t-test). (B) Using microRNA mimics for microRNA-499-5p and microRNA-221-3p in combination leads to an additive effect and no synergetic amplification (n=4). (half doses were used; statistical significance was not achieved, students t-test) (C) Fragments of the 3'UTRs of various genes of interest involved in heart development have been subjected to Luciferase assay analysis using mimics for microRNA-499-5p, microRNA-126-3p and/or microRNA-221-3p. *GATA4* (n=3) was not negatively regulated, *HAPLN1* (n=4/2) showed a trend but needs further replicates for statistical significance, *HAS2* (n=8) showed a trend but sequence of interaction was not identified, *NOTCH1* (n=4/3) and *PAX3* (n=4) were confirmed and lastly *SMAD6* (n=4) showed no response to any of the used microRNA-mimics (statistical significance was tested by students t-test, $p<0.05$ * and $p<0.01$ **).

replication of these experiments, which were unsuccessful (data not shown). The reason for this lies most likely in the microRNA mimic sequence, which was a custom oligo from SIGMA before project start and later swapped for a predesigned microRNA mimic from QIAGEN. Reanalysis of updated sequence information for *ETS1* from RNAseq data (Aken et al., 2016) revealed another binding site within its 3'UTR that follows canonical microRNA binding rules. The 3' UTR was cloned into a different vector system, pmirGLO Dual-Luciferase microRNA Target Expression Vector (Promega, E1330) than previously used, pGL3 Luciferase Reporter Vectors (Promega, E1751 and E1741). This has the advantage of transfecting a single plasmid into cells and thus allowing more accurate normalisation.

Target interaction for microRNA-499-5p and *ETS1* was not confirmed but a trend indicated the effect of the microRNA (normal - control: 1 ± 0.354; miR-499-5p: 0.610 ± 0.228; $p>0.05$; n=3) further mutation of the seed sequence recovered the luciferase expression to normal levels (mutant - control: 1 ± 0.321; miR-499-5p: 1.198 ± 0.567; $p>0.05$; n=3) (Figure 10A, Appendix 8.1). In addition, a candidate target sequence for microRNA-221-3p was found in the 3'UTR and analysed. Once more confirmation could not be confirmed but a trend was present (normal - control: 1 ± 0.354; miR-221-3p: 0.857 ± 0.281; $p>0.05$; n=3), which is consistent with a previous publication (Xu et al., 2016). Mutation of the seed sequence recovered the luciferase expression to normal levels (mutant - control: 1 ± 0.359; miR-221-3p: 1.137 ± 0.433; $p>0.05$; n=3) (Figure 10A, Appendix 8.1). Further microRNA-221-3p was in the list of microRNAs of interest as it follows a similar upregulation pattern as microRNA-499-5p during endocardial cushion development. Following observing these trends of *ETS1* 3'UTR interaction with both microRNAs we wondered if they signal in an additive or synergetic manner. Therefore, another assay involving both microRNAs was performed, which revealed that target suppression is neither additive nor synergetic and resembles the inhibition achieved by microRNA-499-5p alone thus(Figure 10B, Appendix 8.1) (normal - control: 1 ± 0.207; miR-c/499-5p: 0.672 ± 0.181; miR-c/221-3p: 0.914 ± 0.156; miR-499-5p/221-3p: 0.676 ± 0.237; mutant - control: 1 ± 0.273; miR-c/499-5p: 1.057 ± 0.333; miR-c/221-3p: 1.108 ± 0.287; miR-499-5p/221-3p: 1.162 ± 0.405; $p>0.05$; n=4) no amplification occurs using both mimics together.

Besides *ETS1* we identified other genes involved in heart development from literature and subjected those to target interaction analysis using TargetScan (Agarwal et al., 2015). Aim of said analysis was to determine other players during cushion maturation that are affected by our selected microRNAs of interest. UTR sequence information was acquired either from the TargetScan website itself or Ensembl.org including RNAseq data (Aken et al., 2016). Candidate target sites were identified for microRNA-499-5p, microRNA-221-3p, microRNA-126-3p and microRNA-451 for the following genes: *GATA4*, *HAPLN1*, *HAS2*, *NOTCH1*, Neuregulin 1 (*NRG1*), Paired Box 3 (*PAX3*) and Mothers against decapentaplegic homolog 6 (*SMAD6*) and subsequently their 3'UTRs were cloned for luciferase assays analysis (Figure 10C, Appendix 8.1). Some of these UTRs contained multiple target sites of interest as depicted in Table 13. Some of the identified targets have not been cloned due to large PCR products (>1000 bp). Furthermore, microRNA interactions seem to favour sites located at either ends of 3'UTRs rather than sites located in the centre (Grimson et al., 2007).

GATA4 is a downstream target of ETS1. It is expressed early on in heart development and involved in cardiac specification (Meilhac and Buckingham, 2018). Later on, GATA4 plays and important role

Table 13: Target site analysis using TargetScan

The below table shows identified target sites for various genes of interest involved in heart development. The position of the site and their respective type is detailed in the table. All sites except for those marked in grey have been cloned into the luciferase reporter vector for analysis.

Gene_ID	microRNA_family_ID	species_ID	UTR_start	UTR_end	Site_type
ETS1	miR-221-3p	9031	253	259	7mer-m8
ETS1	miR-499-5p	9031	698	705	8mer-1a
ETS1	miR-499-5p	9031	1422	1428	7mer-1a
ETS1	miR-221-3p	9031	4181	4187	7mer-m8
ETS1	miR-221-3p	9031	4340	4345	6mer
GATA4	miR-499-5p	9031	880	886	7mer-m8
HAPLN1	miR-499-5p	9031	975	981	7mer-1a
HAPLN1	miR-499-5p	9031	1065	1071	7mer-m8
HAS2	miR-499-5p	9031	1201	1206	6mer
HAS2	miR-499-5p	9031	1369	1375	7mer-m8
NOTCH1	miR-499-5p	9031	1346	1353	8mer-1a
NRG1	miR-451	9031	510	515	6mer
NRG1	miR-499-5p	9031	1021	1027	7mer-m8
NRG1	miR-221-3p	9031	1362	1368	7mer-1a
PAX3	miR-499-5p	9031	1809	1815	7mer-1a
SMAD6	miR-221-3p	9031	776	782	7mer-1a
SMAD6	mir-126-3p	9031	913	918	6mer
SMAD6	miR-499-5p	9031	994	1001	8mer-1a
SMAD6	miR-221-3p	9031	1092	1097	6mer
SMAD6	miR-221-3p	9031	2013	2018	6mer

in vasculogenesis and angiogenesis (Marín-García, 2014). Luciferase assay invalidated the target site for microRNA-499-5p (Table 14).

HAPLN1 (hyaluronan and Proteoglycan Link Protein 1) is an ECM component that is expressed at the AVC and at lower levels on the OFT during the formation of the endocardial cushions (Lockhart et al., 2011, Wirrig et al., 2007). Luciferase assay showed a trend that indicates target interaction of microRNA-499-5p and the 3'UTR fragment of *HAPLN1* (Table 14, replicates of mutant construct are missing for statistical analysis).

HAS2 is an enzyme synthesising hyaluronan another ECM component essential during heart development. Knockout of *HAS2* in mice has been shown to be embryonic lethal, emphasizing its importance (Camenisch et al., 2000, Lockhart et al., 2011). Luciferase assay showed a trend for reduction in Luciferase expression after microRNA-499-5p-mimic administration however target site mutation does not recover the phenotype (Table 14).

NOTCH1 is an essential transmembrane receptor, which is cleaved upon ligand binding to produce a transcriptional regulator involved in various processes during heart development as for example septation, cushion remodelling, trabeculation and neural crest migration. NOTCH signalling is required for valve development and homeostasis and if absent various malformations arise (MacGrogan et al., 2018a). Luciferase assay confirmed the target site for microRNA-499-5p (Table 14).

NRG1 is a key factor for ventricular trabeculation where its signalling promotes ECM synthesis in the Myocardium (Del Monte-Nieto et al., 2018). Further NRG1 contributes to the formation of the endocardial cushions via ERBB3 and ERBB4 signalling. Mutation in the NRG1 gene led to Hypoplasia (Lin et al., 2012). For our reporter analysis NRG1 was an interesting candidate especially since it was predicted to be targeted by the less common microRNA-451. Unfortunately cloning from chick cDNA was unsuccessful after multiple attempts and the target was dropped for luciferase analysis. In addition, ISH analysis following knockdown of miR-499-5p did not support the idea that *NRG1* is a direct target for this microRNA (see below and (Figure 15).

PAX3 is a relevant gene for neural crest migration into the OFT, where PAX3 positive cells contribute to formation of the OFT valves (Epstein et al., 2000). Additionally, ETS is required for neural crest migration thus linking these two targets of interest. Luciferase assay confirmed the target site for microRNA-499-5p (Table 14). The significance of microRNA-499-5p in the context of PAX3 regulation in the heart is still open since detection of PAX3 transcripts in the OFT is limited(Gao et al., 2010).

SMAD6 is a negative regulator of EMT during endocardial cushion development. Overexpression of SMAD6 leads to reduced EMT whereas knockout to increased EMT leading to Hypoplasia (Desgrosellier et al., 2005). Luciferase assay confirmed the target site for microRNA-499-5p and microRNA-126-3p (but invalidated the target binding site for microRNA-221-3p (Table 14).

When this data is referenced in the following chapters conclusions are based on a previous analysis where the data was treated as paired rather than unpaired. This resulted in more comparisons being significantly different (see Appendix 8.1).

Table 14: Target site analysis using TargetScan

Data corresponding to luciferase assays for candidate genes

Gene_ID	miR-control			miR-499-5p			
	mean	SD	n	mean	SD	n	p
GATA4	1	0.351	3	1.160	0.448	3	0.65105
HAPLN1	1	0.239	4	0.851	0.189	4	0.36782
HAPLN1-499-5p-M	1	0.165	2	1.000	0.025	2	>0.99999
HAS2	1	0.326	8	0.952	0.385	8	0.79067
HAS2-499-5p-M	1	0.424	8	0.948	0.607	8	0.84486
NOTCH1	1	0.155	4	0.719	0.076	4	0.01732
NOTCH1-499-5p-M	1	0.687	3	0.975	0.506	3	0.9627
PAX3	1	0.024	4	0.898	0.044	4	0.0064
PAX3-499-5p-M	1	0.075	4	0.969	0.101	4	0.64239
SMAD6	1	1.019	6	1.094	0.920	4	0.88619
SMAD6-499-5p-M	1	0.288	4	0.979	0.264	4	0.91619

Gene_ID	miR-control			miR-126-3p			
	mean	SD	n	mean	SD	n	p
SMAD6	1	1.019	6	1.139	0.905	4	0.83112
SMAD6-126-3p-M	1	0.663	4	0.993	0.658	4	0.98888

Gene_ID	miR-control			miR-221-3p			
	mean	SD	n	mean	SD	n	p
SMAD6	1	1.019	6	0.402	0.075	4	0.28393

4.3 Development of a technique for *in vivo* knockdown of microRNAs in the chicken heart

The development of the cardiac injection procedure has undergone several optimisation steps before a final protocol for a reliable method was established. At first the standard procedure for injections into somites, which is commonly used in the Münsterberg lab was chosen as a basis, but several modifications were necessary to achieve good survival and AntagomiR delivery to the heart.

One of the first problems was related to heart access, which is covered by an additional membrane. A delicate incision method needed to be established to open this extra membrane since the injection needle wasn't strong enough to pierce trough. Further to this the standard injection needles used in the lab were too long and too flexible (depicted in Movie 1), therefore several different needle shapes had to be analysed until a more rigid version was found.

A second issue was survival of the embryos which initially was poor even just 24 hours after injection. More experience with proper execution of the injection procedure improved survival slightly but the biggest impact came from using a tabletop incubator. Thanks to the incubator the time at temperatures lower than 37°C was minimised, which we believe improved the chick embryos physiology to deal with the stress caused by the "microsurgery". After implementing the table top incubator into the method, survival was easily achieved for three days post injection but also longer, which hasn't been tested extensively.

Further a third issue was proper targeting of the heart. In many attempts the injected AntagomiR entered the blood stream and was flushed into the circulatory system, which would have led to global effects on the embryo rather than heart specific ones. However, the aim was to specifically target the heart, thus we tried to minimise circulation cooling down eggs down to 18°C prior to injection to reduce the heart rate. Unfortunately, this did not improve the situation and even subtle heart beats were sufficient to distribute the AntagomiR across the whole body. Further the reduced temperature had a negative impact on survival, as we explained above that the appropriate egg temperature seemed to help to cope with the stress caused by the procedure. Ultimately, after several experiments we became aware of the interspace in the cardiac wall were the AntagomiR stays and does not diffuse to other areas. After some practice specific targeting of this area was no problem (Movie 1).

Another problem affecting survival was caused by embryos sticking to the eggshell inside the egg which prevented proper sealing. Unfortunately, complete elimination of this issue was not possible, but we were able to minimise its impact by positioning the eggs straight upright prior incubation and avoid any tilt in any direction. Further when still stuck after successful injection, detaching the embryo by applying albumen to flush it down showed better success then PBS or "gentle" detachment with forceps or a syringe needle. Usually working with forceps or a syringe needle close to embryo caused some minor or even major incision that decreased the chance of survival dramatically.

Occasionally another issue caused experimental failure. Once in a while we encountered complete infection of all injected eggs within one batch, why we implemented the additional surface cleaning step of the eggs prior to injection. To reduce the likelihood of infection as the large

opening to execute the procedure offers plenty of risk for infection. Additionally, the used tabletop incubator was disinfected regularly.

All in all, after carefully assessing the different issues we were able to establish a protocol for reliable delivery of AntagomiRs specifically to the heart.

The sub-sections below have been published in (Wittig et al., 2018), few updates, additions and content reorganisation have been made where applicable.

4.3.1 Protocol for cardiac injections

The whole procedure is shown step by step in Movie 1: Cardiac injection procedure.

Movie 1: Cardiac injection procedure

The movie shows all necessary details for carrying out the cardiac injection procedure described in this study.

1. Incubate fertilized chicken eggs
    a. Fertilized chicken eggs are stored at 17°C for up to a week prior to incubation
    b. Eggs are incubated with the blunt end up in a humidified incubator at 37°C
        i. Depending on stage of interest the length of egg incubation has to be adjusted. To obtain HH15 embryos we incubated fertile eggs for approximately 66 h (Hamburger and Hamilton, 1951)
2. Preparation of injection setup:
    a. For 30 eggs prepare 25 ml 1:500 PBS/ Pen Strep (PS) (Gibco Life Technologies; 15140-122) solution and 25 ml PBS/PS-solution with Indian ink (Winsor & Newton)
    b. Prepare Syringes with needles
        i. 1 ml syringe with 25Gx 5/8” needle for ink injection
        ii. 1 ml syringe with 25Gx 5/8” needle for incision of the extra embryonic tissue (EET)
        iii. 10 ml or 2 ml syringe with 21Gx2” needle for albumen removal
    c. Forceps and tweezers for removal of the shell and outer/inner membranes
    d. Adhesive tape for egg sealing
    e. Small table-top incubator for usage during procedure
3. Prepare injection apparatus
    a. Pull needle for microinjection (borosilicate glass capillaries 1.00 mm O.D. x 0.78 mm I.D.)
    b. To enable easy heart manipulation, we recommend shorter needles with a very sharp tip, since long flexible ones will not penetrate the heart and simply bend.
        i. Needle pull settings for Sutter Instruments P-97: P=300, Heat=ramp test value, Pull=150, Vel=80, Time=130.
    c. Load needle with ~1.5 µl AntagomiR at 1 µM (or other) using Microloader™ (Eppendorf) and mount onto microinjector
4. Prior to procedure spray eggs with 70% ethanol to kill surface germs
5. Remove single egg from incubator (Figure 11A)
6. Crack it open at the blunt end using tweezers and remove shell pieces until embryo is easily accessible (Figure 11B)

7. Using syringe (i) in a shallow angle inject ink-mix beneath the embryo for contrast and apply 2 drops PBS/PS-solution on top using a plastic Pasteur pipette to increase elasticity of EET (Figure 11C)
8. Place egg under a stereo-dissecting microscope and use syringe needle (ii) to cut open the vitelline membrane (Figure 11D)
    a. Cut EET around heart until it is freely accessible (Figure 11E)
9. Perform multiple injections in areas of interest (Figure 11F)
    a. Depicted is conus, primitive ventricle and primitive atrium (Figure 11F)
10. Remove needle and visually confirm injection (Figure 11G)
    a. Injected compound (AntagomiR) is conjugated to a fluorophore
11. Slide the needle of the large syringe (iii) down along the inside of the egg shell and remove albumen until the embryo is sufficiently lowered and will not touch the sealing tape (Figure 11H)
    a. If embryo adheres to the egg shell, flush it gently using albumen until it detaches
    b. Apply a few drops PBS/PS-solution
12. Seal the egg using clear adhesive tape
    a. Combine two strips of tape together (parallel) and apply them to the egg. Use a third strip and cross the other two (perpendicular) (Figure 11I)
13. Return the egg to an incubator immediately (for convenience this could be the desk-top incubator).

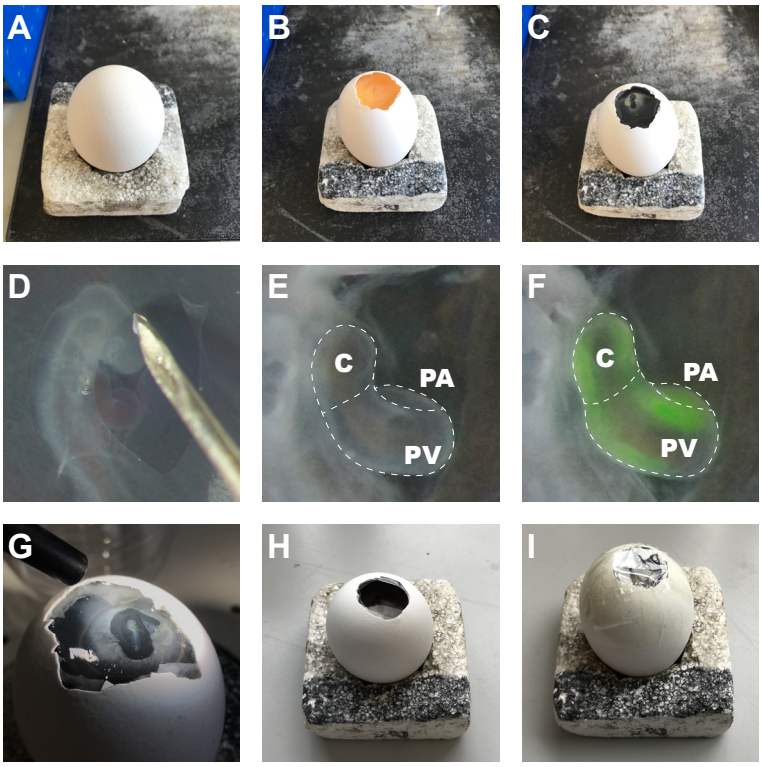

Figure 11: Injection Sequence

Image sequence of procedure steps. (A) Incubated egg for manipulation, (B) egg was cracked open and outer and inner membrane were removed, (C) ink was applied into the yolk sac below the embryo to provide contrast, (D) vitelline membrane and EET were cut open to access the heart, (E) accessible heart for injection, red blood cells are visible in the lumen, (F) injected heart along conus (C) downwards to primitive ventricle (PV) and on the right side the primitive atrium (PA), (G) injection verification, (H) removal of albumen and lowering of embryo, (I) sealing of egg and returning to incubation at 37°C.

4.3.2 Embryo survival and possible timescales of experiments

Several parameters have an impact on survival of the injected chicken embryos. In this study we analysed survival of embryos, injected with AntagomiR or with a scrambled sequence, 24 hours

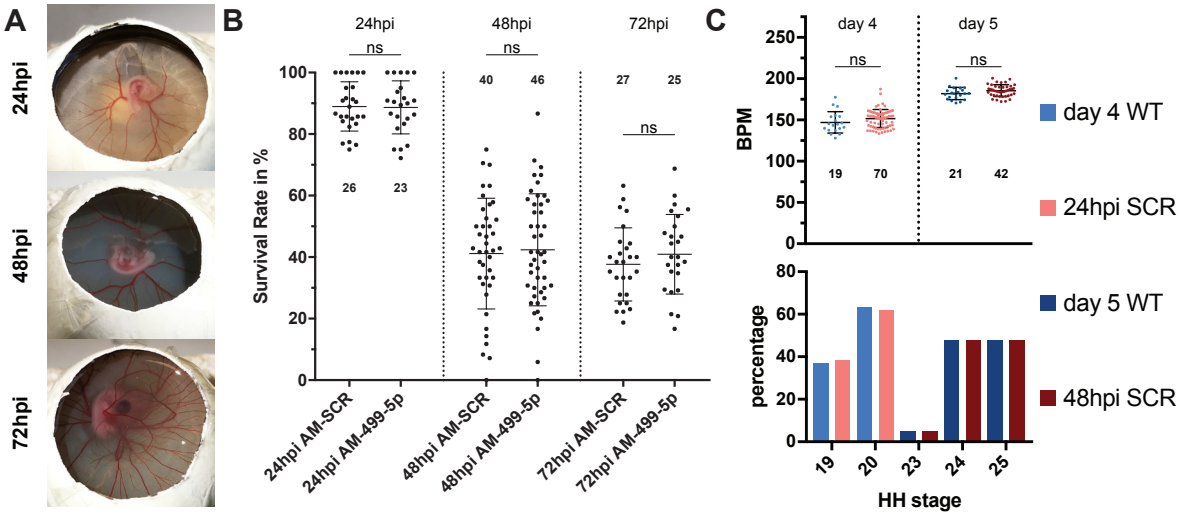

Figure 12: Representative results – embryo survival & impact on heart rate

Embryos survive until at least 72hpi and show no differences in cardiac health. (A) Representative photos of embryos post injection at the 3 time points analysed. (B) Survival analysis for embryos injected with AntagomiR-SCR (control) and AntagomiR-499-5p, a specific microRNA inhibitor shows similar survival rates across 24hpi, 48hpi and 72hpi. (C) Comparison of WT non-manipulated embryos vs control-injected embryos show no significant difference in heart rate. The bottom panel shows the distribution of HH stages that were analysed. We ensured the same proportion of HH19 and HH20 embryos were examined on day 4 (light blue and light red columns) and the same proportion of HH23, HH24 and HH25 embryos were examined on day 5 (dark blue and dark red columns). (B and C Mean ± SD; student t-test for statistical analysis; N in (B) is number of experiments, each experiment comprised between 25 and 30 embryos, N in (C) represents the number of analysed hearts)

post injection (hpi), 48hpi and 72hpi (Krutzfeldt et al., 2005, McGlinn et al., 2009) (representative photos, Figure 12A). For both the non-specific scrambled control, AntagomiR-SCR, and the specific AntagomiR-499-5p embryo survival declined with longer incubation periods (Figure 12B). After 24 hours post injection around 90% (AM-SCR: 88.99 ± 8.04, n=26; AM-499-5p: 88.67 ± 8.63, n=23; $p>0.05$) of embryos had survived and developed normally, this dropped to 40% (AM-SCR: 41.14 ± 18.01, n=40; AM-499-5p: 42.40 ± 18.21, n=46; $p>0.05$) and slightly lower than 40% (AM-SCR: 37.63 ± 11.90, n=27; AM-499-5p: 40.92 ± 12.95; n=25; $p>0.05$) at 48hpi and 72hpi, respectively. The almost identical survival rates observed with control and experimental AntagomiRs suggests that the decrease in survival is due to the manipulation itself. The data presented for AntagomiR-SCR represents the baseline for survival and we assume that survival beyond 72hpi is possible, potentially even up to hatching. In experiments where other AntagomiRs were injected the embryos showed a steeper decline in survival (up to 100% before 48hpi, not shown), suggesting a biological impact affecting survival resulting from this particular knockdown.

Several factors during the procedure should be considered to promote embryo survival. During egg opening, it is vital to avoid damaging the embryonic tissue and the vasculature. Bleeding indicates damage and these embryos cannot be used. In addition, following the microinjection embryos can sometimes adhere to the egg shell and their detachment can result in damage. Incubation with rocking prior to injection may reduce the occurrence of adherence to the shell and it has been reported that agitation during incubation improves hatchability and should therefore promote healthier development (Randles and Romanoff, 1954). In the final step of the procedure, when lowering the embryo after injection, it is essential to avoid contact with sealing tape. To avoid

these confounding issues, we have excluded egg shell adhering embryos in our survival analysis.

To make the heart accessible for injection the vitelline membrane and some of the EET surrounding the heart need to be partially removed. During this, caution is necessary to avoid wounding vessels or the heart to prevent bleeding. The same applies to the actual injection step, since the injection needle is sharp enough to cause small incisions in the heart. Finally, the procedure was optimized by returning the embryos to a heated incubator at 37°C immediately after injection, this improved survival rates.

To determine if the injection procedure had an impact on heart function, we analysed heart rates (HR) of control-injected embryos compared to wildtype (non-manipulated) embryos as a representative variable for cardiac health (Figure 12C top panel). The data revealed no significant differences between the two groups for the first two timepoints analysed, 24hpi and 48hpi (unpaired t-test, $p>0.05$). This also shows that the injected AntagomiR has no non-specific toxicity. The HR becomes faster with increasing age, therefore, to ensure accurate comparison, the same stages of embryo development were used (Figure 12C bottom panel). The quantification of HR requires the heart to be visually accessible and this makes analysis of older embryos (>5 days) difficult. After 5 days of development the allantois is covering the heart and this made HR-quantification challenging even though still possible for some embryos (Spurlin and Lwigale, 2013). However, electrophysiological methods for HR- quantification may still be suitable (Shi et al., 2013). We have also found that injection of some AntagomiRs can induce HR changes and the complete analysis of such phenotypes require detailed follow-up analysis.

4.3.3 Validation of AntagomiR administration

The injected compounds in this study were AntagomiRs, complementary sequences to microRNAs designed to inhibit their function (Krutzfeldt et al., 2005, McGlinn et al., 2009). The AntagomiRs contained two modifications, a 3' cholesterol group to allow cell uptake and a 5' Fluorescein group for tracing purposes. The Fluorescein enables easy localization of AntagomiRs during the procedure, which is helpful for targeting and to avoid injection into the bloodstream, potentially causing systemic rather than heart specific effects. Furthermore, the fluorescent tag enables detection post-injection at 24hpi and 48hpi (Figure 13A). However, fluorescence intensity decreased over time and was no longer detectable at 72hpi. Signal strength may also depend on local retention of the AntagomiR. The AntagomiR-SCR used as a control in this study has no binding partner in the chicken embryo, we found that its signal intensity was reduced, compared to an AntagomiR that is directed against a microRNA expressed in the heart, such as miR-499-5p (Figure 13Bi) (van Rooij et al., 2009). After Antagomir-499-5p injection a much stronger signal was consistently detected using enzyme catalysed immunohistochemistry (IHC) against the FITC-tag. We propose that this is most likely due to binding of the endogenous complementary microRNA, miR-499-5p. In addition to IHC on dissected hearts (Figure 13Bi), we examined whole embryos to confirm specific targeting of the heart only (Figure 13Bii). Specific staining was restricted to the heart shown by two purple stripes. Some faint staining was visible in the body due to trapping, which is a commonly observed drawback of methods involving chromophore conversion (Antin et al., 2007, Lufkin, 2007). However, if this diffuse signal is due to leakage of AntagomiR into other tissues, it would indicate that there was very little if any.

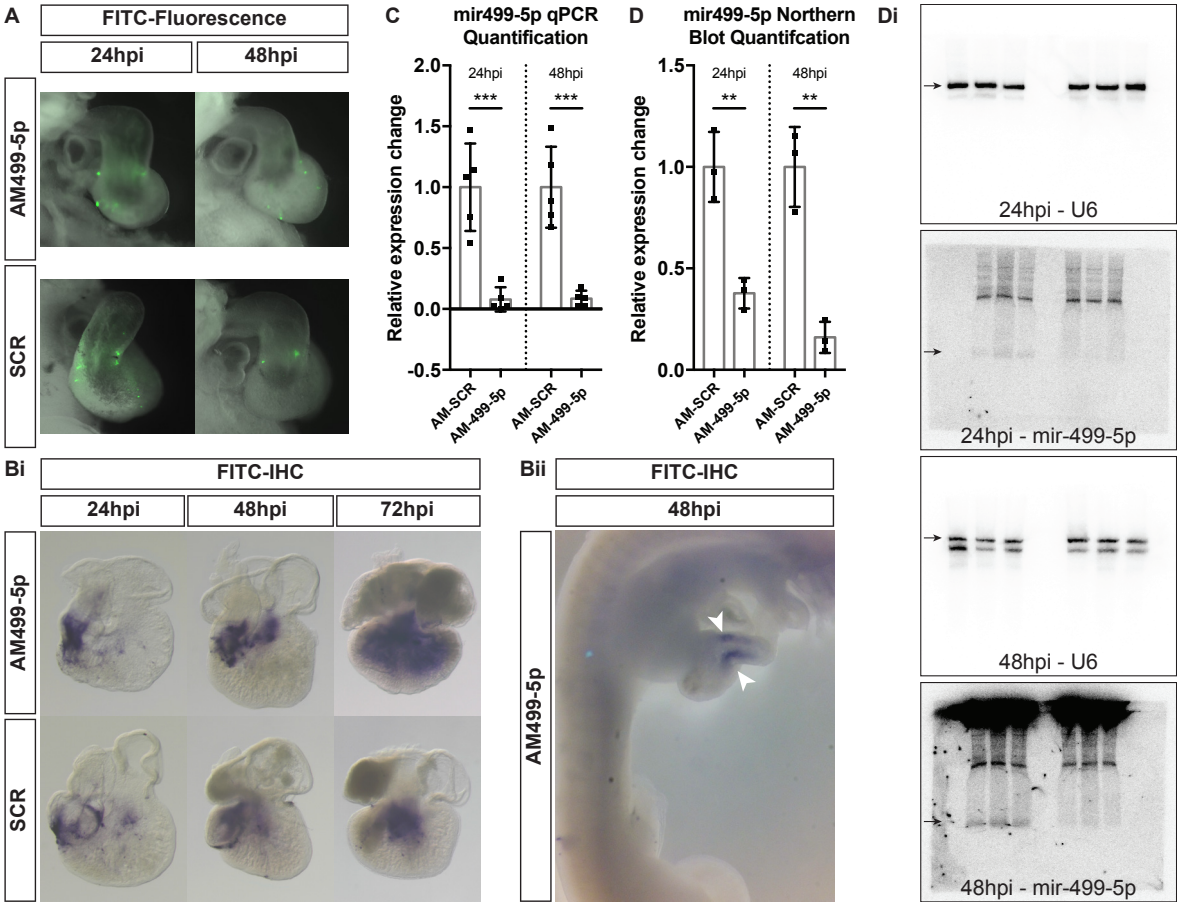

Figure 13: Confirmation of successful AntagomiR delivery

Visual and molecular verification of AntagomiR delivery and microRNA knockdown. (A) Tracing of FITC-tag fluorescence of AntagomiR-SCR and AntagomiR-499-5p at 24hpi and 48hpi. (B) Chromophoric detection of the FITC-tag by IHC. (Bi) AntagomiR-SCR and AntagomiR-499-5p are detected by IHC at 24hpi, 48hpi and 72hpi in dissected hearts. (Bii) Whole embryo IHC for AntagomiR-499-5p. Specific signal is detected in the heart (white arrowheads), faint background staining originates from trapping. (C) qPCR confirmation of miR-499-5p knockdown (unpaired t-test, n=5, 24hpi and 48hpi $p<0.001$) (D) Northern Blot confirmation of miR-499-5p knockdown (unpaired t-test, n=3, 24hpi and 48hpi, $p<0.01$). (Di) Corresponding Northern Blot Images to D, three most left lanes AntagomiR-SCR injected samples and three most right lanes Antagomir-499-5p injected samples (arrow indicates target).

In mice, AntagomiRs were detected for up to three weeks after systemic injection (Krutzfeldt et al., 2005). Consistent with this, IHC against Fluorescein detected AntagomiRs for periods longer than 48hpi (Figure 13B).

Furthermore, knockdown of miR-499-5p can be confirmed by RT-qPCR (24hpi, AM-SCR: 1 ± 0.359, AM-499-5p: 0.078 ± 0.100; 48hpi, AM-SCR: 1 ± 0.332, AM-499-5p: 0.084 ± 0.065, $p<0.001$, n=5)(Figure 13C) and Northern-Blot (24hpi, AM-SCR: 1 ± 0.173, AM-499-5p: 0.377 ± 0.075; 48hpi, AM-SCR: 1 ± 0.197, AM-499-5p: 0.160 ± 0.076, $p<0.01$, n=3)(Figure 13D). Hearts were dissected post incubation, pooled (six for 24hpi & three for 48hpi) and RNA was extracted. Both methods show a significant reduction of miR-499-5p expression at both timepoints, indicating that AntagomiRs are effective and stable in an *in vivo* environment (unpaired t-test, Northern Blot, n=3, 24hpi and 48hpi $p<0.01$, qPCR, n=5, 24hpi and 48hpi $p<0.001$). The miR-499-5p bands on Northern Blots were normalised to U6 and qPCR data was normalised to the expression of other microRNAs, miR-451 and miR-126-3p. These microRNAs were not targeted and showed stable

expression. We have found that detection of U6 by qPCR was inconsistent, especially when using different RNA amounts for cDNA synthesis.

4.3.4 Knockdown confirmation is dependent on extraction method

During our experiments we found that the verification of a successful microRNA-499-5p knockdown using Northern Blot or RT-qPCR is dependent on the chosen RNA extraction method. If the extraction method included TRIzol®, a frequently used and effective solution for RNA extraction (Deng et al., 2005), the knockdown could not be demonstrated by Northern-Blot (Figure 14A, A2) (24hpi, AM-SCR: 1 ± 0.079, AM-499-5p: 2.266 ± 0.281, p<0.05; 48hpi, AM-SCR: 1 ± 0.171, AM-499-

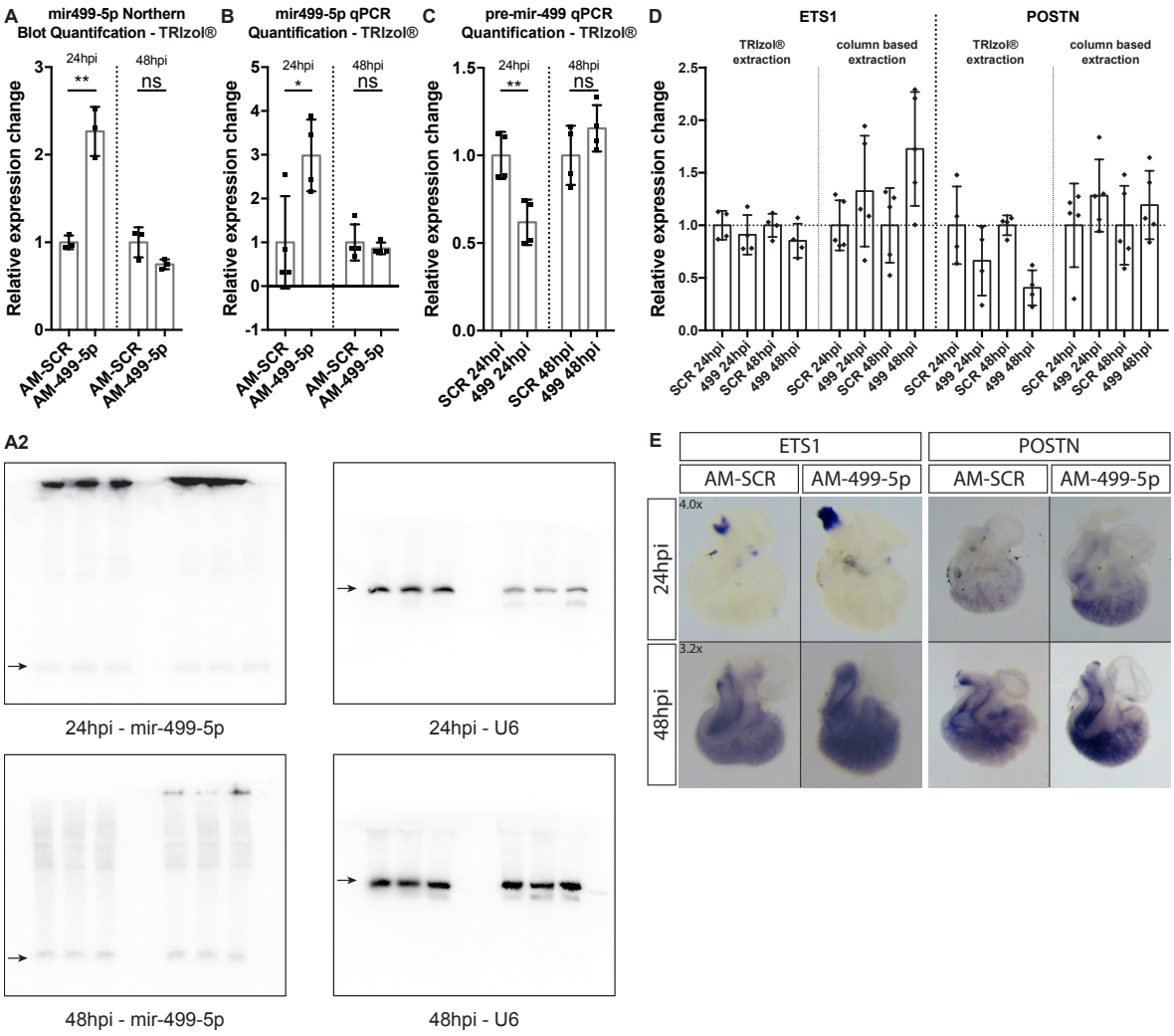

Figure 14: Difference in Results using TRIzol® based RNA extraction

MicroRNA-499-5p knockdown cannot be confirmed using RNA extraction involving TRIzol®. (A) Northern Blot analysis (n=3) shows a significant increase of mircoRNA-499-5p at 24hpi but no significant difference at 48hpi (unpaired t-test, p<0.01; p>0.05) (A2) Northern Blot raw images, three most left lanes AntagomiR-SCR injected samples and three most right lanes Antagomir-499-5p injected samples (arrow indicates mature mir-499-5p band) (B) RT-qPCR analysis confirms Northern blot results (unpaired t-test, 24hpi p<0.05, 48hpi p>0.05, n=4) (C) RT-qPCR quantification of mir-499-5p precursor transcript shows significant reduction at 24hpi but not at 48hpi (unpaired t-test, p<0.01; p>0.05, n=4). (D) Difference in extraction methods expands to RT-qPCR analysis for differentially expressed mRNA's, left *ETS1* expression in TRIzol® samples indicates downtrend whereas in column based extracted samples a clear uptrend is observed. Similar results are shown for Periostin (*POSTN*). (E) ISH analysis indicates derepression of ETS1 and POSTN after 24hpi and 48hpi in miR-499-5p knockdown samples confirming column-based RT-qPCR results.

5p: 0.749 ± 0.056, p>0.05, n=3) and RT-qPCR (Figure 14B) (24hpi, AM-SCR: 1 ± 1.055, AM-499-5p: 2.984 ± 0.820, p<0.05; 48hpi, AM-SCR: 1 ± 0.413, AM-499-5p: 0.863 ± 0.132, p>0.05, n=4). Initially we wondered whether the lack of observable knockdown could be explained by a feedback mechanism, involving the upregulation of miR-499-5p synthesis, however RT-qPCR detection of the longer precursor microRNA in TRIzol® extracted samples did not support this idea (24hpi, AM-SCR: 1 ± 0.135, AM-499-5p: 0.618 ± 0.13, p<0.01; 48hpi, AM-SCR: 1 ± 0.169, AM-499-5p: 1.154 ± 0.133, p>0.05, n=4) (Figure 14C). Another explanation might be, that TRIzol® releases the stable duplex of AntagomiR and microRNA, that had prevented microRNA degradation and thus, more microRNA can be detected in such samples even though microRNA function was inhibited in the treated embryo due to duplex formation. Furthermore, TRIzol® has a known bias regarding GC-content, particularly when extracting microRNAs (Kim et al., 2012). Taking this into consideration, it is preferable to avoid extraction methods that involve TRIzol® when examining microRNAs.

Due to these confounding effects on microRNA analysis we wondered if the observed TRIzol® effect also translates into mRNA analysis. We tested various different candidate genes for which we expected differential expression in the heart after microRNA-499-5p knockdown. Representative RT-qPCR data for *ETS1* and Periostin (*POSTN*) is shown in Figure 14D which reveals opposite trends for differential expression depending on extraction method (Table 15). At present we do not have an explanation for these observed results, but they were reproduced by different researchers within the lab using different sets of biological replicates. Further to this we qualitatively assessed mRNA transcript levels in whole injected hearts by ISH at 24hpi and 48hpi for *ETS1* and *POSTN*. ISH showed for both genes stronger staining after microRNA-499-5p knockdown, indicating increased transcript levels and thus derepression. This confirms the RT-qPCR results obtained from column only extracted RNA samples. Nonetheless, RT-qPCR and ISH results are a not consistent for every gene analysed. For example, *NOTCH1* which shows derepression in knockdown samples of RNAseq and column only based RT-qPCR (Figure 22D) shows the opposite in ISH (Figure 22B) and in knockdown samples of TRIzol® based RT-qPCR (Figure 16O).

Table 15: Extraction methods impact RT-qPCR results

Gene Name	AM-SCR-24hpi		AM-499-5p-24hpi			AM-SCR-48hpi		AM-499-5p-48hpi		
	Mean	SD	Mean	SD	p	Mean	SD	Mean	SD	p
ETS1 – TRIzol®	1	0.137	0.910	0.188	0.469	1	0.110	0.853	0.163	0.185
ETS1 - Column	1	0.239	1.326	0.527	0.244	1	0.356	1.727	0.542	0.036
POSTN - TRIzol®	1	0.370	0.663	0.332	0.223	1	0.095	0.405	0.167	0.001
POSTN - Column	1	0.398	1.283	0.344	0.263	1	0.375	1.193	0.326	0.410

4.4 Functional analysis of target microRNA knockdown *in vivo*

After studying microRNA-499-5p interaction with the *ETS1* 3'UTR and several others it was of interest what effects ablation of the microRNA causes in the chicken heart in regard to physiology and gene expression. Therefore, knockdown studies involving AntagomiRs, using the above introduced cardiac injection method were performed. Antagomirs are chemically synthesized oligonucleotides which are complementary to the microRNA of interest and thus are able to inhibit their biological effect (Krutzfeldt et al., 2005).

During the establishment of the cardiac injection procedure a set of cardiac markers was developed that could be used to analyse the microRNA-499-5p knockdown phenotype. Another aim was to conduct a differential RNAseq experiment to investigate the whole transcriptome, but this required more time for completion. Relevant genes expressed in the heart were selected and ISH probes (Table 8) and RT-qPCR primer pairs (Table 11) for those were designed as tools for the preliminary analysis. As introduced above the primary mode of action for microRNAs in animals is translational repression, therefore measuring RNA levels might not make sense at first sight. Nonetheless, several (reports summarised in (Catalanotto et al., 2016)) have shown that microRNA silencing seems to be a sequential process that is initiated by translational repression and sooner or later followed by mRNA destabilisation/ decay.

4.4.1 Investigating differential expression of cardiac markers prior to RNAseq by ISH

ISH data out of this cardiac marker list was associated with specific topics, pathways or phenotypes and therefore is shown in various sections throughout this thesis (Figure 14E; Figure 20E; Figure 22B, C). Additional ISH data are shown here as starting point for future follow-up experiments and open for discussion.

4.4.1.1 Msh homeobox 1

MSX1 shows a precise staining pattern in the heart. It specifically labels the AVC and the outflow tract (Allen et al., 2001), two locations where septation occurs. Staining at the AVC was detected at both timepoints analysed and became stronger after microRNA-499 knockdown. Further at the later timepoint, 48hpi which is roughly HH24 to HH25 some faint staining in the OFT became apparent (Figure 15).

4.4.1.2 Neuregulin 1

NRG1 is a key factor for ventricular trabeculation where its signalling promotes ECM synthesis in the Myocardium (Del Monte-Nieto et al., 2018). Further NRG1 contributes to the formation of the endocardial cushions via ERBB3 and ERBB4 signalling. Mutation in the NRG1 gene led to Hypoplasia (Lin et al., 2012). In the present ISH *NRG1*s expression is predominantly surrounding the root of the OFT up to the AVC. No expression was detected in the in the ventricular myocardium. Less transcript was detected in the microRNA-499-5p knockdown at both analysed timepoints (Figure 15). These results indicated that *NRG1* is not a direct target of microRNA-499-5p as initially hypothesised by target interaction analysis.

4.4.1.3 Mothers against decapentaplegic homolog 6

SMAD6 is a negative regulator of endothelial-to-mesenchymal transformation during endocardial cushion development. Overexpression of SMAD6 leads to reduced EMT whereas knockout to increased EMT leading to Hypoplasia (Desgrosellier et al., 2005). Expression of *SMAD6* increased after microRNA-499-5p knockdown at 24hpi but stayed relatively consistent at 48hpi. Transcript amounts concentrate in the ventricular region including the AVC and the proximal OFT. Later 48hpi expression diminishes and centres around the proximal OFT (Figure 15).

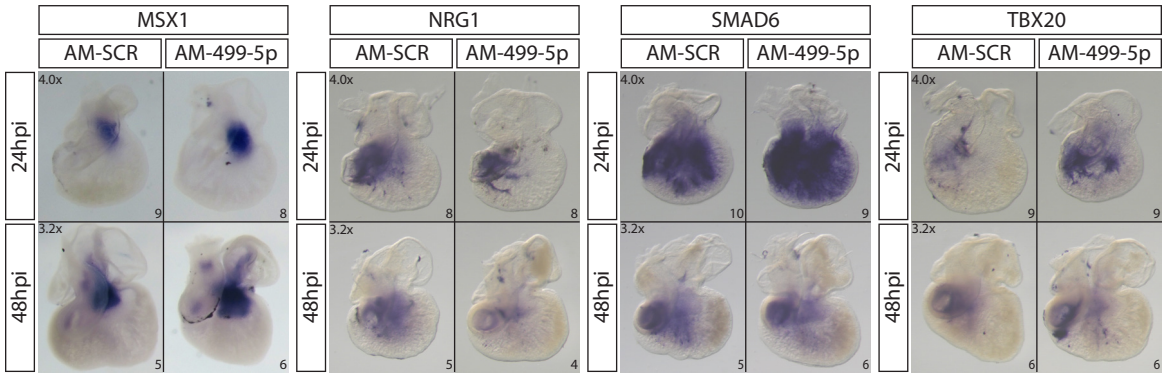

Figure 15: Cardiac marker probes

Shown are ISH reaction on AM-SCR and AM-499-5p injected hearts at 24hpi and 48hpi. MSX1 shows expression at the AVC which increases after microRNA-499-5p knockdown at both analysed timepoints. NRG1 is expressed at the proximal OFT. Its expression reduces at both time points after microRNA-499-5p knockdown. SMAD6 shows global expression at 24hpi which intensifies at 24hpi after knockdown. At 48hpi the expression is more restricted and equal between the conditions. TBX20 shows expression at the proximal OFT up to the AVC. At 24hpi after knockdown more transcript can be detected in contrast to 48hpi where expression seems to be equal between conditions.

4.4.1.4 T-Box gene 20

TBX20 is relevant for chamber specification. It represses *TBX2* expression in the atria and the ventricle and it activates both HEY transcription factors which then can confine the expression of *BMP2* which is essential for AVC specification. In summary TBX20 is a negative regulator of ECM remodelling (MacGrogan et al., 2018a). Interestingly expression was not detected in the atria and in the ventricle only at the junction to the OFT. Overall the ISH indicates an derepression after microRNA-499-5p knockdown at 24hpi and no change in expression at 48hpi (Figure 15).

4.4.2 Differential expression analysis of cardiac markers prior to RNAseq by RT-qPCR based TRIzol® extracted samples

In addition to expression analysis in the heart by ISH we conducted RT-qPCR. Those experiments were exclusively performed before the difference in TRIzol® and non-TRIzol® dependent RNA extraction was detected, which is explained in "4.3.4 Knockdown confirmation is dependent on extraction method", meaning that all experiments in this section involved the former method (TRIzol® mediated extraction).

A large list of genes was investigated at the two earlier time points used in this study, 24hpi and 48hpi. A summary of their differential expression is shown in Figure 16. It is to note that some primers used in the RT-qPCR experiments are not fully optimised and may show multiple TM peaks in a few cases, which indicates lack of target specificity. Such cases are indicated in the chart. A summary of all expression data is found in Table 16.

4.4.2.1 Genes involved in ECM regulation

Several cardiac markers represented members of the ECM. Aggrecan (ACAN) is a proteoglycan which is induced via BMP2 – SOX9 signalling in the heart (Figure 7Ciii). ACAN is bound by HAPLN1 another gene product analysed in this project. Together with hyaluronan, which is synthesized by HAS2 another candidate in this group they ensure structure and stability in the ECM (Lockhart

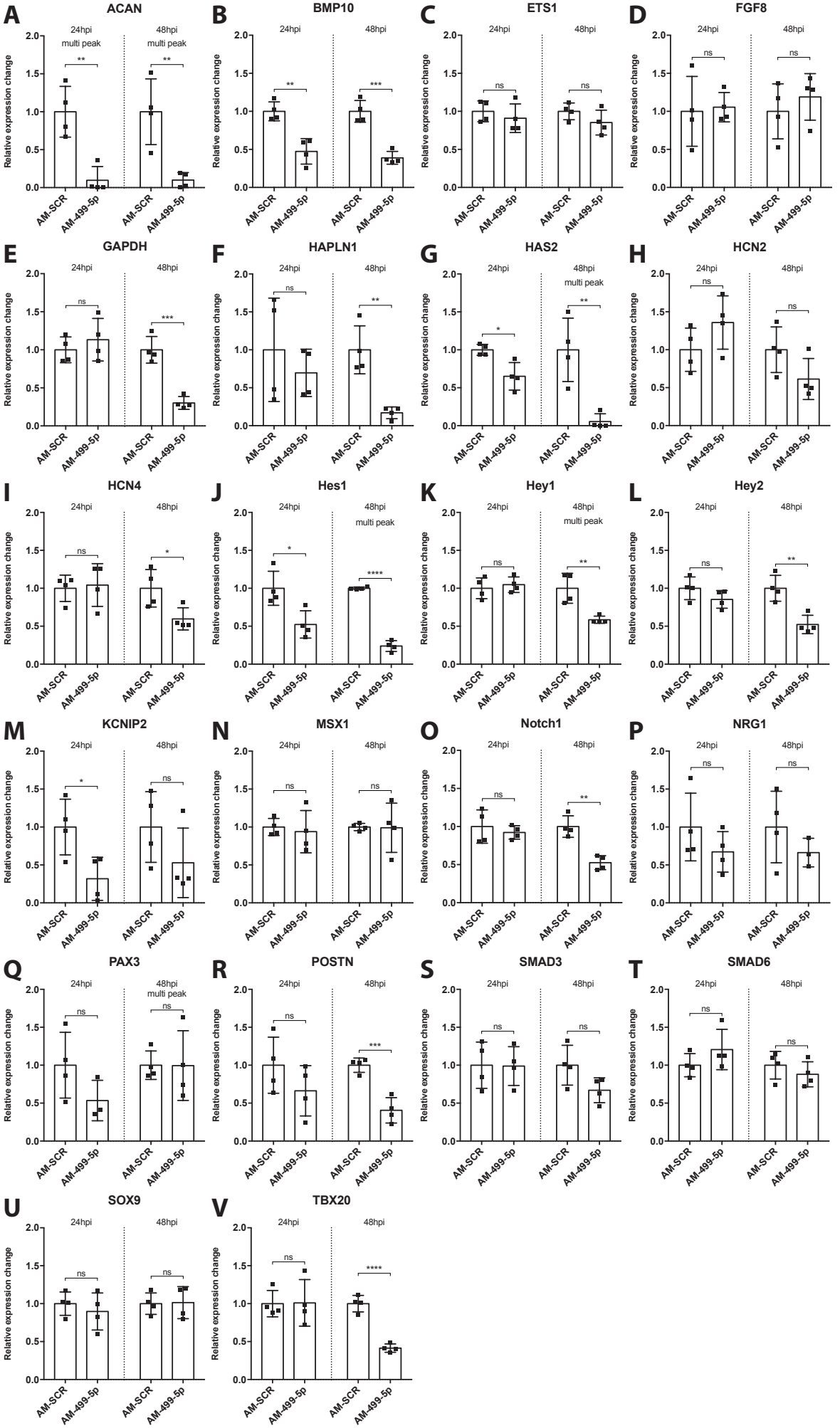
A
ACAN
24hpi
multi peak
48hpi
multi peak
**
**
B
BMP10
24hpi
48hpi
**
***
C
ETS1
24hpi
48hpi
ns
ns
D
FGF8
24hpi
48hpi
ns
ns
E
GAPDH
24hpi
48hpi
ns
***
F
HAPLN1
24hpi
48hpi
ns
**
G
HAS2
24hpi
48hpi
multi peak
*
**
H
HCN2
24hpi
48hpi
ns
ns
I
HCN4
24hpi
48hpi
ns
*
J
Hes1
24hpi
48hpi
multi peak
*
****
K
Hey1
24hpi
48hpi
multi peak
ns
**
L
Hey2
24hpi
48hpi
ns
**
M
KCNIP2
24hpi
48hpi
*
ns
N
MSX1
24hpi
48hpi
ns
ns
O
Notch1
24hpi
48hpi
ns
**
P
NRG1
24hpi
48hpi
ns
ns
Q
PAX3
24hpi
48hpi
multi peak
ns
ns
R
POSTN
24hpi
48hpi
ns
***
S
SMAD3
24hpi
48hpi
ns
ns
T
SMAD6
24hpi
48hpi
ns
ns
U
SOX9
24hpi
48hpi
ns
ns
V
TBX20
24hpi
48hpi
ns
****
Relative expression change
0.0
0.5
1.0
1.5
2.0
AM-SCR
AM-499-5p

Figure 16: RT-qPCR analysis of cardiac markers

Gene expression of cardiac markers was assessed prior to RNAseq by RT-qPCR. Four biological replicates of both conditions per timepoint have been run on a single plate to minimise variation. One outlier each have been removed for NRG1 and PAX3. Assessed genes are: ACAN, BMP10, ETS1, FGF8, GAPDH, HAPLN1, HAS2, HCN2, HCN4, HES1, HEY1, HEY2, KCNIP2, MSX1, NOTCH1, NRG1, PAX3, POSTN, SMAD3, SMAD6, SOX9 and TBX20. For statistical analysis a student's t-test has been performed. Melt curve analysis was performed for all primer pairs at both analysed timepoints and suboptimal peaks (multiple peaks) have been labelled.

et al., 2011). *ACAN* showed significant downregulation within this RT-qPCR analysis and similarly *HAPLN1* and *HAS2* showed a downtrend as well (Figure 16A, F, G) but only significant at the later timepoint 48hpi. Together these results indicate defects in ECM composition after microRNA-499-5p knockdown.

4.4.2.2 Genes involved in NOTCH signalling

Many of the chosen cardiac markers are players within and surrounding the NOTCH pathway. NOTCH signalling is critical for EMT during cushion remodelling but also trabeculation (Del Monte-Nieto et al., 2018, MacGrogan et al., 2018a, MacGrogan et al., 2018b). Luciferase assays indicated that the receptor *NOTCH1* is a direct target of microRNA-499-5p (Figure 10, Appendix 8.1) and therefore derepression should be expected after knockdown. However, the RT-qPCR data showed

Table 16: Expression data of cardiac markers analysed pre RNAseq

Differential expression data of genes expressed in the heart assessed by RT-qPCR on TRIzol® extracted samples.

Gene Name	AM-SCR-24hpi		AM-499-5p-24hpi			AM-SCR-48hpi		AM-499-5p-48hpi		
	Mean	SD	Mean	SD	p	Mean	SD	Mean	SD	p
ACAN	1	0.335	0.097	0.179	0.003	1	0.433	0.100	0.099	0.007
BMP10	1	0.124	0.474	0.167	0.002	1	0.142	0.389	0.084	0.000
ETS1	1	0.137	0.910	0.188	0.468	1	0.110	0.853	0.163	0.185
FGF8	1	0.459	1.054	0.192	0.834	1	0.362	1.190	0.305	0.454
GAPDH	1	0.169	1.132	0.279	0.450	1	0.174	0.302	0.084	0.000
HAPLN1	1	0.682	0.696	0.312	0.449	1	0.316	0.170	0.078	0.002
HAS2	1	0.073	0.651	0.182	0.012	1	0.418	0.055	0.103	0.005
HCN2	1	0.286	1.359	0.352	0.164	1	0.301	0.614	0.271	0.105
HCN4	1	0.173	1.043	0.282	0.804	1	0.247	0.596	0.146	0.031
HES1	1	0.225	0.523	0.180	0.016	1	0.017	0.239	0.071	<0.00001
HEY1	1	0.137	1.048	0.102	0.598	1	0.197	0.586	0.048	0.006
HEY2	1	0.150	0.854	0.116	0.174	1	0.170	0.523	0.122	0.004
KCNIP2	1	0.367	0.318	0.285	0.026	1	0.466	0.528	0.458	0.199
MSX1	1	0.114	0.939	0.279	0.699	1	0.047	0.990	0.324	0.953
NOTCH1	1	0.218	0.923	0.088	0.536	1	0.141	0.525	0.092	0.001
NRG1	1	0.446	0.672	0.267	0.255	1	0.472	0.663	0.188	0.303
PAX3	1	0.433	0.534	0.267	0.165	1	0.187	0.995	0.459	0.983
POSTN	1	0.369	0.663	0.332	0.223	1	0.095	0.405	0.167	0.001
SMAD3	1	0.305	0.989	0.256	0.957	1	0.262	0.670	0.164	0.077
SMAD6	1	0.153	1.206	0.266	0.228	1	0.182	0.880	0.165	0.366
SOX9	1	0.155	0.897	0.244	0.501	1	0.141	1.014	0.211	0.918
TBX20	1	0.174	1.010	0.307	0.956	1	0.109	0.414	0.055	0.000

no change at 24hpi and a significant downtrend at 48hpi. These results are in agreement with ISH data (Figure 22B) discussed at a later point of this study, but in conflict with data retrieved from RNAseq (Figure 22D). The RNAseq was performed on RNA which was extracted without TRIzol®. Consistent with the here shown reduced expression is the downtrend of genes downstream of NOTCH1 such as *HES1*, *HEY1* and *HEY2*. All of those showed a reduction in expression either at both timepoints analysed or at 48hpi (Figure 16J, K, L). *HES1* shows a significant reduction at both timepoints whereas the other two only at 48hpi.

Another downstream target of NOTCH1 in the myocardium is *BMP10* which is relevant for trabeculation (Paige et al., 2015). Expression of *BMP10* also falls in alignment with the here observed downregulation of *NOTCH1*. *BMP10* shows a significant reduction at 24hpi and 48hpi (Figure 16B).

FGF8 expression in the secondary HF myocardium is also downstream of JAG1 dependent NOTCH1. It modulates EMT in adjacent endothelial cells via activation of its secreted factor and its downstream mediator BMP4 (High et al., 2009). In contrast to the other NOTCH1 downstream targets *FGF8* did not show change in expression after microRNA-499-5p knockdown in this RT-qPCR analysis (Figure 16D).

The role of *NRG1* was briefly discussed with the ISH data above (Figure 15), where a subtle reduction was observed. This trend is also reproduced in the RT-qPCR data at both timepoints but did not show significance. Further *TBX20* ISH was also discussed, but in this case the here presented RT-qPCR data shows an opposite trend. No expression change was observed at 24hpi but a significant reduction at 48hpi.

4.4.2.3 Genes involved in cushion maturation and septation

We confirmed *ETS1* as direct target of microRNA-499-5p by luciferase assay and were therefore interested if its expression changes after knockdown. However, the anticipated derepression of ETS1 was not evident (Figure 16C) when assessed by RT-qPCR on TRIzol® extracted samples. Comparing those results with the above mentioned ISH and RT-qPCR data from column extracted RNA (Figure 14D, E) we once more see the differences between the extraction methods. ETS1 is relevant for metalloproteinase induction to regulate ECM and promotes neural crest migration via GATA4 (Gao et al., 2010). A marker for NCC is *PAX3* which showed a downtrend only at 24hpi but overall no significant change in expression (Figure 16Q).

In addition to the ISH data for *MSX1* presented above, this marker was analysed by RT-qPCR which did not confirm the observations from the ISH. Expression values at both 24hpi and 48hpi showed almost equal numbers (Figure 16N).

POSTN shows expression throughout the heart at locations of endocardial cushions and valves and therefore became a target gene of interest (Norris et al., 2004). Expression analysis revealed a reduction after microRNA-499-5p knockdown which is strongly significant at 48hpi (Figure 16R). Once more this data is in contrast to the ISH data shown previously and it is also inconsistent with the RT-qPCR with column based extracted RNA where an increased signal was observed at both timepoints (Figure 14D, E).

SOX9 is relevant in early cushion proliferation and expansion. It's gene product induces the

expression of ACAN a member of the ECM (Figure 7Ciii). The here presented RT-qPCR analysis shows no change in expression (Figure 16U) however an ISH presented later in this study indicated a uptrend at 48hpi (Figure 20E).

Further, two members of the SMAD family are relevant for cushion remodelling. SMAD3 is critical for mediating TGF-β-induced extracellular matrix synthesis and TIMP upregulation (inhibitors of Metalloproteinases) (Dobaczewski et al., 2011). SMAD6 is highly expressed in the cardiac valves and outflow tract of the embryonic heart (Gitler et al., 2003) where it negatively regulates BMP signalling. This process is vital during heart development, as *SMAD6* knockout showed valve defects and aortic ossification (Galvin et al., 2000). *SMAD3* showed a subtle downtrend at 48hpi whereas *SMAD6* showed a subtle uptrend at 24hpi. However, none of these are significant (Figure 16S, T). Even tough insignificant, the *SMAD6* data is in agreement with the previously shown ISH data (Figure 15) where increased signal was observed at 24hpi.

4.4.2.4 Genes involved in Ion transport

As reported above we found that heart rates were not affected by control injections thus suggesting normal cardiac health after the procedure. However, knockdown of microRNA-499-5p does affect heart rate (see below Figure 21A). Therefore, we examined the expression of ion channel changes which could potentially affect the frequency of heart beats. In addition to the most relevant ion channels in the heart HCN2 and HCN4 (Zhao and Gu, 2016) we have analysed KCNIP2. The data shows that their expression is quite variable among replicates but overall a decreasing trend is observed in this analysis (Figure 16H, I, M). *KCNIP2* shows significant reduction at 24hpi but not at 48hpi. *HCN2s* expression change is insignificant at both timepoints and *HCN4* shows only significance at 48hpi. All together these results do not indicate a direct target interaction of microRNA-499-5p with the above genes 3'UTRs.

In conclusion the cardiac marker analysis showed that the majority of the selected cardiac marker genes are differentially expressed. Unfortunately, the conflicting observations between ISH analysis and RT-qPCR make interpretation challenging. Some of the trends seem logical like the reduced expression of NOTCH downstream targets together with the receptor itself, however, this is in conflict with *NOTCH1* being a direct target for microRNA-499-5p. Other results like the *MSX1* ISH and RT-qPCR are also highly contradicting. Furthermore, the previously described impact of the RNA extraction method on RT-qPCR results complicates this analysis further. Some of the data shown later in this report from RNAseq and RT-qPCR of column extracted RNA illustrates different outcomes after microRNA-499-5p knockdown. Therefore, further evidence is required before making conclusions.

4.4.3 RNAseq analysis to assess differential expression in miR-499-5p ablated hearts

In order to identify genome-wide effects of microRNA-499-5p knockdown we performed differential transcriptomics. This would also provide additional candidate target genes. Chicken embryos were injected at HH14-15 and incubated for 24- and 48-hours post injection. Subsequently embryos were dissected, and hearts excised, pooled (six for 24hpi and three for 48hpi) and snap frozen in liquid nitrogen. Once all samples were collected RNA was extracted under identical conditions and stored at -80°C. The sample setup for RNA sequencing included five biological

Table 17: RNAseq sample information

The sample submission for RNAseq contained 16 samples, four of each group, which were AM-SCR and AM-499-5p injected hearts at 24hpi and 48hpi. RNA concentrations and associated ODs for purity are listed below.

Sample Name	Concentration (ng/µl)	Vol (µl)	Note	Total Amount (ng)	Tube Qty	Pre-QC Method	OD 260/280	OD 260/230
A	274.2	25	499-48	6855.0	1	nano	2.09	2.30
B	282	25	499-48	7050.0	1	nano	2.09	2.31
C	259.2	25	499-48	6480.0	1	nano	2.09	2.32
E	289.7	25	499-48	7242.5	1	nano	2.09	2.30
F	312.1	25	SCR48	7802.5	1	nano	2.10	2.27
G	216.2	25	SCR48	5405.0	1	nano	2.09	2.19
H	264.6	25	SCR48	6615.0	1	nano	2.10	2.32
J	250.8	25	SCR48	6270.0	1	nano	2.10	2.26
K	228.4	25	499-24	5710.0	1	nano	2.10	2.30
L	235.4	25	499-24	5885.0	1	nano	2.10	2.29
M	224.6	25	499-24	5615.0	1	nano	2.09	2.32
N	210.4	25	499-24	5260.0	1	nano	2.09	2.31
P	190.3	25	SCR24	4757.5	1	nano	2.09	2.25
R	344.1	25	SCR24	8602.5	1	nano	2.11	2.28
S	224.5	25	SCR24	5612.5	1	nano	2.10	2.28
T	225.9	25	SCR24	5647.5	1	nano	2.09	2.19

replicates of each group, which were AM-SCR injected and AM-499-5p injected hearts at 24hpi and 48hpi, resulting in 20 samples. Prior to sample submission for RNAseq microRNA-499-5p knockdown was confirmed by RT-qPCR (24hpi & 48hpi $p<0.01$) (Figure 13C). After quality assessment of RNA quality four samples of each group were selected for submission as RNA on dry ice to Novogene Co., Ltd in Hongkong (16 samples in total). A summary of submitted samples is listed in the following table including their respective quality assessment values by NanoDrop (Table 17).

Novogene Co., Ltd carried out all steps necessary to gain sequencing information for the submitted samples. The included steps are visualised in Figure 17, where panel A describes the general workflow and B how the individual mRNAs are processed to gain cDNA libraries ready for sequencing.

Obtained data from sequencing of the cDNA libraries was quantified with kallisto (Bray et al., 2016) and further processed with Sleuth (Pimentel et al., 2017). Differential expression was calculated for both timepoints (24hpi and 48hpi) and cutoff at $p<0.05$, the resulting data was used to generate a Venn diagram (Figure 18B). The intersection has further been used to generate a differential expression heat map of known transcripts using a fold change cutoff of 0.75, differentially expressed transcripts were identified, 78 of which were upregulated and 168 downregulated in hearts injected with AntagomiR-499-5p (Figure 18A). Further GO Term enrichment has been performed which revealed changes in neural crest and mesenchyme related processes which are both highly important during cushion development and maturation.

Inhibition of microRNA function should lead to increased expression of direct interaction targets, which have a binding site present in their 3'UTR. Still other genes harbouring no binding site in their UTRs might be repressed or derepressed as well due to secondary signalling effects. Among the

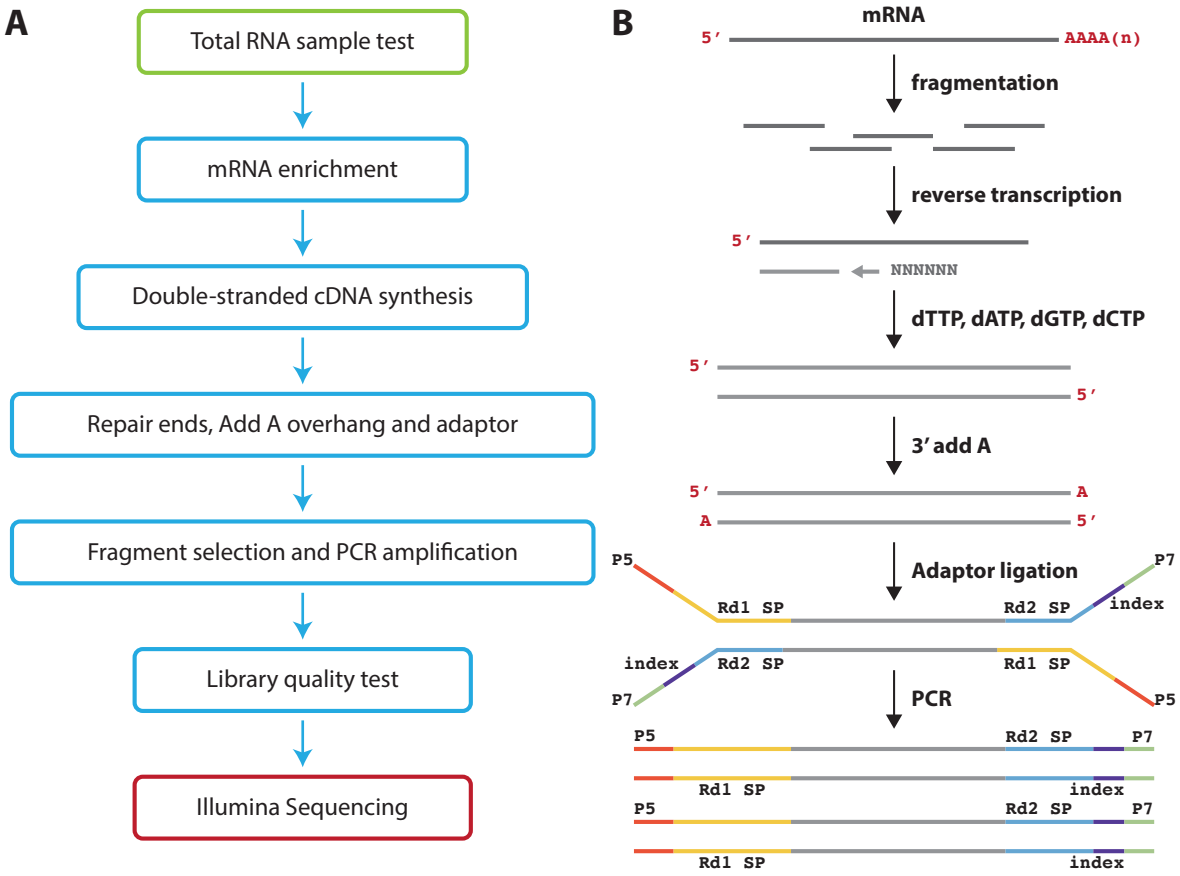

Figure 17: Novogene Co., Ltd RNAseq workflow

(A) Flow chart depicting the steps Novogene Co., Ltd carried out after receiving the RNAseq samples in Hongkong. To guarantee the reliability of the data, quality control was performed at each step of the procedure (B) After the QC procedures, mRNA from eukaryotic organisms is enriched using oligo(dT) beads. Non-coding libraries, rRNA is removed using the Ribo-Zero kit that leaves the mRNA. First, the mRNA is fragmented randomly by adding fragmentation buffer, then the cDNA is synthesized by using mRNA template and random hexamers primer, after which a custom second-strand synthesis buffer (Illumina), dNTPs, RNase H and DNA polymerase I are added to initiate the second-strand synthesis. Second, after a series of terminal repair,A ligation and sequencing adaptor ligation, the double-stranded cDNA library is completed through size selection and PCR enrichment (Information from Novogene Co., Ltd).

derepressed genes were ECM components and regulators as *ACAN*, *HAPLN1* and *MATN4*, a variety of collagens *COL11A1, COL9A1* and *COL9A3* and genes involved in cushion maturation, such as *TWIST1*, *WNT11* and Tenascin C (*TNC*). From the RNAseq data we have focussed on genes involved in ECM regulation and NOTCH signalling. Nonetheless many other differentially expressed genes have been identified (Figure 18A) which need further follow up experiments to determine their role in microRNA-499-5p mediate signalling.

Out of the top scoring genes within the heat map (Figure 18A) only *HAPLN1* has been assessed by luciferase assay (Figure 10C, Appendix 8.1) prior to RNAseq. Nonetheless it was of interested if the predicted targets showed derepression in the differential expression data. The majority of predicted targets showed the expected derepression in the differential expression data, but not all of them. We also noticed that the 24hpi timepoint showed consistently less variation than the later 48hpi timepoint (Figure 19). One of the primary candidates of this study, *ETS1* showed the strongest derepression among all candidates for its second transcript but also significant derepression for its first transcript at 24hpi (Table 18). Noteworthy in this case though is the absolute transcript number

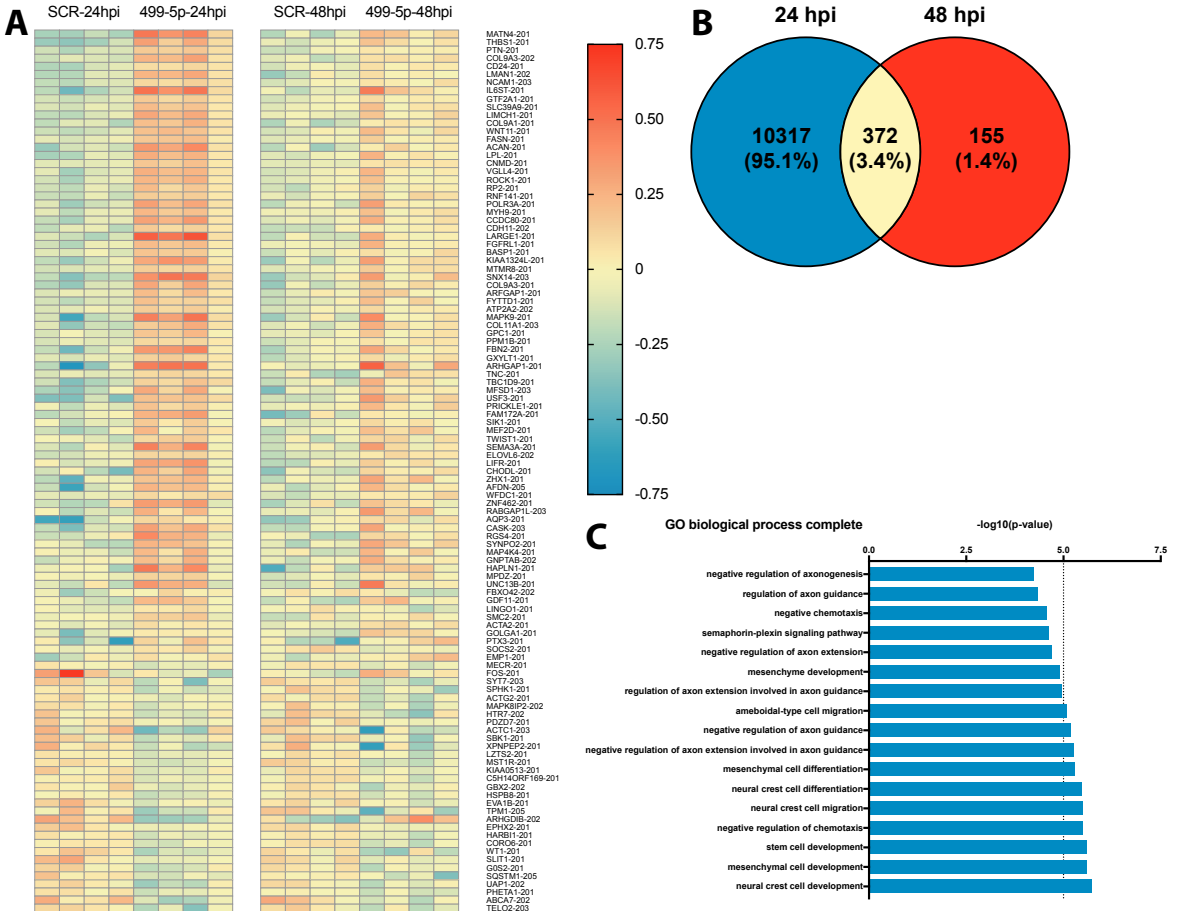

Figure 18: RNAseq AM-SCR vs AM-499-5p at 24 and 48hpi

RNAseq was performed on AM-SCR and AM-499-5p injected chicken hearts 24- and 48-hours post injection. (A) Heatmap shows differentially expressed transcripts from intersection of 24hpi and 48hpi. (B) Venn diagram showing number of differentially expressed transcripts $p<0.05$ at the two time points and their intersection. (C) Graphical representation of "GO biological process complete" analysis of Venn intersection using Panther Overrepresentation Test.

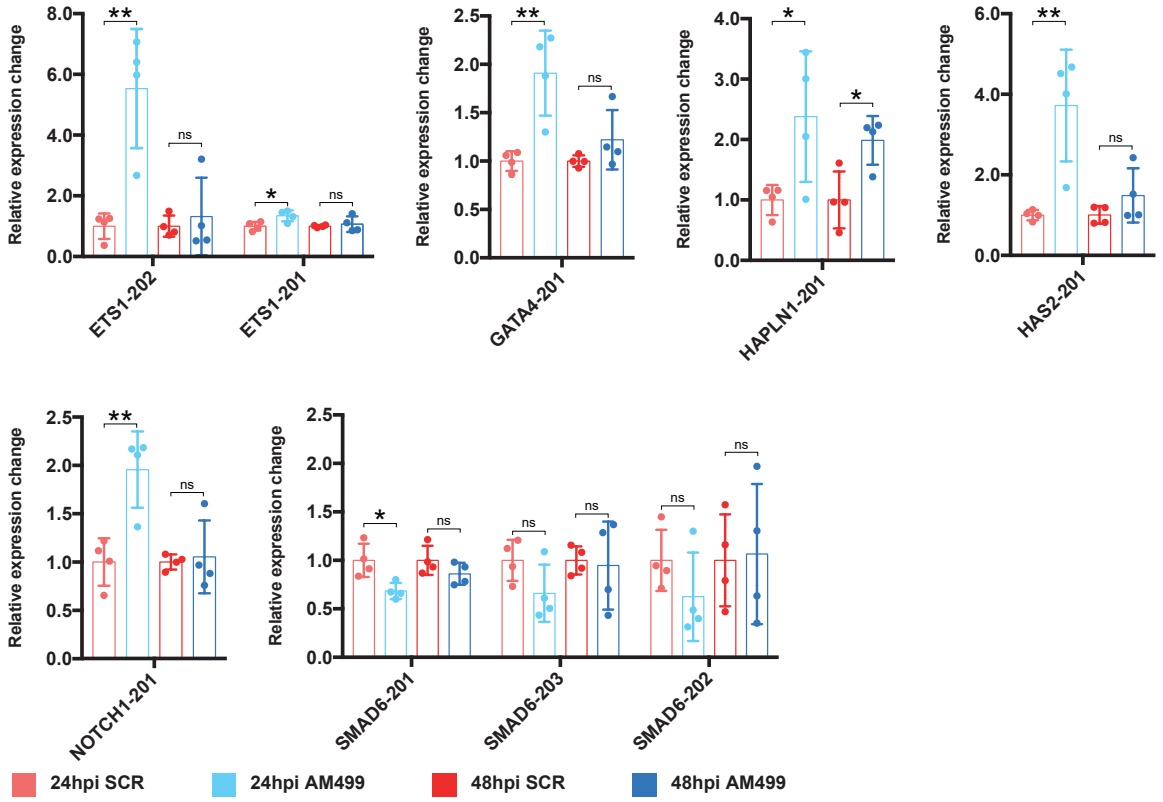

Figure 19: Differential gene expression of Luciferase assayed target candidates

Differential expression data for candidate target gene transcripts previously analysed by Luciferase reporter assays has been extracted for comparison. The RNAseq data was consistent with the Luciferase assay results for ETS1, HAPLN1, HAS2 and NOTCH1. For GATA4 no target interaction could be shown in Luciferase assay, RNAseq however shows upregulation. SMAD6 could be confirmed in Luciferase assays, RNAseq however shows opposite trend from what would be expected for a direct target gene. N=4; unpaired t-test: ** $p<0.01$; * $p<0.05$.

which seems to be relatively small compared to other candidates. Unfortunately, the different roles of *ETS1* transcript isoforms are not yet known, therefore it is unclear what the derepression of its second transcript means. Interestingly, *GATA4* which was invalidated by luciferase assay (Figure 10C, Appendix 8.1) showed a nearly 2-fold derepression at 24hpi in the RNAseq data (Table 18). A potential explanation could reside in the length of the cloned UTR fragment, which might not have harboured the biologically active interaction site. Annotation of 3'UTR for gallus gallus is incomplete and future updates might reveal longer 3'UTRs. The third gene assayed *HAPLN1* is the only one included in the list of top targets. Further it is the only one among the candidates that shows significant derepression at both timepoints 24hpi and 48hpi (Table 18). HAPLN1 as well as the next target HAS2 are important members of the ECM. HAPLN1 delivers structure by bridging hyaluronan and Aggrecan whereas HAS2 synthesises hyaluronan. MicroRNA-499-5p showed target interaction in luciferase assay with the *HAS2* 3'UTR (Figure 10C, Appendix 8.1), but signal depression could not be recovered by mutation therefore the exact site of target interaction was not identified. RNAseq differential expression data confirms the derepression after microRNA-499-5p knockdown (Table 18). The next target in the list is *NOTCH1* which is of major importance for EMT in the endocardial cushions. Target interaction was confirmed (Figure 10C, Appendix 8.1) and RNAseq also showed derepression at 24hpi (Table 18). The last candidate was *SMAD6* which showed luciferase repression in the *in vitro* assay (Figure 10C, Appendix 8.1). However, RNAseq was not consistent with

Table 18: Differential gene expression of Luciferase assayed target candidates

Differential expression data of normalised transcript counts to median of experimental group.

Transcript	AM-SCR-24hpi		AM-499-5p-24hpi			AM-SCR-48hpi		AM-499-5p-48hpi			Transcript Counts	
	Mean	SD	Mean	SD	p	Mean	SD	Mean	SD	p	Median 24hpi	Median 48hpi
ETS1-202	1	0.422	5.533	1.959	0.004	1	0.348	1.321	1.278	0.645	23.63	44.56
ETS1-201	1	0.144	1.342	0.182	0.026	1	0.037	1.067	0.257	0.624	396.00	427.98
GATA4-201	1	0.101	1.909	0.439	0.007	1	0.060	1.220	0.307	0.210	2836.72	3618.89
HAPLN1-201	1	0.249	2.378	1.080	0.047	1	0.471	1.986	0.404	0.019	44.44	34.69
HAS2-201	1	0.128	3.722	1.388	0.008	1	0.221	1.487	0.673	0.218	86.98	107.24
NOTCH1-201	1	0.246	1.956	0.395	0.006	1	0.078	1.053	0.377	0.791	3449.87	4940.17
SMAD6-201	1	0.172	0.684	0.084	0.016	1	0.150	0.861	0.113	0.189	39038.36	32793.14
SMAD6-203	1	0.212	0.660	0.295	0.110	1	0.145	0.947	0.454	0.831	176.80	213.01
SMAD6-202	1	0.315	0.625	0.456	0.225	1	0.475	1.065	0.724	0.885	34.94	41.98

this as it showed reduction for all three detected transcripts after microRNA-499-5p knockdown. This may indicate the possibility for compensating signalling cascades *in vivo* compared to the *in vitro* assay. Interestingly *SMAD6* showed the strongest expression among the candidates (Table 18). In summary, out of the six predicted 3'UTR target interaction sites by bioinformatic tools 4 of them where identified by luciferase assay and five of them showed expected derepression *in vivo* in the chicken heart.

4.4.4 MicroRNA-499-5p knockdown promotes ECM deposition

In addition to RNAseq experiments injected hearts were analysed for changes in morphology. Whole hearts did not indicate obvious differences in volume or mass. Therefore, hearts were embedded and sectioned. To compare sections of AM-SCR and AM-499-5p injected hearts they were stained for H/E (Figure 20A, left panel). Again, no striking morphological defects could be observed by comparing AM-SCR sections against AM-499-5p sections (data not shown). The endocardial cushions are primarily composed of ECM as described above, so we decided to segment the area of the ECM in all sections of each single heart (around 75-100 sections at 20µm per heart) to detect more subtle differences in the 3D context of the heart. Fiji software was used to align sections (TrackEM2) and segment ECM areas (Segmentation Editor) (Figure 20A middle and right panel). Processing of all sections of a single heart (loss <3%, interpolated by Fiji) also allowed 3D volume reconstruction of the heart with its respective ECM labelled (Figure 20B). Next, the ECM volumes per section were calculated and summed up for each heart to acquire heart specific total ECM volumes (Figure 20C). This data indicated a trend in which AM-499-5p injected hearts have larger amounts of ECM compared to AM-SCR injected hearts (72hpi, AM-SCR: 0.323 ± 0.035 mm^3, n=4; AM-499-5p: 0.337 ± 0.028 mm^3, n=8, unpaired students t-test p>0.05), although further replicates are necessary for better statistical evaluation.

Overall this trend was consistent with RNAseq results, which showed among the top targets of the intersection of 24hpi and 48hpi hearts various genes commonly expressed in the ECM (Figure 18A). The majority of those ECM genes were upregulated, underpinning the above observed trend of ECM volume increase. Specifically, among the ECM related genes where *ACAN*, *VCAN*,

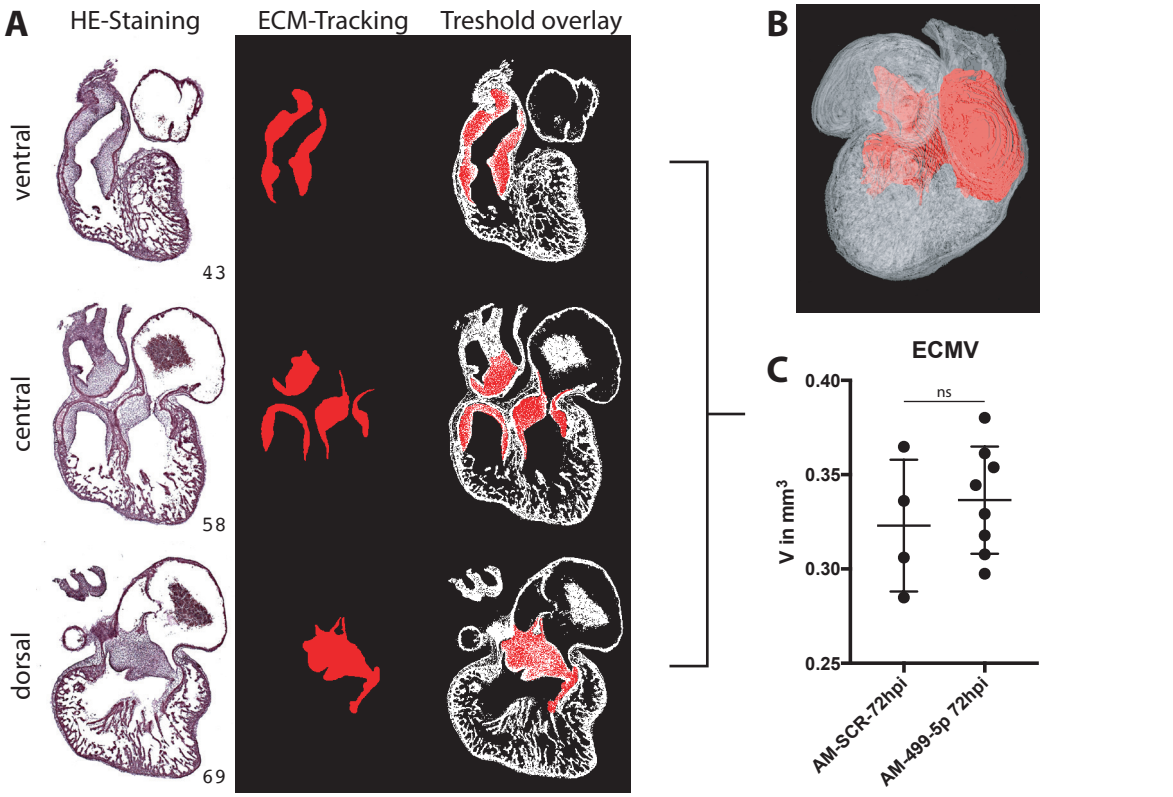
A
HE-Staining
ECM-Tracking
Treshold overlay
ventral
central
dorsal
43
58
69
B
C
ECMV
ns
V in mm³
0.40
0.35
0.30
0.25
AM-SCR-72hpi
AM-499-5p 72hpi

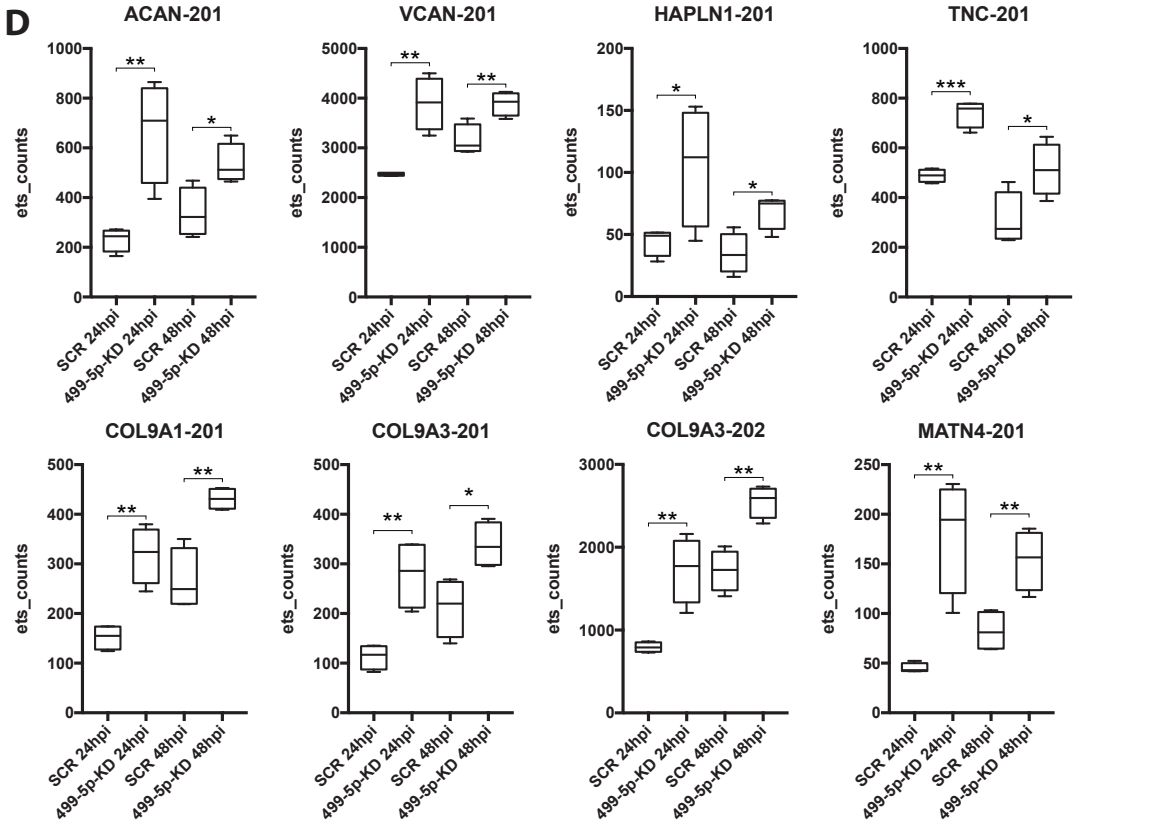
D
ACAN-201
VCAN-201
HAPLN1-201
TNC-201
COL9A1-201
COL9A3-201
COL9A3-202
MATN4-201
ets_counts
SCR 24hpi
499-5p-KD 24hpi
SCR 48hpi
499-5p-KD 48hpi

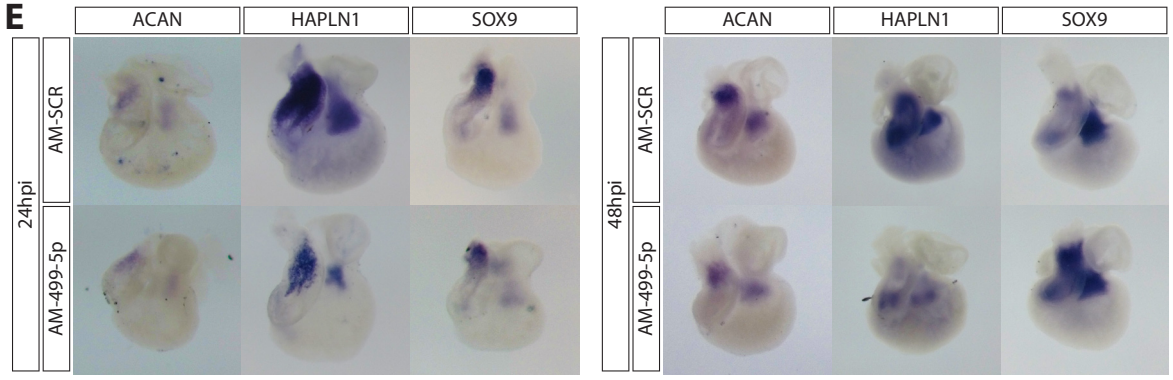
E
ACAN
HAPLN1
SOX9
24hpi
48hpi
AM-SCR
AM-499-5p

Figure 20: ECM volume increases with microRNA-499-5p inhibition

Knockdown of microRNA-499-5p leads to an increase in cardiac ECM volume as well as modulation of various ECM relevant genes. (A) Representative sections of the heart showing the different shapes of ECM areas within the heart. Left panel H/E staining (number corresponds to section of 75-100), middle panel segmented ECM area, right panel overlay of threshold and segmented area. (B) Representative 3D volume rendering of reconstructed heart from sections. (C) Quantification of volume of segmented areas shows difference in AM-SCR and AM-499-5p injected chick hearts. (D) Top targets of RNAseq intersecting 24hpi and 48hpi show many ECM proteins upregulated. (E) ISH for ACAN and HAPLN1 are not consistent with RNAseq data. SOX9 shows downregulation at 24hpi and upregulation at 48hpi in the miR-499-5p knockdown samples.

HAPLN1, *TNC*, Collagen 9A1 and 9A3 (*COL9A1* and *COL9A3*) and Matrilin 4 (*MATN4*). All of those showed significant derepression after microRNA-499-5p knockdown at both timepoints of analysis (Figure 20D and Table 19).

Prior to RNA sequencing several ISH probes have been generated as cardiac markers for the analysis of the microRNA-499-5p knockdown. Three of the available probes detect gene transcripts related to the ECM namely *ACAN*, *HAPLN1* and *SOX9*. Interestingly ISH with the former two probes showed contrasting results when compared to RNAseq results (Figure 20E). *ACAN* shows nearly no change in expression at 24hpi and a subtle down regulation at 48hpi whereas RNAseq shows a strong increase at both timepoints. Similarly, ISH analysis for *HAPLN1* shows an easily visible reduction for both timepoints but a rather strong increase within the RNAseq data (Figure 20D, E). The third gene *SOX9* is relevant for specification in the endocardial cushions as introduced above. Qualitative analysis by ISH showed comparable expression levels at 24hpi for both conditions and an increase at 48hpi particularly in the OFT. *SOX9* was not a top differentially expressed gene in the RNAseq analysis nonetheless the data showed a trend suggesting derepression at both time points analysed (24hpi, AM-SCR: 339.92 ± 123.50, AM-499-5p: 1367.86 ± 430.86; 48hpi, AM-SCR: 586.03 ± 126.26, AM-499-5p: 748.66 ± 393.41, n=4, transcript numbers) thus consistent with the ISH analysis at 48hpi but not at 24hpi.

As described earlier in this thesis (4.3.4 Knockdown confirmation is dependent on extraction method) differences have been observed when comparing ISH results and RNAseq/RT-qPCR depending on the chosen RNA extraction method. This makes the interpretation of the results challenging and inconclusive, in particular with regards to the potential role of microRNA-499-5p in ECM remodelling and in posttranscriptional regulation of ECM related genes within the heart. Overall the 3D morphology analysis indicates an increase in ECM volume which is in agreement with

Table 19: Differential gene expression of ECM related genes from top targets of RNAseq

Differential expression data of transcript counts

Transcript	AM-SCR-24hpi		AM-499-5p-24hpi			AM-SCR-48hpi		AM-499-5p-48hpi		
	Mean	SD	Mean	SD	p	Mean	SD	Mean	SD	p
ACAN-201	231.61	46.80	669.63	202.73	0.0056	338.58	97.92	534.35	80.00	0.0212
VCAN-201	2471.59	33.88	3893.39	528.23	0.0017	3152.48	304.04	3891.63	235.16	0.0085
HAPLN1-201	44.44	11.05	105.67	48.01	0.0474	34.69	16.35	68.92	14.01	0.0191
TNC-201	488.43	25.19	739.21	54.17	0.0002	309.98	105.74	512.94	105.47	0.0347
COL9A1-201	152.13	25.18	318.17	56.64	0.0017	266.87	61.49	431.15	21.41	0.0023
COL9A3-201	112.90	25.23	278.79	69.49	0.0042	212.04	58.36	338.59	45.69	0.0142

RNAseq transcriptomics data. However, the qualitative data obtained by ISH are not consistent with the volume measurements or the RNAseq. To summarise these observations, we can say that the physical increase of the ECM volume is interesting although it requires further replication for more convincing statistical evaluation. Gene expression analysis by RNAseq and ISH showed opposing results therefore it is not possible yet to determine the exact source for the ECM trend and further experiments need to be conducted.

4.4.5 MicroRNA-499-5p knockdown slows down heart beat

During the establishment of the cardiac injection procedure the assessment of heart rates became a useful tool for determining effects of the procedure on cardiac health. The same technique proved to be useful for analysing microRNA-499-5p's contribution to heart rate control.

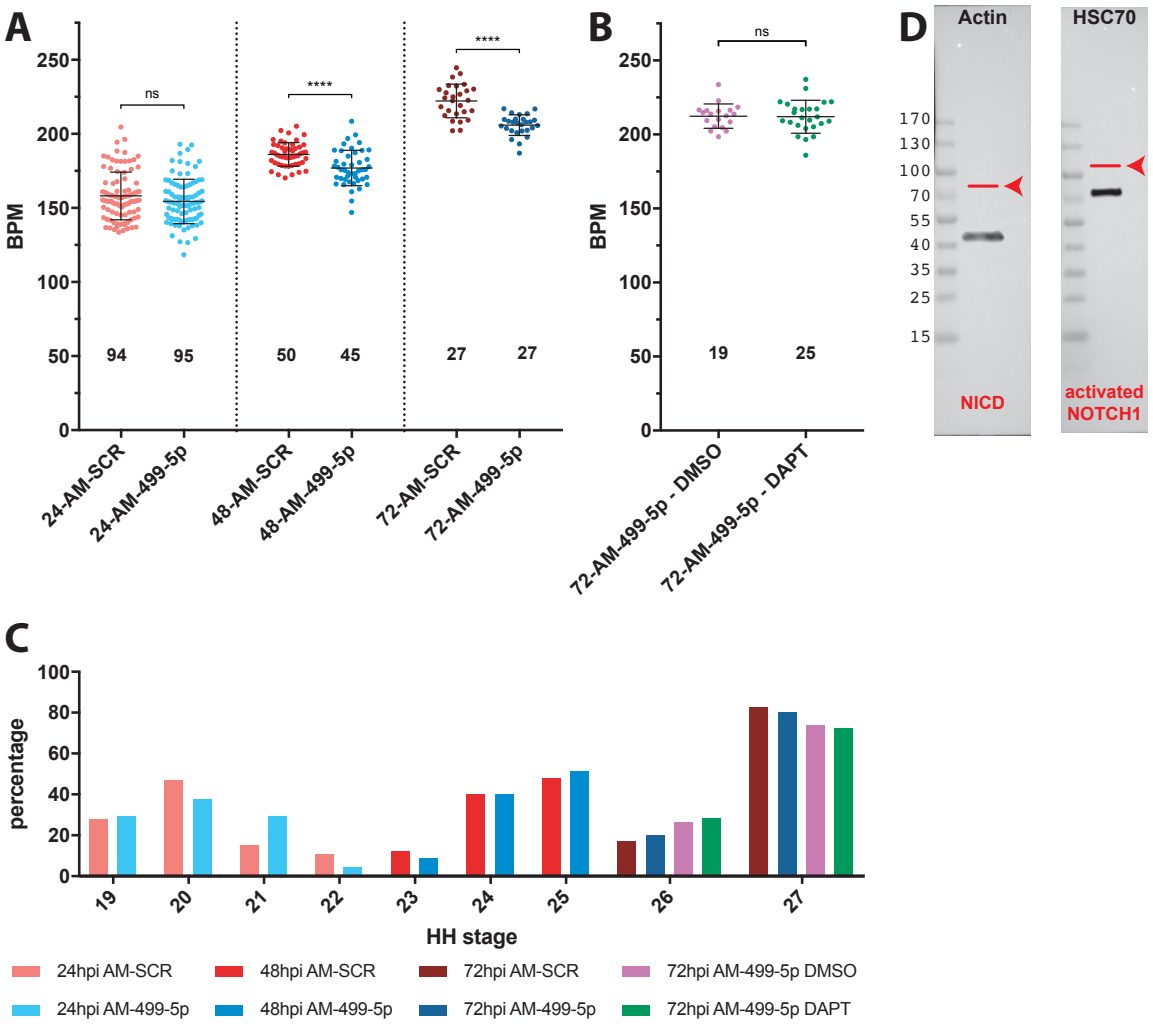

Figure 21: AM-499-5p knockdown impacts heart rate

Knockdown of microRNA-499-5p slows down heartbeat. (A) Heart rates were quantified at 24hpi, 48hpi, and 72hpi which shows an increase with developmental progress. Comparison between treatments reveals a reduction in heart rate after microRNA-499-5p knockdown, which becomes more severe at later timepoints and is significant at 48hpi and 72hpi (students t-test, n depicted below scatter blot). (B) Inhibition of the NOTCH pathway by 5μM DAPT was expected to recover heart rate phenotype but could not be shown at 72hpi (students t-test $p>0.05$, n depicted below scatter blot). (C) Heart rate analysis is dependent on equally developed chicken embryos. Chart shows equal age distribution for 48hpi and 72hpi as well as DMSO/DAPT conditions but not for 24hpi experiments. (D) Confirmation of inhibition of NOTCH signalling was unsuccessful and only loading controls (Actin and HSC70) were detected. Arrow head and red line show predicted size of NICD and activated NOTCH1 respectively.

Embryos injected with AM-SCR and AM-499-5p have been subjected to heart quantification at the three chosen timepoints within this study, 24hpi, 48hpi and 72hpi. The data obtained revealed a reduction in heart rate after AM-499-5p injection compared to AM-SCR injection (Figure 21A) (24hpi, AM-SCR: 158.10 ± 16.11 n=94, AM-499-5p: 154.4 ± 14.99 n=95, p>0.05; 48hpi, AM-SCR: 186.10 ± 8.00 n=50, AM-499-5p: 177.00 ± 11.97 n=45, p<0.0001; 72hpi, AM-SCR: 222.20 ± 11.38 n=27, AM-499-5p: 205.90 ± 6.95 n=27, p<0.0001). This reduction became more pronounced with rising age. At 24hpi the difference is subtle (-3.76 ± 2.26 BPM) but becomes significant at the following time points at 48hpi (-9.08 ± 2.07 BPM) and at 72hpi (-16.31 ± 2.57 BPM). Further to the observed heart rate reduction the data clearly shows an increase of heart rate with rising age regardless of the injected compound. This points out that to appropriately compare heart rates it is necessary to align the actual developmental stage of the analysed embryos. Because the rate of development can vary between embryos, the chosen time points of 24hpi, 48hpi and 72hpi do not reflect the actual developmental stage of chicken embryos. Development of chick embryos is not always consistent and can be affected by season, flock and other factors. Thus accurate comparisons required the identification of the developmental stages of the analysed chicken hearts according to (Hamburger and Hamilton, 1951). Figure 21C shows such an alignment and reveals that there is an equal distribution at the 48hpi and 72hpi time points between the conditions but not at 24hpi. More precisely it shows that the AM-499-5p injected group contains a larger proportion of more developed embryos in comparison to AM-SCR injected ones. This means that any reduction caused by the AM-499-5p injection may have been masked because the heart rate was higher in this group of embryos. Therefore, it is possible that the actual heart rate reduction at 24hpi may be stronger than the data shown here reveals.

Based on published literature reports NOTCH1 is a potential regulator of heart rate. One study showed that overexpression of *NOTCH1* in mice led to a reduction in heart rate (Bhatnagar et al., 2016) whereas another study using induced cardiac-like myocytes from mouse embryonic fibroblasts showed that NOTCH1 inhibition induces cardiac specification via Myocyte Enhancer Factor 2C (MEF2C) which results in beating cardiac cells (Abad et al., 2017). Inspired by these two studies and the observed effects on of microRNA-499-5p on *NOTCH1* in luciferase assay experiments and RNAseq we decided to perform cardiac injections with AM-499-5p and the NOTCH inhibitor DAPT. This was done to test the hypothesis that *NOTCH* derepression was the major cause of the reduced heart rate observed. DAPT is best soluble in DMSO and barely in water, the solvent used for AntagomiRs. Initially experiments used equal doses of AntagomiR (water) and DMSO (50%) for better solubility of DAPT. This led to complete inactivation of AM-499-5p and heart rates were similar to AM-SCR injected hearts (data not shown). We than assessed minimal solubility of DAPT in DMSO and chose AM-499-5p in 10% DMSO as our control and AM-499-5p in 10% DMSO with 5µM DAPT as our treatment condition. Investigations were done only at 72hpi because at that time point previously observed differences were the biggest. Unfortunately, no rescue could be observed and heart rates quantified for both conditions (Figure 21B) showed no significant differences between each other and averaged nearly identical (72hpi, AM-499-5p-10%DMSO: 212.40 ± 8.19, n=19; AM-499-5p-10%DMSO/ 5µM DAPT: 212.00 ± 11.10, n=25, p>0.05). This means that rescuing the heart rate phenotype using DAPT was not possible. Furthermore, we were not able to confirm successful NOTCH1 inhibition after DAPT injection. Western Blots have been conducted using two different

antibodies predicted to work with chick protein against activated NOTCH1 (Table 12) and NOTCH intracellular domain (NICD) (Table 12) but these did not cross react with the respective chick protein in our hands. However, loading controls (Actin, HSC70, Table 12) showed successful execution of the Western Blotting technique (Figure 21D). Taken together this negative data does not yet exclude NOTCH1 signalling as root for the differences in heart rate. Using a different NOTCH inhibitor might offer an alternative or finding a better solution to demonstrate effects on NOTCH signalling are key to progress with these experiments.

4.4.5.1 Identifying a pathway related to heart rate

As already mentioned above a connection between NOTCH signalling and affected heart rates was previously reported in literature (Abad et al., 2017, Bhatnagar et al., 2016). Even though we were not able to recover the heart rate phenotype by NOTCH inhibition via DAPT administration, we investigated further downstream of NOTCH1. In particular we had a look at the pathway described by Abad et al. (2017), which places NICD as an inhibitor of MEF2C signalling. In this context NICD prevents MEF2C from binding promoter regions of genes like *MYH6*, *TNNT2* and *ACTC1*. An expanded version of this pathway where microRNA-499-p is placed in this context is depicted in Figure 22A. To gain a better profile of signalling components we looked at expression of NOTCH1 by ISH, RT-qPCR and RNAseq. Unfortunately, as previously observed results are not strictly in alignment. ISH showed a reduction of NOTCH1 expression, which is contrasting (Figure 22A) to our previously reported luciferase assay results where NOTCH1 was confirmed as a direct target of microRNA-499-5p (Figure 10C, Appendix 8.1). Integrity of the probe was confirmed by sequencing prior to probe synthesis and the expression pattern shown, particularly in the sections which shows predominant expression in the Endocardium confirms NOTCH1 identity. Even though at different timepoints both quantitative methods RT-qPCR and RNAseq indicate derepression of NOTCH1 transcript after microRNA-499-5p knockdown in contrast to ISH (Figure 22D). Further to receptor availability we had a look at NOTCH1 activating ligands *JAG1* and *DLL4* within our RNAseq data set (Figure 22E). *JAG1* shows an uptrend at both analysed timepoints but only significant at 24hpi. *DLL4* similarly indicates derepression at 24hpi but no change at 48hpi. However, significance is not achieved at any timepoint (Table 20).

Table 20: Differential gene expression of players within a NOTCH – MEF2C signalling cascade

Differential expression data of transcript counts

Gene Name	AM-SCR-24hpi		AM-499-5p-24hpi			AM-SCR-48hpi		AM-499-5p-48hpi		
	Mean	SD	Mean	SD	p	Mean	SD	Mean	SD	p
NOTCH1 (RT-qPCR)	1	0.386	1.025	0.417	0.924	1	0.229	1.550	0.324	0.015
NOTCH1-201	1	0.246	1.956	0.395	0.006	1	0.078	1.053	0.377	0.791
JAG1-201	1	0.375	2.509	0.647	0.007	1	0.178	1.370	0.365	0.118
DLL4-201	1	0.258	1.419	0.285	0.072	1	0.054	1.103	0.511	0.704
TNNT2-202	1	0.107	0.544	0.122	0.001	1	0.184	0.926	0.262	0.658
TNNT2-203	1	0.067	0.893	0.061	0.056	1	0.088	0.938	0.100	0.392
TNNT2-204	1	0.185	0.456	0.123	0.003	1	0.149	0.916	0.305	0.638
ACTC1-202	1	0.263	1.590	0.169	0.009	1	0.208	0.790	0.174	0.172
ACTC1-203	1	0.338	0.518	0.318	0.083	1	0.195	0.570	0.287	0.048

Looking further downstream at MEF2C targets *TNNT2* and *ACTC1*, ISH and RNAseq consistently revealed a reduction in transcript levels. ISH showed for both genes a reduced expression in the

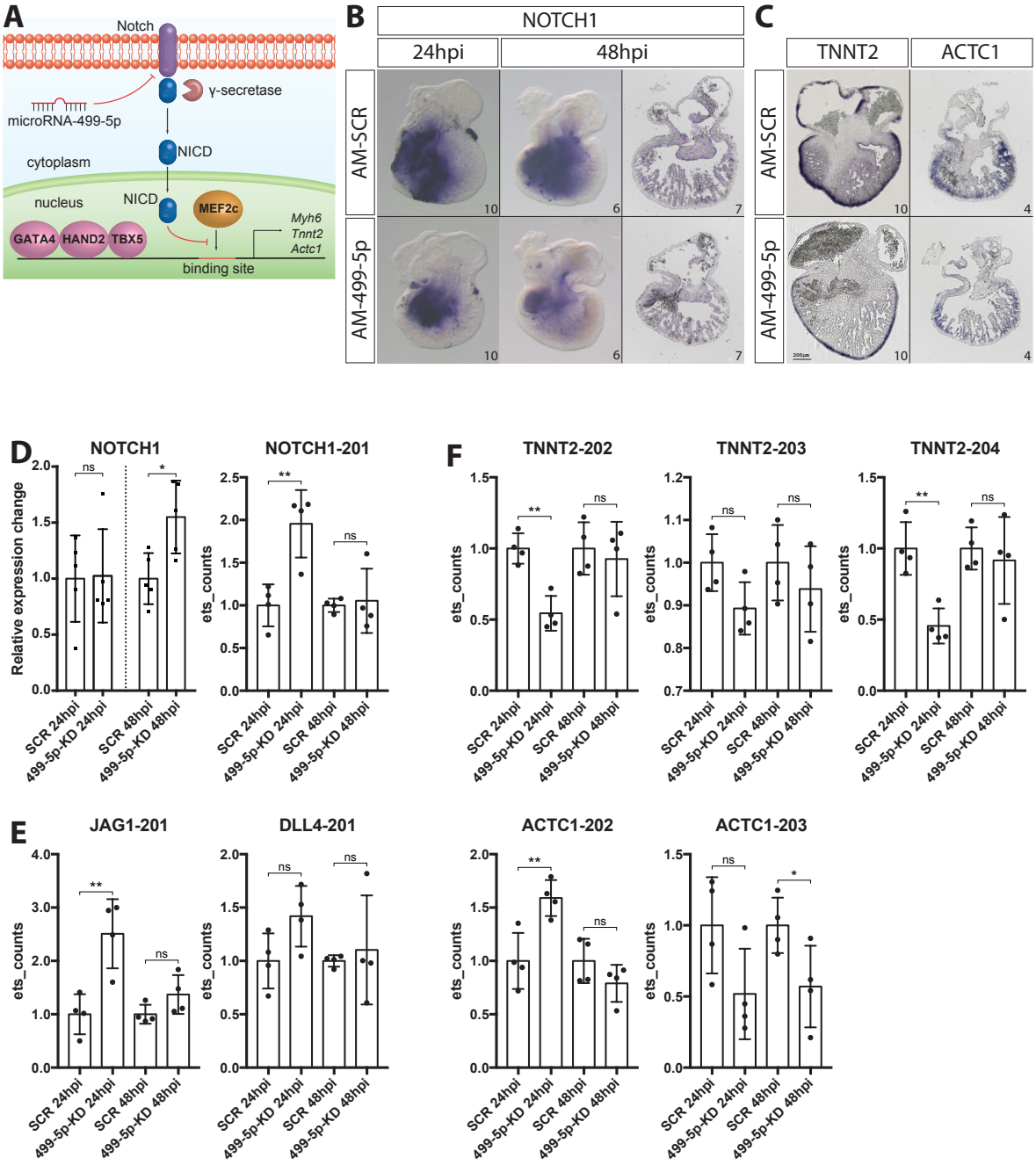

Figure 22: NOTCH signalling cascade affecting cardiac specification

(A) A graphic representation placing microRNA-499-5p into a signalling context where NOTCH activation leads to NICD release which in turn prevents MEF2C binding to its respective promoters. This prevents activation of cardiac specification genes like *MYH6*, *TNNT2* and *ACTC1*. (B) ISH for *NOTCH1* shows reduction in expression after microRNA-499-5p knockdown at both 24hpi and 48hpi. Sections confirm *NOTCH1*s expression is primarily in the Endocardium. (C) ISH of MEF2C targets *TNNT2* and *ACTC1*. Both show reduced expression after microRNA-499-5p knockdown at 48hpi. (D) In contrast to ISH, RT-qPCR (left) and RNAseq (right) indicate upregulation of *NOTCH1* transcript. (E) Data for NOTCH activators *JAG1* and *DLL4* has been extracted from RNAseq. *JAG1* shows a more pronounced uptrend than *DLL4* which only shows indication for upregulation at 24hpi. Together the data supports increased NICD activity and thus less MEF2C mediated signalling. (F) RNAseq data for MEF2C target genes *TNNT2* and *ACTC1*. Most abundant transcripts are represented. All *TNNT2* transcripts show downtrend which is significant for variant 202 and 204 at 24hp and thus confirm ISH results. *ACTC1* transcripts mostly indicate downtrend except for 202 at 24hpi which is significantly upregulated. (Statistical significance determined by students t-test) (D, E, F n=4-5)

myocardium and trabeculae at 48hpi after microRNA-499-5p knockdown (Figure 22C). This trend is also reflected in the RNAseq data. Both genes have a multitude of transcripts, therefore we choose to depict expression data for the most abundant ones which consistently show a downtrend for both genes apart from the 202 transcript of *ACTC1* at 24hpi, which is upregulated (Figure 22F). Specific transcript function is not yet known and will require further experimentation. Overall the downregulation shown by ISH and RNAseq strengthens the hypothesis of reduced MEF2C signalling as reported in (Abad et al., 2017) where similar results were presented. The reduced MEF2C activity is in alignment with the above described factors that indicate increased NOTCH activity. In conclusion we can say that the performed experiments strongly indicated that microRNA-499-p is involved in a signalling cascade where NOTCH signalling prevents activation of MEF2C target genes (Figure 22A).

4.4.6 Outlook – Modulation of microRNA signalling by microRNA LNA mimics

Main focus of this PhD work was to investigate the phenotype of microRNA-499-5p knockdown in hearts of chick embryos. For this purpose, we established the above described cardiac injection procedure which serves as a useful tool throughout the study. As we have introduced above, other compounds than AntagomiRs can be injected with this method. As our focus was on studying microRNA signalling cascades, we were interested in overstimulating such signalling events. In preliminary experiments we injected LNA microRNA mimics which we normally used in luciferase assays in cell culture into the heart. The manufacturer Exiqon has stated before that small LNA modified oligonucleotides can pass the cell membrane without further carrier substances like the cholesterol modification used on our AntagomiRs. Unfortunately, this information is no longer available and other literature reports state the opposite (Chabot et al., 2012). Nonetheless, we took the opportunity and injected several hearts with LNA modified mimics for microRNA-499-5p and assessed gene expression afterwards by RT-qPCR (Figure 23).

The data from the mimic injections showed differential expression between the conditions, although additional replicates are needed. Interestingly *NOTCH1* and *BMP10* showed a subtle downregulation similar to their counterpart experiments with AntagomiR-499-5p and TRIzol® extraction (Figure 16B, O) instead of the expected derepression. Therefore, those results are more in line with the RT-qPCR performed on non-TRIzol® extracted samples as well as the validated target interaction by luciferase assay (Figure 10C, Appendix 8.1). Still the ISH data shown earlier (Figure 22B) doesn't fit with these results and therefore no final conclusion is possible. The third gene assed in this set of experiments was *NRG1* which showed an uptrend which is opposite of its counterpart experiment with AntagomiR-499-5p and TRIzol® extraction and therefore expected. The results obtained for *NRG1* indicated that mimic injections might be a useful tool to study phenotypic and gene expression changes in a scenario with abundant microRNA availability. Considering the unknown delivery mechanism and contradicting literature (Chabot et al., 2012) further controls might be necessary to establish mimic injections as a reliable tool. Taken together this opens an additional avenue for studying microRNA signalling.

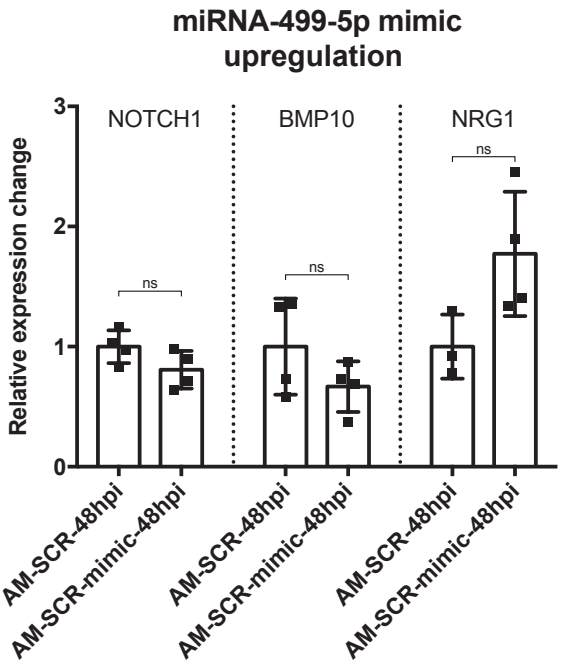

Figure 23: Differential gene expression after microRNA-499-5p mimic upregulation

RT-qPCR performed on cDNA from TRIzol® extracted RNA samples showed differential expression after microRNA-499-5p mimic injection into the heart. AM-SCR was used as a label for both injections. *NOTCH1* and *BMP10* show a downtrend whereas *NRG1* shows a more pronounced uptrend.

5 Discussion

5.1 UTR target verification and relation to *in vivo* results

As introduced *ETS1* was determined to be a target for microRNA-499-5p in a prior PhD-project in the Münsterberg lab (McCormick, 2015). The study showed a significant reduction of luciferase expression after microRNA-499-5p administration. Unfortunately, those results could not be reproduced in the early stages of this project. Reanalysis of available 3'UTR information including RNAseq (Aken et al., 2016) data revealed extended sequence information which allowed cloning of a longer 3'UTR fragment (originally ~400bp, now 1200bp of the total 3'UTR of 4747bp) harbouring a canonical target site for microRNA-499-5p and in addition a putative site for microRNA-221-3p. Further, the initially used mimic for microRNA-499-5p was not specifically designed for chicken sequence but an oligo nucleotide based on human sequence. The difference between these oligo nucleotides is minor and only one nucleotide (Figure 5B) (Kozomara and Griffiths-Jones, 2011, Kozomara and Griffiths-Jones, 2014), but as literature suggest sometimes such small differences are sufficient to affect microRNA binding (Martin et al., 2007). After solving these initial starting issues luciferase assays were successfully performed confirming an interaction between *ETS1* and microRNA-499-5p and also microRNA-221-3p and thus we were able to confirm previously published results (Wei et al., 2012, Wilson et al., 2010, Xu et al., 2016). The two microRNA mimics had reproducible effects on luciferase repression, but the strength of the effect differed: microRNA-499-5p led to a reduction of 39.5% of the *ETS1*-3'UTR luciferase reporter and microRNA-221-3p to only 11.5%. A subsequent, separate analysis for combinatorial regulation showed no synergy averaging at 34.0% (using half of the concentration of each mimic), which is roughly the inhibition caused by microRNA-499-5p alone. Another change in the previous assay procedure in the Münsterberg lab was the swap to a single plasmid system where both luciferases are under control of different strong promoters on the same plasmid (Promega; E1330). One luciferase is controlled by the 3'UTR to be tested (Firefly luciferase) and a second serves as transfection control for normalisation (Renilla luciferase). This change allowed better normalisation and overall showed less variation in data distribution (data not shown). Analysis of *ETS1* in microRNA-499-5p knockdown hearts by ISH confirmed the expected upregulation of the transcription factor at both timepoints analysed in keeping with the luciferase data (Figure 14E). Unfortunately, this was also the first time where we encountered a critical discrepancy between RT-qPCR results depending on the chosen RNA extraction method prior to cDNA synthesis. RT-qPCR using samples from TRIzol® extraction showed a downregulation whereas samples from a non-TRIzol® extraction process revealed differential upregulation after microRNA inhibition (Figure 14D) which is more in agreement with the validated target interaction and ISH data. Nonetheless, further investigation surrounding ETS1 signalling was conducted which is discussed in detail in 5.3.1 ETS1 and microRNA-499-5p – a signalling cascade surrounding the ECM.

In addition to ETS1 we looked for other genes that play an important role in heart development and are predicted to be targets (Agarwal et al., 2015) for our list of microRNAs of interest (Table 1). By doing so we were able to identify gene and signalling networks in which particularly microRNA-499-5p is involved and were able to develop an experimental plan for more in depth

in vivo experiments. We have conducted further luciferase assays experiments, which validated several target interactions, namely *NOTCH1*, *PAX3* and *SMAD6*. Further to those *HAPLN1* indicated target interaction but lacks sufficient replicates as of yet and *HAS2* showed microRNA mediated luciferase repression but this was not recoverable by target site mutation, thus the exact binding site for the microRNA-499-5p mimic is still unclear. Out of all performed assays only one gene, *GATA4* was invalidated as a target. The invalidation of *GATA4* is particularly interesting when compared to the acquired RNAseq data in which *ETS1*, which gene product activates *GATA4*, and *GATA4* itself both showed significant derepression after microRNA-499-5p knockdown at 24hpi. Even at the later timepoint 48hpi an uptrend is still visible but not significant anymore (Figure 19). On the other hand literature has reported that after microRNA-499 transfection into bone marrow cells *GATA4* mRNA expression and that of others has increased (Lu-lu and Bo, 2012), which is contrary to our RNAseq results, that's shows derepression after microRNA-499-5p knockdown. Based on the published data the direct interaction of microRNA-499-5p and *GATA4* is less likely since direct interaction should have led to a stronger repression and not derepression. Possible reasons for the observed differences could be attributed to *in vitro* vs. *in vivo* experiments, feedback mechanisms or even the signalling context within the tissue.

One of ETS1 functions is to coordinate NCC migration in the heart via GATA6 (Gao et al., 2010). A well-known marker for NCC fate prior to arrival at the OFT is PAX3 (Epstein et al., 2000) for which the luciferase assay also revealed subtle but significant repression and thus establishing *PAX3* as an interesting candidate for further investigation. RNAseq data revealed extremely low expression at 24hpi and no detectable transcript at 48hpi, which confirms observations made in mouse that *PAX3* expressions diminishes prior arrival at the OFT (Epstein et al., 2000). Differential expression at 24hpi is extremely variable and therefore no in-depth analysis was possible. A probe for ISH analysis was generated (Table 8) but expression in dissected hearts was too low to compare AM-SCR injected hearts vs. AM-499-5p injected hearts (data not shown). Previously published data for Cre-reporter mice stained for β-galactosidase expression clearly showed *PAX3* cells invading the outflow tract and therefore confirming NCC migration to the heart (Epstein et al., 2000). Nonetheless, a possible reason for the lack of detection of subtle remaining expression could be caused by the localisation of NCC, which are primarily at the distal OFT. All analysis was performed on dissected hearts, for which they were cut off at the sinus venosus and distal OFT. Due to the small size of the heart the exact cut off location might not have been as accurate as necessary to guarantee consistent detection across biological replicates. Taking into account that *PAX3* expression diminishes during migration from the neural folds to the OFT and it's distance to microRNA-499-5p expression locations in the heart the microRNA-499-5p-*PAX3* relationship might not be relevant for cushion maturation. Therefore, for this study *PAX3* has not been followed up any further.

Apart from NCC migration ETS1 also has a regulatory function in ECM regulation by promoting the expression of metalloproteinase which are responsible for degradation (Wei et al., 2012). Two of the analysed reporter constructs were for *HAS2* an ECM synthesising enzyme and *HAPLN1* a bridging protein for ECM components. Both assays couldn't be completed in a sufficient number of replicates within the timeframe of the project but have shown reporter construct repression. In the case of *HAS2* a reduction of 9.8% was observed and for *HAPLN1* 14.3%. Those results together

with literature that reported aberrant ECM deposition in the heart in ETS1-null embryos (Gao et al., 2010) led us to further look into changes in the ECM after microRNA-499-5p knockdown. In fact, top targets showing upregulation/derepression of the intersection of our RNAseq data sets at 24hpi and 48hpi were dominated by ECM components (Figure 18). A more comprehensive discussion about an observed ECM phenotype and related genes follows in a separate section (5.3.1 ETS1 and microRNA-499-5p – a signalling cascade surrounding the ECM).

Another target of interest was SMAD6 due to its expression location at the heart valves and in the OFT. Further, reports indicated severe heart defects in *SMAD6* ablated animals (Galvin et al., 2000). SMAD6 regulates BMP signalling which is as introduced above essential for coordinating EMT in the heart for cushion maturation (Desgrosellier et al., 2005). Target prediction algorithms proposed binding sites for three different microRNAs of which microRNA-499-5p and microRNA-126-3p mimics did affect the luciferase reporter construct. They led to similar reductions of 20.8% and 18.2%, respectively. The microRNA-499-5p phenotype was further investigated in knockdown hearts. ISH revealed an increase in signal for *SMAD6* transcripts (Figure 15) particularly at the 24hpi timepoint, which strengthens the target validation. Once more RT-qPCR (Figure 16T) and RNAseq (Figure 19) showed contradicting results comapred to ISH, leaving the exact trend for differential expression unresolved. This is one of many cases throughout this PhD project were ISH results and RT-qPCR/RNAseq results are not in agreement, specifically when using different RNA extraction methods to extract RNA for cDNA synthesis for the latter two methods. Overall this complicated the analysis tremendously. A more detailed discussion of this issue follows in “RNA extraction – a major challenge for data interpretation”.

The last gene of interest studied for target interaction by luciferase Assays was *NOTCH1*. In heart development NOTCH signalling is involved in many different processes including EMT and trabeculation and disruption of its signalling usually leads to severe malformations or even prenatal death (Del Monte-Nieto et al., 2018, MacGrogan et al., 2018a, MacGrogan et al., 2018b). Our target interaction analysis confirmed microRNA-499-5p interaction with the *NOTCH1* 3’UTR. Luciferase expression was repressed by roughly 27.4%, the strongest reduction after *ETS1* (Figure 10, Appendix 8.1). RNAseq and RT-qPCR (non-TRIzol®) showed an uptrend of NOTCH1 expression which is consistent with the target interaction validation (Figure 22D). However, ISH data (Figure 22B) showed a reduction after microRNA-499-5p knockdown, which requires further explanation. Nonetheless, many of our experiments and the reported role of NOTCH signalling during cushion maturation as we explained above, indicated relevance for NOTCH signalling in the heart. Therefore, we decided to investigate its connection to microRNA-499-5p more and have performed more in depth analysis which is summarised in a dedicated section below (5.3.2 MicroRNA-499-5p signalling regulates NOTCH pathways).

5.2 Establishment of a cardiac injection procedure

This section has been published in Wittig et al. (2018), but was expanded for this PhD thesis for more detail.

In conclusion, the method established for this project can be used for AntagomiR injections and to achieve successful knockdown of microRNA function in the heart. The injected compound

can easily be replaced and thus the technique is also suitable for delivery of morpholinos, or plasmid constructs, or viral particles to achieve transient knockdown or area specific expression of genes of interest. For example, injection of LNA modified microRNA mimics, usually used for tissue culture experiments to promote microRNA mediated silencing gave a promising outlook as a tool for increasing availability of microRNAs *in vivo* and thus enhance their signalling. Preliminary experiments showed differential expression changes for *NOTCH1*, *BMP10* and *NRG1* (Figure 23). Also, it is possible to combine multiple AntagomiRs into a single injection to study synergistic, antagonistic or additive effects of microRNA inhibition or to combine AntagomiRs with drugs that possibly can rescue inhibitory effects of the former as we have tried with AntagomiR-499-5p and the NOTCH inhibitor DAPT (Figure 21B).

The method can be applied to variety of stages of chicken development and thus allows the study of different processes of heart development. Most suitable are HH13 to HH18, after turning of the chicken embryo and before the heart encapsulating tissue becomes too rigid for dissection to gain access (Martinsen, 2005, Wittig and Münsterberg, 2016). Injections at older developmental stages will allow the specific targeting of only the atria or ventricles, similarly at younger stages it is possible to restrict injections to parts of the primitive heart tube. Strikingly, following delivery the administered AntagomiR was locally restricted to the heart (Figure 11F and Figure 13A, B) and not affected by the circulating bloodstream. Therefore, this procedure allows studying the impact of microRNA-inhibition and other injectable compounds on the heart only, which presents an important advantage to approaches used previously (Davidson et al., 2001, Goehringer et al., 2009), where injection were made into blood vessels and thus caused systemic effects. This spatial restriction is helpful to avoid possible effects on other organs caused by systemic microRNA knockdown and will improve the analysis of phenotypes.

The method allows the downstream analysis of different parameters to assess the phenotype, including morphology, histology, gene expression changes and changes in physiology. Here, we quantified the heart rate of injected embryos and compared it to wildtype siblings. Quantification of zebrafish heart rates has been done using a high frame rate camera (Musso et al., 2014), this was adopted for this study. Video recordings of the heart allow automated heart rate quantification using Fiji software and furthermore allow calculation of input and output volumes. The latter requires visual access to both, atria and ventricles (Musso et al., 2014), which is rarely the case past 48hpi in chick since at that stage the embryo is covered by the allantois (Spurlin and Lwigale, 2013). However, by selecting recorded videos where all heart chambers are fully visible, it would be possible to determine cardiac input and output volumes. Alternatively, the heart rate can be determined with electrodes producing an electrocardiogram as shown by Shi et al. (2013) in the chicken embryo. Electrophysiological experiments surrounding the conduction system of the heart could involve patch clamp, pulse wave, action potential and/or ECG measurements (Borghetti et al., 2018, Shi et al., 2013). Morphological changes in the heart post-injection can be analysed by serial sectioning and 3D reconstruction as we have shown ourselves (Figure 20) but also as published before (Wang et al., 2015b). Further optical projection tomography (Sharpe et al., 2002) or histological staining procedures (Alturkistani et al., 2015) are suitable techniques for downstream analysis.

To assess successful administration and resulting knockdown of miR499-5p, we employed

Northern Blot analysis and quantitative RT-PCR. Such analysis can be further expanded for genes of interest to determine differential expression and thus dissect pathways relevant for the targeted microRNA. In order to understand the functional relevance of microRNAs and their corresponding targets and to decipher the microRNA network in heart development, we further processed heart samples for RNAseq to obtain a broader picture of differentially expressed genes (Figure 18). We showed that the RNA extraction method used, column-based or TRIzol® based, affects the ability to verify the knockdown. The reasons for this are still unclear, but we feel that it is an important observation to report. For further molecular analyses, non-TRIzol® extracted samples are preferable. This extraction method enables confirmation of microRNA knockdown after AntagomiR administration (Figure 13C, D)(Krutzfeldt et al., 2005, Velu and Grimes, 2012) and avoids the reported GC-bias of TRIzol® for microRNAs (Kim et al., 2012).

Taken together the cardiac injection method presented here enabled us to investigate microRNA functions during intermediate heart development in the chicken embryo. Advantages of this knockdown approach are the targeted local delivery at specific stages of development and the short timeframe in which results can be obtained. Establishing the injection procedure allowed us to investigate a microRNA-499-5p knockdown phenotype using several different methods as discussed below.

5.3 Analysis of a microRNA-499-5p knockdown phenotype

During the development of the cardiac injection procedure we established various tools to analyse effects of microRNA-499 ablation. Among those tools were a variety of ISH probes (Table 8) for genes relevant for heart development but also involved in hypothesized signalling cascades affected by microRNA-499-5p.

Five of the markers have been selected for their involvement in ECM formation. ACAN is a cartilage specific protein and expressed in the heart (Darnell et al., 2007). Cartilage is an essential component of the cardiac cushions and when *SOX9* a major driver for expression of cartilage genes is knocked out defects in cushion development can be observed finally leading to the death of the embryo (Akiyama et al., 2004). On the other hand, excessive amounts of cartilage has a critical impact on cardiac development as well. ETS1 is known to be an inhibitor of chondrogenic differentiation. Unsurprisingly when knocked out the cartilage homeostasis gets disrupted and an aberrant mass of cartilage peripheral to the aorta forms which is accompanied by septal defects (Gao et al., 2010). Further in the marker list is VCAN another structural component of the ECM which can form aggregates together with hyaluronan when linked via HAPLN1. HAPLN1 is involved in homeostasis of cartilage and also allows interaction of ACAN and hyaluronan, which is synthesised by the last marker in this group HAS2. Further it is also expressed in the heart (Lockhart et al., 2011, Wirrig et al., 2007)

Another group of markers was chosen surrounding a NOTCH – MEF2C signalling cascade which is relevant for cardiac specification. In Addition to *NOTCH1* and ***MEF2C*** probes for *ACTC1*, cardiac actin and *TNNT2*, cardiac Troponin have been generated. *TNNT2* and *ACTC1* are expressed in the myocardium, the muscle-layer of the heart. Since the MyomiRs regulate muscle composition these markers were a logical choice to study the microRNA-499-5p knockdown phenotype (Abad

et al., 2017). Also closely related to NOTCH signalling is NRG1, which is relevant for coordinating Trabeculation in the Myocardium (Del Monte-Nieto et al., 2018) and is also another marker for endocardial cushion development (Gitler et al., 2003).

Other probes generated cannot be as easily grouped as the ones above but still were expected to be useful tools for investigation. *MSX1* was selected, because it is specifically expressed at the AV junction (Allen et al., 2001), the location were the septum intermedium forms (Person et al., 2005). *PDLIM5* shows overlapping expression to ETS1 and microRNA-499-5p in the sinus venosus. Expression of the gene results in a scaffold protein which supports protein kinases in striated muscles. Its function is thought to be connected to cardiomyocyte expansion (Pruitt et al., 2012, Wu et al., 2004), making it an interesting target for analysis in the heart. *POSTN* is a gene specifically expressed in the endocardium (Norris et al., 2004). As introduced, the endocardium emits signals necessary for endocardial cushion formation early in development (Person et al., 2005), making it an obvious choice as a marker. Furthermore *TBX3* expression is not restricted to the heart but highly specific within the heart to the valves (Darnell et al., 2007). *TBX3* was chosen as marker since the valves are the major interest of this study. *AMHC* is exclusively expressed in the heart. It is coded by myosin heavy chain genes and it was shown that intragenic microRNAs from this cluster regulate its expression by feedback (Liu and Olson, 2010). GATA4 is a downstream target of ETS1. As explained earlier microRNAs have usually a small impact on expression of a single gene and more likely target multiple genes in a pathway. Moreover, a target site for miR-499 was predicted in the *GATA4* 3'UTR (Agarwal et al., 2015, Lewis et al., 2005) making it an ideal candidate. Similar to GATA4, PAX3 has a connection to ETS1 which recruits neural crest cells to the OFT during septation. *PAX3* is a gene specifically expressed in NCC and was a predicted target of microRNA-499-5p (Epstein et al., 2000, Gao et al., 2010). *TBX18* is a major marker of the PEO (Ishii et al., 2010). Its expression overlaps with what we have seen for microRNA-499 in our study, which led to the selection of *TBX18* as another potential marker for phenotypic analysis. *SMAD6* is expressed in the heart valves and in the OFT (Galvin et al., 2000) and was another predicted target for microRNA-499-5p, therefore phenotypic analysis after knockdown by ISH just seemed logical. Last, but not least *PITX2* was included in the marker list as specific marker for the atria, which should allow easy determination of morphological changes after microRNA-499-5p knockdown.

In summary a useful set of probes was established for downstream analysis of microRNA-499-5p knockdown and the majority of them were presented within the different results sections of this PhD-thesis. ISH experiments have been performed for all established probes (Table 8) but some of them yielded very weak signals in the heart, showed no differential expression changes after microRNA-499-5p knockdown or could not be connected to a particular signalling cascade surrounding ETS1 or NOTCH1 in the heart, which were the main targets for investigation.

In addition to the large set of probes even more primers pairs for RT-qPCR have been established which in part have been used to confirm RNAseq results. Unfortunately experiments before RNAseq led to different results due to the differences in RNA extraction methods. An explanation for those differences is not available yet but highly important. Further analysis of gene expression requires tight controls and is best analysed by multiple independent methods to ensure no bias caused by the chosen RNA extraction method.

5.3.1 ETS1 and microRNA-499-5p – a signalling cascade surrounding the ECM

Analysis of *ETS1* gene expression in chicken embryos has been performed in several studies in the past (Bollerot et al., 2005, Darnell et al., 2007, Tahtakran and Selleck, 2003) including one study showing immunoreactivity in the heart (Macias et al., 1998). Expression is consistent among several developmental stages (HH17 to HH25) and is dominant in the OFT of the heart as well as the sinus venosus and the connecting omphalo-mesenteric vein, which is found dorsally to the heart. This places *ETS1* expression in locations important for cushion formation and valve generation. Particularly, OFT staining previously reported was strong which we were able to confirm in ISH analysis in our *in vivo* microRNA knockdown experiments (Figure 14E). This location emphasizes ETS1 involvement in NCC recruiting.

Expression of miR-499 via ISH has not yet been studied in chick, only a study in medaka has been conducted fairly recently (Bhuiyan et al., 2013). Nevertheless, in Medaka it was already shown that miR-499 is expressed in the heart. Still miR-499s expression in the heart has been previously confirmed by RISC pulldown in mice (Matkovich et al., 2011). We conducted ISH analysis for microRNA-499-5p in WT embryos using LNA probes (Exiqon) which confirmed its location in the heart (data not shown) but obtaining specific spatial localisation was difficult due to excessive background staining. The sinus venous seemed to be the major region of expression. Interestingly, expression was also observed in the OFT at HH19 very faintly and HH25 more pronounced along the aortico-pulmonary ridges. This expression is overlapping with the one of *ETS1* and therefore supported its regulatory role regarding ETS1. A summary of the expression locations is depicted in a schematic (Figure 24).

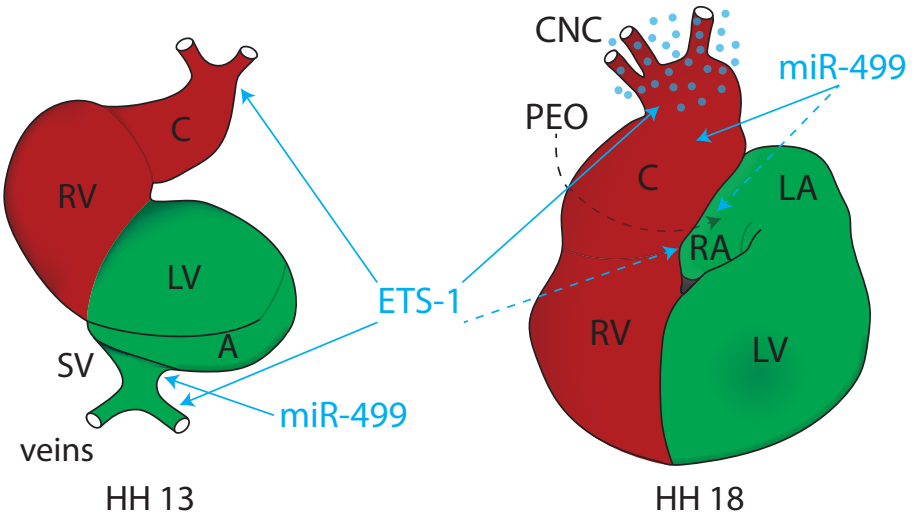

Figure 24: Expression locations of ETS1 and miR-499

Reported expression locations of ETS1 and microRNA-499-5p from preliminary data in the heart. ETS1 is expressed in the sinus venous, the OFT (C) and the omphalo-mesenteric vein (not illustrated). MiR-499 expression can be detected in the sinus venous and/or PEO and the OFT. (A) atrium, (CNC) cardiac neural crest, (C) Conus, (LA) left atrium, (LV) left ventricle, (PEO) pro-epicardial organ, (RA) right atrium, (RV) right ventricle, (SV) sinus venosus.

Literature suggested that ETS1 signalling plays a crucial role in ECM regulation in general (Trojanowska, 2000) and particularly in the heart, where any kind of misregulation often leads into malformations or disease (Gao et al., 2010). Investigating a potential link of microRNA-499-5p and

ETS1 was the original aim of this project and we believe, that we were able to shed some new light onto their signalling relationship. In a first instance target interaction was confirmed by luciferase assay as discussed earlier, after which *in vivo* knockdown experiments followed that were analysed by various techniques including ISH and RNAseq. As reported previously *in vitro* luciferase assay results do not always led to expected results in subsequent *in vivo* experiments (Liu and Olson, 2010), but in our case ISH (Figure 14E), RT-qPCR (Figure 14D) and RNAseq (Figure 19) confirmed an derepression of *ETS1* after microRNA-499-5p knockdown.

ETS1 has long been known to regulate enzymes involved in ECM degradation such as matrix metalloproteinases (MMPs) and their inhibitors (TIMPs), but literature has also suggested a signalling role in collagen and tenascin regulation (Jinnin et al., 2004, Trojanowska, 2000). Furthermore, other literature also reported a link between JAG1/DLL4 mediated Tencascin C activation via NOTCH (Midwood et al., 2016), another gene of interest from our target interaction analysis (Figure 10C, Appendix 8.1). Interestingly Tenascin C and several Collagens are among the top targets of the intersection of our 24hpi and 48hpi RNAseq data set. More precisely they showed the smallest p-values within the dataset and thus their differential expression is the most significant (Figure 18A). Intrigued by this data we were interested to see if these changes in gene expression lead to an increase in ECM material which can be measured by volume calculations. To do so we sectioned AM-SCR and AM-499-5p injected hearts and 3D reconstructed the captured images to measure ECM surface areas in all sections which allowed volume calculation. Interestingly the quantified volumes (Figure 20C) showed an uptrend in microRNA-499-5p knockdown samples, that supported the observed upregulation/derepression shown in the RNAseq results (Figure 18A). Further other ECM components, such as *ACAN*, *VCAN* and *HAPLN1*, showed strong upregulation/derepression in RNAseq data as well (Figure 20D) which is in agreement with the observed ECM volume increase. Taking together the findings thus far, microRNA-499-5p can be positioned as a fine tune inhibitor of ETS1 signalling for ECM remodelling. Unfortunately, not all results obtained were in agreement. Further ISH experiments surrounding important players in ECM composition and specification showed partially contradictory results. Namely *ACAN* and *HAPLN1* showed decreased signal intensities in ISH analysis (Figure 20E) which is opposing to the obtained RNAseq data (Figure 20D). The third assessed gene by ISH is *SOX9*, which previously has been reported for a role of mesenchyme proliferation in endocardial cushions and later specification by inducing *ACAN* expression at the same site (MacGrogan et al., 2018b). Other reports position SOX9 as a pan-neural crest regulator together with ETS1 of migratory NCC (Simoes-Costa et al., 2014) which contribute to the OFT. Together this highlighted the importance of SOX9 in this signalling context. Our data showed at 24hpi no obvious differences in signal intensities but an increase in the OFT at 48hpi (Figure 20E). No direct connection to microRNA-499-5p modulation has been made, but the upregulation could be a consequence of other signalling events disrupted by the lack of microRNA-499-5p activities. The OFT is one of the two locations were endocardial cushions arise and mature which requires proper coordination of ECM synthesis and degradation. As previously reported SOX9 and ETS1 together are relevant for stimulating NCC to become migratory. Along with this stimulation COL9A3 and others get activated (Simoes-Costa et al., 2014). Interestingly, two transcripts of *COL9A3* are among the top targets of our differential expression data for the intersection of the 24hpi and 48hpi dataset. All in all, the majority of the presented data point towards a misregulation of ECM signalling surrounding

ETS1 mediated transcriptional activation.

Another aspect of ETS1s signalling role is the activation of ECM degradation enzymes. Among those are MMP1, MMP3, MMP9 (Matrix-Metalloproteinases) and Plasminogen Activator, Urokinase (PLAU). The activation of those metalloproteinases has shown to promote cell migration (Wei et al., 2012) but direct evidence that ETS1 contributes to mesenchyme invasion into the endocardial cushions via this process has not been reported yet. Nonetheless, many reports have stated ETS1s relevance for induction of EMT in heart and NCC (Gilles et al., 2000-2013, Macias et al., 1998, Nie and Bronner, 2015). Differential expression of *MMPs* did not attract our immediate attention. Looking at our RNAseq data more closely we noticed no detectable expression for *MMP1* and *MMP3*. Expression for *MMP9* and *PLAU* was detected but transcript numbers were low. Specifically, a downtrend of roughly 30% was observed for *MMP9* but biological replicates showed too much variability for significance (data not shown). Data for *PLAU* showed a subtle uptrend at 24hpi and nearly identical expression at 48hpi, which both was insignificant (data not shown). In conclusion not much information about MMP signalling could be retrieved from the RNAseq data which could have led to other experiments.

To summarise reported signalling relations with respect to expression changes observed here we illustrated a new schematic for ETS1 signalling (Figure 24). ETS1 signalling is initiated via MEK-ERK signalling which in turn gets activated by FGF (Wang et al., 2015a) or RAS/RAF (Wei et al., 2012). Subsequently ETS1 itself can signal towards ECM degradation via MMPs (Wei et al., 2012) or ECM synthesis by activating Tenascin-C (Jinnin et al., 2004, Trojanowska, 2000) and Collagen 9A3 (Simoes-Costa et al., 2014). In addition, we have positioned microRNA-499-5p within the ETS1 signalling cascade (Figure 25).

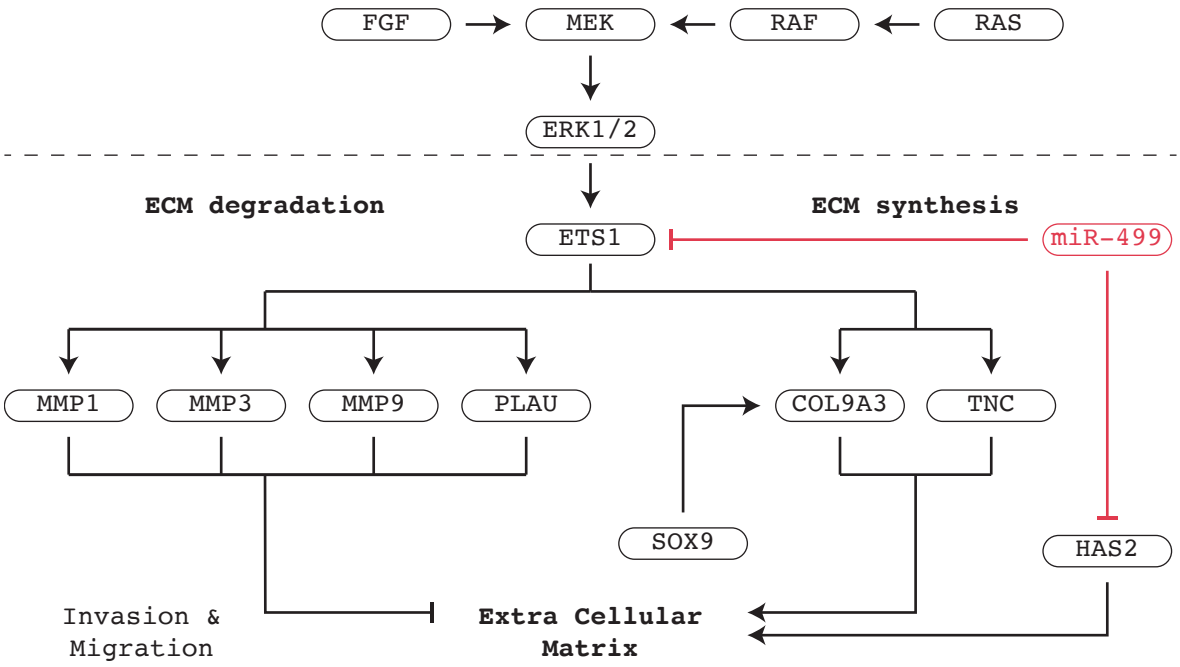

Figure 25: ECM synthesis and degradation initiated by ETS1

The schematic shows a summary of literature reported ETS1 signalling in the context of the here presented data. Further signalling functions of microRNA-499-5p (red) have been placed in context which indicate function in promoting and suppressing ECM synthesis.

5.3.2 MicroRNA-499-5p signalling regulates NOTCH pathways

During the development of our cardiac injection procedure we started using heart rate assessment as measurement for cardiac health. The method was useful also during the analysis for knockdown phenotypes, as previously reported in other species (Musso et al., 2014). Therefore, we employed heart rate assessment in this study to learn more about the microRNA-499-5p knockdown phenotype. Strikingly, the microRNA knockdown had a significant impact on heart rate that became more severe with longer incubation periods post injection. This suggests that microRNA-499-5p could interfere in a signalling cascade responsible for heart rate control. NOTCH signalling has an impact on heart rate via regulation of cellular identity through differentiation of cardiomyocytes into cardiac conduction system-like cells (Abad et al., 2017). We were able to show an interaction of microRNA-499-5p with the 3'UTR of *NOTCH1* (Figure 10C, Appendix 8.1) and were able to observe derepression of *NOTCH1* expression after knockdown via RT-qPCR and RNAseq (Figure 22D). Confusingly, ISH data (Figure 22B) did not confirm *NOTCH1* derepression but we kept looking further and found that ligand availability (Figure 22E) increased and thus signalling could still have been elevated. Moreover, increased conditionally activated NICD has been reported to affect heart rate negatively in transgenic mice (Bhatnagar et al., 2016). The authors recorded ECG data under different conditions that revealed a reduction in heart rate and bradycardia along with a sinus pause in NICD overexpressing animals. Morphological differences were not observed, which is similar to our current findings. In another study NOTCH signalling was studied in a similar context where they were able to show an increase in the number of cells with an organized sarcomere structure after NOTCH inhibition via DAPT, a common NOTCH inhibitor (Abad et al., 2017). Preliminary experiments in this respect were unsuccessful due to technical issues, but we are planning to revisit them to reproduce these observations in the chicken heart.

Further to the morphological observations made by Abad et al. (2017) they observed gene expression changes surrounding MEF2C signalling. Precisely, they showed upregulation of *TNNT2* and *ACTC1* after NOTCH inhibition. Interestingly, we observed the inverted scenario, both by ISH and RNAseq (Figure 22C, F) analysis where the above mentioned genes are downregulated in AM-499-5p injected hearts, which we hypothesised leads to increased NOTCH signalling. Strikingly, in another report it was shown that hCMPCs showed increased expression of *TNNT2* and *ACTC1* upon microRNA-499 supplementation and *ACTC1* repression on microRNA-499 inhibition. These published reports are in agreement with our observed results (Sluijter et al., 2010). Further, the same authors showed that cardiac differentiation is enhanced upon microRNA-499 addition which is similar to the observed effects by Abad et al. (2017) after NOTCH inhibition via DAPT.

In yet another report it was shown that *TNNI2* and *TNNT3* expression was downregulated in transgenic mice where microRNA-499 was upregulated (Wang et al., 2011). TNNIs and TNNTs work together in the troponin complex to facilitate muscle contraction in skeletal and cardiac muscle. Transcripts for *TNNI2* and *TNN3* were examined in our RNAseq data but their expression was low and differential expression was insignificant (data not shown). Interesting however is that our transcriptomics data indicates a downregulation after microRNA-499p knockdown which is in conflict with the reported downregulation of *TNNI2* and *TNN3* in transgenic animals overexpressing microRNA-499. Possible reasons for this are plentiful, it could be species differences between chick

and mouse, it could be a feedback signalling loop that requires a specific amount of microRNA-499-5p for maintaining normal expression but the results could also be affected by the here reported impact of RNA extraction on quantitative analysis. Researchers from the earlier mentioned report (Bhatnagar et al., 2016) observed reduced gene expression of *SCN5A* and Connexin 40 (*CX40*, *GJA5*) in transgenic animals overexpressing NICD. These two genes are major players in cardiac conduction and usually their loss is connected to altered heart rates (Gosselin-Badaroudine et al., 2012, Paige et al., 2015, van Eif et al., 2018). We checked those genes in our microRNA-499-5p knockdown differential expression data as well and observed significant upregulation at 24hpi and a still persistent uptrend at 48hpi (data not shown). Once more this data is in contrast to previously published literature. Nonetheless, our experiments are using different approaches compared to those reported in the literature, therefore the answer to those differences may lie in methodological, species or signalling pathway related differences. Additional experiments are required to answer those questions and to more accurately define microRNA-499-5ps signalling role.

Coming back to the heart rate, the origin of this discussion. The heart rate is established by a combination of cardiac contraction and cardiac conduction. The latter is a process mediated by ion signalling, which mostly relies on calcium, sodium and potassium channels (Barry and Townsend, 2010).Thanks to these ion channels, a coordinated depolarisation of electrically coupled heart muscle cells (cardiomyocytes) in the atria and ventricles is possible which ultimately leads to periodic contraction of the heart. The heart rate is regulated by the autonomic nervous system, which stimulates the sinoatrial node (SAN). Electrical signals from the SAN are transferred to the atrioventricular node and then to the ventricular conduction system to complete one full heart beat (van Eif et al., 2018). Interestingly, it was shown, that TNNT2 and other troponins contribute to cardiac muscle contraction. Specifically, TNNT2 causes significant potentiation of $Ca2^{+}$-signal-mediation. The intensity of this process was altered in heterozygous knockout animals (Kajioka et al., 2012), which need higher $Ca2^{+}$ doses to produce the same effect. As described in our results we have observed reduced *TNNT2* expression in microRNA-499-5p samples. Considering its reported function in calcium mediated muscle contraction we'd like to connect the here reported reduced heart rate to misregulation of *TNNT2* function. Possibly, the present $Ca2^{+}$ concentrations are not sufficient to mediate normal contraction. To strengthen the connection between NOTCH signalling and our observations, we tried rescuing the microRNA-499-5p knockdown phenotype by simultaneous injection of the NOTCH inhibitor DAPT. Unfortunately, heart rate analysis did not reveal a reversal to control conditions (Figure 21B). During this analysis we noted that high doses of DMSO (50%) abolished AntagomiR function, which potentially masked the results (data not shown). Reduced DMSO (10%) amounts did not show such an effect, but we were not able to confirm NICD downregulation due to the lack of antibodies cross reacting with chick protein (Figure 21D). In addition to our own experiments, a recent report has shown that *TNNT2* downregulation is accompanied by down regulation of *TBX3*, a marker for the maturing conduction system (England et al., 2016), which could also be shown in our RNAseq data (data not shown). Moreover, in another report a prolonged QRS duration, HV interval and QT interval were observed in a heterozygous *TNNT2* mutant strain, which suggested conduction delays and repolarisation abnormalities. These differences have not been seen in haploinsufficient mice in which TNNT2 protein levels stayed the same (Ahmad et al., 2008). Nonetheless the gathered data and literature information indicate

that the observed reduction in heart rate might be connected to both the cardiac contraction and conduction system. Future experiments should try to strengthen the link between microRNA-499-5p, NOTCH and TNNT2 signalling, assess TNNT2 protein levels and investigate further down the TBX3 signalling cascade.

In summary we were able to report a strong heart rate phenotype after microRNA-499-5p knockdown which was accompanied by expression changes of troponin genes which points towards a role of microRNA-499-5p in heart rate control. All in all, our results and that of published work (Abad et al., 2017, Sluijter et al., 2010) indicates that this signalling is coordinated via a NOTCH pathway (Figure 22A).

5.4 RNA extraction – a major challenge for data analysis

Commonly used techniques for RNA extraction are phenol/chloroform extraction, TRIzol® mediated extraction or simply column-based extraction kits from different manufacturers (Deng et al., 2005) During this research project we have used the latter two of them. In literature both extraction variants have been used extensively (Deng et al., 2005) and reports about differences have only been published for specific contexts like the GC bias for microRNA extraction when using a TRIzol® based procedure on low cell numbers (Kim et al., 2012). However, using different methods during this project posed a hurdle for data analysis, since the data obtained of the different methods showed in part conflicting results (Appendix 8.2). Extraction kits in our lab were available from different vendors, but the cleanest and most consistent results were achieved by using Zymo products, which include Proteinase-K treatment, DNAse treatment, a gDNA removal column step and a special lysis buffer that prevents RNA degradation. Similarly, we have used a column clean up approach from Zymo after RNA precipitation originating from TRIzol® phase separation, that also included Proteinase-K treatment and DNAse treatment. The actual problem did not arise during extraction but during downstream analysis particularly when quantifying gene expression by RT-qPCR or RNAseq. The first time we encountered issues, was during experiments confirming a successful microRNA-499-5p knockdown (Figure 14 A, B), which showed an increase instead of confirming loss or reduction when using samples whose extraction involved TRIzol®. At the same time another microRNA related project was running in the Münsterberg laboratory and other researchers (Dr. Estefanía Lozano-Velasco) conducting identical experiments for other microRNAs have made similar observations, i.e. apparent upregulation instead of knockdown (data not shown). Previously RNA extraction for microRNAs has been performed using kit-based approaches in the lab but here the aim was to obtain higher yields of total RNA for RNAseq/transcriptomics, which usually can be achieved by TRIzol® extraction. Reverting extraction procedures to kit-based approaches showed the expected knockdown of microRNA-499-5p in AM-499-5p injected samples (Figure 13B, C). Possible reasoning for the observed differences involved a physiological feedback response in the form of microRNA precursor upregulation, which was quickly disproved (Figure 14C). Another hypothesis evolved around microRNA-AntagomiR duplex stability which prevents degradation *in vivo* but gets released after TRIzol® contact and thus allowing detection of more microRNA in RT-qPCR (although duplex formation would render the microRNA non-functional *in vivo*). Interestingly original research about AnatgomiRs showed knockdown confirmation by Northern Blot using TRIzol® extracted samples (Krutzfeldt et al., 2007, Krutzfeldt et al., 2005). The fact, that the authors used the identical

reagent as we in this study makes our observations even more confusing. Nonetheless we feel that our experiments were carefully planned and executed, indeed some of the presented results have been published after peer review (Wittig et al., 2018). Experiments attempting to resolve the issue around the extraction method have been repeated several times involving different researchers (sample generation: J.G. Wittig, M. Robles-García and Dr. E. Lozano-Velasco; RNA extraction: J.G. Wittig and Dr. E. Lozano-Velasco; RT-qPCR: J.G. Wittig and Dr. E. Lozano-Velasco; Northern-Blot: Dr. M. Billmeier) however, without being able to reach a definitive conclusion. In contrast, the observed method difference for AntagomiR knockdown confirmation expanded to differential expression analysis of genes of interest (mRNA) (Figure 14D) where our hypothesised explanation that TRIzol® releases the AntagomiR-microRNA duplex has no impact. Initially, we thought that accidental sample swapping was the most likely source of error, however similar results have been obtained by independent researchers in our lab using different samples and microRNAs of interest, which makes us confident to exclude human error and conclude that a technical aspect of the different methods must interfere in the context of our lab and potentially in others as well. Interestingly, we were able to show identical results as (Sluijter et al., 2010) for *ACTC1* downregulation on microRNA-499 inhibition, since both studies used kit-based extraction approaches. However, when comparing our data for *TNNI2* and *TNNT3*, which both showed downregulation in RNAseq of microRNA-499-5p knockdown samples (data not shown) to gene expression analysis performed on TRIzol® extracted samples for microRNA-499 TG animals (overexpresseion), our results are contradicting, as Wang et al. (2011) showed downregulation of these genes as well. This suggests that the difference between the methods is more widespread than anticipated and might not be caused by human error and not be specific to our lab. For further experiments we have chosen to proceed with non-TRIzol® based extraction approaches since those allowed us to obtain confirmation of successful AntagomiR knockdown of microRNA-499-5p (Figure 13B, C). Moreover, reports have previously noted a bias of TRIzol® regarding GC-content, particularly when extracting microRNAs (Kim et al., 2012), thus we do not recommend extraction methods that involve TRIzol® when examining microRNAs.

As of now, no definite explanation for the differences observed between the different extraction methods could be made and thus we cannot say which method delivers the “right” results or by what the difference is caused. With our current understanding, we feel that the ISH results, even though not quantitative deliver the “more trustworthy” results. The ISH procedure contains less steps, which can introduce errors like RNA extraction, primer or RT-qPCR probe design or generation of sequencing libraries. The ISH probes used in the project are custom designed from chicken cDNA which were cloned into a pGEM-T-Easy vector and sequenced prior to probe synthesis. Probe sequences were chosen to not overlap with any other genes and thus should solely identify one gene of interest at a time. Considering the unknown cause of difference for the gene quantification results depending on RNA extraction method, we believe that ISH is the more reliable method for qualitatively assessing differential gene expression.

6 Outlook and future prospects

In summary this project has meaningfully contributed to the progression of science. During this project we were able to develop a method for cardiac injection that is not affected by blood circulation and thus allowed us to study microRNA-499-5p knockdown in a locally restricted fashion. Said knockdown analysis led us to connect signalling of the microRNA to two major transcription factors, ETS1 and NOTCH1 in the heart. New insight has been given into signalling cascades surrounding those transcription factors. For ETS1 new evidence has been shown promoting its signalling role in ECM synthesis rather than its more commonly known role in ECM degradation. Further a connection was made for microRNA-499-5p to a previously published NOTCH signalling cascade that affects heart rate. With respect to this we have shown a strong reduction in heart rate after microRNA-499-5p knockdown which hasn't been reported before.

Our investigation was led by confirmation of target interaction studies by luciferase assays in which we have validated other microRNAs in addition to microRNA-499-5p. This data will give a great starting point for further investigations surrounding microRNA-126-3p, microRNA-221-3p and microRNA-451, which all showed increased transcript levels in the heart during cushion formation.

To our trouble our data analysis was complicated by the described differences in quantifying gene expression depending on RNA extraction method. Solving this issue is great importance to conduct future experiments with clear conscience. Unfortunately, as of yet we do not have a possible solution for this problem.

For future experiments we recommend including more rescue studies like the attempted NOTCH inhibition via DAPT to establish a stronger link between signalling components. Particularly interesting could be further studies involving microRNA mimic injections to be able to analyse both scenarios of increased and reduced microRNA modulation *in vivo*. In general emphasis should be put on showing microRNA target interaction *in vivo* since several reports showed difference in *in vivo* and *in vitro* results. A possible approach for this could involve RISC pulldown studies as the one previously reported by Matkovich et al. (2011), where target genes of microRNA-499 have been isolated. Combination of such methods we the recent trend towards single cell analysis could deliver a completely new spectrum of information available about microRNA target interaction. Said single cell technologies should also be considered for RNAseq since the heart is a highly complex organ with many different tissue layers and cell types. As we have introduced signalling in the heart to initiate EMT and cushion maturation requires very specific and localised expression. The RNAseq performed in this study was able to show overall trends of differential gene expression but one or the other effect might have been masked due to upregulation/derepression in one region and downregulation in another.

All in all, this study revealed new insights into microRNA-499-5p signalling and has revealed novel avenues for further research.

7 References

Abad, M., Hashimoto, H., Zhou, H., Morales, M. G., Chen, B., Bassel-Duby, R. & Olson, E. N. 2017. NOTCH Inhibition Enhances Cardiac Reprogramming by Increasing MEF2C Transcriptional Activity. Stem Cell Reports, 8, 548-560.

Agarwal, V., Bell, G. W., Nam, J. W. & Bartel, D. P. 2015. Predicting effective microRNA target sites in mammalian mRNAs. Elife, 4.

Ahmad, F., Banerjee, S. K., Lage, M. L., Huang, X. N., Smith, S. H., Saba, S., Rager, J., Conner, D. A., Janczewski, A. M., Tobita, K., Tinney, J. P., Moskowitz, I. P., Perez-Atayde, A. R., Keller, B. B., Mathier, M. A., Shroff, S. G., Seidman, C. E. & Seidman, J. G. 2008. The role of cardiac troponin T quantity and function in cardiac development and dilated cardiomyopathy. PLoS One, 3, e2642.

Aken, B. L., Ayling, S., Barrell, D., Clarke, L., Curwen, V., Fairley, S., Fernandez Banet, J., Billis, K., Garcia Giron, C., Hourlier, T., Howe, K., Kahari, A., Kokocinski, F., Martin, F. J., Murphy, D. N., Nag, R., Ruffier, M., Schuster, M., Tang, Y. A., Vogel, J. H., White, S., Zadissa, A., Flicek, P. & Searle, S. M. 2016. The Ensembl gene annotation system. Database (Oxford), 2016.

Akiyama, H., Chaboissier, M. C., Behringer, R. R., Rowitch, D. H., Schedl, A., Epstein, J. A. & De Crombrugghe, B. 2004. Essential role of Sox9 in the pathway that controls formation of cardiac valves and septa. Proc Natl Acad Sci U S A, 101, 6502-7.

Allen, S. P., Bogardi, J. P., Barlow, A. J., Mir, S. A., Qayyum, S. R., Verbeek, F. J., Anderson, R. H., Francis-West, P. H., Brown, N. A. & Richardson, M. K. 2001. Misexpression of noggin leads to septal defects in the outflow tract of the chick heart. Dev Biol, 235, 98-109.

Alturkistani, H. A., Tashkandi, F. M. & Mohammedsaleh, Z. M. 2015. Histological Stains: A Literature Review and Case Study. Glob J Health Sci, 8, 72-9.

Andrews, S. 2010. FastQC: a quality control tool for high throughput sequence data [Online]. Available: http://www.bioinformatics.babraham.ac.uk/projects/fastqc [Accessed].

Antin, P. B., Kaur, S., Stanislaw, S., Davey, S., Konieczka, J. H., Yatskievych, T. A. & Darnell, D. K. 2007. Gallus expression in situ hybridization analysis: a chicken embryo gene expression database. Poult Sci, 86, 1472-7.

Balic, A., Garcia-Morales, C., Vervelde, L., Gilhooley, H., Sherman, A., Garceau, V., Gutowska, M. W., Burt, D. W., Kaiser, P., Hume, D. A. & Sang, H. M. 2014. Visualisation of chicken macrophages using transgenic reporter genes: insights into the development of the avian macrophage lineage. Development, 141, 3255-65.

Barry, S. P. & Townsend, P. A. 2010. Chapter Three - What Causes a Broken Heart—Molecular Insights into Heart Failure. In: Jeon, K. W. (ed.) International Review of Cell and Molecular Biology. Academic Press.

Bartel, D. P. 2004. MicroRNAs: genomics, biogenesis, mechanism, and function. Cell, 116, 281-97.

Bartel, D. P. 2009. MicroRNAs: target recognition and regulatory functions. Cell, 136, 215-33.

Bellairs, R. & Osmond, M. 2014. Atlas of Chick Development, Elsevier Science.

Bergmann, O., Bhardwaj, R. D., Bernard, S., Zdunek, S., Barnabe-Heider, F., Walsh, S., Zupicich, J., Alkass, K., Buchholz, B. A., Druid, H., Jovinge, S. & Frisen, J. 2009. Evidence for cardiomyocyte

renewal in humans. Science, 324, 98-102.

Betel, D., Wilson, M., Gabow, A., Marks, D. S. & Sander, C. 2008. The microRNA.org resource: targets and expression. Nucleic Acids Res, 36, D149-53.

Bhatnagar, S., Lipovsky, C., Qiao, J., Hicks, S., Li, R., Khandekar, A., Guzy, R., Nichols, C., Efimov, I. & Rentschler, S. 2016. The Role of NOTCH Signaling on Heart Rate and Atrial Conduction. Undergraduate Research Symposium Posters: Washington University in St. Louis.

Bhuiyan, S. S., Kinoshita, S., Wongwarangkana, C., Asaduzzaman, M., Asakawa, S. & Watabe, S. 2013. Evolution of the myosin heavy chain gene MYH14 and its intronic microRNA miR-499: muscle-specific miR-499 expression persists in the absence of the ancestral host gene. Bmc Evolutionary Biology, 13.

Bollerot, K., Romero, S., Dunon, D. & Jaffredo, T. 2005. Core binding factor in the early avian embryo: cloning of Cbfbeta and combinatorial expression patterns with Runx1. Gene Expr Patterns, 6, 29-39.

Bonnet, X. 1894. Charles Bonnet's Idea of the Development of the Chick. Science, 23, 71-2.

Borghetti, G., Eisenberg, C. A., Signore, S., Sorrentino, A., Kaur, K., Andrade-Vicenty, A., Edwards, J. G., Nerkar, M., Qanud, K., Sun, D., Goichberg, P., Leri, A., Anversa, P., Eisenberg, L. M., Jacobson, J. T., Hintze, T. H. & Rota, M. 2018. NOTCH signaling modulates the electrical behavior of cardiomyocytes. Am J Physiol Heart Circ Physiol, 314, H68-H81.

Bouabe, H. & Okkenhaug, K. 2013. Gene targeting in mice: a review. Methods Mol Biol, 1064, 315-36.

Bray, N. L., Pimentel, H., Melsted, P. & Pachter, L. 2016. Near-optimal probabilistic RNA-seq quantification. Nat Biotechnol, 34, 525-7.

Bustin, S. A., Benes, V., Garson, J. A., Hellemans, J., Huggett, J., Kubista, M., Mueller, R., Nolan, T., Pfaffl, M. W., Shipley, G. L., Vandesompele, J. & Wittwer, C. T. 2009. The MIQE guidelines: minimum information for publication of quantitative real-time PCR experiments. Clin Chem, 55, 611-22.

Camenisch, T. D., Spicer, A. P., Brehm-Gibson, T., Biesterfeldt, J., Augustine, M. L., Calabro, A., Jr., Kubalak, S., Klewer, S. E. & Mcdonald, J. A. 2000. Disruption of hyaluronan synthase-2 abrogates normal cardiac morphogenesis and hyaluronan-mediated transformation of epithelium to mesenchyme. J Clin Invest, 106, 349-60.

Catalanotto, C., Cogoni, C. & Zardo, G. 2016. MicroRNA in Control of Gene Expression: An Overview of Nuclear Functions. Int J Mol Sci, 17.

Chabot, S., Orio, J., Castanier, R., Bellard, E., Nielsen, S. J., Golzio, M. & Teissie, J. 2012. LNA-based oligonucleotide electrotransfer for miRNA inhibition. Mol Ther, 20, 1590-8.

Chen, J. & Wang, D. Z. 2012. microRNAs in cardiovascular development. J Mol Cell Cardiol, 52, 949-57.

Chen, J. F., Mandel, E. M., Thomson, J. M., Wu, Q., Callis, T. E., Hammond, S. M., Conlon, F. L. & Wang, D. Z. 2006. The role of microRNA-1 and microRNA-133 in skeletal muscle proliferation and differentiation. Nat Genet, 38, 228-33.

Cordes, K. R., Sheehy, N. T., White, M. P., Berry, E. C., Morton, S. U., Muth, A. N., Lee, T. H., Miano,

J. M., Ivey, K. N. & Srivastava, D. 2009. miR-145 and miR-143 regulate smooth muscle cell fate and plasticity. Nature, 460, 705-10.

Cui, C., Filla, M. B., Jones, E. A., Lansford, R., Cheuvront, T., Al-Roubaie, S., Rongish, B. J. & Little, C. D. 2013. Embryogenesis of the first circulating endothelial cells. PloS one, 8, e60841.

Darnell, D. K., Kaur, S., Stanislaw, S., Davey, S., Konieczka, J. H., Yatskievych, T. A. & Antin, P. B. 2007. GEISHA: an in situ hybridization gene expression resource for the chicken embryo. Cytogenet Genome Res, 117, 30-5.

Davidson, M. J., Jones, J. M., Emani, S. M., Wilson, K. H., Jaggers, J., Koch, W. J. & Milano, C. A. 2001. Cardiac gene delivery with cardiopulmonary bypass. Circulation, 104, 131-3.

Del Monte-Nieto, G., Ramialison, M., Adam, A. a. S., Wu, B., Aharonov, A., D'uva, G., Bourke, L. M., Pitulescu, M. E., Chen, H., De La Pompa, J. L., Shou, W., Adams, R. H., Harten, S. K., Tzahor, E., Zhou, B. & Harvey, R. P. 2018. Control of cardiac jelly dynamics by NOTCH1 and NRG1 defines the building plan for trabeculation. Nature, 557, 439-445.

Deng, M. Y., Wang, H., Ward, G. B., Beckham, T. R. & Mckenna, T. S. 2005. Comparison of six RNA extraction methods for the detection of classical swine fever virus by real-time and conventional reverse transcription-PCR. J Vet Diagn Invest, 17, 574-8.

Desgrosellier, J. S., Mundell, N. A., Mcdonnell, M. A., Moses, H. L. & Barnett, J. V. 2005. Activin receptor-like kinase 2 and SMAD6 regulate epithelial-mesenchymal transformation during cardiac valve formation. Dev Biol, 280, 201-10.

Dobaczewski, M., Chen, W. & Frangogiannis, N. G. 2011. Transforming growth factor (TGF)-beta signaling in cardiac remodeling. J Mol Cell Cardiol, 51, 600-6.

England, J., Granados-Riveron, J., Polo-Parada, L., Kuriakose, D., Moore, C., Brook, J. D., Rutland, C. S., Setchfield, K., Gell, C., Ghosh, T. K., Bu'lock, F., Thornborough, C., Ehler, E. & Loughna, S. 2017. Tropomyosin 1: Multiple roles in the developing heart and in the formation of congenital heart defects. J Mol Cell Cardiol, 106, 1-13.

England, J., Pang, K. L., Parnall, M., Haig, M. I. & Loughna, S. 2016. Cardiac troponin T is necessary for normal development in the embryonic chick heart. J Anat, 229, 436-49.

Epstein, J. A., Li, J., Lang, D., Chen, F., Brown, C. B., Jin, F., Lu, M. M., Thomas, M., Liu, E., Wessels, A. & Lo, C. W. 2000. Migration of cardiac neural crest cells in Splotch embryos. Development, 127, 1869-78.

Evsen, L. & Doetzlhofer, A. 2016. Gene Transfer into the Chicken Auditory Organ by In Ovo Micro-electroporation. J Vis Exp.

Fischer, A. H., Jacobson, K. A., Rose, J. & Zeller, R. 2008. Hematoxylin and eosin staining of tissue and cell sections. CSH Protoc, 2008, pdb prot4986.

Fu, Y., Jiang, W., Zhao, Y., Huang, Y., Zhang, H., Wang, H. & Pu, J. 2018. A Simple and Efficient Method for In Vivo Cardiac-specific Gene Manipulation by Intramyocardial Injection in Mice. J Vis Exp.

Galvin, K. M., Donovan, M. J., Lynch, C. A., Meyer, R. I., Paul, R. J., Lorenz, J. N., Fairchild-Huntress, V., Dixon, K. L., Dunmore, J. H., Gimbrone, M. A., Jr., Falb, D. & Huszar, D. 2000. A role for smad6 in development and homeostasis of the cardiovascular system. Nat Genet, 24, 171-4.

Gao, Z., Kim, G. H., Mackinnon, A. C., Flagg, A. E., Bassett, B., Earley, J. U. & Svensson, E. C. 2010. Ets1

is required for proper migration and differentiation of the cardiac neural crest. Development, 137, 1543-51.

Gilles, C., Newgreen, D. F., Sato, H. & Thompson, E. W. 2000-2013. Matrix Metalloproteases and Epithelial-to-Mesenchymal Madame Curie Bioscience Database. Austin (TX): Landes Bioscience.

Gitler, A. D., Lu, M. M., Jiang, Y. Q., Epstein, J. A. & Gruber, P. J. 2003. Molecular markers of cardiac endocardial cushion development. Dev Dyn, 228, 643-50.

Goehringer, C., Rutschow, D., Bauer, R., Schinkel, S., Weichenhan, D., Bekeredjian, R., Straub, V., Kleinschmidt, J. A., Katus, H. A. & Muller, O. J. 2009. Prevention of cardiomyopathy in delta-sarcoglycan knockout mice after systemic transfer of targeted adeno-associated viral vectors. Cardiovasc Res, 82, 404-10.

Goljanek-Whysall, K., Sweetman, D., Abu-Elmagd, M., Chapnik, E., Dalmay, T., Hornstein, E. & Munsterberg, A. 2011. MicroRNA regulation of the paired-box transcription factor PAX3 confers robustness to developmental timing of myogenesis. Proc Natl Acad Sci U S A, 108, 11936-41.

Gosselin-Badaroudine, P., Keller, D. I., Huang, H., Pouliot, V., Chatelier, A., Osswald, S., Brink, M. & Chahine, M. 2012. A proton leak current through the cardiac sodium channel is linked to mixed arrhythmia and the dilated cardiomyopathy phenotype. PLoS One, 7, e38331.

Grimson, A., Farh, K. K., Johnston, W. K., Garrett-Engele, P., Lim, L. P. & Bartel, D. P. 2007. MicroRNA targeting specificity in mammals: determinants beyond seed pairing. Mol Cell, 27, 91-105.

Grocott, T., Thomas, P. & Munsterberg, A. E. 2016. Atlas Toolkit: Fast registration of 3D morphological datasets in the absence of landmarks. Scientific reports, 6, 20732.

Hamburger, V. & Hamilton, H. L. 1951. A series of normal stages in the development of the chick embryo. J Morphol, 88, 49-92.

Harris, I. S. & Black, B. L. 2010. Development of the endocardium. Pediatr Cardiol, 31, 391-9.

Havens, M. A., Reich, A. A. & Hastings, M. L. 2014. Drosha promotes splicing of a pre-microRNA-like alternative exon. PLoS Genet, 10, e1004312.

Henderson, D. J., Chaudhry, B. & Pompa, J. L. D. L. 2018. Development of the arterial valves. In: Pérez-Pomares, J. M. & Kelly, R. (eds.) The ESC Textbook of Cardiovascular Development. Oxford University Press.

High, F. A., Jain, R., Stoller, J. Z., Antonucci, N. B., Lu, M. M., Loomes, K. M., Kaestner, K. H., Pear, W. S. & Epstein, J. A. 2009. Murine Jagged1/NOTCH signaling in the second heart field orchestrates Fgf8 expression and tissue-tissue interactions during outflow tract development. J Clin Invest, 119, 1986-96.

Inui, M., Martello, G. & Piccolo, S. 2010. MicroRNA control of signal transduction. Nat Rev Mol Cell Biol, 11, 252-63.

Ishii, Y., Garriock, R. J., Navetta, A. M., Coughlin, L. E. & Mikawa, T. 2010. BMP signals promote proepicardial protrusion necessary for recruitment of coronary vessel and epicardial progenitors to the heart. Dev Cell, 19, 307-16.

Jinnin, M., Ihn, H., Asano, Y., Yamane, K., Trojanowska, M. & Tamaki, K. 2004. Tenascin-C upregulation by transforming growth factor-beta in human dermal fibroblasts involves SMAD3, Sp1, and Ets1. Oncogene, 23, 1656-67.

Kain, K. H., Miller, J. W., Jones-Paris, C. R., Thomason, R. T., Lewis, J. D., Bader, D. M., Barnett, J. V. & Zijlstra, A. 2014. The chick embryo as an expanding experimental model for cancer and cardiovascular research. Developmental dynamics, 243, 216-28.

Kajioka, S., Takahashi-Yanaga, F., Shahab, N., Onimaru, M., Matsuda, M., Takahashi, R., Asano, H., Morita, H., Morimoto, S., Yonemitsu, Y., Hayashi, M., Seki, N., Sasaguri, T., Hirata, M., Nakayama, S. & Naito, S. 2012. Endogenous cardiac troponin T modulates Ca(2+)-mediated smooth muscle contraction. Sci Rep, 2, 979.

Kalhor, R., Kalhor, K., Mejia, L., Leeper, K., Graveline, A., Mali, P. & Church, G. M. 2018. Developmental barcoding of whole mouse via homing CRISPR. Science, 361.

Kiezun, A., Artzi, S., Modai, S., Volk, N., Isakov, O. & Shomron, N. 2012. miRviewer: a multispecies microRNA homologous viewer. BMC Res Notes, 5, 92.

Kim, Y.-K., Yeo, J., Kim, B., Ha, M. & Kim, V. N. 2012. Short Structured RNAs with Low GC Content Are Selectively Lost during Extraction from a Small Number of Cells. Molecular Cell, 46, 893-895.

Kirby, M. L. 1989. Plasticity and predetermination of mesencephalic and trunk neural crest transplanted into the region of the cardiac neural crest. Dev Biol, 134, 402-12.

Kirby, M. L. & Waldo, K. L. 1995. Neural crest and cardiovascular patterning. Circ Res, 77, 211-5.

Kozomara, A. & Griffiths-Jones, S. 2011. miRBase: integrating microRNA annotation and deep-sequencing data. Nucleic Acids Res, 39, D152-7.

Kozomara, A. & Griffiths-Jones, S. 2014. miRBase: annotating high confidence microRNAs using deep sequencing data. Nucleic Acids Res, 42, D68-73.

Kraus, P., Sivakamasundari, V., Xing, X. & Lufkin, T. 2014. Generating mouse lines for lineage tracing and knockout studies. Methods Mol Biol, 1194, 37-62.

Kretzschmar, K. & Watt, F. M. 2012. Lineage tracing. Cell, 148, 33-45.

Krueger, F. 2015. Trim Galore - A Wrapper Tool Around Cutadapt and FastQC to Consistently Apply Quality and Adapter Trimming to FastQ Files [Online]. Available: https://www.bioinformatics.babraham.ac.uk/projects/trim_galore/ [Accessed].

Krutzfeldt, J., Kuwajima, S., Braich, R., Rajeev, K. G., Pena, J., Tuschl, T., Manoharan, M. & Stoffel, M. 2007. Specificity, duplex degradation and subcellular localization of antagomirs. Nucleic Acids Res, 35, 2885-92.

Krutzfeldt, J., Rajewsky, N., Braich, R., Rajeev, K. G., Tuschl, T., Manoharan, M. & Stoffel, M. 2005. Silencing of microRNAs in vivo with 'antagomirs'. Nature, 438, 685-9.

Lambeth, L. S., Ohnesorg, T., Cummins, D. M., Sinclair, A. H. & Smith, C. A. 2014. Development of retroviral vectors for tissue-restricted expression in chicken embryonic gonads. PLoS One, 9, e101811.

Lawrence, J. B. & Singer, R. H. 1985. Quantitative analysis of in situ hybridization methods for the detection of actin gene expression. Nucleic Acids Res, 13, 1777-99.

Le Douarin, N. 1973. A biological cell labeling technique and its use in expermental embryology. Dev Biol, 30, 217-22.

Lewis, B. P., Burge, C. B. & Bartel, D. P. 2005. Conserved seed pairing, often flanked by adenosines,

indicates that thousands of human genes are microRNA targets. Cell, 120, 15-20.

Li, C., Wen, A., Shen, B., Lu, J., Huang, Y. & Chang, Y. 2011. FastCloning: a highly simplified, purification-free, sequence- and ligation-independent PCR cloning method. BMC Biotechnol, 11, 92.

Li, Z., Xu, R. & Li, N. 2018a. Correction to: MicroRNAs from plants to animals, do they define a new messenger for communication? Nutr Metab (Lond), 15, 74.

Li, Z., Xu, R. & Li, N. 2018b. MicroRNAs from plants to animals, do they define a new messenger for communication? Nutr Metab (Lond), 15, 68.

Lin, C. J., Lin, C. Y., Chen, C. H., Zhou, B. & Chang, C. P. 2012. Partitioning the heart: mechanisms of cardiac septation and valve development. Development, 139, 3277-99.

Liu, N., Bezprozvannaya, S., Williams, A. H., Qi, X., Richardson, J. A., Bassel-Duby, R. & Olson, E. N. 2008. microRNA-133a regulates cardiomyocyte proliferation and suppresses smooth muscle gene expression in the heart. Genes Dev, 22, 3242-54.

Liu, N. & Olson, E. N. 2010. MicroRNA regulatory networks in cardiovascular development. Dev Cell, 18, 510-25.

Livak, K. J. & Schmittgen, T. D. 2001. Analysis of relative gene expression data using real-time quantitative PCR and the 2(-Delta Delta C(T)) Method. Methods, 25, 402-8.

Lockhart, M., Wirrig, E., Phelps, A. & Wessels, A. 2011. Extracellular matrix and heart development. Birth Defects Res A Clin Mol Teratol, 91, 535-50.

Lu-Lu, Z. & Bo, Y. 2012. MIR-499 INDUCES CARDIAC DIFFERENTIATION OF RAT BONE MARROW-DERIVED MESENCHYMAL STEM CELLS. Heart, 98, E52-E52.

Lufkin, T. 2007. In situ hybridization of whole-mount mouse embryos with RNA probes: hybridization, washes, and histochemistry. CSH Protoc, 2007, pdb prot4823.

Luo, X., Yang, B. & Nattel, S. 2015. MicroRNAs and atrial fibrillation: mechanisms and translational potential. Nat Rev Cardiol, 12, 80-90.

Macdonald, J., Taylor, L., Sherman, A., Kawakami, K., Takahashi, Y., Sang, H. M. & Mcgrew, M. J. 2012. Efficient genetic modification and germ-line transmission of primordial germ cells using piggyBac and Tol2 transposons. Proceedings of the National Academy of Sciences of the United States of America, 109, E1466-72.

Macgrogan, D., Munch, J. & De La Pompa, J. L. 2018a. NOTCH and interacting signalling pathways in cardiac development, disease, and regeneration. Nat Rev Cardiol, 15, 685-704.

Macgrogan, D., Pérez-Pomares, J. M., Chaudhry, B., De La Pompa, J. L. & Henderson, D. J. 2018b. From cushions to leaflets: morphogenesis of cardiac atrioventricular valves. In: Pérez-Pomares, J. M. & Kelly, R. (eds.) The ESC Textbook of Cardiovascular Development. Oxford University Press.

Macias, D., Perez-Pomares, J. M., Garcia-Garrido, L., Carmona, R. & Munoz-Chapuli, R. 1998. Immunoreactivity of the ets-1 transcription factor correlates with areas of epithelial-mesenchymal transition in the developing avian heart. Anat Embryol (Berl), 198, 307-15.

Marín-García, J. 2014. Chapter 9 - Molecular Determinants of Cardiac Neovascularization, Academic Press.

Martin, M. M., Buckenberger, J. A., Jiang, J., Malana, G. E., Nuovo, G. J., Chotani, M., Feldman, D. S., Schmittgen, T. D. & Elton, T. S. 2007. The human angiotensin II type 1 receptor +1166 A/C polymorphism attenuates microRNA-155 binding. J Biol Chem, 282, 24262-9.

Martinsen, B. J. 2005. Reference guide to the stages of chick heart embryology. Dev Dyn, 233, 1217-37.

Matkovich, S. J., Van Booven, D. J., Eschenbacher, W. H. & Dorn, G. W. 2011. RISC RNA Sequencing for Context-Specific Identification of In Vivo MicroRNA Targets. Circulation Research, 108, 18-U50.

Mccormick, D. 2015. Investigating microRNAs during cardiac Development in the Chick. PhD PhD Thesis, University of East Anglia.

Mcglinn, E., Yekta, S., Mansfield, J. H., Soutschek, J., Bartel, D. P. & Tabin, C. J. 2009. In ovo application of antagomiRs indicates a role for miR-196 in patterning the chick axial skeleton through Hox gene regulation. Proc Natl Acad Sci U S A, 106, 18610-5.

Meilhac, S. M. & Buckingham, M. E. 2018. The deployment of cell lineages that form the mammalian heart. Nat Rev Cardiol, 15, 705-724.

Mercado-Pimentel, M. E. & Runyan, R. B. 2007. Multiple transforming growth factor-beta isoforms and receptors function during epithelial-mesenchymal cell transformation in the embryonic heart. Cells Tissues Organs, 185, 146-56.

Mi, H., Muruganujan, A., Huang, X., Ebert, D., Mills, C., Guo, X. & Thomas, P. D. 2019. Protocol Update for large-scale genome and gene function analysis with the PANTHER classification system (v.14.0). Nat Protoc, 14, 703-721.

Midwood, K. S., Chiquet, M., Tucker, R. P. & Orend, G. 2016. Tenascin-C at a glance. J Cell Sci, 129, 4321-4327.

Morton, S. U., Scherz, P. J., Cordes, K. R., Ivey, K. N., Stainier, D. Y. & Srivastava, D. 2008. microRNA-138 modulates cardiac patterning during embryonic development. Proc Natl Acad Sci U S A, 105, 17830-5.

Musso, G., Tasan, M., Mosimann, C., Beaver, J. E., Plovie, E., Carr, L. A., Chua, H. N., Dunham, J., Zuberi, K., Rodriguez, H., Morris, Q., Zon, L., Roth, F. P. & Macrae, C. A. 2014. Novel cardiovascular gene functions revealed via systematic phenotype prediction in zebrafish. Development, 141, 224-35.

Nie, S. & Bronner, M. E. 2015. Dual developmental role of transcriptional regulator Ets1 in Xenopus cardiac neural crest vs. heart mesoderm. Cardiovasc Res, 106, 67-75.

Norris, R. A., Kern, C. B., Wessels, A., Moralez, E. I., Markwald, R. R. & Mjaatvedt, C. H. 2004. Identification and detection of the periostin gene in cardiac development. Anat Rec A Discov Mol Cell Evol Biol, 281, 1227-33.

O'brien, J., Hayder, H., Zayed, Y. & Peng, C. 2018. Overview of MicroRNA Biogenesis, Mechanisms of Actions, and Circulation. Front Endocrinol (Lausanne), 9, 402.

Paige, S. L., Plonowska, K., Xu, A. & Wu, S. M. 2015. Molecular regulation of cardiomyocyte differentiation. Circ Res, 116, 341-53.

Pall, G. S. & Hamilton, A. J. 2008. Improved northern blot method for enhanced detection of small

RNA. Nat Protoc, 3, 1077-84.

Person, A. D., Klewer, S. E. & Runyan, R. B. 2005. Cell biology of cardiac cushion development. Int Rev Cytol, 243, 287-335.

Pimentel, H., Bray, N. L., Puente, S., Melsted, P. & Pachter, L. 2017. Differential analysis of RNA-seq incorporating quantification uncertainty. Nat Methods, 14, 687-690.

Plein, A., Fantin, A. & Ruhrberg, C. 2015. Neural crest cells in cardiovascular development. Curr Top Dev Biol, 111, 183-200.

Porrello, E. R. & Olson, E. N. 2014. A neonatal blueprint for cardiac regeneration. Stem Cell Res, 13, 556-70.

Pruitt, K. D., Tatusova, T., Brown, G. R. & Maglott, D. R. 2012. NCBI Reference Sequences (RefSeq): current status, new features and genome annotation policy. Nucleic Acids Res, 40, D130-5.

Qayyum, S. R., Webb, S., Anderson, R. H., Verbeek, F. J., Brown, N. A. & Richardson, M. K. 2001. Septation and valvar formation in the outflow tract of the embryonic chick heart. Anat Rec, 264, 273-83.

Randles, C. A. & Romanoff, A. L. 1954. A Preliminary Study on the Hatchability of Chicken Eggs Subjected to Shaking Agitation. Poultry Science, 33, 374-377.

Rehmsmeier, M., Steffen, P., Hochsmann, M. & Giegerich, R. 2004. Fast and effective prediction of microRNA/target duplexes. RNA, 10, 1507-17.

Rozbicki, E., Chuai, M., Karjalainen, A. I., Song, F., Sang, H. M., Martin, R., Knolker, H. J., Macdonald, M. P. & Weijer, C. J. 2015. Myosin-II-mediated cell shape changes and cell intercalation contribute to primitive streak formation. Nature cell biology, 17, 397-408.

Schachterle, W., Rojas, A., Xu, S. M. & Black, B. L. 2012. ETS-dependent regulation of a distal Gata4 cardiac enhancer. Dev Biol, 361, 439-49.

Sharpe, J., Ahlgren, U., Perry, P., Hill, B., Ross, A., Hecksher-Sorensen, J., Baldock, R. & Davidson, D. 2002. Optical projection tomography as a tool for 3D microscopy and gene expression studies. Science, 296, 541-5.

Shi, L., Goenezen, S., Haller, S., Hinds, M. T., Thornburg, K. L. & Rugonyi, S. 2013. Alterations in pulse wave propagation reflect the degree of outflow tract banding in HH18 chicken embryos. Am J Physiol Heart Circ Physiol, 305, H386-96.

Shieh, J. T., Huang, Y., Gilmore, J. & Srivastava, D. 2011. Elevated miR-499 levels blunt the cardiac stress response. PLoS One, 6, e19481.

Shinji, H., Phillip, K. & Mark, E. C. 2014. microRNA as Biomarkers and Regulator of Cardiovascular Development and Disease. Current Pharmaceutical Design, 20, 2347-2370.

Simoes-Costa, M., Tan-Cabugao, J., Antoshechkin, I., Sauka-Spengler, T. & Bronner, M. E. 2014. Transcriptome analysis reveals novel players in the cranial neural crest gene regulatory network. Genome Res, 24, 281-90.

Singh, P., Schimenti, J. C. & Bolcun-Filas, E. 2015. A mouse geneticist's practical guide to CRISPR applications. Genetics, 199, 1-15.

Sluijter, J. P., Van Mil, A., Van Vliet, P., Metz, C. H., Liu, J., Doevendans, P. A. & Goumans, M. J.

2010. MicroRNA-1 and -499 regulate differentiation and proliferation in human-derived cardiomyocyte progenitor cells. Arterioscler Thromb Vasc Biol, 30, 859-68.

Sole, A., Mencia, N., Villalobos, X., Noe, V. & Ciudad, C. J. 2013. Validation of miRNA-mRNA interactions by electrophoretic mobility shift assays. BMC Res Notes, 6, 454.

Song, J., Yue, Q. & Munsterberg, A. 2011. Time-lapse imaging of chick cardiac precursor cells. Methods Mol Biol, 769, 359-72.

Spurlin, J., 3rd & Lwigale, P. 2013. A technique to increase accessibility to late-stage chick embryos for in ovo manipulations. Dev Dyn, 242, 148-54.

St Johnston, D. 2015. The renaissance of developmental biology. PLoS biology, 13, e1002149.

Stankunas, K., Ma, G. K., Kuhnert, F. J., Kuo, C. J. & Chang, C. P. 2010. VEGF signaling has distinct spatiotemporal roles during heart valve development. Dev Biol, 347, 325-36.

Stern, C. D. 2004. The chick embryo--past, present and future as a model system in developmental biology. Mechanisms of development, 121, 1011-3.

Stern, C. D. 2005. The chick; a great model system becomes even greater. Dev Cell, 8, 9-17.

Tahtakran, S. A. & Selleck, M. A. 2003. Ets-1 expression is associated with cranial neural crest migration and vasculogenesis in the chick embryo. Gene Expr Patterns, 3, 455-8.

Tian, J., An, X. & Niu, L. 2017. Role of microRNAs in cardiac development and disease. Exp Ther Med, 13, 3-8.

Tijsen, A. J., Pinto, Y. M. & Creemers, E. E. 2012. Non-cardiomyocyte microRNAs in heart failure. Cardiovasc Res, 93, 573-82.

Trojanowska, M. 2000. Ets factors and regulation of the extracellular matrix. Oncogene, 19, 6464-71.

Van Eif, V. W. W., Devalla, H. D., Boink, G. J. J. & Christoffels, V. M. 2018. Transcriptional regulation of the cardiac conduction system. Nat Rev Cardiol, 15, 617-630.

Van Rooij, E. & Olson, E. N. 2012. MicroRNA therapeutics for cardiovascular disease: opportunities and obstacles. Nat Rev Drug Discov, 11, 860-72.

Van Rooij, E., Quiat, D., Johnson, B. A., Sutherland, L. B., Qi, X., Richardson, J. A., Kelm, R. J., Jr. & Olson, E. N. 2009. A family of microRNAs encoded by myosin genes governs myosin expression and muscle performance. Dev Cell, 17, 662-73.

Van Rooij, E., Sutherland, L. B., Qi, X., Richardson, J. A., Hill, J. & Olson, E. N. 2007. Control of stress-dependent cardiac growth and gene expression by a microRNA. Science, 316, 575-9.

Velu, C. S. & Grimes, H. L. 2012. Utilizing antagomiR (antisense microRNA) to knock down microRNA in murine bone marrow cells. Methods Mol Biol, 928, 185-95.

Veron, N., Qu, Z., Kipen, P. A., Hirst, C. E. & Marcelle, C. 2015. CRISPR mediated somatic cell genome engineering in the chicken. Dev Biol, 407, 68-74.

Wang, C., Kam, R. K., Shi, W., Xia, Y., Chen, X., Cao, Y., Sun, J., Du, Y., Lu, G., Chen, Z., Chan, W. Y., Chan, S. O., Deng, Y. & Zhao, H. 2015a. The Proto-oncogene Transcription Factor Ets1 Regulates Neural Crest Development through Histone Deacetylase 1 to Mediate Output of Bone Morphogenetic Protein Signaling. J Biol Chem, 290, 21925-38.

Wang, C. W., Budiman Gosno, E. & Li, Y. S. 2015b. Fully automatic and robust 3D registration of serial-section microscopic images. Sci Rep, 5, 15051.

Wang, J. X., Jiao, J. Q., Li, Q., Long, B., Wang, K., Liu, J. P., Li, Y. R. & Li, P. F. 2011. miR-499 regulates mitochondrial dynamics by targeting calcineurin and dynamin-related protein-1. Nat Med, 17, 71-8.

Wang, S., Aurora, A. B., Johnson, B. A., Qi, X., Mcanally, J., Hill, J. A., Richardson, J. A., Bassel-Duby, R. & Olson, E. N. 2008. The endothelial-specific microRNA miR-126 governs vascular integrity and angiogenesis. Dev Cell, 15, 261-71.

Wei, W., Hu, Z., Fu, H., Tie, Y., Zhang, H., Wu, Y. & Zheng, X. 2012. MicroRNA-1 and microRNA-499 downregulate the expression of the ets1 proto-oncogene in HepG2 cells. Oncol Rep, 28, 701-6.

Wilson, K. D., Hu, S., Venkatasubrahmanyam, S., Fu, J. D., Sun, N., Abilez, O. J., Baugh, J. J., Jia, F., Ghosh, Z., Li, R. A., Butte, A. J. & Wu, J. C. 2010. Dynamic microRNA expression programs during cardiac differentiation of human embryonic stem cells: role for miR-499. Circ Cardiovasc Genet, 3, 426-35.

Wirrig, E. E., Snarr, B. S., Chintalapudi, M. R., O'neal J, L., Phelps, A. L., Barth, J. L., Fresco, V. M., Kern, C. B., Mjaatvedt, C. H., Toole, B. P., Hoffman, S., Trusk, T. C., Argraves, W. S. & Wessels, A. 2007. Cartilage link protein 1 (Crtl1), an extracellular matrix component playing an important role in heart development. Dev Biol, 310, 291-303.

Wittig, G. J. & Münsterberg, A. 2016. The Early Stages of Heart Development: Insights from Chicken Embryos. Journal of Cardiovascular Development and Disease, 3.

Wittig, J. G., Billmeier, M., Lozano-Velasco, E., García, M. R. & Münsterberg, A. E. 2018. Cardiac injections of AntagomiRs as a novel tool for knockdown of miRNAs during heart development. Developmental Biology.

Wu, M., Li, Y., Ji, C., Xu, J., Zheng, H., Zou, X., Gu, S., Lou, Y., Xie, Y. & Mao, Y. 2004. Cloning and identification of a novel human gene PDLIM5, a homolog of AD-associated neuronal thread protein (AD7c-NTP). DNA Seq, 15, 144-7.

Xu, J., Liu, Y., Deng, M., Li, J., Cai, H., Meng, Q., Fang, W., Long, X. & Ke, J. 2016. MicroRNA221-3p modulates Ets-1 expression in synovial fibroblasts from patients with osteoarthritis of temporomandibular joint. Osteoarthritis Cartilage.

Yalcin, H. C., Shekhar, A., Rane, A. A. & Butcher, J. T. 2010. An ex-ovo chicken embryo culture system suitable for imaging and microsurgery applications. J Vis Exp.

Yang, X., Dormann, D., Munsterberg, A. E. & Weijer, C. J. 2002. Cell movement patterns during gastrulation in the chick are controlled by positive and negative chemotaxis mediated by FGF4 and FGF8. Developmental cell, 3, 425-37.

Zamir, E. A., Czirok, A., Cui, C., Little, C. D. & Rongish, B. J. 2006. Mesodermal cell displacements during avian gastrulation are due to both individual cell-autonomous and convective tissue movements. Proceedings of the National Academy of Sciences of the United States of America, 103, 19806-11.

Zamir, E. A., Rongish, B. J. & Little, C. D. 2008. The ECM moves during primitive streak formation--computation of ECM versus cellular motion. PLoS biology, 6, e247.

References

Zhao, X. & Gu, T. 2016. Dysfunctional Hyperpolarization-Activated Cyclic Nucleotide-gated Ion Channels in Cardiac Diseases. Braz J Cardiovasc Surg, 31, 203-6.

Zhao, Y., Ransom, J. F., Li, A., Vedantham, V., Von Drehle, M., Muth, A. N., Tsuchihashi, T., Mcmanus, M. T., Schwartz, R. J. & Srivastava, D. 2007. Dysregulation of cardiogenesis, cardiac conduction, and cell cycle in mice lacking miRNA-1-2. Cell, 129, 303-17.

Zhao, Y., Samal, E. & Srivastava, D. 2005. Serum response factor regulates a muscle-specific microRNA that targets Hand2 during cardiogenesis. Nature, 436, 214-20.

8 Appendix

8.1 *In vitro* confirmation of target interaction (paired analysis)

In this analysis below samples for Luciferase assay were treated as paired samples, thus normalisation sets control values to one. Since statistical significane against a group of samples all at one is achieved easier comparison was performed against the corresponding experiment using the mutated plasmid.

Prior to project start ETS1 was selected as a promising target for microRNA-499-5p target interaction. Target sequence analysis at that point of time revealed only a cryptic binding site according to microRNA nomenclature (Bartel, 2004, Bartel, 2009). Cryptic binding sites signal in a non-canonical manner and are less well understood. Nevertheless, luciferase assays using an UTR sequence with this cryptic binding site led to a reduction of luciferase expression, concluding successful target interaction (data not shown). Initial experiments within this PhD project addressed replication of these experiments, which were unsuccessful (data not shown). The reason for this lies most likely in the microRNA mimic sequence, which was a custom oligo from SIGMA before project start and later swapped for a predesigned microRNA mimic from QIAGEN. Reanalysis of updated sequence information for ETS1 from RNAseq data (Aken et al., 2016) revealed another binding site within its 3'UTR that follows canonical microRNA binding rules. The 3' UTR was cloned into a different vector system, pmirGLO Dual-Luciferase microRNA Target Expression Vector (Promega, E1330) than previously used, pGL3 Luciferase Reporter Vectors (Promega, E1751 and E1741). This has the advantage of transfecting a single plasmid into cells and thus allowing more accurate normalisation.

Target interaction for microRNA-499-5p and ETS1 was confirmed (miR-499-5p: 0.6056 ± 0.03405, miR-499-5p-M: 1.048 ± 0.0396; $p<0.001$) and mutation of the seed sequence recovered the luciferase expression to normal levels (Figure 10A, Appendix 8.1). In addition, a candidate target sequence for microRNA-221-3p was found in the 3'UTR and confirmed, consistent with a previous publication (Xu et al., 2016). Mutation of the seed sequence recovered the luciferase expression to normal levels (miR-221-3p: 0.8844 ± 0.02546, miR-221-3p-M: 1.021 ± 0.03576; $p<0.01$) (Figure 10A, Appendix 8.1). Further microRNA-221-3p was in the list of microRNAs of interest as it follows a similar upregulation pattern as microRNA-499-5p during endocardial cushion development. Following confirmation of ETS1 3'UTR interaction with both microRNAs we wondered if they signal in an additive or synergetic manner. Therefore, another assay involving both microRNAs was performed, which revealed that target suppression is additive (Figure 10B, Appendix 8.1) (control/miR-499-5p: 0.6857 ± 0.1198, control/miR-221-3p: 0.9264 ± 0.1422, miR-499-5p/miR-221-3p: 0.6603 ± 0.164) and no amplification occurs due to cooperative occurs.

Besides ETS1 many other genes involved in heart development became of interest during this study and were subjected to target interaction analysis using TargetScan (Agarwal et al., 2015). UTR sequence information was acquired either from the TargetScan website itself or Ensembl.org including RNAseq data (Aken et al., 2016). Candidate target sites were identified for microRNA-499-5p, microRNA-221-3p, microRNA-126-3p and microRNA-451 for the following genes: GATA4, HAPLN1, HAS2, NOTCH1, Neuregulin 1 (NRG1), Paired Box 3 (PAX3) and Mothers against

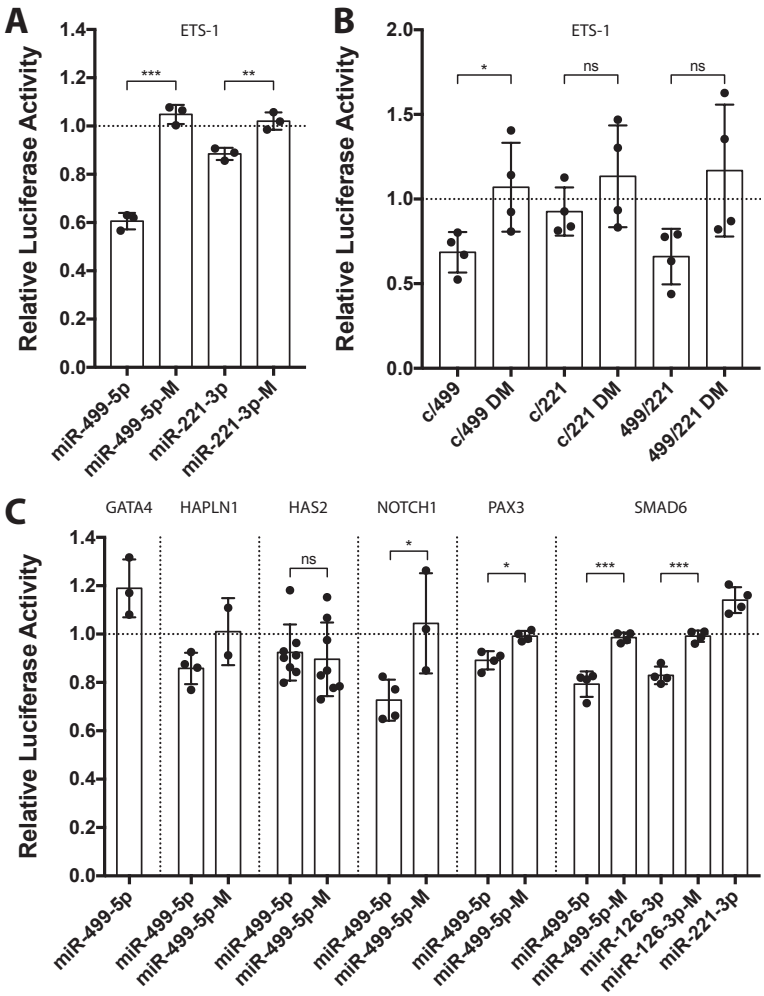

Figure 26: Validation of 3'UTR interactions via Luciferase Assays.

Luciferase Assay analysis of target genes. Columns labelled with used microRNA-mimic and an additional M stands for seed sequence mutated vector (A) Confirmation of microRNA-499-5p and microRNA-221-3p target interaction with the ETS-1 3'UTR. Mutation of both seed sequences individually recovered expression to base levels respectively (n=3). (B) Using microRNA mimics for microRNA-499-5p and microRNA-221-3p in combination leads to an additive effect and no symbiotic amplification (n=4). (C) Fragments of the 3'UTRs of various genes of interest involved in heart development have been subjected to Luciferase assay analysis using mimics for microRNA-499-5p, microRNA-126-3p and/or microRNA-221-3p. GATA4 (n=3) was not negatively regulated, HAPLN1 (n=4/2) was confirmed but needs further replicates for statistical significance, HAS2 (n=8) was confirmed but sequence of interaction was not identified, NOTCH1 (n=4/3) and PAX3 (n=4) were confirmed and lastly SMAD6 (n=4) was regulated by microRNA-499-5p and microRNA-126-3p, but not by microRNA-221-3p. (statistical analysis students t-test, unpaired, $p<0.05$ *, $p<0.01$ **, $p<0.001$ ***)

decapentaplegic homolog 6 (SMAD6) and subsequently their 3'UTRs were cloned for luciferase assays analysis (Figure 10C, Appendix 8.1). Some of these UTRs contained multiple target sites of interest as depicted in Table 13. Some of the identified targets have not been cloned due to large PCR products. Furthermore, microRNA interactions seem to favour sites located at either ends of 3'UTRs rather than sites located in the centre (Grimson et al., 2007).

GATA4 is a downstream target of ETS1. It is expressed early on in heart development and involved in cardiac specification (Meilhac and Buckingham, 2018). Later on, GATA4 plays and important role in vasculogenesis and angiogenesis (Marín-García, 2014). luciferase assay invalidated the target site for microRNA-499-5p (miR-499-5p: 1.189 ± 0.1195).

HAPLN1 (hyaluronan and Proteoglycan Link Protein 1) is an ECM component that is expressed at the AVC and at lower levels on the OFT during the formation of the endocardial cushions (Lockhart et al., 2011, Wirrig et al., 2007). Luciferase assay confirmed target interaction of microRNA-499-5p and the 3'UTR fragment of HAPLN1 (mir-499-5p: 0.8575 ± 0.06508, miR-499-5p-M: 1.01 ± 0.1387, replicates of mutant construct are missing for statistical analysis).

HAS2 is an enzyme synthesising hyaluronan another ECM component essential during heart development. Knockout of HAS2 in mice has been shown to be embryonic lethal, emphasizing its

importance (Camenisch et al., 2000, Lockhart et al., 2011). Luciferase assay confirmed a reduction in luciferase expression after microRNA-499-5p-mimic administration however target site mutation does not recover the phenotype (miR-499-5p: 0.9237 ± 0.1161, miR-499-5p-M: 0.8953 ± 0.1522).

NOTCH1 is an essential transmembrane receptor, which is cleaved upon ligand binding to produce a transcriptional regulator involved in various processes during heart development as for example septation, cushion remodelling, trabeculation and neural crest migration. NOTCH signalling is required for valve development and homeostasis and if absent various malformations arise (MacGrogan et al., 2018a). Luciferase assay confirmed the target site for microRNA-499-5p (miR-499-5p: 0.7265 ± 0.08496, miR-499-5p-M: 1.044 ± 0.2075, $p<0.05$).

NRG1 is a key factor for ventricular trabeculation where its signalling promotes ECM synthesis in the Myocardium (Del Monte-Nieto et al., 2018). Further NRG1 contributes to the formation of the endocardial cushions via ErbB3 and ErbB4 signalling. Mutation in the NRG1 gene led to Hypoplasia (Lin et al., 2012). For our reporter analysis NRG1 was an interesting candidate especially since it was predicted to be targeted by the less common microRNA-451. Unfortunately cloning from chick cDNA was unsuccessful after multiple attempts and the target was dropped for luciferase analysis. In addition, ISH analysis following knockdown of miR-499-5p did not support the idea that NRG1 is a direct target for this microRNA (see below and (Figure 15).

PAX3 is a relevant gene for neural crest migration into the OFT, where PAX3 positive cells contribute to formation of the OFT valves (Epstein et al., 2000). Additionally, ETS is required for neural crest migration thus linking these two targets of interest (Gao et al., 2010). Luciferase assay confirmed the target site for microRNA-499-5p (miR-499-5p: 0.8913 ± 0.03781, miR-499-5p-M: 0.9916 ± 0.021, $p<0.05$).

SMAD6 is a negative regulator of endothelial-to-mesenchymal transformation during endocardial cushion development. Overexpression of SMAD6 leads to reduced EMT whereas knockout to increased EMT leading to Hypoplasia (Desgrosellier et al., 2005). Luciferase assay confirmed the target site for microRNA-499-5p (miR-499-5p: 0.7929 ± 0.05265, miR-499-5p-M: 0.9854 ± 0.02045, $p<0.001$) and microRNA-126-3p (miR-126-3p: 0. 0.8289 ± 0.03656, miR-126-3p-M: 0.991 ± 0.02356, $p<0.001$) but invalidated the target binding site for microRNA-221-3p (miR-221-3p: 1.14 ± 0.05348).

8.2 Comparison of different RNA extraction methods tested during this PhD project

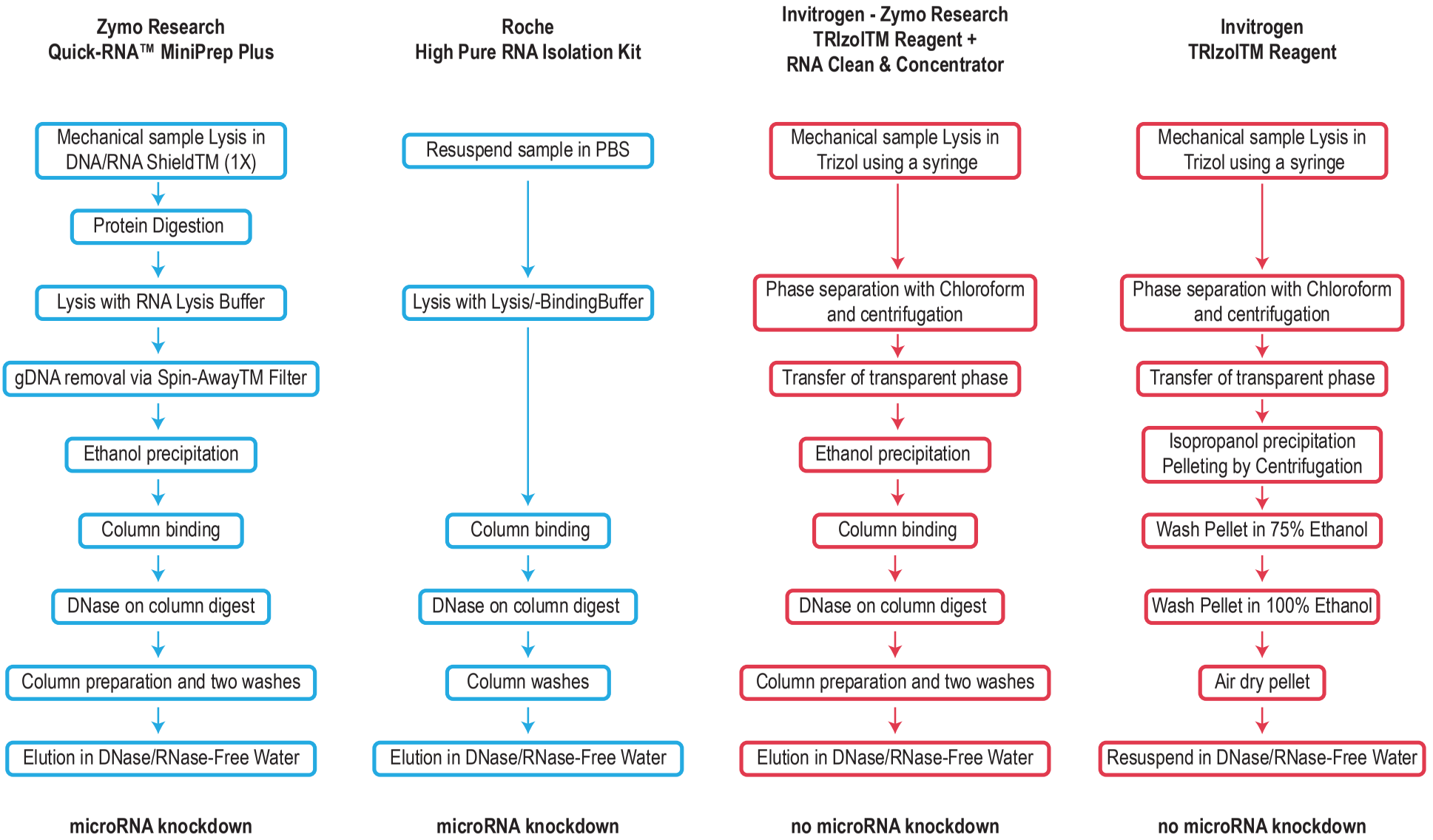

The page on the left shows a flow chart of various methods used for RNA extraction during this PhD-project. The first two a fully column based, the third used a combination of TRIzol® and subsequent column clean up and the last one is based purely on TRIzol® and centrifugation. Differences in downstream results have been observed as soon as TRIzol® was implicated in the procedure.

8.3 The Early Stages of Heart Development: Insights from Chicken Embryos

Johannes G. Wittig and Andrea Münsterberg *

Journal of
Cardiovascular
Development and Disease

MDPI

Review

The Early Stages of Heart Development: Insights from Chicken Embryos

Johannes G. Wittig and Andrea Münsterberg *

School of Biological Sciences, University of East Anglia, Norwich Research Park, Norwich NR4 7TJ, UK; j.wittig@uea.ac.uk
* Correspondence: a.munsterberg@uea.ac.uk; Tel.: +44-1603-592232

Academic Editors: Rolf Bodmer and Georg Vogler
Received: 4 March 2016; Accepted: 30 March 2016; Published: 5 April 2016

Abstract: The heart is the first functioning organ in the developing embryo and a detailed understanding of the molecular and cellular mechanisms involved in its formation provides insights into congenital malformations affecting its function and therefore the survival of the organism. Because many developmental mechanisms are highly conserved, it is possible to extrapolate from observations made in invertebrate and vertebrate model organisms to humans. This review will highlight the contributions made through studying heart development in avian embryos, particularly the chicken. The major advantage of chick embryos is their accessibility for surgical manipulation and functional interference approaches, both gain- and loss-of-function. In addition to experiments performed *in ovo*, the dissection of tissues for *ex vivo* culture, genomic, or biochemical approaches is straightforward. Furthermore, embryos can be cultured for time-lapse imaging, which enables tracking of fluorescently labeled cells and detailed analysis of tissue morphogenesis. Owing to these features, investigations in chick embryos have led to important discoveries, often complementing genetic studies in mice and zebrafish. As well as including some historical aspects, we cover here some of the crucial advances made in understanding early heart development using the chicken model.

Keywords: chick embryo; fate mapping; heart fields; morphogenesis; *in ovo* studies

1. Introduction

The detailed mechanistic understanding of developmental processes is a major requirement to be able to identify the embryonic origin of diseases and to develop future therapeutic interventions. Different model organisms have been established to study patterning and organogenesis in developing embryos. Important metazoan model organisms include the nematode (*Caenorhabditis elegans*), the fruit fly (*Drosophila melanogaster*), the tunicate (*Ciona intestinalis*), a few species of sea urchin, the teleost fish (*Danio rerio*), the African claw-toed frog (*Xenopus laevis*), the mouse (*Mus musculus*), and the chicken (*Gallus gallus*). All of these have different advantages and have made significant contributions to our understanding of developmental processes. The focus of this review will be the chicken, specifically its role in our current understanding of early heart formation.

The chicken is a "classic" model organism and the first meaningful information obtained through its use arose in the 17th century, when it was shown that embryos are not preformed but develop body parts progressively. Further fundamental discoveries were dependent on the development of optical microscopes, which made it possible to discover the three germ layers: ectoderm, mesoderm, and endoderm. A comment on Charles Bonnet's ideas on "fecundation" and development of the germ (egg) was published in the late 19th century [1]. Since then developmental biology research has changed dramatically owing to advances in genetics and in cell and molecular biology, which enabled much progress and a "golden age" for the discipline [2]. Analyses have become more sophisticated, focusing on discrete regions in the developing animal.

The chick embryo is ideal for studying the early development of the heart, the first functioning organ in the embryo. A major advantage is that the chick develops *ex utero* in an egg, which allows easy accessibility during all stages of development post-laying. This ease of access enables *in ovo* manipulations and observation of the embryo, such as dissection, grafting, micro-injection, and labeling, and this has made the chicken popular, even before the molecular age [3–5]. Particularly powerful have been grafting and ablation experiments. When combined with the use of quail/chick chimeras [6], this approach allowed the tracing of grafted cells before genetic labeling became possible. Establishing methods for *ex ovo* development and introduction of constructs encoding fluorescently labeled proteins by electroporation has facilitated the imaging of cell movement in live embryos using advanced microscopy [7,8]. Advanced tools for image registration allow for the alignment and comparison of multiple specimens in the absence of morphological landmarks [9]. By directly labeling the extracellular matrix, it has also been possible to measure active *versus* passive motion of cells, including cardiac progenitors, during gastrulation [10,11]. The use of CRISPR/Cas9-mediated genome editing via targeted electroporation allows the generation of genetic mosaics; combined with imaging the behavior of mutant cells can then be studied in detail, for example in developing somites [12]. Furthermore, improved methods for transgenesis and the availability of lines, both quail and chick, transgenic for fluorescent markers expressed either ubiquitously or restricted to specific cell lineages, has enhanced the utility of avian models [13–15].

Finally, the mature chick heart comprises four chambers with in- and out-flow tracts, and despite some differences, for example during septation and aortic arch remodeling [16], it resembles the human anatomy more closely than other non-mammalian model organisms. Owing to those features, and the available tool-kit described above, avian embryos will almost certainly continue to contribute significant insights into the development of the heart.

2. Cardiac Development and Morphogenesis

2.1. Mapping Studies and Characterization of Cardiogenic Fields

In the chick embryo, systematic observations and comparative analyses were boosted when Hamburger and Hamilton established a classification scheme for developmental stages that was universally adopted [17]. A recent reference guide maps the stages of heart development onto the HH-stage series [18]. In addition, the series has been refined for the stages of gastrulation [19], which starts with the formation of the primitive streak in the midline of the embryo.

In the early chick gastrula (Hamburger-Hamilton, HH stage 3), cardiac progenitors are located in the mid-primitive streak, from which they ingress to enter the mesoderm bilaterally [20–23]. By HH4, the late gastrula/early neurula stage, the contribution of the primitive streak to the heart ceases [21,24]. At that stage precardiac areas are organized into bilateral heart fields located in the lateral plate mesoderm, which subsequently splits into the somatic and splanchnic layers, the latter comprising cardiogenic cells. Bilateral heart fields were originally characterized by culturing isolated cells and testing their potential to generate spontaneously contracting cardiomyocytes [20,25].

Early studies tracing cardiac cells in gastrula stage embryos used isotope labeling and autoradiography, thus defining bilateral heart fields that are initially separate but then fuse to generate the tubular heart at early somite stages [26]. In mouse embryos, the timing is different and the heart field mesoderm merges together across the midline at the 1-somite stage (E7.5), forming a "crescent" [27,28].

Additional insights regarding the origin of cells contributing to the heart as well as the aortic arches derived arteries were obtained through interspecies grafts that generate quail–chick chimeras. This approach, developed by Lièvre and Le Douarin [29], was important for studies in avian model systems and a reliable and sensitive alternative to methods involving radioactive isotopes [25]. Using quail–chick chimeras and fluorescent vital dye injections, a more precise fate map was generated [21]. This showed that cardiomyocyte and endocardial precursors arise from a rostral portion of the

HH3 primitive streak, and that the craniocaudal organization of cells within the streak reflects the craniocaudal arrangement of the linear heart tube [21], extending the earlier cardiogenic "potency map" of the primitive streak by DeHaan [20]. The linear heart tube becomes extended and refined by additional cell populations contributing to the mature heart (see Section 2.3).

2.2. Pre-Gastrula and Gastrula Stages

2.2.1. Specification and Migration of Cardiac Progenitor Cells

Cardiogenic potential can be detected in pre-streak, blastula stage embryos prior to gastrulation before the heart fields emerge. Pre-streak stage chick embryos are a flat disc composed of two layers, the epiblast (upper layer) and the hypoblast (lower layer). Cardiac progenitors are found within the posterior half of the epiblast [30] and these cells have cardiogenic potential in culture [31,32]. These authors also showed that the hypoblast is required to induce cardiac myogenesis in the early epiblast, and furthermore, that Tgfβ/activin is sufficient to substitute for its cardiogenic-inducing ability [31,32]. In contrast, BMP-2 and BMP-4 inhibit cardiogenesis at this stage, consistent with studies that show that BMP antagonists, such as chordin, can induce the expression of the early marker, smooth-muscle alpha actin (SMA), in cultured posterior epiblasts at pre-gastrula stages [33]. In mice, transplantation experiments combined with embryo culture showed that epiblast cells can acquire a cardiac fate independent of ingression through the primitive streak [34]. Thus, in both chicks and mice, ingression itself is not necessary for fate specification.

Soon after gastrulation, prospective cardiac cells migrate to the anterior lateral mesoderm and the bilateral heart fields contain prospective endocardial and myocardial cells, indicating that cardiac fates are allocated in the primitive streak or earlier prior to cell migration. This idea was confirmed using lineage tracing with low titers of a replication-defective retrovirus expressing LacZ. The labeled cells gave rise to either myocardial or endocardial derivatives [35].

Using chick embryos and *ex vivo* tissue recombination experiments it was possible to identify the origin of signals in the endoderm underlying the bilateral heart field mesoderm in the anterior lateral plate that trigger the commitment to the cardiac lineage [36]. Pioneering studies identified the crucial role of BMP signaling post-gastrulation. Beads soaked in recombinant BMP-2 could induce ectopic expression of early cardiac markers, such as the transcription factors GATA-4 and Nkx-2.5. Furthermore, recombinant BMP-2 or BMP-4 protein induced myocardial differentiation and beating in explants of non-cardiogenic mesoderm, while exposure to the secreted protein Noggin, a BMP-antagonist, completely inhibited differentiation of precardiac mesoderm [37,38]. The competency to respond to BMP-2/4 alone was stage dependent [39] and restricted to anterior mesoderm explants. Subsequently it was shown that interactions between BMP-2 and FGF-4 pathways are important for the induction of cardiac cell fate in the posterior mesoderm [40] by directly targeting the transcription factor Nkx2.5 [41].

Additional experiments conducted in both chick and Xenopus gastrula stage embryos revealed that inhibition of canonical Wnt/β-catenin signaling is critical for heart development [42,43], whereas β-catenin-dependent Wnt signaling in the posterior lateral mesoderm induced hematopoiesis [42]. The Wnt family of secreted proteins initiates several signal transduction pathways, recently reviewed in the context of heart development [44]. Antagonists of β-catenin-dependent Wnt signaling that promote cardiogenesis include dickkopf (Dkk1) and crescent. In chicks, crescent is expressed in anterior endoderm during gastrulation and can induce the expression of cardiac genes in posterior, non-cardiogenic tissues *in vitro* [42]. The conditional genetic ablation of β-catenin in early mouse embryos also led to a proposed cell fate switch and ectopic heart formation [45]. These observations are consistent with the idea that β-catenin-dependent Wnt signaling represses cardiogenesis; however, this is context dependent. At an early stage of development, prospective cardiac cells are exposed to canonical Wnt-ligands: both Wnt-3a and Wnt-8c (known as Wnt8a in mouse and human) are expressed in the primitive streak. Indeed, during the differentiation of embryonic stem cell derived

embryoid bodies, Wnt/β-catenin signaling is initially required for induction of mesoderm and thus cardiomyogenesis. Therefore, this pathway either enhances or inhibits cardiogenic differentiation depending on the stage of development; it has been proposed that canonical signaling retains cardiac precursors in a proliferative precursor state, whereas non-canonical signaling promotes their differentiation (reviewed in [44,46]).

Taken together, work in avian embryos demonstrated that inhibitors of β-catenin-dependent Wnt signaling act in concert with BMP and FGF signaling molecules to specify cells to cardiac fates during early neurula stages. These insights led to efforts to differentiate human pluripotent stem cells into cardiomyocytes [47]. Additional data indicate that FGF and BMP signaling pathway interactions are regulated by negative feedback loops involving microRNAs, particularly miR-130 and miR-133 [48,49].

Furthermore, β-catenin-independent (or non-canonical) signaling is important for cardiogenesis. Wnt binding to frizzled receptors and signaling through Dvl can activate alternative pathways, including the planar cell polarity (PCP) and Wnt/Ca^{2+} pathways [44]. Known mediators of the Wnt/PCP pathway involve the ligand Wnt-11 and the small GTPase RhoA. In chicken embryos, RhoA controls tissue polarity and cell movement of cardiogenic progenitors [50,51]. Live-imaging and cell tracking of cardiac progenitors have shown that during gastrulation a combination of BMP-2/4- and Wnt/GSK3β-mediated signals is involved in controlling the migration of these cells towards the bilateral heart fields [52]. This work also showed that the two pathways are integrated by differential phosphorylation of Smad-1: (1) at the carboxy-terminus in response to BMP-receptor activation; and (2) in the linker region by GSK3β kinase.

These observations suggest that the control of migration is intimately linked with that of cell fate specification—the same players and pathways are involved in both processes and this is illustrated in Figure 1. However, the downstream effectors and molecular switches that control the cells' response depending on their competency and differentiation status remain to be identified.

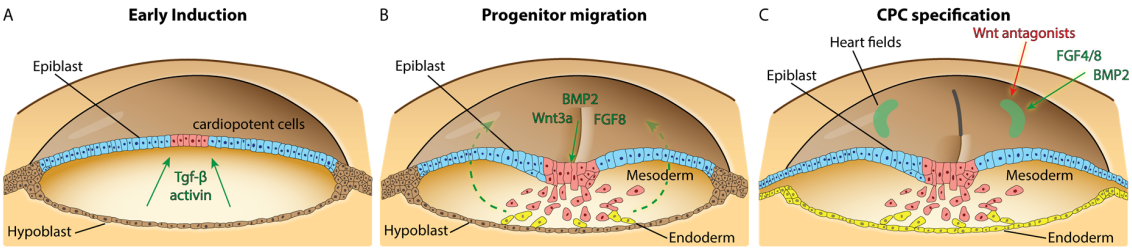

Figure 1. Cardiogenic signals in pre-gastrula, gastrula, and neurula stage embryos. Schematic representation of a pre-gastrula chick embryo (**A**) with epiblast and hypoblast layers. Cardiopotent cells identified in the posterior epiblast respond to Tgf-β/activin signaling. The diagram in (**B**) represents a HH3 gastrula with prospective mesoderm (**red**) and endoderm cells (**yellow**) ingressing through the primitive streak. Wnt3a, BMP2, and FGF8 are expressed in the primitive streak and control migration trajectories of cardiac progenitor cells, indicated by **green** stippled arrows, towards the bilateral heart fields. (**C**) Representation of a neurula stage embryo, approximately HH5. Gastrulation continues at the primitive streak, which is regressing; an endoderm layer has formed, and cardiogenic cells are located in bilateral heart fields in the anterior lateral plate mesoderm. A combination of BMP2, FGF4/8, and inhibitors of canonical Wnt signaling act to specify cardiac fate.

Effects of BMPs on progenitor cell migration in addition to effects on fate acquisition are also consistent with observations in genetically altered mice. For example, the conditional deletion of BMP receptor type 1a using mesoderm-posterior-1-Cre (MesP1-cre), which acts in cardiogenic progenitors, results in the absence of the entire cardiac crescent and the restricted expression of myocardial progenitor markers Nkx2-5 and the LIM homeobox 1 transcription factor, Isl1, to a small remaining cardiac field [53]. Consistent with the findings in chick embryos, these authors also showed that sustained activation of canonical Wnt signaling led to increased Isl1 expression but inhibited heart

tube formation at the eight-somite stage [50,53]. Thus far it has not been possible to observe cardiac progenitor cell migration in real time using mice; however, advanced imaging approaches will soon be able to address this challenge [54].

2.2.2. Establishment of Left–Right Asymmetry

Shortly after the emergence of cardiogenic progenitors from the primitive streak and around the time that they arrive in the heart fields, the bilateral symmetry of the early embryo is broken. Ultimately this leads to the striking left–right asymmetry in the placement and differentiation of organs, which is seen in all vertebrates. Experiments in chick embryos have made major contributions to our understanding of the mechanisms involved in this process. For a review see [55]. In particular, the gene network that provides left–right information was characterized in chick embryos [56]. Initial breaking of symmetry starts at Hensen's node, the organizing center at the anterior end of the fully extended HH4 primitive streak. Several signaling molecules are asymmetrically expressed, including activin receptor IIa, Sonic hedgehog (Shh), and cNR1 (the chick homologue of mouse nodal); the experimental manipulation of these pathways, through implantation of growth factor soaked beads or cell pellets, affects heart *situs* [56]. Furthermore, recent work showed that *N*-cadherin is involved in asymmetric gene expression and the leftward cell movements in Hensen's node [57].

In mice, the use of a nodal-lacZ reporter allele confirmed its asymmetric expression on the left side [58]. Although the mechanisms leading to initial breaking of symmetry are different in mice and chicks [59,60], in both species the transcription factor Pitx2 acts downstream of nodal and Shh signaling. In chick embryos misexpression of Pitx2 is sufficient to produce reversed heart looping [61]. The literature on genetic manipulations of Pitx2 is extensive and cannot be covered here; suffice it to say that cardiac laterality defects are usually observed (for example [62], and references in [55]).

The signaling molecules expressed on the left side interact with a right-sided program, initiated by BMP-4 at Hensen's node inducing FGF8, which in turn activates Snai1, a Zn-finger transcriptional repressor. Snai1 is necessary for the formation of the proepicardium (PE), which in the chick develops only on the right side—a vestigial PE on the left undergoes apoptosis. Ectopic expression of FGF8 or Snail on the left led to bilateral PE formation [63]. In the mouse, the PE, which is characterized by expression of WT1 and TBX18, develops bilaterally. This may reflect differences in FGF8, which is a determinant of the right side in the chick but mediates left side identity in mice [59,64].

2.3. Discovery of Additional Heart Fields

Classic mapping experiments using labeling with iron oxide particles followed by time-lapse photography indicated that new segments are added to the linear heart tube during looping, in particular to generate outflow myocardium [65,66]. Cells residing in the ventral region of the subcephalic fold of HH9^{-} were shown to be included at the cephalic end of the heart tube by HH12. Similar labeling showed that precursors for the right and left primitive atria are not yet present in the HH8–9 straight heart tube [67] but become incorporated later during loop stages. Building on this early work, the origins of secondarily added cell populations were characterized in more detail in both the chick and mouse, using fluorescent dye or genetic labeling, respectively [68–70]. This showed that cell populations contributing to the outflow tract (OFT) are located in the pharyngeal mesoderm and the splanchnic mesoderm anterior, and immediately adjacent to the straight heart tube. These regions have been termed the anterior and secondary heart fields (AHF/SHF), respectively, and their derivatives are shown in Figure 2. The cells contributing to the OFT express the transcription factors Nkx2.5 and GATA-4. They are also positive for HNK-1 immunostaining as they translocate into the heart [69,70]. Using vital dye injections and tissue grafting it was possible to map the location and ingression sites of prospective AHF and SHF cells in the primitive streak of gastrula stage HH3 chick embryos [71]. This work showed that during early somite stages the Isl1-positive AHF progenitors were located in the cranial paraxial mesoderm and the pharyngeal mesoderm [71], also consistent with

studies that identified a close relationship between these progenitors and some craniofacial skeletal muscles, in both the chick and mouse [72,73].

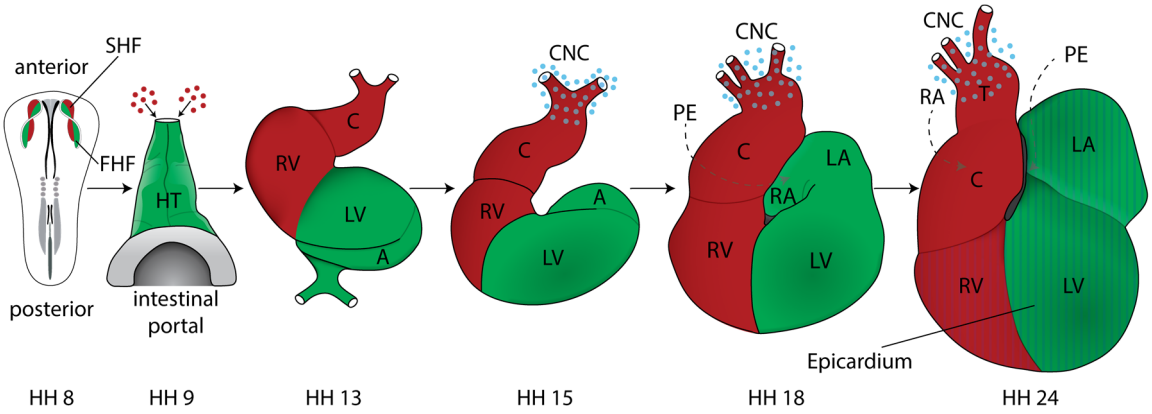

Figure 2. Cardiac morphogenesis in chick embryos. Schematic ventral views of HH8 to HH24 chick hearts. Fate mapping revealed the location of first and second heart fields (FHF, SHF), marked in green and red. Fusion generates a primitive heart tube by HH9; secondarily added cell populations have not yet entered (red dots). In all images, components of the heart derived predominantly from FHF are in green and components derived predominantly from SHF and also AHF are in red. During dextral-looping the straight heart tube transforms into a C-shaped bend by HH13 and SHF/AHF-derived cells contribute to the heart; primitive atria move dorsocranially. Further positional changes are indicated. The proepicardium (PE) is located on the dorsal side (stippled grey arrow); it generates the epicardium. The expansion of the epicardium over the heart by HH24 is indicated by stripes. The cardiac neural crest (CNC), shown as blue spots, contributes to outflow tract septation and remodeling of the great arteries. See text for details. A, atrium; C, conus, CNC, cardiac neural crest; HT heart tube; LA/RA, left/right atrium; LV/RV, left/right ventricle; T, truncus arteriosus.

In vivo live imaging in quail embryos was used to determine the origins of the endocardium. This identified an endocardium-forming field located medial to and distinct from the first and second heart fields. These progenitors are restricted in their potential and enter the heart from the arterial pole [74]. Conditional genetic ablations showed that in the mouse the origins of the endocardium are more heterogeneous [74,75] and are specified by a gene network initiated by the early cardiac transcription factor Nkx2.5 [76].

In the mouse, cells that generate in particular the right ventricle and outflow myocardium were characterized through the expression of an FGF-10 lacZ knock-in allele in the pharyngeal mesoderm [68]. The second heart field populations of cells are reviewed in detail in [77,78]. Additional makers have since been identified and genetic studies in mice have helped to explain congenital heart defects that affect the OFT, comprising the aortic and pulmonary trunk [79]. OFT septation and the remodeling of the great arteries also depend on the neural crest (see below), which adds to the complexity of some mutant phenotypes.

Work in chick embryos investigating a signaling mechanism within the AHF niche showed that BMP and FGF crosstalk coordinates the balance between proliferation and differentiation of cardiac progenitors [80]. Close interaction with cardiac neural crest cells was also shown to be required for the regulation of AHF cell differentiation [81]. Furthermore, studies in both the chick and the mouse have revealed the close relationship between head skeletal muscles and AHF/SHF-derived cardiac muscles, which share overlapping expression of a genetic program that is evolutionarily conserved [73,82–84] (reviewed in [85,86]).

More recently the origin of pacemaker cells (PC) of the sinoatrial node (SAN) was identified in a "tertiary" heart field. Using electrophysiological measurements in chick embryos, it was shown that mesoderm cells in a region posterior to the HH8 stage heart fields generate action potentials. By late

looping stages these cells contribute PCs of the sinoatrial node. This work also revealed that Wnt8c promotes PC fate [87]. Prior to this, voltage sensitive dyes had been used to monitor spontaneous action potential activity, which was detected at 7–8 somite stages in the pre-beating heart using optical recording [88].

2.4. Formation and Transformation of the Straight Heart Tube

Insights regarding the origin of cardiac precursors in pre-gastrula stage embryos and cardiogenic fields at gastrula stages were not among the first investigations into heart formation in the chick. Studies about morphology and how an organ acquires its final form were conducted much earlier. For example, the process of heart looping was first observed in 1758 by Albrecht Haller (cited in [89]), who noticed a transformation of the heart tube into a loop-like shape during heart maturation. Even though it was discovered early, a comprehensive summary of this phenomenon did not appear in the literature until 1922, when the term "cardiac looping" was introduced [90].

Insights into the formation of the heart tube itself included the discovery of the bilateral heart fields, which migrate to the midline and fuse [26]. Initial experiments conducted to analyze the process of fusion determined a craniocaudal course of the merging of the endocardial and myocardial heart primordia [25]. However, this observation was revised to show that fusion occurs in a central region and progresses in cranial and caudal directions, similar to what had been observed in mouse embryos [66].

Our understanding of the molecular and cellular drivers of the fusion process is still limited, but evidence in the chick supports a mechanical role for the endoderm at the anterior intestinal portal. Tracking experiments combined with the use of the myosin-II inhibitor, Blebbistatin, and computational modeling showed that shortening of the endoderm, driven by cytoskeletal contractions, is involved in motion of the heart fields towards the midline [91]. Disruption of the fusion process leads to *cardia bifida*, a severe malformation of the heart, which can be experimentally induced. For example, after surgical incision along the midline of a HH7 chick embryo, two separate contractile tubes form [92]. *Cardia bifida* was also observed in MesP1 null mice, most likely because the migration of mesoderm progenitors was affected [93]. Furthermore, in chick embryos *cardia bifida* was seen after inhibition of the RhoA GTPase, by siRNA, or by electroporating mutant forms of RhoA into cardiac progenitors in the HH3 primitive streak [50,51]. This implicates RhoA-mediated regulation of cytoskeleton dynamics in directional movements of cardiogenic progenitors. The effects of RhoA mutants mimicked what was seen after overexpression of Wnt3a, which controls cardiac progenitor cell migration (see above), potentially through chemotactic guidance [50]. Interestingly, non-canonical Wnt-signaling via Rho GTPase was shown to be important during midline conversion of organ primordia, including heart tube assembly in zebrafish [94]. *Cardia bifida* will lead to embryonic death rather than a congenital heart defect. Nevertheless, mechanistic studies resulting in *cardia bifida* will provide important information about the relative contributions of the primary germ layers and signaling pathways involved in early heart morphogenesis.

After formation of the straight heart tube the looping process begins—reviewed and updated by Männer J. [95]. Major advances made during the late 20th century describe cardiac looping in four phases: (1) the pre-looping phase (HH8–9); (2) the phase of dextral looping, leading to the transformation of the originally straight heart tube into a C-shaped bend/loop whose convexity is directed toward the right of the body (HH9^{+}–13); (3) the phase of transformation of the C-shaped heart loop into the S-shaped heart loop (HH14–16); and (4) a phase of late positional changes of the primitive outflow tract (conus) with respect to the atria, with the process being completed by HH24 [95]. For more information about heart looping and a series of pictures, see Figure 2 and the following reviews and books [95–97].

Despite the fact that detailed observations and descriptions of heart looping were acquired some time ago, our understanding of the relevant mechanical forces is still in its infancy. Important biomechanical processes include major morphogenetic events such as cranial flexure, which is intimately linked with the caudal shift of the ventricular bend. Some evidence suggests that the

bending head and neck regions lead to a compression of the heart loop; however, the converse scenario whereby the caudal shift exerts a pulling force on the head cannot be completely excluded at present [95]. Additional mechanical force is exerted by increased blood flow and blood pressure, and it is evident that altered hemodynamics can contribute to laterality and congenital heart defects [96]. Modern imaging approaches, including light sheet microscopy, which can image live tissues without inducing photo-damage, and computational modeling in combination with studies of cell behavior are key technologies for advancing this field [8,54]. For a summary of approaches for the heart in chicks and other model organisms, see [98].

2.5. Cardiac Neural Crest

Experiments using avian embryos, particularly quail–chick chimeras, enabled the analysis of neural crest cell (NCC) migration and differentiation [29,99]. This approach revealed an important contribution by NCCs to the heart. Specifically, replacing chick NCCs arising from the posterior hindbrain adjacent to somites 1–3 with that of quail NCC showed that these cells contribute to the aortico-pulmonary and conotruncal septa; thus they were called "cardiac" NCCs [100,101], although they also contribute to non-cardiac tissues. Cardiac NCCs are crucial for the remodeling of the pharyngeal arteries into an aortic arch, and for septation of the outflow tract into the pulmonary artery and aorta. In mouse embryos, the use of genetic labels such as Wnt1-cre and ROSA26 reporter lines enabled the tracking of cardiac neural crest cell derived tissues [102].

More recently, it has been shown in chick embryos that the chemokine stromal cell-derived factor-1 (SDF1) and its cognate receptor, Cxcr4, are important for the migration of cardiac NCCs towards the heart. This suggested that SDF1 acts as a chemoattractant for cardiac NCCs. Misregulation of SDF1 signaling caused cardiac anomalies including incomplete septation of the aorta and pulmonary trunk (also described as Persistent truncus arteriosus or PTA), and ventricular septal defects (VSD) [103]. The experiments in chicks were consistent with observations demonstrating that mice deficient for Sdf1 or its receptors, Cxcr4 and Cxcr7, exhibit ventricular septal defects [104]. The important role of cardiac NCCs for the etiology of common congenital birth defects, including outflow tract septation defects, has been reviewed (for example, [16]).

2.6. Cardiac Chambers

Following heart looping, maturation of the heart into four chambers, two atria and two ventricles, is initiated. The primitive atrium becomes divided by the formation of a septum primum. This septum initiates from the dorsocranial atrial wall at HH14 and grows towards the developing endocardial cushions in the atrioventricular canal (AVC). It has been shown that reciprocal myocardial–endocardial interactions coordinate the formation of valves [105] that optimize blood flow. In addition, qPCR analysis of microRNAs demonstrated distinct expression profiles within the atrial, ventricular, and atrioventricular canal regions of the developing chick heart. In particular miR-23b, miR-199a, and miR-15a displayed increased expression during early AVC development and characterization of target genes suggests that they are involved in regulating epithelial-mesenchymal transition (EMT) signaling pathways [106].

Around the same time, the chamber walls undergo morphological changes. At first, the myocardial layer of the ventricular walls forms protrusions, called trabeculae, which project into the chamber lumen and are covered by a layer of endocardium. The process of trabeculae formation begins at HH16 at the outer curvature of the primitive ventricle—later trabeculae contribute to ventricular septation. Trabeculae grow in length; when growth ceases their shape and morphology change. During this phase of remodeling, trabeculae start to thicken at their anchors in the chamber wall. In the chick, a compact myocardium with a mature trabeculae network is formed around halfway through gestation, by approximately HH34. Throughout embryonic stages the increased surface area generated by trabeculae supports nutrition and oxygen uptake prior to vascularization. Post-birth trabeculae prevent suction, specifically the flow of blood back into the atria. For a more detailed description readers are referred to reviews [107,108] and the references therein.

2.7. The Proepicardium

Concomitant with the initiation of trabeculation, cells of the proepicardium migrate to the post-looped heart to form its outermost layer, the epicardium, which invades the myocardial wall, resulting in establishment of the coronary vasculature and an increased number of cardiac fibroblasts in the myocardial wall [109–111]. Failed fusion of the proepicardium to the heart results in severe coronary and heart defects and a better understanding of its precise roles will be needed to develop new therapies [112]. Loss-of-PE-function can be induced by photoablation and this induces long-lasting abnormalities in the heart, including a thin myocardium and defects in the coronary vasculature [113]. Interestingly, the epicardium of the distal OFT has a different embryonic origin and gene expression profile, as shown by transplantation and mapping studies [114]. Quail–chick grafting also demonstrated that the PE contributes hemangioblasts but not lymphangioblasts [115]. In both the chick and the mouse. RANKL/NFATC1 signaling induces expression of extracellular matrix-degrading enzymes, which is important for the invasion of epicardial cells into the myocardium [116]. Work in chick embryos examined PE origin [117] and showed that myocardium-derived BMP signals induce the protrusion of Tbx18/WT1-positive proepicardial cells toward the looping heart tube [118]. In both humans and chicks, Tbx5 is implicated in the migration of proepicardial cells [119]. Genetic lineage tracing in mice identified a sub-compartment of proepicardial cells positive for Scleraxis (Scx) and Semaphorin3D (Sema3D), which give rise to coronary vascular endothelium and contribute to the early sinus venosus and cardiac endocardium [120].

3. Conclusions

Compared to mammalian model organisms, the chick has discrete advantages for experimental embryology. Due to long generation times, genetic approaches are not straightforward in the chicken; however, *in ovo* accessibility allows transient gain- and loss-of-function approaches, which compensates for this shortfall. In this review we have illustrated how approaches in the chick model have facilitated important insights into the origin of cardiogenic cells and the developmental signals involved in their specification and migration. The timeline in Figure 3 summarizes some crucial milestones. No doubt, ongoing and future work using avian species will provide more original insights into the molecular and cellular mechanisms that underpin the early development of the vertebrate heart.

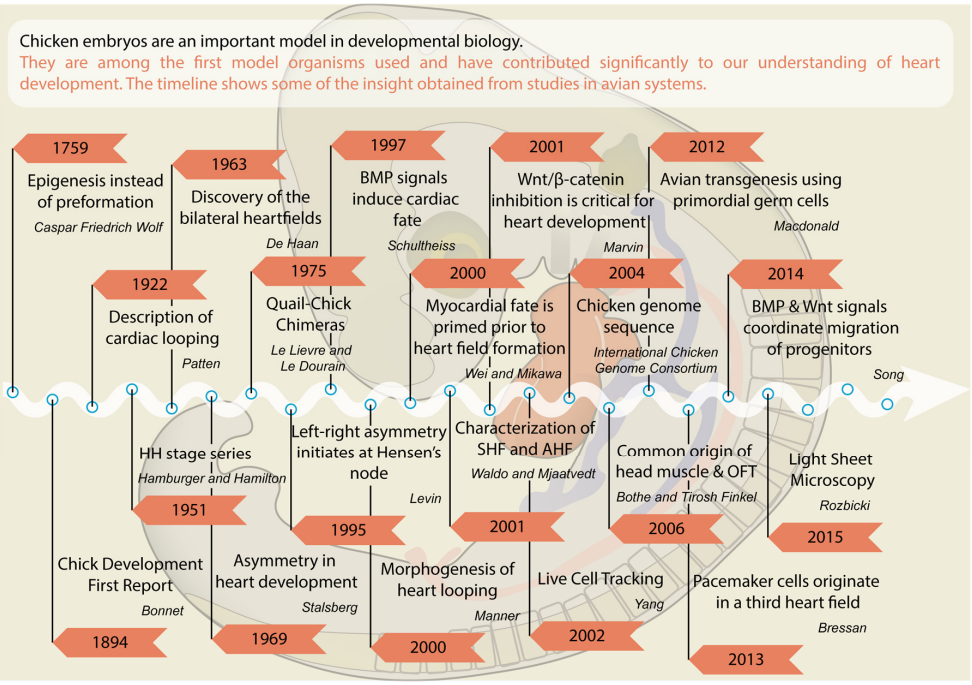

Figure 3. Timeline of important discoveries in chick embryos.

Acknowledgments: The authors would like to thank Grant Wheeler for commenting on the manuscript. J.G.W. is funded by a grant from the British Heart Foundation (BHF FS/15/41/31564) to A.M. Research in the laboratory was supported by BHF grant PG/11/118/29292 and BBSRC grant BB/K003437/1 to A.M.

Author Contributions: J.G.W. prepared illustrations; J.G.W. and A.M. wrote the manuscript.

Conflicts of Interest: The authors declare no conflict of interest.

Abbreviations

The following abbreviations are used in this manuscript:

AHF/SHF	anterior/secondary heart field
HH	Hamburger-Hamilton
NCC	neural crest cells
OFT	outflow tract
PC	pacemaker cell
PE	proepicardium

References

1. B, X. Charles Bonnet's idea of the development of the chick. *Science* **1894**, *23*, 71–72. [CrossRef] [PubMed]
2. St Johnston, D. The renaissance of developmental biology. *PLoS Biol.* **2015**, *13*, e1002149. [CrossRef] [PubMed]
3. Stern, C.D. The chick; a great model system becomes even greater. *Dev. Cell* **2005**, *8*, 9–17. [PubMed]
4. Kain, K.H.; Miller, J.W.; Jones-Paris, C.R.; Thomason, R.T.; Lewis, J.D.; Bader, D.M.; Barnett, J.V.; Zijlstra, A. The chick embryo as an expanding experimental model for cancer and cardiovascular research. *Dev. Dyn.* **2014**, *243*, 216–228. [CrossRef] [PubMed]
5. Stern, C.D. The chick embryo-past, present and future as a model system in developmental biology. *Mech. Dev.* **2004**, *121*, 1011–1013. [CrossRef] [PubMed]
6. Le Douarin, N. A biological cell labeling technique and its use in experimental embryology. *Dev. Biol.* **1973**, *30*, 217–222. [CrossRef]
7. Yang, X.; Dormann, D.; Münsterberg, A.E.; Weijer, C.J. Cell movement patterns during gastrulation in the chick are controlled by positive and negative chemotaxis mediated by fgf4 and fgf8. *Dev. Cell* **2002**, *3*, 425–437. [CrossRef]
8. Rozbicki, E.; Chuai, M.; Karjalainen, A.I.; Song, F.; Sang, H.M.; Martin, R.; Knolker, H.J.; MacDonald, M.P.; Weijer, C.J. Myosin-ii-mediated cell shape changes and cell intercalation contribute to primitive streak formation. *Nat. Cell Biol.* **2015**, *17*, 397–408. [CrossRef] [PubMed]
9. Grocott, T.; Thomas, P.; Münsterberg, A.E. Atlas toolkit: Fast registration of 3D morphological datasets in the absence of landmarks. *Sci. Rep.* **2016**, *6*, 20732. [CrossRef] [PubMed]
10. Zamir, E.A.; Czirok, A.; Cui, C.; Little, C.D.; Rongish, B.J. Mesodermal cell displacements during avian gastrulation are due to both individual cell-autonomous and convective tissue movements. *Proc. Natl. Acad. Sci. USA* **2006**, *103*, 19806–19811. [CrossRef] [PubMed]
11. Zamir, E.A.; Rongish, B.J.; Little, C.D. The ECM moves during primitive streak formation–computation of ECM versus cellular motion. *PLoS Biol.* **2008**, *6*, e247. [CrossRef] [PubMed]
12. Veron, N.; Qu, Z.; Kipen, P.A.; Hirst, C.E.; Marcelle, C. Crispr mediated somatic cell genome engineering in the chicken. *Dev. Biol.* **2015**, *407*, 68–74. [CrossRef] [PubMed]
13. Cui, C.; Filla, M.B.; Jones, E.A.; Lansford, R.; Cheuvront, T.; Al-Roubaie, S.; Rongish, B.J.; Little, C.D. Embryogenesis of the first circulating endothelial cells. *PLoS ONE* **2013**, *8*, e60841. [CrossRef] [PubMed]
14. Balic, A.; Garcia-Morales, C.; Vervelde, L.; Gilhooley, H.; Sherman, A.; Garceau, V.; Gutowska, M.W.; Burt, D.W.; Kaiser, P.; Hume, D.A.; *et al*. Visualisation of chicken macrophages using transgenic reporter genes: Insights into the development of the avian macrophage lineage. *Development* **2014**, *141*, 3255–3265. [CrossRef] [PubMed]
15. Macdonald, J.; Taylor, L.; Sherman, A.; Kawakami, K.; Takahashi, Y.; Sang, H.M.; McGrew, M.J. Efficient genetic modification and germ-line transmission of primordial germ cells using piggybac and tol2 transposons. *Proc. Natl. Acad. Sci. USA* **2012**, *109*, E1466–E1472. [CrossRef] [PubMed]

16. Plein, A.; Fantin, A.; Ruhrberg, C. Neural crest cells in cardiovascular development. *Curr. Top. Dev. Biol.* **2015**, *111*, 183–200. [PubMed]
17. Hamburger, V.; Hamilton, H.L. A series of normal stages in the development of the chick embryo. *J. Morphol.* **1951**, *88*, 49–92. [CrossRef] [PubMed]
18. Martinsen, B.J. Reference guide to the stages of chick heart embryology. *Dev. Dyn.* **2005**, *233*, 1217–1237. [CrossRef] [PubMed]
19. Lopez-Sanchez, C.; Puelles, L.; Garcia-Martinez, V.; Rodriguez-Gallardo, L. Morphological and molecular analysis of the early developing chick requires an expanded series of primitive streak stages. *J. Morphol.* **2005**, *264*, 105–116. [CrossRef] [PubMed]
20. DeHaan, R.L. Organization of the cardiogenic plate in the early chick embryo. *Acta Embryol. Morphol. Exp.* **1963**, *6*, 26–38.
21. Garcia-Martinez, V.; Schoenwolf, G.C. Primitive-streak origin of the cardiovascular system in avian embryos. *Dev. Biol.* **1993**, *159*, 706–719. [CrossRef] [PubMed]
22. Bellairs, R. The primitive streak. *Anat. Embryol. (Berl.)* **1986**, *174*, 1–14. [CrossRef] [PubMed]
23. Rosenquist, G.C. Location and movements of cardiogenic cells in the chick embryo: The heart-forming portion of the primitive streak. *Dev. Biol.* **1970**, *22*, 461–475. [CrossRef]
24. Psychoyos, D.; Stern, C.D. Fates and migratory routes of primitive streak cells in the chick embryo. *Development* **1996**, *122*, 1523–1534. [PubMed]
25. Stalsberg, H.; DeHaan, R.L. The precardiac areas and formation of the tubular heart in the chick embryo. *Dev. Biol.* **1969**, *19*, 128–159. [CrossRef]
26. Rosenquist, G.C.; DeHaan, R.L. *Migration of precardiac cells in the chick embryo: A radioautographic study*; Carnegie Institution of Washington: Washington, DC, USA, 1966.
27. DeRuiter, M.C.; Poelmann, R.E.; VanderPlas-de Vries, I.; Mentink, M.M.; Gittenberger-de Groot, A.C. The development of the myocardium and endocardium in mouse embryos. Fusion of two heart tubes? *Anat. Embryol. (Berl.)* **1992**, *185*, 461–473. [CrossRef] [PubMed]
28. Colas, J.F.; Lawson, A.; Schoenwolf, G.C. Evidence that translation of smooth muscle alpha-actin mrna is delayed in the chick promyocardium until fusion of the bilateral heart-forming regions. *Dev. Dyn.* **2000**, *218*, 316–330. [CrossRef]
29. Le Lievre, C.S.; Le Douarin, N.M. Mesenchymal derivatives of the neural crest: Analysis of chimaeric quail and chick embryos. *J. Embryol. Exp. Morphol.* **1975**, *34*, 125–154. [PubMed]
30. Hatada, Y.; Stern, C.D. A fate map of the epiblast of the early chick embryo. *Development* **1994**, *120*, 2879–2889. [PubMed]
31. Ladd, A.N.; Yatskievych, T.A.; Antin, P.B. Regulation of avian cardiac myogenesis by activin/tgfbeta and bone morphogenetic proteins. *Dev. Biol.* **1998**, *204*, 407–419. [CrossRef] [PubMed]
32. Yatskievych, T.A.; Ladd, A.N.; Antin, P.B. Induction of cardiac myogenesis in avian pregastrula epiblast: The role of the hypoblast and activin. *Development* **1997**, *124*, 2561–2570. [PubMed]
33. Matsui, H.; Ikeda, K.; Nakatani, K.; Sakabe, M.; Yamagishi, T.; Nakanishi, T.; Nakajima, Y. Induction of initial cardiomyocyte alpha-actin–smooth muscle alpha-actin–in cultured avian pregastrula epiblast: A role for nodal and bmp antagonist. *Dev. Dyn.* **2005**, *233*, 1419–1429. [CrossRef] [PubMed]
34. Tam, P.P.; Parameswaran, M.; Kinder, S.J.; Weinberger, R.P. The allocation of epiblast cells to the embryonic heart and other mesodermal lineages: The role of ingression and tissue movement during gastrulation. *Development* **1997**, *124*, 1631–1642. [PubMed]
35. Wei, Y.; Mikawa, T. Fate diversity of primitive streak cells during heart field formation in ovo. *Dev. Dyn.* **2000**, *219*, 505–513. [CrossRef]
36. Schultheiss, T.M.; Xydas, S.; Lassar, A.B. Induction of avian cardiac myogenesis by anterior endoderm. *Development* **1995**, *121*, 4203–4214. [PubMed]
37. Schultheiss, T.M.; Burch, J.B.; Lassar, A.B. A role for bone morphogenetic proteins in the induction of cardiac myogenesis. *Genes Dev.* **1997**, *11*, 451–462. [CrossRef] [PubMed]
38. Andree, B.; Duprez, D.; Vorbusch, B.; Arnold, H.H.; Brand, T. Bmp-2 induces ectopic expression of cardiac lineage markers and interferes with somite formation in chicken embryos. *Mech. Dev.* **1998**, *70*, 119–131. [CrossRef]
39. Schlange, T.; Andree, B.; Arnold, H.H.; Brand, T. Bmp2 is required for early heart development during a distinct time period. *Mech. Dev.* **2000**, *91*, 259–270. [CrossRef]

40. Alsan, B.H.; Schultheiss, T.M. Regulation of avian cardiogenesis by fgf8 signaling. *Development* **2002**, *129*, 1935–1943. [PubMed]
41. Lee, K.H.; Evans, S.; Ruan, T.Y.; Lassar, A.B. Smad-mediated modulation of yy1 activity regulates the bmp response and cardiac-specific expression of a gata4/5/6-dependent chick nkx2.5 enhancer. *Development* **2004**, *131*, 4709–4723. [CrossRef] [PubMed]
42. Marvin, M.J.; Di Rocco, G.; Gardiner, A.; Bush, S.M.; Lassar, A.B. Inhibition of wnt activity induces heart formation from posterior mesoderm. *Genes Dev.* **2001**, *15*, 316–327. [CrossRef] [PubMed]
43. Schneider, V.A.; Mercola, M. Wnt antagonism initiates cardiogenesis in Xenopus laevis. *Genes Dev.* **2001**, *15*, 304–315. [CrossRef] [PubMed]
44. Ruiz-Villalba, A.; Hoppler, S.; van den Hoff, M.J. Wnt signaling in the heart fields: Variations on a common theme. *Dev. Dyn.* **2016**, *245*, 294–306. [CrossRef] [PubMed]
45. Lickert, H.; Kutsch, S.; Kanzler, B.; Tamai, Y.; Taketo, M.M.; Kemler, R. Formation of multiple hearts in mice following deletion of beta-catenin in the embryonic endoderm. *Dev. Cell* **2002**, *3*, 171–181. [CrossRef]
46. Tzahor, E. Wnt/beta-catenin signaling and cardiogenesis: Timing does matter. *Dev. Cell* **2007**, *13*, 10–13. [CrossRef] [PubMed]
47. Noseda, M.; Peterkin, T.; Simoes, F.C.; Patient, R.; Schneider, M.D. Cardiopoietic factors: Extracellular signals for cardiac lineage commitment. *Circ. Res.* **2011**, *108*, 129–152. [CrossRef] [PubMed]
48. Lopez-Sanchez, C.; Franco, D.; Bonet, F.; Garcia-Lopez, V.; Aranega, A.; Garcia-Martinez, V. Negative fgf8-bmp2 feed-back is regulated by mir-130 during early cardiac specification. *Dev. Biol.* **2015**, *406*, 63–73. [CrossRef] [PubMed]
49. Lopez-Sanchez, C.; Franco, D.; Bonet, F.; Garcia-Lopez, V.; Aranega, A.; Garcia-Martinez, V. Reciprocal repression between fgf8 and mir-133 regulates cardiac induction through bmp2 signaling. *Data in brief* **2015**, *5*, 59–64. [CrossRef] [PubMed]
50. Yue, Q.; Wagstaff, L.; Yang, X.; Weijer, C.; Münsterberg, A. Wnt3a-mediated chemorepulsion controls movement patterns of cardiac progenitors and requires rhoa function. *Development* **2008**, *135*, 1029–1037. [CrossRef] [PubMed]
51. Kaarbo, M.; Crane, D.I.; Murrell, W.G. Rhoa is highly up-regulated in the process of early heart development of the chick and important for normal embryogenesis. *Dev. Dyn.* **2003**, *227*, 35–47. [CrossRef] [PubMed]
52. Song, J.; McColl, J.; Camp, E.; Kennerley, N.; Mok, G.F.; McCormick, D.; Grocott, T.; Wheeler, G.N.; Münsterberg, A.E. Smad1 transcription factor integrates bmp2 and wnt3a signals in migrating cardiac progenitor cells. *Proc. Natl. Acad. Sci. USA* **2014**, *111*, 7337–7342. [CrossRef] [PubMed]
53. Klaus, A.; Saga, Y.; Taketo, M.M.; Tzahor, E.; Birchmeier, W. Distinct roles of wnt/beta-catenin and bmp signaling during early cardiogenesis. *Proc. Natl. Acad. Sci. USA* **2007**, *104*, 18531–18536. [CrossRef] [PubMed]
54. Udan, R.S.; Piazza, V.G.; Hsu, C.W.; Hadjantonakis, A.K.; Dickinson, M.E. Quantitative imaging of cell dynamics in mouse embryos using light-sheet microscopy. *Development* **2014**, *141*, 4406–4414. [CrossRef] [PubMed]
55. Ramsdell, A.F. Left-right asymmetry and congenital cardiac defects: Getting to the heart of the matter in vertebrate left-right axis determination. *Dev. Biol.* **2005**, *288*, 1–20. [CrossRef] [PubMed]
56. Levin, M.; Johnson, R.L.; Stern, C.D.; Kuehn, M.; Tabin, C. A molecular pathway determining left-right asymmetry in chick embryogenesis. *Cell* **1995**, *82*, 803–814. [CrossRef]
57. Mendes, R.V.; Martins, G.G.; Cristovao, A.M.; Saude, L. N-cadherin locks left-right asymmetry by ending the leftward movement of Hensen's node cells. *Dev. Cell* **2014**, *30*, 353–360. [CrossRef] [PubMed]
58. Collignon, J.; Varlet, I.; Robertson, E.J. Relationship between asymmetric nodal expression and the direction of embryonic turning. *Nature* **1996**, *381*, 155–158. [CrossRef] [PubMed]
59. Meyers, E.N.; Martin, G.R. Differences in left-right axis pathways in mouse and chick: Functions of fgf8 and shh. *Science* **1999**, *285*, 403–406. [CrossRef] [PubMed]
60. Schlueter, J.; Brand, T. Left-right axis development: Examples of similar and divergent strategies to generate asymmetric morphogenesis in chick and mouse embryos. *Cytogenet. Genome Res.* **2007**, *117*, 256–267. [CrossRef] [PubMed]
61. Logan, M.; Pagan-Westphal, S.M.; Smith, D.M.; Paganessi, L.; Tabin, C.J. The transcription factor pitx2 mediates situs-specific morphogenesis in response to left-right asymmetric signals. *Cell* **1998**, *94*, 307–317. [CrossRef]

62. Tessari, A.; Pietrobon, M.; Notte, A.; Cifelli, G.; Gage, P.J.; Schneider, M.D.; Lembo, G.; Campione, M. Myocardial pitx2 differentially regulates the left atrial identity and ventricular asymmetric remodeling programs. *Circ. Res.* **2008**, *102*, 813–822. [CrossRef] [PubMed]
63. Schlueter, J.; Brand, T. A right-sided pathway involving fgf8/snai1 controls asymmetric development of the proepicardium in the chick embryo. *Proc. Natl. Acad. Sci. USA* **2009**, *106*, 7485–7490. [CrossRef] [PubMed]
64. Schulte, I.; Schlueter, J.; Abu-Issa, R.; Brand, T.; Manner, J. Morphological and molecular left-right asymmetries in the development of the proepicardium: A comparative analysis on mouse and chick embryos. *Dev. Dyn.* **2007**, *236*, 684–695. [CrossRef] [PubMed]
65. de la Cruz, M.V.; Sanchez Gomez, C.; Arteaga, M.M.; Arguello, C. Experimental study of the development of the truncus and the conus in the chick embryo. *J. Anat.* **1977**, *123*, 661–686. [PubMed]
66. Arguello, C.; de la Cruz, M.V.; Gomez, C.S. Experimental study of the formation of the heart tube in the chick embryo. *J. Embryol. Exp. Morphol.* **1975**, *33*, 1–11. [PubMed]
67. de La Cruz, M.V.; Sanchez-Gomez, C.; Palomino, M.A. The primitive cardiac regions in the straight tube heart (stage 9) and their anatomical expression in the mature heart: An experimental study in the chick embryo. *J. Anat.* **1989**, *165*, 121–131. [PubMed]
68. Kelly, R.G.; Brown, N.A.; Buckingham, M.E. The arterial pole of the mouse heart forms from fgf10-expressing cells in pharyngeal mesoderm. *Dev. Cell* **2001**, *1*, 435–440. [CrossRef]
69. Mjaatvedt, C.H.; Nakaoka, T.; Moreno-Rodriguez, R.; Norris, R.A.; Kern, M.J.; Eisenberg, C.A.; Turner, D.; Markwald, R.R. The outflow tract of the heart is recruited from a novel heart-forming field. *Dev. Biol.* **2001**, *238*, 97–109. [CrossRef] [PubMed]
70. Waldo, K.L.; Kumiski, D.H.; Wallis, K.T.; Stadt, H.A.; Hutson, M.R.; Platt, D.H.; Kirby, M.L. Conotruncal myocardium arises from a secondary heart field. *Development* **2001**, *128*, 3179–3188. [PubMed]
71. Camp, E.; Dietrich, S.; Münsterberg, A. Fate mapping identifies the origin of SHF/AHFprogenitors in the chick primitive streak. *PLoS ONE* **2012**, *7*, e51948. [CrossRef] [PubMed]
72. Nathan, E.; Monovich, A.; Tirosh-Finkel, L.; Harrelson, Z.; Rousso, T.; Rinon, A.; Harel, I.; Evans, S.M.; Tzahor, E. The contribution of islet1-expressing splanchnic mesoderm cells to distinct branchiomeric muscles reveals significant heterogeneity in head muscle development. *Development* **2008**, *135*, 647–657. [CrossRef] [PubMed]
73. Lescroart, F.; Kelly, R.G.; Le Garrec, J.F.; Nicolas, J.F.; Meilhac, S.M.; Buckingham, M. Clonal analysis reveals common lineage relationships between head muscles and second heart field derivatives in the mouse embryo. *Development* **2010**, *137*, 3269–3279. [CrossRef] [PubMed]
74. Milgrom-Hoffman, M.; Harrelson, Z.; Ferrara, N.; Zelzer, E.; Evans, S.M.; Tzahor, E. The heart endocardium is derived from vascular endothelial progenitors. *Development* **2011**, *138*, 4777–4787. [CrossRef] [PubMed]
75. Misfeldt, A.M.; Boyle, S.C.; Tompkins, K.L.; Bautch, V.L.; Labosky, P.A.; Baldwin, H.S. Endocardial cells are a distinct endothelial lineage derived from flk1+ multipotent cardiovascular progenitors. *Dev. Biol.* **2009**, *333*, 78–89. [CrossRef] [PubMed]
76. Ferdous, A.; Caprioli, A.; Iacovino, M.; Martin, C.M.; Morris, J.; Richardson, J.A.; Latif, S.; Hammer, R.E.; Harvey, R.P.; Olson, E.N.; *et al.* Nkx2–5 transactivates the ets-related protein 71 gene and specifies an endothelial/endocardial fate in the developing embryo. *Proc. Natl. Acad. Sci. USA* **2009**, *106*, 814–819. [CrossRef] [PubMed]
77. Dyer, L.A.; Kirby, M.L. The role of secondary heart field in cardiac development. *Dev. Biol.* **2009**, *336*, 137–144. [CrossRef] [PubMed]
78. Vincent, S.D.; Buckingham, M.E. How to make a heart: The origin and regulation of cardiac progenitor cells. *Curr. Top. Dev. Biol.* **2010**, *90*, 1–41. [PubMed]
79. Buckingham, M.; Meilhac, S.; Zaffran, S. Building the mammalian heart from two sources of myocardial cells. *Nature reviews. Genetics* **2005**, *6*, 826–835. [CrossRef] [PubMed]
80. Hutson, M.R.; Zeng, X.L.; Kim, A.J.; Antoon, E.; Harward, S.; Kirby, M.L. Arterial pole progenitors interpret opposing fgf/bmp signals to proliferate or differentiate. *Development* **2010**, *137*, 3001–3011. [CrossRef] [PubMed]
81. Tirosh-Finkel, L.; Zeisel, A.; Brodt-Ivenshitz, M.; Shamai, A.; Yao, Z.; Seger, R.; Domany, E.; Tzahor, E. Bmp-mediated inhibition of fgf signaling promotes cardiomyocyte differentiation of anterior heart field progenitors. *Development* **2010**, *137*, 2989–3000. [CrossRef] [PubMed]

82. Bothe, I.; Dietrich, S. The molecular setup of the avian head mesoderm and its implication for craniofacial myogenesis. *Dev. Dyn.* **2006**, *235*, 2845–2860. [CrossRef] [PubMed]
83. Tirosh-Finkel, L.; Elhanany, H.; Rinon, A.; Tzahor, E. Mesoderm progenitor cells of common origin contribute to the head musculature and the cardiac outflow tract. *Development* **2006**, *133*, 1943–1953. [CrossRef] [PubMed]
84. Bothe, I.; Tenin, G.; Oseni, A.; Dietrich, S. Dynamic control of head mesoderm patterning. *Development* **2011**, *138*, 2807–2821. [CrossRef] [PubMed]
85. Grifone, R.; Kelly, R.G. Heartening news for head muscle development. *Trends in genetics : TIG* **2007**, *23*, 365–369. [CrossRef] [PubMed]
86. Diogo, R.; Kelly, R.G.; Christiaen, L.; Levine, M.; Ziermann, J.M.; Molnar, J.L.; Noden, D.M.; Tzahor, E. A new heart for a new head in vertebrate cardiopharyngeal evolution. *Nature* **2015**, *520*, 466–473. [CrossRef] [PubMed]
87. Bressan, M.; Liu, G.; Mikawa, T. Early mesodermal cues assign avian cardiac pacemaker fate potential in a tertiary heart field. *Science* **2013**, *340*, 744–748. [CrossRef] [PubMed]
88. Kamino, K.; Hirota, A.; Fujii, S. Localization of pacemaking activity in early embryonic heart monitored using voltage-sensitive dye. *Nature* **1981**, *290*, 595–597. [CrossRef] [PubMed]
89. Needham, J.; Hughes, A. *A history of embryology*, 2nd ed.; Cambridge University Press: London, UK, 1959.
90. Patten, B.M. The formation of the cardiac loop in the chick. *Am. J. Anat.* **1922**, *30*, 373–397. [CrossRef]
91. Varner, V.D.; Taber, L.A. Not just inductive: A crucial mechanical role for the endoderm during heart tube assembly. *Development* **2012**, *139*, 1680–1690. [CrossRef] [PubMed]
92. DeHaan, R.L. Cardia bifida and the development of pacemaker function in the early chick heart. *Dev. Biol.* **1959**, *1*, 586–602. [CrossRef]
93. Kitajima, S.; Takagi, A.; Inoue, T.; Saga, Y. Mesp1 and mesp2 are essential for the development of cardiac mesoderm. *Development* **2000**, *127*, 3215–3226. [PubMed]
94. Matsui, T.; Raya, A.; Kawakami, Y.; Callol-Massot, C.; Capdevila, J.; Rodriguez-Esteban, C.; Izpisua Belmonte, J.C. Noncanonical wnt signaling regulates midline convergence of organ primordia during zebrafish development. *Genes Dev.* **2005**, *19*, 164–175. [CrossRef] [PubMed]
95. Manner, J. Cardiac looping in the chick embryo: A morphological review with special reference to terminological and biomechanical aspects of the looping process. *Anat. Rec.* **2000**, *259*, 248–262. [CrossRef]
96. Manner, J. The anatomy of cardiac looping: A step towards the understanding of the morphogenesis of several forms of congenital cardiac malformations. *Clin. Anat.* **2009**, *22*, 21–35. [CrossRef] [PubMed]
97. de la Cruz, M.; Sanchez-Gomez, C. Straight tube heart. Primitive cardiac cavities vs. Primitive cardiac segments. In *Living Morphogenesis of the Heart*; de la Cruz, M., Markwald, R., Eds.; Birkhäuser Boston: Boston, MA, USA, 1998; pp. 85–98.
98. Goenezen, S.; Rennie, M.Y.; Rugonyi, S. Biomechanics of early cardiac development. *Biomech. Model. Mechanobiol.* **2012**, *11*, 1187–1204. [CrossRef] [PubMed]
99. Le Douarin, N.M. The avian embryo as a model to study the development of the neural crest: A long and still ongoing story. *Mech. Dev.* **2004**, *121*, 1089–1102. [CrossRef] [PubMed]
100. Kirby, M.L.; Gale, T.F.; Stewart, D.E. Neural crest cells contribute to normal aorticopulmonary septation. *Science* **1983**, *220*, 1059–1061. [CrossRef] [PubMed]
101. Waldo, K.; Miyagawa-Tomita, S.; Kumiski, D.; Kirby, M.L. Cardiac neural crest cells provide new insight into septation of the cardiac outflow tract: Aortic sac to ventricular septal closure. *Dev. Biol.* **1998**, *196*, 129–144. [CrossRef] [PubMed]
102. Zhang, Y.; Ruest, L.B. Analysis of neural crest cell fate during cardiovascular development using cre-activated lacz/beta-galactosidase staining. *Methods Mol. Biol.* **2012**, *843*, 125–138. [PubMed]
103. Escot, S.; Blavet, C.; Hartle, S.; Duband, J.L.; Fournier-Thibault, C. Misregulation of sdf1-cxcr4 signaling impairs early cardiac neural crest cell migration leading to conotruncal defects. *Circ. Res.* **2013**, *113*, 505–516. [CrossRef] [PubMed]
104. Sierro, F.; Biben, C.; Martinez-Munoz, L.; Mellado, M.; Ransohoff, R.M.; Li, M.; Woehl, B.; Leung, H.; Groom, J.; Batten, M.; *et al*. Disrupted cardiac development but normal hematopoiesis in mice deficient in the second cxcl12/sdf-1 receptor, cxcr7. *Proc. Natl. Acad. Sci. USA* **2007**, *104*, 14759–14764. [CrossRef] [PubMed]

105. Bressan, M.; Yang, P.B.; Louie, J.D.; Navetta, A.M.; Garriock, R.J.; Mikawa, T. Reciprocal myocardial-endocardial interactions pattern the delay in atrioventricular junction conduction. *Development* **2014**, *141*, 4149–4157. [CrossRef] [PubMed]
106. Bonet, F.; Duenas, A.; Lopez-Sanchez, C.; Garcia-Martinez, V.; Aranega, A.E.; Franco, D. Mir-23b and mir-199a impair epithelial-to-mesenchymal transition during atrioventricular endocardial cushion formation. *Dev. Dyn.* **2015**, *244*, 1259–1275. [CrossRef] [PubMed]
107. Samsa, L.A.; Yang, B.; Liu, J. Embryonic cardiac chamber maturation: Trabeculation, conduction, and cardiomyocyte proliferation. *Am. J. Med. Genet. C Semin. Med. Genet.* **2013**, *163C*, 157–168. [CrossRef] [PubMed]
108. Moorman, A.F.; Christoffels, V.M. Cardiac chamber formation: Development, genes, and evolution. *Physiol. Rev.* **2003**, *83*, 1223–1267. [CrossRef] [PubMed]
109. Mikawa, T.; Gourdie, R.G. Pericardial mesoderm generates a population of coronary smooth muscle cells migrating into the heart along with ingrowth of the epicardial organ. *Dev. Biol.* **1996**, *174*, 221–232. [CrossRef] [PubMed]
110. Reese, D.E.; Mikawa, T.; Bader, D.M. Development of the coronary vessel system. *Circ. Res.* **2002**, *91*, 761–768. [CrossRef] [PubMed]
111. Kattan, J.; Dettman, R.W.; Bristow, J. Formation and remodeling of the coronary vascular bed in the embryonic avian heart. *Dev. Dyn.* **2004**, *230*, 34–43. [CrossRef] [PubMed]
112. Olivey, H.E.; Compton, L.A.; Barnett, J.V. Coronary vessel development: The epicardium delivers. *Trends Cardiovasc. Med.* **2004**, *14*, 247–251. [CrossRef] [PubMed]
113. Manner, J.; Schlueter, J.; Brand, T. Experimental analyses of the function of the proepicardium using a new microsurgical procedure to induce loss-of-proepicardial-function in chick embryos. *Dev. Dyn.* **2005**, *233*, 1454–1463. [CrossRef] [PubMed]
114. Perez-Pomares, J.M.; Phelps, A.; Sedmerova, M.; Wessels, A. Epicardial-like cells on the distal arterial end of the cardiac outflow tract do not derive from the proepicardium but are derivatives of the cephalic pericardium. *Dev. Dyn.* **2003**, *227*, 56–68. [CrossRef] [PubMed]
115. Wilting, J.; Buttler, K.; Schulte, I.; Papoutsi, M.; Schweigerer, L.; Manner, J. The proepicardium delivers hemangioblasts but not lymphangioblasts to the developing heart. *Dev. Biol.* **2007**, *305*, 451–459. [CrossRef] [PubMed]
116. Combs, M.D.; Braitsch, C.M.; Lange, A.W.; James, J.F.; Yutzey, K.E. Nfatc1 promotes epicardium-derived cell invasion into myocardium. *Development* **2011**, *138*, 1747–1757. [CrossRef] [PubMed]
117. Schlueter, J.; Brand, T. Subpopulation of proepicardial cells is derived from the somatic mesoderm in the chick embryo. *Circ. Res.* **2013**, *113*, 1128–1137. [CrossRef] [PubMed]
118. Ishii, Y.; Garriock, R.J.; Navetta, A.M.; Coughlin, L.E.; Mikawa, T. Bmp signals promote proepicardial protrusion necessary for recruitment of coronary vessel and epicardial progenitors to the heart. *Dev. Cell* **2010**, *19*, 307–316. [CrossRef] [PubMed]
119. Hatcher, C.J.; Diman, N.Y.; Kim, M.S.; Pennisi, D.; Song, Y.; Goldstein, M.M.; Mikawa, T.; Basson, C.T. A role for tbx5 in proepicardial cell migration during cardiogenesis. *Physiol. Genomics* **2004**, *18*, 129–140. [CrossRef] [PubMed]
120. Katz, T.C.; Singh, M.K.; Degenhardt, K.; Rivera-Feliciano, J.; Johnson, R.L.; Epstein, J.A.; Tabin, C.J. Distinct compartments of the proepicardial organ give rise to coronary vascular endothelial cells. *Dev. Cell* **2012**, *22*, 639–650. [CrossRef] [PubMed]

8.4 Cardiac injections of AntagomiRs as a novel tool for knockdown of miRNAs during heart development

Johannes G. Wittig, Martina Billmeier, Estefanía Lozano-Velasco, Miguel Robles-García, Andrea E. Münsterberg *

Developmental Biology 445 (2019) 163–169

Contents lists available at ScienceDirect

Developmental Biology

journal homepage: www.elsevier.com/locate/developmentalbiology

Cardiac injections of AntagomiRs as a novel tool for knockdown of miRNAs during heart development

Johannes G. Wittig, Martina Billmeier, Estefanía Lozano-Velasco, Miguel Robles-García, Andrea E. Münsterberg*

School of Biological Sciences, University of East Anglia, Norwich Research Park, Norwich NR4 7TJ, UK

ARTICLE INFO

Keywords:
Chicken embryo
Micromanipulation
Microinjection
Heart development
MicroRNA
AntagomiR

ABSTRACT

Background: Studying microRNA networks during heart development is essential to obtain a better understanding of developmental defects and diseases associated with the heart and to identify novel opportunities for therapeutics. Here we highlight the advantages of chicken embryos as a vertebrate model for studying intermediate processes of heart development. Avians develop a four-chambered heart closely resembling human anatomy and they develop *ex utero*, which makes them easily accessible. Furthermore, embryos are available all year with a steady supply.

Results: In this report we established a novel method for the knockdown of microRNA function by microinjecting AntagomiRs into the chicken heart *in ovo*. Our approach enables the targeted delivery of antagomirs into a locally restricted area and is not impacted by circulation. After further embryo development the successful miRNA knockdown was confirmed. Loss of function phenotypes can be evaluated rapidly, compared to more time-consuming genetic ablation experiments. The local application avoids potential systemic effects of microRNA knockdown, therefore allowing the assessment of impacts on heart development only. The method can be adjusted for different stages of chicken embryos (HH13–HH18) as well as for knockdown or targeted overexpression of coding genes.

Conclusion: In conclusion our method allows targeted and locally restricted delivery of Antagomirs to the heart leading to successful knockdown of microRNA function. This method enables rapid phenotypic assessment, for example by gene expression analysis of multiple cardiac genes.

1. Introduction

The study of heart development contributed important insights into the normal process of organ patterning and growth control but also revealed factors involved in pathological development leading to a better understanding of congenital heart disease. MicroRNAs are small non-coding RNA molecules of approximately 23 base pairs in size that regulate gene expression (Bartel, 2009). It has been demonstrated previously that they play a significant role in both cardiac development and disease (Chen and Wang, 2012; Liu and Olson, 2010), however the details of how individual microRNAs regulate gene networks remain to be elucidated. Thus, further work is needed to acquire new insights and to potentially translate this knowledge into new avenues for medical care. Cardiac microRNA networks have been studied in a number of model organisms each of them with different advantages for analysis. Two models closely resembling human heart anatomy, with a four-chambered heart comprising two atria and two ventricles, are the mouse (*Mus musculus*) and the chicken (*Gallus gallus*). The fact that mice develop *in utero* whereas chicken embryos develop *in ovo* has a strong impact on accessibility and therefore applicable methods. Commonly used approaches for altering gene expression in mice include Cre-mediated tissue specific (conditional) recombination of a selected target gene, CRISPR-mediated genome editing, or transgenic overexpression of genes of interest, allowing for permanent and/or inducible genetic alterations (Bouabe and Okkenhaug, 2013; Singh et al., 2015). Furthermore, lineage tracing experiments that reveal cell relationships have been used extensively in mice by applying genetic labelling methods (Kalhor et al., 2018; Kraus et al., 2014). In chicken, tissue grafting, electroporation and microinjections are the most commonly used techniques. The embryo is highly accessible *in ovo* and allows stage-specific manipulations with subsequent read out (Bellairs and Osmond, 2014; Stern, 2005). Even though a different subset of techniques is used in chicken embryos lineage tracing has also been employed to study cell fate (Kretzschmar and Watt, 2012), for

* Corresponding author.
E-mail address: A.Munsterberg@uea.ac.uk (A.E. Münsterberg).

https://doi.org/10.1016/j.ydbio.2018.11.008
Received 19 October 2018; Received in revised form 12 November 2018; Accepted 14 November 2018
Available online 26 November 2018

example the contributions of cardiac neural crest to outflow tract septation and of the second heart field to the right ventricle were first identified in the chicken (Wittig and Münsterberg, 2016).

Genetic approaches in mice have significantly increased our understanding of heart development, however, these are time-consuming and their spatio-temporal control is limited by the ability to control the activity of the Cre recombinase, thus making the study of specific events during heart development more challenging. The precise local administration of pharmacological agents to the mouse heart is difficult due to in utero development and therefore lack of access to the embryonic heart. Injections into the vasculature lead to systemic delivery and thus an impact on tissues other than the heart cannot be excluded (Goehringer et al., 2009; Krutzfeldt et al., 2005). In chicken, the effective delivery of viral based expression constructs needs high concentrations (Lambeth et al., 2014), leading to potential DNA toxicity effects. A general complication is that due to heart contractions, injected compounds are quickly washed out into circulation (Davidson et al., 2001). Virus based transduction is slightly less affected by this since the virus binds to cell surface receptors. Effective binding can be improved by slowing the heart temporarily through embryo cooling. However, nucleic acid-based constructs or synthetic compounds can quickly disperse and their successful delivery and uptake requires steady local administration and/or temporary heart arrest, which could have non-specific effects on development.

For our study we chose the chicken embryo as model organism, its developmental stages are well-defined (Hamburger and Hamilton, 1951) and the heart is readily accessible, particularly the early and intermediate stages, which closely resemble human anatomy (Wittig and Münsterberg, 2016). Embryos are cheap to obtain and are incubated to the desired stage in controlled conditions. This facilitates *in ovo* manipulations with precise temporal and site-specific targeting and permits the study of different phases of intermediate heart development, including S-shape (heart) looping, chamber remodelling, trabeculation and septa formation. Following manipulation and further embryo development subsequent visual assessment and gene expression analysis is possible and does not require sacrificing the parent animal. Therefore, the use of chicken embryos complements the analysis of genetically modified embryos of other model species (Bellairs and Osmond, 2014).

The injection technique into the chicken heart illustrated here can be applied to different subsections of the heart and thus overcomes some of the above-mentioned drawbacks. Furthermore, the targeted injections could be performed with plasmid constructs – combined with Lipofectamin (England et al., 2017), or with virus particles, synthetic compounds, antisense morpholinos or microRNA mimics and inhibitors. Delivery of microRNA inhibitors, AntagomiRs (Table 1), is the primary focus of this report as it represents a new tool for studying the functions of individual or multiple microRNAs during intermediate heart development, during which the heart tube is remodelled into a mature chambered heart. Once mastered, this method can be used for heart-specific knockdown and gain-of-function studies and allows medium-throughput screening of multiple genes of interest.

2. Results

2.1. Protocol for cardiac injections

The whole procedure is shown step by step in Movie 1: Cardiac injection procedure.

1. Incubate fertilized chicken eggs.
   a. Fertilized chicken eggs are stored at 17 °C for up to a week prior to incubation.
   b. Eggs are incubated with the blunt end up in a humidified incubator at 37 °C.
      i. Depending on stage of interest the length of egg incubation has to be adjusted. To obtain HH15 embryos we incubated fertile eggs for approximately 66 h (Hamburger and Hamilton, 1951).
2. Preparation of injection setup:
   a. For 30 eggs prepare 25 ml 1:500 PBS/ Pen Strep (PS) (Gibco Life Technologies) solution and 25 ml PBS/PS-solution with Indian ink (Winsor & Newton).
   b. Prepare Syringes with needles.
      i. 1 ml syringe with 25Gx 5/8″ needle for ink injection.
      ii. 1 ml syringe with 25Gx 5/8″ needle for incision of the extra embryonic tissue (EET).
      iii. 10 ml or 2 ml syringe with 21Gx2″ needle for albumen removal.
   c. Forceps and tweezers for removal of the shell and outer/inner membranes.
   d. Adhesive tape for egg sealing.
   e. Small table-top incubator for usage during procedure.
3. Prepare injection apparatus.
   a. Pull needle for microinjection (borosilicate glass capillaries 1.00 mm O.D. × 0.78 mm I.D.).
   b. To enable easy heart manipulation, we recommend shorter needles with a very sharp tip, since long flexible ones will not penetrate the heart and simply bend.
      i. Needle pull settings for Sutter Instruments P-97: P = 300, Heat = ramp test value, Pull = 150, Vel = 80, Time = 130.
   c. Load needle with ~1.5 µl AntagomiR at 1 µM (or other) using Microloader™ (Eppendorf) and mount onto microinjector
4. Prior to procedure spray eggs with 70% Ethanol to kill surface germs.
5. Remove single egg from incubator (Fig. 1A).
6. Crack it open at the blunt end using tweezers and remove shell pieces until embryo is easily accessible (Fig. 1B).
7. Using syringe (i) in a shallow angle inject ink-mix beneath the embryo for contrast and apply 2 drops PBS/PS-solution on top using a plastic Pasteur pipette to increase elasticity of extra-embryonic tissues (EET) (Fig. 1C).
8. Place egg under a stereo-dissecting microscope and use syringe needle (ii) to cut open the vitelline membrane (Fig. 1D).
   a. Cut EET around heart until it is freely accessible (Fig. 1E).
9. Perform multiple injections in areas of interest (Fig. 1F).
   a. Depicted are conus, primitive ventricle and primitive atrium (Fig. 1F).
10. Remove needle and visually confirm injection (Fig. 1G).
    a. Injected compound (AntagomiR) is conjugated to a fluorophore.
11. Slide the needle of the large syringe (iii) down along the inside of the egg shell and remove albumen until the embryo is sufficiently lowered and will not touch the sealing tape (Fig. 1H).
    a. If embryo adheres to the egg shell, flush it gently using albumen until it detaches.
    b. Apply a few drops PBS/PS-solution.
12. Seal the egg using clear adhesive tape.
    a. Combine two strips of tape together (parallel) and apply them to the egg. Use a third strip and cross the other two (perpendicular) (Fig. 1I).

Table 1
AntagomiRs used in this study.

AntagomiR name	Sequence
AntagomiR-SCR	5′-(FL)mC(*)mA(*)mUmCmCmAmUmCmAmCmUmCmAmCmUmCmCmAmU(*)mC(*)mA(*)mU(3′-Chl)-3′
AntagomiR-499-5p	5′-(FL)mC(*)mU(*)mAmAmAmCmAmUmCmAmCmUmAmCmAmAmGmUmCmU(*)mU(*)mA(*)mA(3′-Chl)-3′

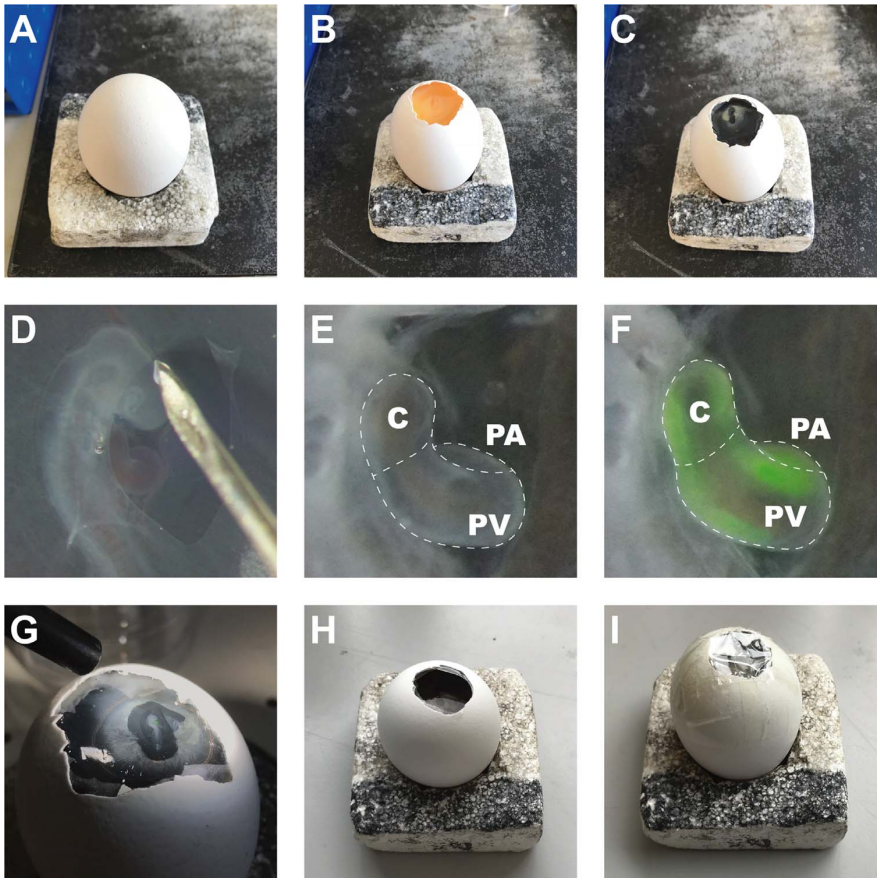

Fig. 1. Injection sequence. Image sequence of procedure steps. (A) Incubated egg for manipulation, (B) egg was cracked open and outer and inner membrane were removed, (C) ink was applied into the yolk below the embryo to provide contrast, (D) vitelline membrane and EET were cut open to access the heart, (E) accessible heart for injection, red blood cells are visible in the lumen, (F) injected heart along conus (C) downwards to primitive ventricle (PV) and on the right side the primitive atrium (PA), (G) injection verification, (H) removal of albumen and lowering of embryo, (I) sealing of egg and returning to incubation at 37 °C.

13. Return the egg to an incubator immediately (for convenience this could be the desk-top incubator).

Supplementary material related to this article can be found online at doi:10.1016/j.ydbio.2018.11.008.

2.2. Embryo survival and possible timescales of experiments

Several parameters have an impact on survival of the injected chicken embryos. In this study we analysed survival of embryos, injected with AntagomiR or with a scrambled sequence, 24 h post injection (hpi), 48 hpi and 72 hpi (Krutzfeldt et al., 2005; McGlinn et al., 2009) (representative photos, Fig. 2A). For both the non-specific scrambled control, AntagomiR-SCR, and the specific AntagomiR-499-5p embryo survival declined with longer incubation periods (Fig. 2B). After 24 h post injection around 90% of embryos had survived and developed normally, this dropped to 40% and 35% at 48 hpi and 72 hpi. The almost identical survival rates observed with control and experimental AntagomiRs suggests that the decrease in survival is due to the manipulation itself. The data presented for AntagomiR-SCR represents the baseline for survival and we assume that survival beyond 72 hpi is possible, potentially even up to hatching. In experiments where other AntagomiRs were injected the embryos showed a steeper decline in survival (up to 100% before 48 hpi, not shown), suggesting a biological impact affecting survival resulting from this particular knockdown.

Several factors during the procedure should be considered to promote embryo survival. During egg opening, it is vital to avoid damaging the embryonic tissue and the vasculature. Bleeding indicates damage and these embryos cannot be used. In addition, following the microinjection embryos can sometimes adhere to the egg shell and their detachment can result in damage. Incubation with rocking prior to injection may reduce the occurrence of adherence to the shell and it has been reported that agitation during incubation improves hatchability and should therefore promote healthier development (Randles and Romanoff, 1954). In the final step of the procedure, when lowering the embryo after injection, it is essential to avoid contact with sealing tape. To avoid these confounding issues, we have excluded egg shell adhering embryos in our survival analysis.

To make the heart accessible for injection the vitelline membrane and some of the EET surrounding the heart need to be partially removed. During this, caution is necessary to avoid wounding vessels or the heart to prevent bleeding. The same applies to the actual injection step, since the injection needle is sharp enough to cause small incisions in the heart. Finally, the procedure was optimized by returning the embryos to a heated incubator at 37 °C immediately after injection, this improved survival rates.

To determine if the injection procedure had an impact on heart function, we analysed heart rates (HR) of control-injected embryos compared to wildtype (non-manipulated) embryos as a representative variable for cardiac health (Fig. 2C top panel). The data revealed no significant differences between the two groups for the first two time-points analysed, 24 hpi and 48 hpi (unpaired *t*-test, $p > 0.05$). This also

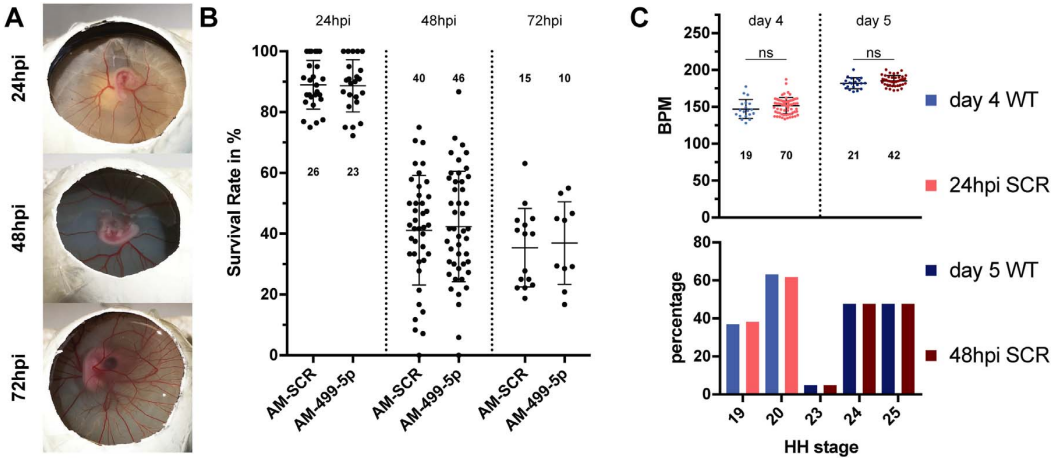

Fig. 2. Representative results – embryo survival & impact on heart rate. Embryos survive until at least 72 hpi and show no differences in cardiac health. (A) Representative photos of embryos post injection at the 3 time points analysed. (B) Survival analysis for embryos injected with AntagomiR-SCR (control) and AntagomiR-499-5p, a specific microRNA inhibitor. (C) Comparison of WT non-manipulated embryos *vs* control-injected embryos show no significant difference in heart rate. The bottom panel shows the distribution of HH stages that were analysed. We ensured the same proportion of HH19 and HH20 embryos were examined on day 4 (light blue and light red columns) and the same proportion of HH23, HH24 and HH25 embryos were examined on day 5 (dark blue and dark red columns). (N in (B) is number of experiments, each experiment comprised between 25 and 30 embryos, N in (C) represents the number of analysed hearts).

shows that the injected AntagomiR has no non-specific toxicity. The HR becomes faster with increasing age, therefore, to ensure accurate comparison, the same stages of embryo development were used (Fig. 2C bottom panel). The quantification of HR requires the heart to be visually accessible and this makes analysis of older embryos (> 5 days) difficult. After 5 days of development the allantois is covering the heart and this made HR-quantification challenging even though still possible for some embryos (Spurlin and Lwigale, 2013). However, electrophysiological methods for HR- quantification may still be suitable (Shi et al., 2013). We have also found that injection of some AntagomiRs can induce HR changes and the complete analysis of such phenotypes requires detailed follow-up experiments.

2.3. Validation of AntagomiR administration

The injected compounds in this study were AntagomiRs, complementary sequences to microRNAs designed to inhibit their function (Krutzfeldt et al., 2005; McGlinn et al., 2009). The AntagomiRs contained two modifications, a 3′ cholesterol group to allow cell uptake and a 5′ Fluorescein group for tracing purposes. The Fluorescein enables easy localization of AntagomiRs during the procedure, which is helpful for targeting and to avoid injection into the bloodstream, potentially causing systemic rather than heart specific effects. Furthermore, the fluorescent tag enables detection post-injection at 24 hpi and 48 hpi (Fig. 3A). However, fluorescence intensity decreased over time and was no longer detectable at 72 hpi. Signal strength may also depend on local retention of the AntagomiR. The AntagomiR-SCR used as a control in this study has no binding partner in the chicken embryo, we found that its signal intensity was reduced, compared to an AntagomiR that is directed against a microRNA expressed in the heart, such as miR-499-5p (Fig. 3Bi) (van Rooij et al., 2009). After Antagomir-499-5p injection a much stronger signal was consistently detected using enzyme catalysed immunohistochemistry (IHC) against the FITC-tag. We propose that this is most likely due to binding of the endogenous complementary microRNA, miR-499-5p. In addition to IHC on dissected hearts (Fig. 3Bi), we examined whole embryos to confirm specific targeting of the heart only (Fig. 3Bii). Specific staining was restricted to the heart shown by two purple stripes. Some faint staining was visible in the body due to trapping, which is a commonly observed drawback of methods involving chromophore conversion (Antin et al., 2007; Lufkin, 2007). However, if this diffuse signal is instead due to leakage of AntagomiR into other tissues, it would indicate that there was very little if any.

In mice, AntagomiRs were detected for up to three weeks after systemic injection (Krutzfeldt et al., 2005). Consistent with this, IHC against Fluorescein detected AntagomiRs for periods longer than 48 hpi (Fig. 3B).

Furthermore, Knockdown of miR-499-5p can be confirmed by Northern-Blot (Fig. 3C, Supplement 1) and qPCR (Fig. 3D). Hearts were dissected post incubation, pooled (six for 24 hpi & three for 48 hpi) and RNA was extracted. Both methods show a significant reduction of miR-499-5p expression at both timepoints, indicating that AntagomiRs are effective and stable in an *in vivo* environment (unpaired *t*-test, Northern Blot, $n = 3$, 24 hpi and 48 hpi $p < 0.01$, qPCR, $n = 5$, 24 hpi and 48 hpi $p < 0.001$). The miR-499-5p bands on Northern Blots were normalised to U6 and qPCR data was normalised to the expression of other microRNAs, miR-451 and miR-126-3p. These microRNAs were not targeted and showed stable expression. We have found that detection of U6 by qPCR was inconsistent, especially when using different RNA amounts for cDNA synthesis.

In addition, we found that the molecular verification using Northern Blot and qPCR is dependent on the chosen RNA extraction method. If the extraction method included Trizol, a frequently used solution, the knockdown could not be demonstrated (Supplement 2A, B). Initially we wondered whether the lack of observable knockdown could be explained by a feedback mechanism, involving the upregulation of miR-499-5p synthesis, however qPCR detection of the longer precursor microRNA in Trizol extracted samples did not support this idea (Supplement 2C). Another explanation might be, that Trizol releases the stable duplex of AntagomiR and microRNA and thus, more microRNA can be detected in these samples even though microRNA function is still inhibited. Furthermore, Trizol has a known bias regarding GC-content, particularly when extracting microRNAs (Kim et al., 2012). Taking this into consideration, we do not recommend extraction methods that involve Trizol when examining microRNAs.

3. Discussion

In conclusion, our method can be used for AntagomiR injections and to achieve successful knockdown of microRNA function in the heart. The injected compound can easily be replaced and thus the technique is also suitable for delivery of morpholinos, or plasmid

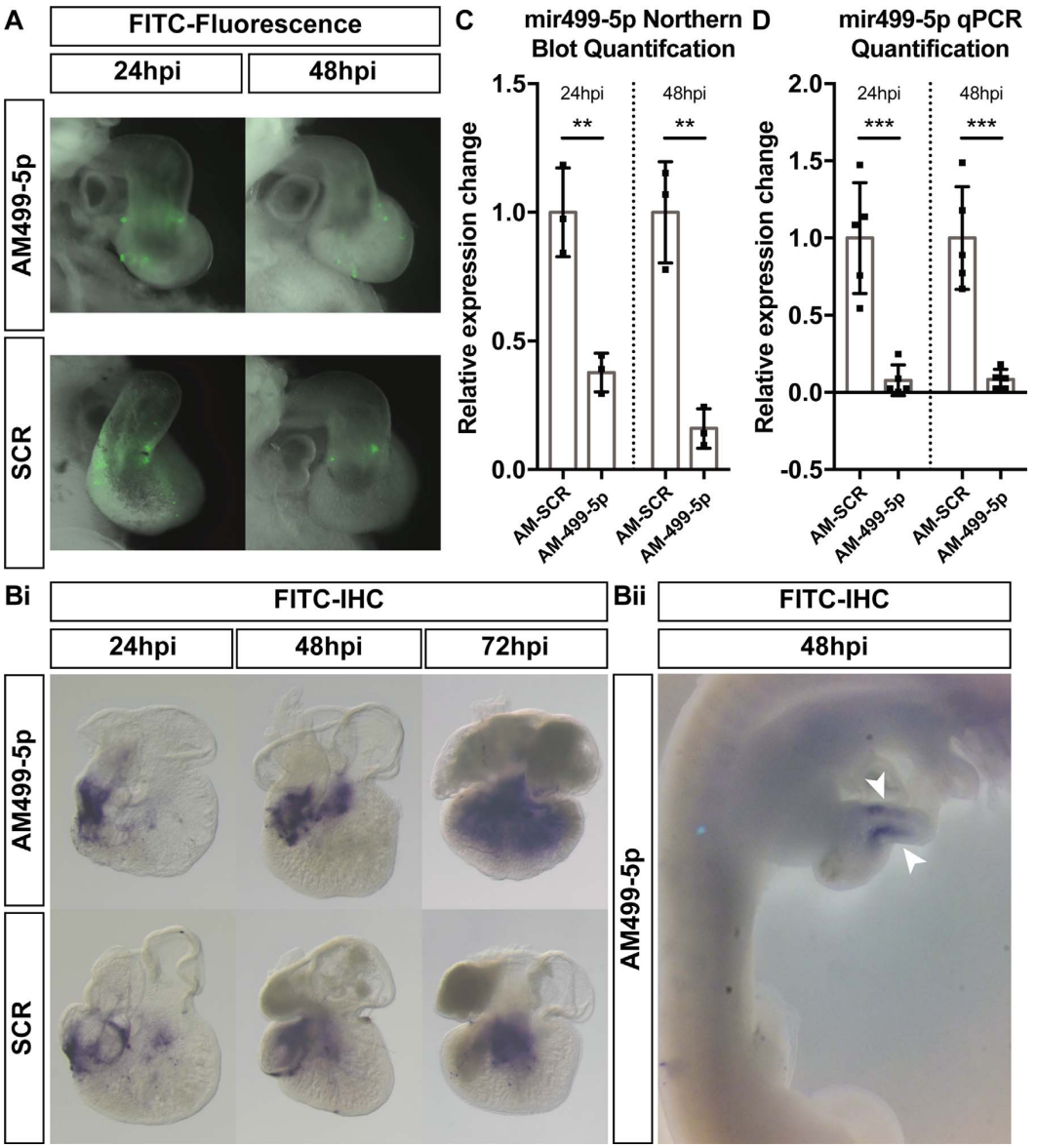

Fig. 3. Confirmation of successful AntagomiR delivery. Visual and molecular verification of AntagomiR delivery and microRNA knockdown. (A) Tracing of FITC-tag fluorescence of AntagomiR-SCR and AntagomiR-499-5p at 24 hpi and 48 hpi. (B) Chromophoric detection of the FITC-tag by IHC. (Bi) AntagomiR-SCR and AntagomiR-499-5p are detected by IHC at 24 hpi, 48 hpi and 72 hpi in dissected hearts. (Bii) Whole embryo IHC for AntagomiR-499-5p. Specific signal is detected in the heart (white arrowheads), faint background staining originates from trapping. (C) Northern Blot confirmation of miR-499-5p knockdown (unpaired *t*-test, n = 3, 24 hpi and 48 hpi, $p < 0.01$). (D) qPCR confirmation of miR-499-5p knockdown (unpaired *t*-test, n = 5, 24 hpi and 48 hpi $p < 0.001$).

constructs, or viral particles to achieve transient knockdown or area specific expression of genes of interest. For example, in preliminary experiments injection of LNA modified microRNA mimics, usually used for tissue culture experiments to promote miRNA mediated silencing, showed target RNA expression changes (data not shown). Also, it is possible to combine multiple AntagomiRs into a single injection to study synergistic, antagonistic or additive effects of microRNA inhibition. The method can be applied to a variety of stages of chicken development and thus allows the study of different processes of heart development. Most suitable are HH13–HH18, after turning of the chicken embryo and before the heart encapsulating tissue becomes too rigid for dissection to gain access (Martinsen, 2005; Wittig and Münsterberg, 2016). Injections at older developmental stages will allow the specific targeting of only the atria or ventricles, similarly at younger stages it is possible to restrict injections to parts of the primitive heart tube. Strikingly, following delivery the administered AntagomiR was locally restricted to the heart (Fig. 1F and Fig. 3A, B) and not affected by the circulating bloodstream. Therefore, this procedure allows studying the impact of microRNA-inhibition on the heart only, which presents an important advantage to approaches used previously (Davidson et al., 2001; Goehringer et al., 2009). This spatial restriction is helpful to avoid effects on other organs caused by systemic microRNA knockdown and will improve the interpretation of phenotypes.

The method allows the downstream analysis of different parameters to assess the phenotype, including morphology, histology, gene expression changes and changes in physiology. Here, we quantified the heart rate of injected embryos and compared it to wildtype siblings. Quantification of zebrafish heart rates has been done using a high frame rate camera (Musso et al., 2014), this was adopted for this study. Video recordings of the heart allow automated heart rate quantification using Fiji software and furthermore allow calculation of input and output volumes. The latter requires visual access to both, atria and ventricles (Musso et al., 2014), which is rarely the case past 48 hpi since at that stage the embryo is covered by the allantois (Spurlin and Lwigale, 2013). However, by selecting recorded videos where all heart chambers are fully visible, it is possible to determine cardiac input and output volumes. Alternatively, the heart rate can be determined with electrodes producing an electrocardiogram as shown by Shi et al. (2013) in the chicken embryo. Electrophysiological experiments surrounding the conduction system of the heart could involve patch clamp, pulse wave, action potential and/or ECG measurements (Borghetti et al., 2018; Shi et al., 2013). Morphological changes in the heart post-injection can be analysed by serial sectioning and 3D reconstruction (Wang et al., 2015), optical projection tomography (Sharpe et al., 2002) or histological staining procedures (Alturkistani et al., 2015).

To assess successful administration and resulting knockdown of miR499-5p, we employed Northern Blot analysis and quantitative RT-PCR. Such analysis can be further expanded for genes of interest to determine differential expression and thus dissect pathways relevant for the targeted microRNA. In order to understand the functional relevance of miRNAs and their corresponding targets and to decipher the miRNA network in heart development, the samples can be further processed for RNAseq to obtain a broader picture of differentially expressed genes. We showed that the RNA extraction method used, column-based or Trizol based, affects the ability to verify the knockdown. The reasons for this are still unclear, but we feel that it is an important observation to report. For further molecular analyses, non-Trizol extracted samples are preferable. This extraction method enables confirmation of microRNA knockdown after AntagomiR administration (Fig. 3C, D) (Krutzfeldt et al., 2005; Velu and Grimes, 2012) and avoids the reported GC-bias of Trizol for microRNAs (Kim et al., 2012).

Taken together the cardiac injection method presented here facilitates investigation of microRNA functions during intermediate heart development in the chicken embryo. Advantages of this knockdown approach are the targeted local delivery at specific stages of development and the short timeframe in which results can be obtained.

4. Material and methods

4.1. AntagomiR design

AntagomiRs are fully complementary to the microRNA of interest and include a 5′ Fluorescein and 3′ Cholesterol addition. Further the backbone consists of 2-O-methyl RNA and contains phosphorothioate bonds at the three most 3′ and two most 5′ bases (McGlinn et al., 2009).

4.2. Embryos

Fertilized Dekalb White chicken eggs (Henry Stewart & Co. Ltd., Fakenham, UK) were incubated at 37 °C until needed. Stage HH14–16 embryos (~ 66 h) were used for the cardiac injection procedure (Hamburger and Hamilton, 1951).

4.3. Fluorescence microscopy

AnatagomiR delivery was confirmed using a LEICA MZ16F microscope with a LEICA DFC 300FX camera to track the fluorescence of the Fluorescein tag. Brightfield and green channel images were taken and merged in Adobe Photoshop CC.

4.4. Heart rate assessment

To asses heart rates, a single injected egg was removed from the incubator and a circular opening was cut in the tape seal. The egg was immediately placed under the microscope and a 15–30 s clip at 1080 p/120 fps was recorded (RIBCAGE H5PRO). Subsequently the embryo was dissected and processed for other methods. Collected video clips were played in slow motion using Apple QuickTime and heart beats were counted manually by J.G.W. and M.R-G. Beats per minute were calculated accordingly $BPM = \frac{n_{beats}}{t_{recording}} * 60s$.

4.5. Immunohistochemistry

Endogenous phosphatases of dissected hearts have been inactivated at 67 °C in HYB buffer overnight. Following several washes according to previously described procedures (Goljanek-Whysall et al., 2011) an antibody against Fluorescein (Anti-Fluorescein-AP, Fab fragments, Roche) was applied and incubated overnight. Again, following several washes colour was developed for all samples simultaneously using BCIP/NBT.

4.6. RNA extraction and RT-qPCR

RNA and miRNA isolation from pools of dissected hearts was performed using Quick-RNA™ MiniPrep Plus (Zymo Research) according to the manufacturer's protocols. We used RNA Clean & Concentrator™-5 (Zymo Research) in the case of Trizol Reagent (Invitrogen™) treated samples. cDNA was synthesized from 200 ng RNA in a 20 µl reaction using a Maxima First Strand cDNA synthesis kit (Thermo Fisher Scientific). For miRNAs, cDNA was synthesized from 10 ng in a 10 µl reaction using miRCURY LNA RT Kit (Qiagen). RT-qPCR was performed on a 7500 Real-Time PCR System (Applied Biosystems) using SYBR Green PCR Master Mix (Thermo Fisher Scientific) according to the manufacturer's instructions. MicroRNA specific primers have been designed by Qiagen (mir-449-5p: YP02111236, mir-451: YP02110557, mir-126-3p: YP02111065). Primers used for the miR-499 precursor are F: 5′-TTTGAGG GAGCGGCAGTTAA-3′ and R: 5′-TGAGGAGAGAAGTAGCACAGACT-3′ (Sigma-Aldrich). RT-qPCR was normalised to β-Actin for mRNA, and miR-451 and miR-126-3p for micro RNA. Analysis was done according Livak and Schmittgen (2001) and significance was determined by unpaired *t*-test using GraphPad Prism.

4.7. Northern blot

Northern blot analysis was performed as previously described (Pall and Hamilton, 2008). Briefly, 10 µg of total RNA was resolved on a 15% denaturing urea polyacrylamide gel. The RNA was transferred to a Hybond-NX nylon membrane (GE Healthcare) by semidry-blotting for 1 h at 20 V and chemically crosslinked using 1-Ethyl-3-(3-dimethylaminopropyl) carbodiimide (Sigma Aldrich) at 60 °C for 2 h.

For Northern blot hybridization the membranes were pre-hybridized using Perfect Hyb buffer (Sigma Aldrich) and the antisense DNA oligonucleotides (Sigma-Aldrich) were end-labelled using 3000 Ci/mmol of [γ-^{32}P]-ATP (Perkin Elmer). The hybridization of the membranes with the 5′-^{32}P labelled DNA oligonucleotide was performed overnight at 37 °C. The membranes were washed twice with 0.2x SSC and 0.1% SDS for 20 min and exposed to a phosphor imager screen for autoradiography. The membrane was imaged using the Typhoon Scanner and band intensities were quantified with the Image Quant Software (GE Healthcare).

For re-probing of the membranes with the loading control, U6, the membranes were stripped with 0.1% SDS for 5 h at 80 °C.

Antisense DNA oligonucleotide probe sequences used were:

The miR499-5p miRCURY LNA miRNA detection (Qiagen) probe was used for the detection of miRNA 499–5p (5′-CTA AACATCACTACAAGTCTTA-3′) and the membrane was re-probed with U6 snRNA as a loading control (5′-GCTAATCTTCTCTGTATCGTTCC-3′).

Acknowledgements

We would like to thank Tamas Dalmay for discussion, and Gerry Giese and members of the Münsterberg and Grocott lab for critical review of the video of the procedure presented in this study.

Funding

This work was supported by the British Heart Foundation FS/15/41/31564, a H2020 Marie Skłodowska-Curie Actions Individual Fellowship (705089), a BBSRC grant (BB/N007034/1) and the Eastern Academic Research Consortium.

Competing interests

The authors declare no competing or financial interests.

Appendix A. Supplementary material

Supplementary data associated with this article can be found in the online version at doi:10.1016/j.ydbio.2018.11.008.

CRediT authorship contribution statement

Johannes G. Wittig: Conceptualization, Methodology, Validation, Formal analysis, Investigation, Visualization, **Martina Billmeier:** Investigation, **Estefanía Lozano-Velasco:** Conceptualization, Methodology, Investigation, **Miguel Robles -García:** Investigation, **Andrea E. Münsterberg:** Conceptualization, Supervision, Project administration, Funding acquisition, Writing - review & editing.

References

Alturkistani, H.A., Tashkandi, F.M., Mohammedsaleh, Z.M., 2015. Histological stains: a literature review and case study. Glob. J. Health Sci. 8, 72–79.
Antin, P.B., Kaur, S., Stanislaw, S., Davey, S., Konieczka, J.H., Yatskievych, T.A., Darnell, D.K., 2007. Gallus expression in situ hybridization analysis: a chicken embryo gene expression database. Poult. Sci. 86, 1472–1477.
Bartel, D.P., 2009. MicroRNAs: target recognition and regulatory functions. Cell 136, 215–233.
Bellairs, R., Osmond, M., 2014. Atlas of Chick Development. Elsevier Science. http://dx.doi.org/10.1016/C2010-0-65149-2.
Borghetti, G., Eisenberg, C.A., Signore, S., Sorrentino, A., Kaur, K., Andrade-Vicenty, A., Edwards, J.G., Nerkar, M., Qanud, K., Sun, D., Goichberg, P., Leri, A., Anversa, P., Eisenberg, L.M., Jacobson, J.T., Hintze, T.H., Rota, M., 2018. Notch signaling modulates the electrical behavior of cardiomyocytes. Am. J. Physiol. Heart Circ. Physiol. 314, H68–H81.
Bouabe, H., Okkenhaug, K., 2013. Gene targeting in mice: a review. Methods Mol. Biol. 1064, 315–336.
Chen, J., Wang, D.Z., 2012. microRNAs in cardiovascular development. J. Mol. Cell. Cardiol. 52, 949–957.
Davidson, M.J., Jones, J.M., Emani, S.M., Wilson, K.H., Jaggers, J., Koch, W.J., Milano, C.A., 2001. Cardiac gene delivery with cardiopulmonary bypass. Circulation 104, 131–133.
England, J., Granados-Riveron, J., Polo-Parada, L., Kuriakose, D., Moore, C., Brook, J.D., Rutland, C.S., Setchfield, K., Gell, C., Ghosh, T.K., Bu'Lock, F., Thornborough, C., Ehler, E., Loughna, S., 2017. Tropomyosin 1: multiple roles in the developing heart and in the formation of congenital heart defects. J. Mol. Cell. Cardiol. 106, 1–13.
Goehringer, C., Rutschow, D., Bauer, R., Schinkel, S., Weichenhan, D., Bekeredjian, R., Straub, V., Kleinschmidt, J.A., Katus, H.A., Muller, O.J., 2009. Prevention of cardiomyopathy in delta-sarcoglycan knockout mice after systemic transfer of targeted adeno-associated viral vectors. Cardiovasc Res. 82, 404–410.
Goljanek-Whysall, K., Sweetman, D., Abu-Elmagd, M., Chapnik, E., Dalmay, T., Hornstein, E., Munsterberg, A., 2011. MicroRNA regulation of the paired-box transcription factor Pax3 confers robustness to developmental timing of myogenesis. Proc. Natl. Acad. Sci. USA 108, 11936–11941.
Hamburger, V., Hamilton, H.L., 1951. A series of normal stages in the development of the chick embryo. J. Morphol. 88, 49–92.
Kalhor, R., Kalhor, K., Mejia, L., Leeper, K., Graveline, A., Mali, P., Church, G.M., 2018. Developmental barcoding of whole mouse via homing CRISPR. Science 361.
Kim, Y.K., Yeo, J., Kim, B., Ha, M., Kim, V.N., 2012. Short structured RNAs with low GC content are selectively lost during extraction from a small number of cells. Mol. Cell 46, 893–895.
Kraus, P., Sivakamasundari, V., Xing, X., Lufkin, T., 2014. Generating mouse lines for lineage tracing and knockout studies. Methods Mol. Biol. 1194, 37–62.
Kretzschmar, K., Watt, F.M., 2012. Lineage tracing. Cell 148, 33–45.
Krutzfeldt, J., Rajewsky, N., Braich, R., Rajeev, K.G., Tuschl, T., Manoharan, M., Stoffel, M., 2005. Silencing of microRNAs in vivo with 'antagomirs'. Nature 438, 685–689.
Lambeth, L.S., Ohnesorg, T., Cummins, D.M., Sinclair, A.H., Smith, C.A., 2014. Development of retroviral vectors for tissue-restricted expression in chicken embryonic gonads. PLoS One 9, e101811.
Liu, N., Olson, E.N., 2010. MicroRNA regulatory networks in cardiovascular development. Dev. Cell 18, 510–525.
Livak, K.J., Schmittgen, T.D., 2001. Analysis of relative gene expression data using real-time quantitative PCR and the 2(-Delta Delta C(T)) Method. Methods 25, 402–408.
Lufkin, T., 2007. In situ hybridization of whole-mount mouse embryos with RNA probes: hybridization, washes, and histochemistry. CSH Protoc 2007, pdb prot4823.
Martinsen, B.J., 2005. Reference guide to the stages of chick heart embryology. Dev. Dyn. 233, 1217–1237.
McGlinn, E., Yekta, S., Mansfield, J.H., Soutschek, J., Bartel, D.P., Tabin, C.J., 2009. In ovo application of antagomirs indicates a role for miR-196 in patterning the chick axial skeleton through Hox gene regulation. Proc. Natl. Acad. Sci. USA 106, 18610–18615.
Musso, G., Tasan, M., Mosimann, C., Beaver, J.E., Plovie, E., Carr, L.A., Chua, H.N., Dunham, J., Zuberi, K., Rodriguez, H., Morris, Q., Zon, L., Roth, F.P., MacRae, C.A., 2014. Novel cardiovascular gene functions revealed via systematic phenotype prediction in zebrafish. Development 141, 224–235.
Pall, G.S., Hamilton, A.J., 2008. Improved northern blot method for enhanced detection of small RNA. Nat. Protoc. 3, 1077–1084.
Randles, C.A., Romanoff, A.L., 1954. A preliminary study on the hatchability of chicken eggs subjected to shaking agitation. Poult. Sci. 33, 374–377.
Sharpe, J., Ahlgren, U., Perry, P., Hill, B., Ross, A., Hecksher-Sorensen, J., Baldock, R., Davidson, D., 2002. Optical projection tomography as a tool for 3D microscopy and gene expression studies. Science 296, 541–545.
Shi, L., Goenezen, S., Haller, S., Hinds, M.T., Thornburg, K.L., Rugonyi, S., 2013. Alterations in pulse wave propagation reflect the degree of outflow tract banding in HH18 chicken embryos. Am. J. Physiol. Heart Circ. Physiol. 305, H386–H396.
Singh, P., Schimenti, J.C., Bolcun-Filas, E., 2015. A mouse geneticist's practical guide to CRISPR applications. Genetics 199, 1–15.
Spurlin, J., 3rd, Lwigale, P., 2013. A technique to increase accessibility to late-stage chick embryos for in ovo manipulations. Dev. Dyn. 242, 148–154.
Stern, C.D., 2005. The chick; a great model system becomes even greater. Dev. Cell 8, 9–17.
van Rooij, E., Quiat, D., Johnson, B.A., Sutherland, L.B., Qi, X., Richardson, J.A., Kelm, R.J., Jr., Olson, E.N., 2009. A family of microRNAs encoded by myosin genes governs myosin expression and muscle performance. Dev. Cell 17, 662–673.
Velu, C.S., Grimes, H.L., 2012. Utilizing antagomiR (antisense microRNA) to knock down microRNA in murine bone marrow cells. Methods Mol. Biol. 928, 185–195.
Wang, C.W., Budiman Gosno, E., Li, Y.S., 2015. Fully automatic and robust 3D registration of serial-section microscopic images. Sci. Rep. 5, 15051.
Wittig, G.J., Münsterberg, A., 2016. The early stages of heart development: insights from chicken embryos. J. Cardiovasc. Dev. Dis. 3.